On the Tracks of *Brachylophosaurus*: Simulation-Based Examinations on the Locomotion of Hadrosaurs

Dissertation

der Mathematisch-Naturwissenschaftlichen Fakultät

der Eberhard Karls Universität Tübingen

zur Erlangung des Grades eines

Doktors der Naturwissenschaften

(Dr. rer. nat.)

vorgelegt von

Dipl. Geol. Alexander Hohloch

aus Sindelfingen

Tübingen

2013

Tag der mündlichen Qualifikation:	26.11.2013
Dekan:	Prof. Dr. Wolfgang Rosenstiel
1. Berichterstatter:	Prof. Dr. Hans-Ulrich Pfretzschner
2. Berichterstatter:	Prof. Dr. Hervé Bocherens

Table of contents

Abstract	2
Zusammenfassung	4
Acknowledgements	7
1. Introduction	**8**
2. State of the art	**11**
2.1 Hadrosaurian locomotion	11
2.2 Hadrosaurian and iguanodontian tracks and trackways	21
3. Material	**27**
3.1 Pectoral girdle	32
3.2 Forelimb	34
3.3 Pelvic girdle	37
3.4 Hindlimb	39
4. Methods	**44**
4.1 Digitizing hadrosaur bones	44
4.2 Rework digitized bones	51
4.3 Creating the hadrosaur model - the skeleton	62
4.4 Creating the hadrosaur model - the body	78
4.5 Running simulations	89
4.6 Model review	105
5. Simulations	**117**
5.1 Quadrupedal locomotion	118
5.1.1 Results	118
5.1.2 Discussion	129
5.2 Bipedal locomotion	160
5.2.1 Results	160
5.2.2 Discussion	166
5.3 Other body postures	176
5.3.1 Results	176
5.3.2 Discussion	179
6. Conclusions	**180**
7. References	**184**

Abstract

The locomotion of hadrosaurs is a long-term debated topic in dinosaur research, including different approaches which often provide controversial results. Although hadrosaurs are commonly regarded as facultative bipeds today, walking quadrupedally according to circumstances, the variety of hadrosaurian locomotion is still not understood completely.

Here, computer based simulations, which are used increasingly in dinosaur research during the last decade, can contribute to a better understanding of hadrosaurian balance and postures, range of motion, body mass distribution, and motion sequences, using CAD (computer aided design) and NASTRAN-based CAE (computer aided engineering) software.

For the simulations shown in this work a 3D model of the hadrosaurine hadrosaur species *Brachylophosaurus canadensis* was created, based on skeletal material of three specimens from the Judith River Formation in Montana which is of Campanian age. The bones of fore- and hindlimb as well as shoulder and pelvic girdle were digitized using a mechanical Immersion MicroScribe-3D® point digitizer together with the Rhinoceros 3.0® CAD program.

In combination with a detailed *Parasaurolophus* desk model, which was digitized to get a preliminary 3D model body, photos from museum mounts, and skeletal drawings, in part with body outlines, it was possible to create a realistic *Brachylophosaurus* NURBS (non-uniform rational B-Spline) model in Rhinoceros 3.0®. For using the model in simulations with MSC.visualNastran 4D®, it had to be transformed into a rigid polygon body and cut into functional parts (e.g. head or tail) using the Geomagic Qualify 8.0® CAQ (computer aided quality assurance) program. Finally, the body parts were connected with joints in MSC.visualNastran 4D® to achieve mobility of the model.

In the motion sequences quadrupedal locomotion was simulated first. Before starting a simulation, e.g. the cross gait, an initial posture of body, arms, and legs had to be defined. Here, to find correct positions of arms and legs in combination with the right placement of hands and feet, tracks and trackways were used. These were necessary as guideline for each gait, and also as control factor, as a widely accordance between model and fossil trackway is essential for a realistic way of motion.

In case of cross and pace gait only the former matches with the fossil track record, indicating that hadrosaurs preferred this kind of quadrupedal locomotion. However, in most trackways used as guidelines in this work a ‘regular’ quadrupedal gait like the cross gait is not possible due to the differences in length between arms and legs. While moving forward both hands lost contact with the ground as step length of the hindfeet is too large.

Therefore, to solve this problem, the so-called ‘semibipedal’ gait was developed within this work, representing a quadrupedal way of motion with the arms used like ‘hiking sticks’ which were extended and retracted alternately in a repeating interval. This kind of motion compensates the lesser length of the hadrosaurian forelimbs and was apparently used most of the time when hadrosaurs walked quadrupedally. However, there is no uniform ‘semibipedal’ gait as step and stride length of the tracks as well as orientation and placement of hand- and footprints vary between different trackways. The simulations show also that the arms were used as additional body support, but the legs played the major supportive role in bearing the body mass.

In bipedal locomotion simulations are relatively similar as there is of course also a great similarity between the fossil bipedal trackways. Nevertheless, differences in step and stride length of the footprints also occur, and the simulations indicate further that hadrosaurs may have used different body postures when walking bipedally, e.g. a horizontally or a more erect body posture. In addition, the motion sequences show that increasing step length, in combination with higher velocities, has no influence on walking stability.

Gait change from quadrupedal to bipedal locomotion was also tested successfully within the simulations as well as different body postures like high-browsing or low-browsing stance. However, in case of motions which are not documented by tracks it is usually not possible to verify if they were actually used.

In all simulations the center of mass of the model moves within a small range and the differences between quadrupedal and bipedal locomotion are relatively small, indicating that the use of the arms would have influenced locomotion only to a minor extent.

In summary, the simulation results show the variety of hadrosaurian locomotion and range of motion and how these may have appeared. However, if each hadrosaur species was able to use this wide capability of motions and postures remains unsolved and cannot be answered by the simulations.

Zusammenfassung

Die Fortbewegung der Hadrosaurier ist seit langem Gegenstand der Diskussion in der Dinosaurierforschung, wobei unterschiedliche Ansätze häufig widersprüchliche Ergebnisse erbracht haben. Obwohl Hadrosaurier inzwischen in der Regel als sich fakultativ biped fortbewegende Tiere angesehen werden, die sich bei Bedarf auch quadruped fortbewegen konnten, ist die Vielfalt ihrer Fortbewegungsmöglichkeiten nach wie vor nicht gänzlich verstanden.

Computergestützte Simulationen, die in den letzten Jahren zunehmend in der Dinosaurierforschung Einzug gehalten haben, können hier zu einem besseren Verständnis der Körperhaltungen, Bewegungsspielräume, Gewichtsverteilung und Bewegungsabläufe von Hadrosauriern beitragen. Hierzu werden CAD (computer aided design) und auf NASTRAN basierende CAE (computer aided engineering) Computerprogramme verwendet.

Für die in dieser Arbeit gezeigten Simulationen wurde ein 3D Modell des Hadrosauriers *Brachylophosaurus canadensis* erstellt. Dieses basiert auf dem Skelettmaterial dreier Exemplare aus der Judith River Formation in Montana, die stratigraphisch in das Campanium (obere Oberkreide) einzuordnen ist. Die Knochen des Vorder- und Hinterbeines und von Schulter- und Beckengürtel wurden mit Hilfe des Immersion MicroScribe-3D® Freiarmdigitalisiergerätes digitalisiert, unter Verwendung des Rhinoceros 3.0® CAD Programms.

In Verbindung mit einem detaillierten Tischmodell eines *Parasaurolophus*, das digitalisiert wurde um einen vorläufigen 3D Körper für das Hadrosaurier Modell zu erhalten, Bildern von Skeletten aus musealen Sammlungen und Skelettzeichnungen mit Körperumrissen war es möglich ein realistisches NURBS (non-uniform rational B-Spline) Modell eines *Brachylophosaurus* in Rhinoceros 3.0® zu erstellen. Um dieses Modell in den Simulationen mit dem MSC.visualNastran 4D® Programm nutzen zu können, musste es in einen in sich geschlossenen, nicht deformierbaren Polygonköper umgewandelt und in funktionelle Einheiten (z.B. Kopf oder Schwanz) unterteilt werden. Dies geschah mit Hilfe des Geomagic Qualify 8.0® CAQ (computer aided quality assurance) Programms. Abschließend wurden die Körperabschnitte in MSC.visualNastran 4D® mit Gelenken verbunden um das Modell beweglich zu machen.

Hinsichtlich der Bewegungsabläufe wurde zunächst die quadrupede Fortbewegung simuliert. Vor dem Start einer Simulation, z.B. des Kreuzgangs, musste die Ausgangsstellung des Körpers und der Arme und Beine festgelegt werden. Spuren und Spurabfolgen wurden genutzt um die korrekte Position der Arme und Beine in Verbindung mit der richtigen Platzierung der Hände und Füße zu ermitteln. Spuren dienten als Vorlage und Kontrollmöglichkeit für die einzelnen Gangarten, da eine weitgehende Übereinstimmung zwischen der Spurabfolge im Fossilbericht und des Modells unabdingbar ist für eine realistische Fortbewegung.

In den Simulationen von Kreuz- und Passgang wurde diese Übereinstimmung nur mit dem Kreuzgang erzielt. Dies deutet darauf hin, dass Hadrosaurier diese Art der quadrupeden Fortbewegung bevorzugt haben. Die meisten Spurabfolgen, die als Vorlage in den Simulationen genutzt wurden, sind jedoch nicht durch einen “normalen” quadrupeden Gang entstanden, da dies durch den Längenunterschied zwischen Armen und Beinen nicht möglich gewesen wäre. Während der Vorwärtsbewegung verlieren beide Hände den Kontakt zum Boden, da die Schrittlänge der Hinterbeine zu groß ist.

Um dieses Problem zu lösen wurde im Rahmen dieser Arbeit der sogenannte ‘semibipede’ Gang entwickelt, der eine quadrupede Fortbewegungsweise darstellt bei der die Arme wie ‘Wanderstöcke’ genutzt werden. Hierbei werden sie in einem sich wiederholenden Intervall abwechselnd gestreckt und zurückgezogen. Diese Gangart gleicht die kürzere Länge der Vorderbeine aus und wurde bei der quadrupeden Fortbewegung von den Hadrosauriern offenbar bevorzugt genutzt. Es existiert jedoch kein einheitlicher ‘semibipeder’ Gang, da sowohl die Schrittlänge als auch die Ausrichtung und Position der Hand- und Fußabdrücke zwischen den verschiedenen Spurabfolgen variieren. Die Simulationen zeigen darüber hinaus, dass die Arme als zusätzliche Stütze dienten, die Beine jedoch die Hauptlast des Körpergewichts trugen.

Die Simulationen der bipeden Fortbewegung weisen eine große Ähnlichkeit auf, da auch in den zugehörigen fossilen Spurabfolgen keine merklichen Unterschiede erkennbar sind, mit Ausnahme z.B. der Schrittlänge. Die Simulationen weisen jedoch darauf hin, dass sich biped fortbewegende Hadrosaurier möglicherweise unterschiedlicher Körperhaltungen bedient haben, z.B. eine mehr horizontale Ausrichtung des Körpers oder eine stärker aufrechte Haltung. Darüber hinaus zeigen die Simulationen, dass eine vergrößerte

Schrittlänge in Verbindung mit höheren Laufgeschwindigkeiten keinen Einfluss auf die Stabilität der Fortbewegung hat.

Ferner wurde in den Simulationen auch der Übergang von quadrupeder zu bipeder Fortbewegung erfolgreich getestet, als auch verschiedene Körperhaltungen, einschließlich unterschiedlicher Fresshöhen. Hinsichtlich von Bewegungsabläufen, die nicht durch Spuren nachgewiesen sind, ist es jedoch in der Regel nicht möglich zu belegen ob diese tatsächlich genutzt wurden.

Der Schwerpunkt des Modells bewegt sich in allen Simulationen innerhalb eines engen Bereichs, wobei die Unterschiede zwischen quadrupeder und bipeder Fortbewegung verhältnismäßig gering sind. Dies deutet darauf hin, dass der Gebrauch der Arme auf die Fortbewegung nur einen geringen Einfluss ausübt.

Insgesamt zeigen die Ergebnisse der Simulationen das breite Spektrum der Fortbewegung und Bewegungsspielräume der Hadrosaurier und wie diese ausgesehen haben könnten. Ob jedoch jede einzelne Hadrosaurier Art in der Lage war dieses breite Spektrum an Bewegungen und Körperhaltungen zu nutzen bleibt ungelöst und kann durch die Simulationen nicht beantwortet werden.

Acknowledgements

My special thanks go to my Ph.D. supervisor Prof. H.-U. Pfretzschner from the Institute for Geosciences of the University of Tübingen for his support and help with all questions and problems which occurred within this work. He helped me to develop this project and had always a helpful comment on my work. Our discussions were of great importance to me, to reflect my results and to get new ideas.

Further, I want to thank Heinrich Mallison from the Museum für Naturkunde, Berlin for his support and help with the CAD and CAE software and especially for his previous work on *Plateosaurus*, which made my work much easier. Without the techniques he developed and improved it would have been much more difficult to realize this work.

Special thanks go also to my colleague Juliane Hinz, who had always an ear for my problems and time for discussing my work. She was a great help with all kind of computer and software problems. Many thanks for the great teamwork during the last years.

I also want to thank the Phillips County Museum and the Great Plains Dinosaur Museum and Field Station (former Dinosaur Field Station) in Malta, Montana, especially Mr. Nate Murphy, for the possibility to digitize the *Brachylophosaurus* bone material. Thanks to all members of the staff for their friendliness and hospitality.

Last but not least I want to thank my family and friends for their support, and that they always believed in me.

1. Introduction

Hadrosaurs, the so-called duck-billed dinosaurs, are virtually the best known dinosaur group. Their common remains range from fully articulated skeletons to disarticulated and isolated material, added by eggshells, embryos, hatchlings, and juveniles, as well as footprints and trackways, skin impressions, and coprolites (HORNER et al. 2004).

They were the most diverse and abundant large herbivores of the Late Cretaceous and also the last major clade of ornithopods to evolve in the Mesozoic (HORNER et al. 2004).

The Hadrosauridae are a monophyletic group of derived iguanodontian ornithopod dinosaurs. Their monophyly has long been presumed (e.g. LULL & WRIGHT 1942; OSTROM 1961), based on a large number of unique features in their skeletons and skulls, and all more recent cladistic analyses (e.g. WEISHAMPEL et al. 1993; FORSTER & SERENO 1994) strongly support this hypothesis (FORSTER 1997; HORNER et al. 2004).

Traditionally, the members of the Hadrosauridae have been divided into two subtaxa, each diagnosed by its own unique features. These two subtaxa are the Hadrosaurinae or "flat-headed" hadrosaurids, and the Lambeosaurinae or "crested" hadrosaurids. This differentiation has been supported by phylogenetic analyses (e.g. WEISHAMPEL et al. 1993; SERENO 1999) (FORSTER 1997; HORNER et al. 2004).

Most taxa of the Lambeosaurinae show strange modifications of the nasal bones, building up crests and pipes (Figure 1). The Hadrosaurinae in contrast possess simpler skull forms (Figure 2) (SANDER 1994).

Figure 1: The lambeosaurine hadrosaur *Parasaurolophus walkeri* (PAUL 2010).

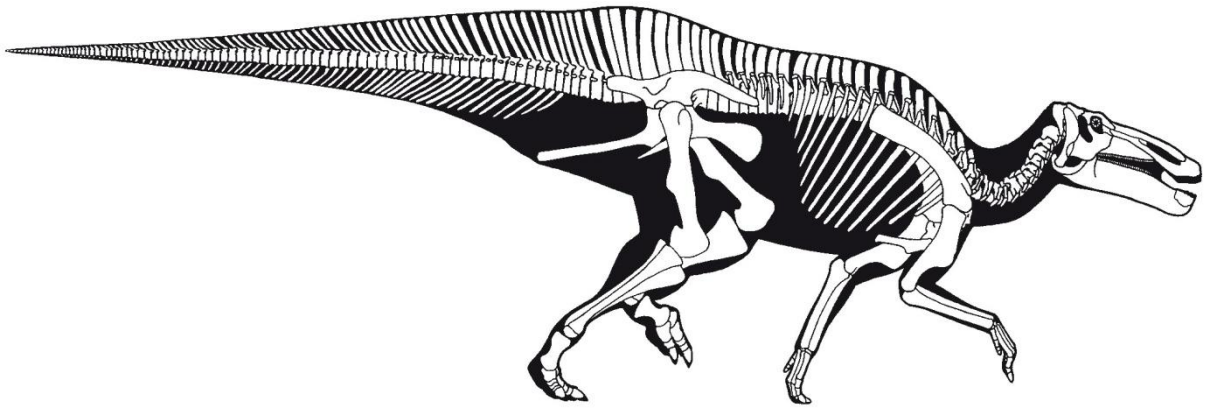

Figure 2: The hadrosaurine hadrosaur *Shantungosaurus giganteus*, the largest known hadrosaur (PAUL 2010).

Despite the abundance of hadrosaur remains, only few morphological studies have focused on the postcrania of these animals, as in general the skull shows the most distinctive morphological characters. The characters based on the postcranium, which are included in phylogenetic analyses, provide very little resolution at lower phylogenetic levels, as among genera and species. They mainly serve to differentiate lambeosaurines from hadrosaurines and hadrosaurids from outgroup taxa. Most genera and species are therefore based primarily on the basis of cranial characters (HORNER et al. 2004; PRIETO-MARQUEZ 2007).

The distribution of hadrosaurs was nearly worldwide. Their fossils were found in North and South America, central and eastern Asia, Europe, and the Antarctic Peninsula (WEISHAMPEL and WEISHAMPEL 1983; WEISHAMPEL 1990; WEISHAMPEL et al. 2004). A North American origin of the clade seems to be most likely (HORNER et al. 2004) although an Asian origin of the group was under discussion (MILNER and NORMAN 1984).

Hadrosaurid remains are found in diverse biotopes, including intermontane and terrestrial foredeep basins (HORNER et al. 2004), and material from Montana (USA) and Alberta (CND) indicates that there is some habitat differentiation among hadrosaurid species (RUSSELL 1967a, 1967b; DODSON 1971; HORNER 1983; HORNER et al. 2001).

Hadrosaurs show body lengths up to 15 m and body weights from less than 1 kg hatching to several tones in adulthood. The largest hadrosaurs may have weighed about 16 t (FORSTER 1997; HORNER et al. 2004).

Based on osteohistological studies (HORNER et al. 2000, 2001), it is evident that hadrosaurids experienced growth rates comparable with living endotherms (PADIAN and

HORNER 2004). *Maiasaura peeblesorum* apparently grew from 0.5 m hatchling size (Figure 3) to about 7 m adult size in 6 to 8 years (HORNER et al. 2000).

Figure 3: Nestling of *Maiasaura peeblesorum* (PAUL 2010).

Regarding the growth rates and adult size, as well as the abundance of hadrosaur specimens during the Late Cretaceous, it is evident that these animals were the dominant terrestrial herbivores of their time. They were active foragers on ground cover and low arboreal foliage from conifers and deciduous trees and shrubs (WEISHAMPEL 1984; HORNER et al. 2004). The broad, complex occlusal surfaces and dental batteries of hadrosaurs, as well as their large gut capacity, were well suited for a food of low-quality, high-fiber vegetation (FARLOW 1987; HORNER et al. 2004).

Colonial nesting is known in *Maiasaura peeblesorum*, which may be widespread among hadrosaurs. There was also parental care of both hadrosaurine and lambeosaurine juveniles for some time following hatching (HORNER and MAKELA 1979; HORNER 1982, 1984, 1999, 2000; HORNER et al. 2004).

Bone bed occurrences, which are often monospecific (VARRICCHIO and HORNER 1993; HORNER et al. 2004), provide further evidence for gregariousness and the possibility of migrations (PAUL 1997a; FIORILLO and GANGLOFF 2001).

Several amazing cranial features in hadrosaurs may have developed in parent-offspring interactions, herding, intraspecific social behavior, and species recognition. These features focus mainly on the modification of the nasal cavity and associated lateral diverticula (HOPSON 1975; WEISHAMPEL 1981a, 1981b). Also, there is morphometric support for sexual dimorphism in the crest of lambeosaurine species (DODSON 1975; HORNER et al. 2004).

2. State of the art

Since hadrosaurs played such a dominating role in the terrestrial fauna of the Upper Cretaceous, studies of their adaptations on locomotion were always of great interest, with different approaches often producing controversial results.

The main discussions focused on the questions if or to what extent hadrosaurs used their forelimbs in locomotion (obligatory or facultative bipedality), exist differences between the two subfamilies (Hadrosaurinae and Lambeosaurinae) concerning locomotion, and which role played the ossified tendons of the vertebral column?

Tracks and trackways of hadrosaurs, and their close relatives the iguanodonts, were also examined in detail over the years and provided lots of information over locomotion and behavior of these animals.

2.1 Hadrosaurian locomotion

When LEIDY (1858) examined the skeleton of *Hadrosaurus*, the first well preserved hadrosaur specimen, he already noted the great disparity between the lengths of the fore- and hindlimbs of this dinosaur. He assumed that *Hadrosaurus* had a bipedal stance, balancing upright on its hindlimbs and tail like a kangaroo, but added that a quadrupedal stance may have also been possible. Further, Leidy speculated that *Hadrosaurus* may have had an aquatic way of life, a viewpoint repeated by later paleontologists who thought these animals water bound and incapable of habitual terrestrial locomotion (FORSTER 1997).

BROWN (1912) studied the *Edmontosaurus* mummy at the American Museum of Natural History in New York and assumed that its hand phalanges were partly imbedded in skin. OSBORN (1912) was of the opinion that this would indicate a webbed hand, which he interpreted as an aquatic adaptation for paddling about in water. This view became one of the primary arguments for researchers who favored an aquatic habit for hadrosaurs (FORSTER 1997).

After OSTROM (1964) implied the paleogeographic and paleobotanical evidence that hadrosaurs lived in lowland coastal plains in warm temperate to subtropical climates. In his point of view indicate the nature of dental apparatus, skeletal structure, associated flora,

and preserved stomach contents that hadrosaurs were terrestrial bipeds adapted to feed on the resistant tissues of land plants rather than soft aquatic plants. Due to the absence of defensive structures, he regarded the large flat tail and webbed manus as protective adaptations that permitted the hadrosaurs to escape terrestrial predators by swimming.

In contrast, BAKKER (1986) interpreted the webbing of the hands as digital pads that were deformed during mummification. These digital pads would have cushioned the fingertips during quadrupedal locomotion. In addition, the hadrosaurian metacarpals show scars along their lengths, indicating that they were tightly bound together in life. This would be a poor arrangement for a paddle, but an excellent adaptation for weight support on land (FORSTER 1997).

Although these supposed digital pads and tightly bound metacarpals are adaptations for quadrupedal locomotion, the disparity in forelimb to hindlimb lengths, which Leidy already noted in 1858, remains outside the range of known obligatory quadrupeds. As the forelimbs of hadrosaurs are shorter and more lightly built than the long, robust hindlimbs, stride length and limb strength during quadrupedal locomotion would be limited. This means that a quadrupedally walking hadrosaur could only have run as fast as its front legs would allow (FORSTER 1997).

GALTON (1970) believed that the hindlimbs of hadrosaurs carried all the weight and that these animals were bipedal except when resting. For him the bipedality is clearly shown by the length of the hindlimb relative to the trunk and to the forelimb, the non-graviportal nature of the forelimb with an elongated radius, ulna, and metacarpals, the absence of any epidermal callouses or tubercule enlargements on the mittened manus, the well-developed fourth trochanter on the femur, the progressive changes in size of the centra and the height of the neural arches on either side of the sacrum, the upward turn of the centra at the base of the tail, and the rhomboidal network of ossified tendons.

After Galton show the ramrod straight vertebral column, the shallow iliac part of the acetabular curve, and the slender pubic peduncle that while running bipedally the straight part of the column was probably held more or less horizontal. Therefore, he rejected an upright, kangaroo-like posture for hadrosaurs as supposed by LEIDY (1858).

MARYANSKA and OSMOLSKA (1983, 1984) considered hadrosaurs as terrestrial bipeds, but added that these animals occasionally moved around on all four legs, e.g. when they remained in swamps or marshes or while resting and feeding. Further, they believed that the

recognized curvature of the vertebral column has its explanation in the static of the skeleton during bipedal progression. Therefore, they agreed with GALTON (1970) that hadrosaurs were bipedal runners which held the vertebral column horizontally during locomotion.

After MARYANSKA and OSMOLSKA (1984) leads the sloping of the thoracic vertebral column to the effective shortening of the hadrosaur trunk region. This caused the backward shift of the center of gravity, closer to the hip joint. So, together with the vertically held neck and the short deep trunk, the preacetabular weight of the animal could be much more easily counterbalanced by the horizontally held tail during bipedal locomotion. While running or walking bipedally, hadrosaurs might have regulated the shift of the center of gravity by thrusting the head back and forth, as do some walking birds (DAGG 1977). In their opinion the downward bend of the cranial portion of the thoracic vertebral column had still another effect as it caused a lowering of the shoulder joint and a backward shift of the sternum. This could enable the forelimbs to reach the ground more easily (BAKKER 1978), which might be significant for some locomotory and feeding habits.

Based on the size of adult hadrosaurs, their habitual (although not obligatory) bipedality and their ability to raise the vertebral column to an upright position, these animals may have used a considerably high reach to obtain food. In contrast to BAKKER (1978), it seems therefore that hadrosaurs could be high-browsers, although low-browsing played possibly also a role in their feeding habits.

Further, MARYANSKA and OSMOLSKA (1984) believed that hadrosaurs had to retreat to places where they would not be threatened by carnivores, in order to grind their food. Swamps, marshes, or river banks may constitute such safe places for hadrosaurs. Here, due to their “webbed” hands, they could move around more easily on all fours than could the heavy, obligatorily bipedal theropods.

GODEFROIT et al. (2001) proposed an osteological reconstruction of the lambeosaurine hadrosaur *Charonosaurus jiayinensis* from the Late Cretaceous Yuliangze Formation of north-eastern China. Their comparisons of postcranial features indicate that *Charonosaurus* was probably less well-adapted for quadrupedal gait than *Iguanodon benissartensis*, but may have shown a more efficient bipedal gait.

In larger specimens of *Iguanodon* the pectoral girdle forms a kind of continuous solid arch, particularly well adapted for weight-supporting during quadrupedal locomotion. Here, the scapula and coracoid are even completely fused as in adult specimens of obligate

quadruped dinosaurs. In contrast, the pectoral girdle of *Charonosaurus* and other hadrosaurs appears less well adapted for weight-supporting, as the coracoid is smaller and more slender, the scapula/coracoid suture is less thickened transversely, and intersternal ossifications have not been observed (GODEFROIT et al. 2001).

Therefore, they concluded that neither the pectoral girdle nor the forelimb of *Charonosaurus jiayinensis*, and of hadrosaurs in general, display the weight-supporting adaptations observed by NORMAN (1980) in *Iguanodon bernissartensis*. In their opinion the results confirm the hypothesis of GALTON (1970) that hadrosaurs were primarily bipeds. However, they added that the forelimb of *Charonosaurus* was notably powerful, although the movements were apparently rather limited. Further, the anatomy of the pelvic girdle and of the hindlimb bones reveals that the musculature of the hindlimb was also particularly powerful. Therefore, like other hadrosaurs, this species was probably better adapted for bipedal stance than was *Iguanodon* (GODEFROIT et al. 2001).

DILKES (2001) examined the ontogenetic growth in the forelimb and hindlimb of the hadrosaur *Maiasaura peeblesorum* from the Upper Cretaceous Two Medicine Formation of Montana by multivariate and bivariate morphometrics, and the biomechanics of beam theory. His results support a hypothesis of an age-dependent selection of stance. Thus, juvenile *Maiasaura* walked primarily as bipeds, but as an individual matured, its predominant stance shifted to quadrupedality.

Concerning the forelimb, morphometric results show a probable allometric enlargement of postural muscles, an allometric increase in the lever arms of protractor muscles, and an increased robustness of the humerus to increase its resistance to bending stresses. In contrast, the hindlimb shows a relative decrease in the resistance of the femur and tibia to bending stresses. Further, there is an allometric enlargement of the fourth trochanter of the femur and positive allometry of the lengths of metatarsals III and IV.

In their opinion is the most likely explanation for the different growth patterns that the hindlimb was sufficiently robust at a young age to accommodate increased postural and locomotory stresses through largely isometric growth. Contrary, in older individuals a behavioral shift to quadrupedality requires an allometric response in the forelimb. Osteological adaptations for weight-bearing in the manus include metacarpals that are firmly united and articulated in an arc configuration that was more resistant to bending than if the metacarpals were aligned in a transverse row. Hyperextension was possible at the

metacarpal-phalangeal joints, the phalanges were bound together by skin and probably ligaments and the manus had a broad contact with the ground. Flexor muscles that attached to the caudal surface of the metacarpals probably reinforced the reduced carpus and lessened the chance of collapse during quadrupedality (DILKES 2001).

EGI and WEISHAMPEL (2002) examined variation in juvenile and adult humeral morphology between the two subfamilies of Hadrosauridae. Their sample consisted of five hadrosaurine and four lambeosaurine genera and included humeri from 28 to 65 cm in length. Nineteen landmarks associated with articular surfaces and muscle attachments were digitized from photographs of humeri in posterolateral view. This data were analyzed using three morphometric techniques: Bookstein's coordinates, Resistant-Fit Theta-Rho-Analysis, and Euclidean Distance Matrix Analysis.

Differences in humeral shape were greater between the adults of the two subfamilies than between the juveniles, and the differences between adults and juveniles were larger in lambeosaurine than in hadrosaurine genera.

The adult lambeosaurine hadrosaurs show lateral and distal enlargement of the distal part of the deltopectoral crest and relative shortening of the shaft distal to the deltopectoral crest, resulting in the increased performance of the shoulder muscles. The morphological change of the humerus during growth seems to be closely combined with the reduction of the humeral length relative to antebrachium. The morphological variations in hadrosaurid humeri relate to structural adaptations to bear increased body size to some extent, but also to a behavioral specialization among some genera during growth (EGI and WEISHAMPEL 2002).

It has been suggested that some postcranial characters, such as the proportions of limb bones and the morphology of the humerus, show variation within the family. BROWN (1913) and LULL and WRIGHT (1942) assumed that the Lambeosaurinae can be distinguished from the Hadrosaurinae in having relatively short humeri with a greatly projected deltopectoral crest.

After EGI and WEISHAMPEL (2002) show the taxonomic differences which they recognized, together with the intraspecific variation of humeri in *Maiasaura peeblesorum* examined by DILKES (1993, 2001), that the claim that skeletal morphology is highly conservative within the Hadrosauridae should be reexamined.

Their results reveal that adult lambeosaurines differed morphologically from adult hadrosaurines in having the relatively further distally and more anterolaterally expanded

deltopectoral crest, the relatively larger humeral head, and the anterolaterally more expanded lateral tuberosity. Further, humeral length is reduced relatively as body size increases in lambeosaurines. According to the humeral shape, the differences in relative humeral length between lambeosaurines and other taxa become clearer among larger forms. In adult lambeosaurines, and some adult hadrosaurines, the humeral shaft becomes wider relative to humeral length than in juveniles. Also, the humeral head is relatively larger in most of the adult forms than in the juveniles.

The relatively thicker humerus and larger humeral head in those adult lambeosaurine and hadrosaurine individuals can be considered as a structural adaptation to bear increased body mass, but the results cannot address the question whether quadrupedal gaits were used more frequently in adult lambeosaurines and hadrosaurines than in juveniles. For EGI and WEISHAMPEL (2002) seems the increased width of the humeral shaft in adult lambeosaurines and some adult hadrosaurines to suggest that the forelimb was heavily involved in body support and that quadrupedal stance was at least a part of locomotion in these animals. As the morphological differences in the humerus between the two groups are minimal between juveniles, but become substantial in adults, they may be related to the increased loading on the forelimb due to larger body mass and possibly to changes in locomotion during growth.

The relative length of the humerus changes in a way that the humerus occupies a smaller portion in the entire forelimb length in adult lambeosaurines than in hadrosaurines and in juvenile lambeosaurines. This reduction of humeral length relative to forelimb length in adult lambeosaurines may be a cursorial adaptation analogous to those in recent ungulates. However, more evidences, such as an elongation of antebrachium and hand length segments relative to body size, are needed to prove this hypothesis (EGI and WEISHAMPEL 2002).

ZELENITSKY et al. (2006) scanned humeri and femora from an ontogenetic series (embryonic to adult individuals) of *Hypacrosaurus stebingeri* in a CT scanner to investigate the locomotory behavior in lambeosaurine hadrosaurs. Their plots indicate that both forelimbs and hindlimbs are subject to the same loading regime throughout ontogeny. They interpreted these results as evidence that *Hypacrosaurus* used its forelimbs during locomotion at all growth stages, although the extent to which they use a quadrupedal stance cannot be determined.

These results differ from those obtained for *Maiasaura peeblesorum* (DILKES 1993, 2001), for which the biomechanical properties of the forelimbs scaled differently from those of the hindlimbs, indicating a transition from bipedal to quadrupedal stance during ontogeny. If the conclusions reached for *Hypacrosaurus* and *Maiasaura* can be extrapolated to their respective subfamilies (Lambeosaurinae respectively Hadrosaurinae), such a difference in locomotory behavior between the two groups could help explain the larger hatchling size, the larger egg size, and the more robust humeri of lambeosaurine hadrosaurs (ZELENITSKY et al. 2006).

HARTMAN (2004) described how the forelimbs of *Brachylophosaurus canadensis* (Hadrosaurinae) are designed in a way to reduce the range of movement of the distal elements to within a parasagittal plane. This is comparable to the forelimbs of ungulates which have a similar reduction in degrees of freedom of joint rotation. Combined with the elongate distal forelimb elements (lower arm and hand) and tightly bound metacarpals, this would indicate that *Brachylophosaurus* spent much of its time in a quadrupedal stance, perhaps even engaging in rapid quadrupedal locomotion.

Moreno et al. (2004, 2007) examined morphological changes in pedal phalanges through ornithopod evolution. During this evolution a change of posture occurred from bipedalism to facultative quadrupedalism with a consequent forward shift of the center of mass. Pedal morphology was modified accordingly, as the basal digitigrade posture became more subunguligrade. During this transition the ornithopod pes was drastically altered from the plesiomorphic dinosaurian morphology with four digits, claw-shaped unguals, strongly concavo-convex joints, phalanges longer than wide, excavated collateral ligament fossae, presence of sagittal ridge, and prominent processes for the attachment of tendons to a more derived condition with tridactyly, modification of the unguals into hooves, phalanges wider and thinner than long, lack of collateral ligament fossae, loss of sagittal ridge and tendon attachment processes, and relatively flattened articular surfaces. These changes are particularly noteworthy regarding the overall conservatism in pedal morphology in the Dinosauria.

The analyses of the external morphology, two-dimensional models (using finite element analysis), and internal bone structure show that this evolutionary shift was accompanied by a loss of digit mobility and flexibility. Further, pedal posture was modified

to better align the pes with the main direction of the ground reaction force, thus becoming well suited to carry high loads.

After Moreno et al. (2007) possess hadrosaurids a derived pedal morphology, including flattened phalanges, absence of collateral ligament fossae, and loss of processes for the attachment of flexor and extensor tendons. This morphology indicates that hadrosaurids had a more upright pedal posture than basal ornithopods, which was closely aligned to the main direction of the ground reaction force during standing. In addition, the lack of a stress concentrator (phalanx neck) and the reduction of joint curvature allowed the hadrosaurid pes to support high loads more effectively than the primitive ornithopod pes.

SELLERS et al. (2009) documented the use of an 8000 core computer to produce mechanically and physiologically plausible gaits and trackway patterns for a hadrosaur (*Edmontosaurus annectens*), evaluating a large range of locomotor possibilities in terms of running speed. Their anatomical reconstruction is capable of running and hopping bipedal gaits, trot, pace and single foot symmetrical quadrupedal gaits, and asymmetrical galloping gaits. The results show that hopping is the fastest gait, followed by quadrupedal galloping, and bipedal running. However, they added that the hopping gait is unlikely for this animal, implying that either the anatomical and physiological reconstruction is incorrect or that there are important constraints that are currently not included in the simulation.

Trackway geometries derived from the modeled gaits are very basic yet, due to the simplicity of the ground/foot contact model used, but they show the future potential of this technology for interpreting and predicting trackway geometry.

After SELLERS et al. (2009) demonstrate the simulations a wide range of possible locomotor modes. While bipedality seems to be the most likely option, a high-speed quadrupedal hadrosaur should not be ruled out as a serious locomotor possibility for this group of dinosaurs.

Like their close relatives the iguanodonts hadrosaurs possess stiff, ossified tendons. These are arranged in a trellis-like pattern, respectively rhomboidal lattice, along the lateral sides of the neural spines, down the dorsum of their back, sacrum, and tail (Figure 4). Some rostral tendons lie on the dorsal rib shafts. In the bipedal stance body and tail are cantilevered over the sacrum and hindlimbs. This construction creates large tensile forces across the top of the vertebral column that must be resisted to avoid bending across the

sacrum. The arrangement of the tendons in a trellis-like pattern seems to be an efficient system to counter these tensile forces. Although tendons are strong, ossification increases their tensile strength, allowing them to hold the vertebral column horizontal with greater ease. Further, the tendons apparently reduced ventral displacement of the tail and restricted its dorsoventral mobility, while probably allowing some degree of lateral motion (FORSTER 1997; HORNER et al. 2004).

Figure 4: Ossified tendons along the neural spines of *Brachylophosaurus canadensis* (MOR 794) from lateral view (photo by the author).

Evaluating the function of ossified tendons, ORGAN (2006) constructed finite element models of the vertebral column for two ornithopod taxa. These genera are *Tenontosaurus*, which shows the plesiomorphic condition of longitudinally arrayed tendons along the spinous processes, and *Brachylophosaurus*, which exhibits a lattice of tendons along the spinous processes. Both models predict that ossified tendons stiffened the vertebral column, especially the tail. However, the derived lattice of ossified tendons in *Brachylophosaurus* shows that in hadrosaurs, iguanodonts, and relatives, spinal stiffness is more increased than in the plesiomorphic condition.

Caudofemoral muscles which retracted the hindlimb during locomotion in ornithopods arise from the fourth trochanter of the femur and attach it to the tail. Increased

tail stiffness caused by intratendinous ossification may have influenced locomotion by rigidly anchoring M. caudofemoralis longus to the tail. This would allow a more forceful retraction of the hindlimb by reducing ventral flexion of the tail during muscle contraction. In addition, the ossified tendons may have been important for storing elastic energy throughout the gait cycle. Moreover, the lattice of ossified tendons stiffened the trunk and tail nearly equally in *Brachylophosaurus*, which indicates the evolution of a postural function by passively supporting the epaxial musculature in maintaining a horizontal vertebral column (ORGAN 2006).

After Forster (1997) it can be summarized that hadrosaurs have to be seen as terrestrial animals, and that they were able to switch between bipedal and quadrupedal gaits according to circumstances. When all evidence is taken together, hadrosaurs appear to have been primarily bipedal, particularly at higher speeds, but probably often walked on all four legs while walking and browsing on low vegetation.

In contrast, MAIDMENT et al. (2012) and MAIDMENT and BARRETT (2012) regard hadrosaurs as predominantly quadrupedal, e.g. due to the pronation ability and weight-bearing adaptations of the manus. In their examinations they studied stance and gait in quadrupedal ornithischian dinosaurs and the evolution of ornithischian quadrupedalism. Concerning the function of the hindlimb, hadrosaurs show few of the quadrupedal adaptations present in ceratopsids and thyreophorans and appear to have retained many of the bipedality features of their bipedal ancestors, despite their assumed quadrupedal stance, such as placing the feet on the midline during locomotion as indicated by trackways. The elongate and slender epipodials of hadrosaurs might indicate that they display more cursorial adaptations in the forelimb than other quadrupedal ornithischians, correlating with a possibly higher locomotor performance. This could relate to an ability to run faster, but could also relate to more energetically efficient low speed locomotion. Alternatively, the slender epipodials could indicate that the hadrosaurian forelimbs were less heavily modified for weight-bearing than in other quadrupedal groups. However, after MAIDMENT et al. (2012), this does not negate their ability to walk quadrupedally.

2.2 Hadrosaurian and iguanodontian tracks and trackways

Simulations of locomotion in dinosaurs require the possibility to compare simulating results with the real circumstances. Here, tracks and trackways provide a good idea how locomotion in these animals may have looked like, making them to an important control factor in this kind of scientific work. The question whether the tracks that are made by the model are in accordance with fossil trackways or not helps to confirm or reject the different body postures or gaits in the simulations.

Since hadrosaurs derived from higher evolved iguanodonts, both groups have a very similar shape of hands and feet. Therefore, main criteria to distinguish their tracks are the stratigraphic age of the trackways and geographic differences in their distribution areas. As the tracks of both groups are so similar, trackways of iguanodonts are also used in this work for developing and controlling gait simulations.

In this chapter a short summary is given about today´s knowledge of hadrosaurian and iguanodontian tracks and trackways.

For general definitions concerning dinosaur tracks see Figures 5 & 6.

Ornithopods, especially the large iguanodontids and hadrosaurs of the Cretaceous, were responsible for leaving a variety of trackways, showing bipedal and quadrupedal locomotion of the track-makers (LOCKLEY 1991). Trackways of large ornithopods, which were attributed to iguanodontids and hadrosaurs, have been found at least from a dozen localities in the Lower and Upper Cretaceous of Europe, North and South America, and eastern Asia (LOCKLEY and WRIGHT 2001). Jurassic trackways attributed to ornithopods represent small, gracile animals that were mainly bipedal. In contrast, ornithopod tracks form the Cretaceous are often large and frequently indicate quadrupedally walking animals with well-padded hindfeet and small forefeet (LOCKLEY and WRIGHT 2001).

There are several types of manus tracks in ornithopod trackways. The manus impression shape can be rounded, subrounded, transversely elongated, (slightly) bilobate, crescentic, or subtriangular (MORATALLA et al. 1992; LOCKLEY and WRIGHT 2001). Remarkably is the fact that two types can be present in the same trackway, suggesting that the shape depends not only on anatomical features but also on substrate and locomotion (MORATALLA

et al. 1992). Manus emplacement occurs along an arc from anterior to lateral of the pes impressions, but they are generally placed anterolaterally (LOCKLEY and WRIGHT 2001).

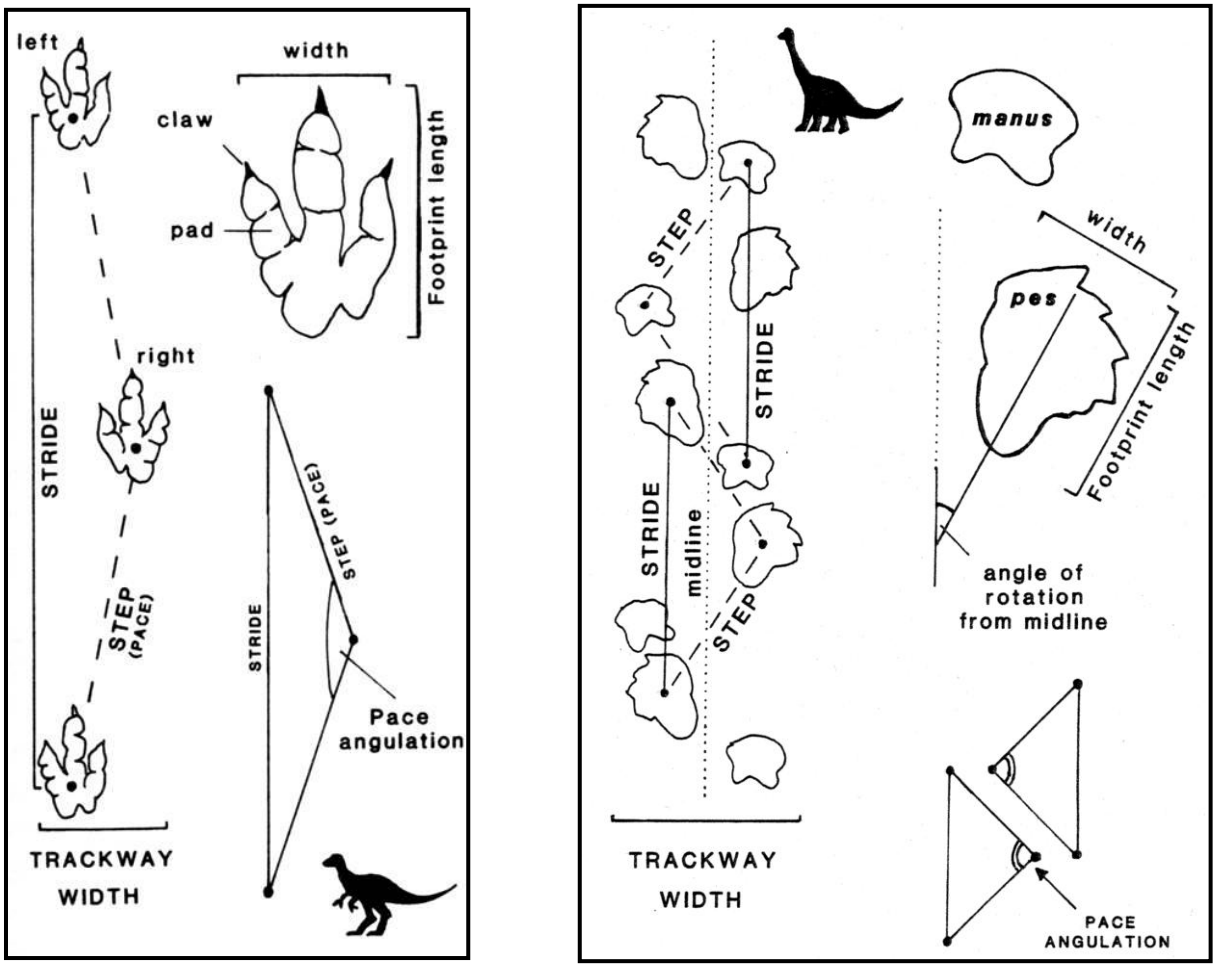

Figure 5 (left): Trackway of a bipedal dinosaur showing step (pace), stride, and other measurable parameters that give clues about locomotion. Also, the main features of an individual track are shown, including claw and pad impressions (LOCKLEY 1991).
Figure 6 (right): Trackway of a quadrupedal dinosaur showing standard features (LOCKLEY 1991).

In iguanodonts the manus was pentadactyl and considerably smaller than the foot. The overall size of the manus varied among species. In *Camptosaurus* it was scarcely one quarter the size of the foot, whereas in *Iguanodon* it was well over half the size. Usually, digits I-III terminated in blunt claws and digits IV and V were completed by rounded nubbins of bone. In contrast, *Iguanodon* had expanded and hoof-like tips on digits II and III. The mesaxonic pes was basically a more robust version of that in smaller ornithopods, but with some minor variations. The foot was either tetradactyl or tridactyl and the three or four functional digits always terminated in broad and somewhat flattened claws with rounded tips (THULBORN 1990). In their bipedal gait iguanodonts produced moderately narrow

trackways with prints of the hindfeet arranged in a definite zig-zag series. The footprints are rotated inwards and there is rarely any trace of a tail-drag. Footprint width is only a little less than footprint length, and in some cases it may be slightly greater. Sometimes, the toes were so thick and fleshy that the resulting footprint has the outline of a clover-leaf. The imprint of digit III is generally the longest and widest, while that of digit IV is only a bit shorter and may be nearly as broad. Digit II is often smaller (THULBORN 1990).

Trackways of the ichnogenus *Caririchnium*, from the Lower Cretaceous of Colorado (USA), were attributed by LOCKLEY (1986) to iguanodonts that travelled quadrupedally. *Caririchnium* shows large tridactyl pes prints, which show slight inwards rotation and form a fairly narrow zig-zag trackway. The small manus prints are located just in front of the pes prints, having an irregular elliptical or bean-shaped outline with no clear indications of separate digits.

XING et al. (2012) examined an unusual, three-dimensionally preserved, large hadrosauriform pes track from the 'mid'-Cretaceous Lotus track site (Jiaguan Formation) of south-central China, which they attribute to the ichnospecies *Caririchnium lotus*. The pes print permits reconstruction of the footfall, weight-bearing, and kick-off phases of the step cycle. Large-scale modifications of the pes during the step cycle indicate that the track-maker was capable of locomotory modifications in response to substrate consistency beyond the expected shift between bipedal and quadrupedal postures. Further, an unusual curvature to the trace of one of the outer digits indicates substantial transverse mobility. The other digits show lesser degrees of transverse movement accompanied by extension of the digits during footfall. The absence of overprinted scale-scratch marks and toe drags are consistent with a vertical kick-off of the pes and simultaneous flexion of the digits. Therefore, this track suggests that pedal mobility in *Caririchnium lotus*, and perhaps in hadrosauriforms in general, was greater than previously suspected.

MEYER and THÜRING (2003) reported on an iguanodontid trackway showing manus impressions from the Schrattenkalk Formation (Late Aptian) from the Swiss central Alps. However, the overall outlines as well as the sizes and shapes of pes and manus of these specimens differ from all other known European Cretaceous iguanodontid footprints. Manus position indicates that one individual placed its hand close to the midline of the trackway, with the dorsal surface of the manus facing forward. The manus shape shows a rounded to slightly oval outline.

A quadrupedal ornithopod trackway from the Early Cretaceous of La Rioja, Spain, is described by MORATALLA et al. (1992). Footprint structure and size suggest that the trackway can be attributed to an iguanodontid dinosaur using a quadrupedal gait. The depth of manus prints is clearly less than that of the pes prints, suggesting that the center of gravity of the body mass of the track-maker was located near the hindlimbs. This point of view is supported by the smaller size of manus prints and also by their position well outside the pes prints, indicating that the manus only made light contact with the ground. There is a regular distance, meaning a relatively constant stride length, between manus impressions, assuming a 'harmonic' quadrupedal progression in which the limb movements are well coordinated. Again a rotation of pes tracks with respect to the manus tracks can be observed. While the pes prints show inward rotation, manus prints show outward rotation. The reason for this inward rotation of pes prints is not clear. Probably it is due to a slight pelvic rotation and the swinging of the tail as a counterbalance during walking. The authors conclude that data from quadrupedal ornithopod trackways indicate that these animals used a similar type of locomotion during both bipedal and quadrupedal gaits, showing an inward rotation of the pes prints. The use of an optional quadrupedal gait seems therefore not to modify significantly the slight rotation of the pelvic girdle or the counterbalancing role of the tail during progression (MORATALLA et al. 1992).

After WRIGHT (1999) are the most modern reconstructions of quadrupedally walking iguanodontid dinosaurs made in a way that the animals placed their forelimbs slightly closer to the midline than the hindlimbs, with the dorsal surface of the manus facing forwards. In her opinion this posture is problematical because it would have required rotation of the radius around the ulna, which would lead to distortion and dislocation of the joints at the wrist or elbow. In contrast to that, WRIGHT (1999) described quadruped ornithopod trackways from the Purbeck Limestone Group (Upper Jurassic-Lower Cretaceous, UK). The trackways are attributed to an iguanodontid dinosaur showing manus impressions, which are oriented with the palmar surfaces facing inwards towards the trackway midline and digit I therefore faced anteriorly rather than medially. In addition, the manus tracks lie in two lines on either side of the single line formed by the pes tracks, which indicates that the animal in its quadrupedal gait placed the forefeet in a wider trackway than the hindfeet. WRIGHT (1999) concluded that this orientation of the manus obviates the need for unnatural twisting of the bones of the lower forelimbs. Also, she argues that these trackways show

foot emplacement patterns which are characteristic of a facultative quadruped animal, as the forelimbs of this track-maker were not placed beneath the body midline and therefore were not necessary for weight-bearing and balance in locomotion. The width of the angulation pattern of the manus tracks, which is about the width of the shoulder girdle of *Iguanodon atherfieldensis*, leads her to the conclusion that the arms would have been held in a vertical position when the forelimbs were in contact with the ground.

After THULBORN (1990) hadrosaurs possess a tetradactyl manus with a greater hoof at the tip of digit III, and a smaller one on digit II, whereas digit IV ended in a bluntly rounded nubbin. In his view the body mass of the animal was carried on digits II and III, and to a lesser extent on digit IV. The slender and divergent digit V had only a minor supportive role. The orientation of the hoof-like extremities indicates that the fingers were steeply inclined so that a quadrupedal hadrosaur, as also *Iguanodon*, would have walked on its fingertips. The foot resembled that of iguanodontids in practically every respect. It was tridactyl and mesaxonic, with three stout and broad-spreading toes, which ended in blunt hoof-like claws. The hadrosaurian foot is often thought to have differed from the iguanodontian foot in having extensive interdigital webs. Hadrosaur hands and feet are so similar to those of certain iguanodonts that it is difficult to identify their tracks with certainty. Usually, tracks have been attributed to hadrosaurs, and not to iguanodonts, for four reasons: first, because they are of adequate age (Late Cretaceous or slightly earlier); secondly, because they are found in geographic regions known to have been frequented by hadrosaurs; thirdly, because they are sometimes found together with hadrosaur body fossils (e.g. LANGSTON 1960); and finally, because they might in some instances show traces of interdigital webbing. In their bipedal gait hadrosaurs produced fairly narrow trackways with foot prints arranged in a slightly zig-zag pattern. The prints are turned inwards to the midline of the trackway, and there is rarely any trace of a tail-drag. Each tridactyl and mesaxonic footprint is about as wide as long and the three toe prints are short, broad, and strongly rounded in outline. Digits II and IV are slightly shorter than digit III and are almost similar in size, shape, and angle of divergence (THULBORN 1990).

CURRIE (1983) reported numerous tracks of quadrupedal hadrosaurs, attributed to the ichnogenus *Amblydactylus*, in the Lower Cretaceous of British Columbia, Canada. The handprints are described as roughly crescent shaped and lacking any details indicating a

separation into separate digits. The trackway evidence also strongly suggests that these dinosaurs were gregarious.

In CURRIE et al. (1991) Cretaceous dinosaur footprints are described, which were discovered in the J Sandstone of the South Platte Formation (Dakota Group) in Colorado and the St. Mary River Formation of southwestern Alberta. They exhibit foot pad skin impressions of large ornithopods. Whereas the trackway of the South Platte Formation is belonging to *Caririchnium*, an iguanodontid ichnogenus, the tracks of the St. Mary River Formation are attributed to hadrosaurs. Their handprints are semilunate in shape and are located anterolateral to digits III and IV of the footprints. These indicate that at least some mature hadrosaurs were facultative bipeds and walked digitigrade. Digits II, III, and IV of the manus were encased in a mitten of skin and had little independence of movement. Only digit II was capable of some independent motion, but it was still joined to the rest of the manus by a web of skin (CURRIE et al. 1991).

After THULBORN (1989) were semibipedal ornithopod dinosaurs, such as iguanodonts and hadrosaurs, able to switch between bipedal and quadrupedal gaits according to circumstances. The shift from quadrupedal to bipedal gait comprises a number of correlated changes in the tracks left by the feet: an increase in stride length and pace angulation, and a simultaneous decrease in trackway width. The increase in stride length may indicate that these animals rather used the bipedal gait for more rapid locomotion. In the quadrupedal gait the feet took strides of moderate length, which produced a broad trackway with reduced pace angulation and consistent step length. This consistency implies that the hindlimbs supported much of the track-maker´s body mass. In contrast, the manus prints have an erratic distribution and their somewhat unpredictable placement implies that the forelimbs had no major supportive role (THULBORN 1989). An amazing feature is that the forefeet left a wider trackway than the hindfeet and that step length for the forefeet often exceeds step length for the hindfeet. As the forelimbs were shorter than the hindlimbs, this remarkably wide spacing of the forelimbs indicates that the shoulder region was depressed below the level of the hips. Therefore, THULBORN (1989) concluded that it is probable that head, neck, and shoulders were carried close to the ground and that the elbows were stuck out sideways to some extent. This would produce a low-slung and somewhat sprawling gait, which was most likely used in slow progression.

3. Material

The creation of the hadrosaur model used in the simulations based on digitized bones of three specimens of the hadrosaurine hadrosaur *Brachylophosaurus canadensis* (Figure 7) from the Judith River Formation in Montana (USA), which is Campanian in age (late Upper Cretaceous). The fossils are part of the collections of the Phillips County Museum and the Great Plains Dinosaur Museum and Field Station (former Dinosaur Field Station) in Malta, Montana. All three skeletons are not mounted, but lying in their original finding positions, each exposed from one side (Figures 8 – 11).

Taxonomy:

Ornithopoda MARSH 1881
Iguanodontia DOLLO 1888
Dryomorpha SERENO 1986
Ankylopollexia SERENO 1986
Styracosterna SERENO 1986
Hadrosauriformes SERENO 1997
Hadrosauroidea SERENO 1986
Hadrosauridae COPE 1869
Hadrosaurinae LAMBE 1918
Brachylophosaurus STERNBERG 1953
Brachylophosaurus canadensis STERNBERG 1953
(After HORNER et al. 2004 / MCDONALD et al. 2010 / MCDONALD 2012)

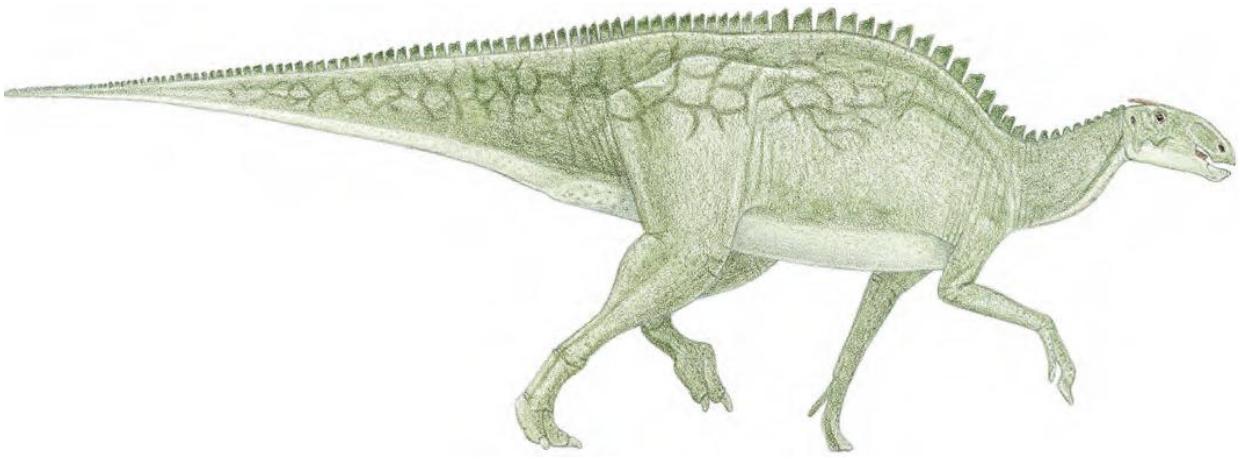

Figure 7: Flesh reconstruction of *Brachylophosaurus canadensis* (PAUL 2010).

Figure 8: *Brachylophosaurus canadensis* skeleton MOR 794 (called “Elvis”) from caudal view: a nearly complete, adult, articulated skeleton (maybe a male), lacking only the distal part of the tail (photo by H.Mallison).

Figure 9: The anterior part of the MOR 794 skeleton from lateral view (photo by the author).

Figure 10: *Brachylophosaurus canadensis* skeleton JRF 200W (called “Roberta”) from craniolateral view: an incomplete, adult, mainly articulated skeleton (maybe a female) (photo by H.Mallison).

Figure 11: *Brachylophosaurus canadensis* skeleton JRF 116H (called “Peanut”) from lateral view: an incomplete, juvenile, mainly disarticulated skeleton (maybe a male) (photo by the author).

Referred specimens of *Brachylophosaurus canadensis* with the bones digitized respectively:

- **MOR 794** (called “Elvis” / Figures 8 & 9 & 12): a nearly complete, adult, articulated skeleton (maybe a male), lacking only the distal part of the tail
    - pelvic girdle sinistral (only digitized from the left side as articulated)
    - femur cast dextral (with incomplete femoral head)

Figure 12: Skeletal reconstruction of *Brachylophosaurus* specimen MOR 794 (Scott Hartman / [www.skeletaldrawing.com]).

- **JRF 200W** (called “Roberta” / Figure 10): an incomplete, adult, mainly articulated skeleton (maybe a female)

  Forelimb:
    - incomplete scapula sinistral (only digitized from the left side as articulated)
    - coracoid sinistral
    - sternal dextral
    - humerus dextral
    - ulna dextral
    - radius dextral
    - carpal dextral
    - metacarpal II sinistral with phalanx I sinistral / phalanx II sinistral / phalanx III dextral
    - metacarpal III dextral with phalanx I dextral
    - metacarpal IV dextral with phalanx I sinistral
    - metacarpal V sinistral with phalanx I sinistral / phalanx II sinistral

Hindlimb:

- fibula dextral
- metatarsal II sinistral with phalanx I sinistral / phalanx II dextral / phalanx III dextral
- metatarsal III sinistral with phalanx I sinistral / phalanx II dextral / phalanx III dextral / phalanx IV dextral
- metatarsal IV sinistral with phalanx I dextral / phalanx II dextral / phalanx III dextral / phalanx IV dextral / phalanx V dextral

- **JRF 116H** (called "Peanut" / Figure 11): an incomplete, juvenile, mainly disarticulated skeleton (maybe a male)
  - phalanx II and phalanx III of mcIII dextral
  - phalanx II and phalanx III of mcIV dextral
  - phalanx III of mcV dextral

Further, a single tibia (sinistral) was digitized, belonging also to a *Brachylophosaurus* (pers. comm. Mr. Nate Murphy (former staff of the Dinosaur Field Station)).

As it was not possible to digitize an astragalus and calcaneus of *Brachylophosaurus*, both bones were taken from bone material of *Dryosaurus lettowvorbecki* (Tendaguru Beds, Upper Jurassic of Tanzania, East Africa) from the collection of the Institute for Geosciences of the University of Tübingen, Germany. The astragalus sinistral (GPIT/RE/6421) and the calcaneus dextral (GPIT/RE/5248) were digitized and transformed (see chapter 4.2). *Dryosaurus lettowvorbecki* was originally named by VIRCHOW (1919) as *Dysalotosaurus lettowvorbecki*. GALTON (1977, 1981) renamed the species as *Dryosaurus lettowvorbecki*, based on the supposed great similarity with *Dryosaurus altus* from North America. However, recent studies reject this synonymy, regarding the original genus *Dysalotosaurus* as valid (BARRETT et al. 2011; HÜBNER and RAUHUT 2010; HÜBNER 2012).

The skeletal elements of *Brachylophosaurus canadensis*, which were digitized in the same scale, consist of the bones of the pectoral girdle and pelvis as well as the fore- and hindlimb. In the following the digitized bones are briefly described and their images are shown. For a more detailed description of the postcranial osteology of *Brachylophosaurus canadensis* see PRIETO-MARQUEZ (2007).

3.1 Pectoral girdle

The scapula (Figure 13) is a bladelike bone that projects caudally from its articulation with the coracoid and the humerus in the pectoral girdle. The proximal end is mediolaterally thicker, with articular facets for the coracoid and the humerus. The scapula is slightly arched to follow the contour of the rib cage. It is convex laterally while the medial surface is rather flat (PRIETO-MARQUEZ 2007).

Figure 13: Left scapula of *Brachylophosaurus* specimen MOR 794 from lateral view (photo by H.Mallison).

The coracoid (Figure 14) is formed by a quadrangular central body, which contains two articular facets and two anteriorly located processes. The articular facets include the articulation with the scapula and the anterior contribution to the glenoid. The first process consists of a short anteromedial projection of bone, which is rounded on its end. The second process is longer, projecting posteroventrally and shows a rounded tip that ends near the sternal. The coracoid foramen is located proximally, near the articular surfaces, and the glenoid faces caudolaterally (PRIETO-MARQUEZ 2007).

The coracoid is thicker proximally than distally and exposes the scapular and humeral articular surfaces. The scapular facet differs clearly from the glenoid and is located dorsomedially on the proximal end of the bone, while the glenoid facet is situated caudolateroventrally (PRIETO-MARQUEZ 2007).

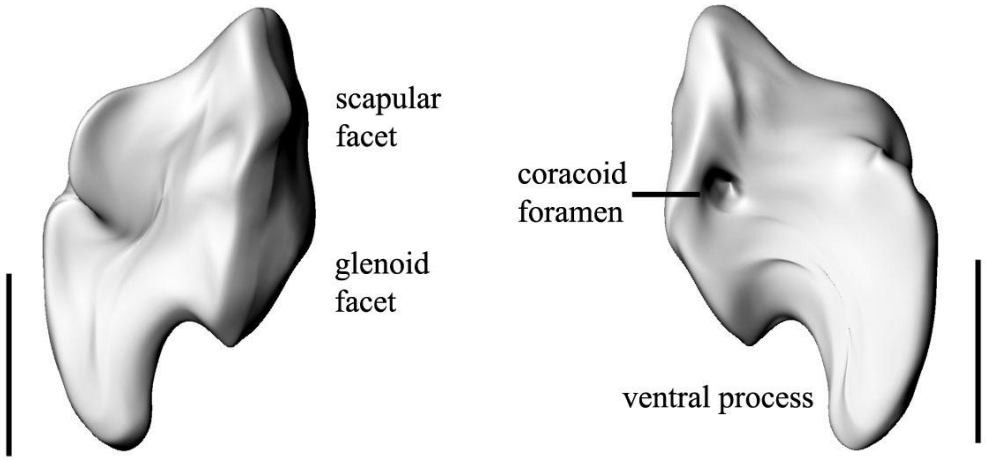

Figure 14: Digitized left coracoid from cranial (left) and caudal view (right); scale bars = 8 cm.

The sternals (Figure 15) are paired elements that were joined together by cartilage at their proximomedial ends. They are flattened and elongated bones with a paddle like expanded anterior part, located at the end of the shaft. The shaft is mediolaterally compressed, ellipsoidal in cross section, and somewhat extended at its caudal most end. The medial side of the sternals is slightly concave, especially on the fanlike blade. There is no evidence of attachment of the sternals to the ribs, by either ligaments or cartilage, whereas the connection to the coracoids, if any, was ligamentous (LULL & WRIGHT 1942; HORNER et al. 2004; PRIETO-MARQUEZ 2007).

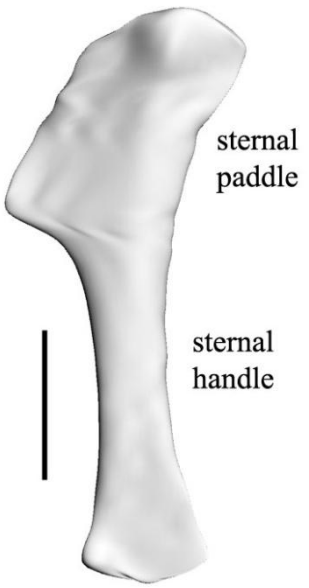

Figure 15: Digitized left sternal from ventral view; scale bar = 10 cm.

3.2 Forelimb

The humerus (Figure 16) head is massive, rounded, and triangular in cross section. On the caudomedial side, at midlength of the proximal half of the bone, a rugose depression is located where the M. latissimus dorsi attached (DILKES 2000). The deltopectoral crest projects anterolaterally and extends along the proximal half of the bone, which is concave on the medial side. From proximal to distal the deltopectoral crest narrows gradually (PRIETO-MARQUEZ 2007).

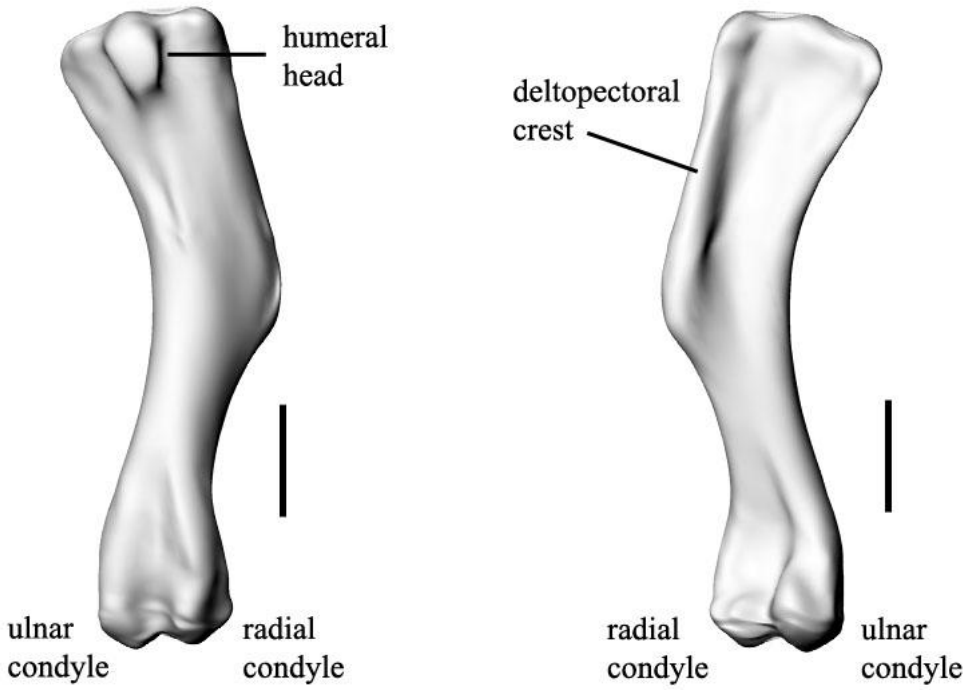

Figure 16: Digitized right humerus from caudal (left) and cranial view (right); scale bars = 10 cm.

The width of the humerus perpendicular to its long axis increases gradually distally. It is greatest at the level of the distal end of the deltopectoral crest, which projects little more than half the diameter of the humerus. Caudal to the deltopectoral crest the shaft is almost cylindrical (PRIETO-MARQUEZ 2007).

The lateral radial and medial ulnar condyles form the distal end of the humerus, in which the ulnar condyle is larger than the radial one. A deep notch separates the condyles from each other for reception of the olecranon process of the ulna (PRIETO-MARQUEZ 2007).

The ulna (Figure 17) is the longest bone in the forelimb. It is little expanded distally, but mostly proximally, with two anterodorsally directed flanges. These flanges enclose a wide radial notch for reception of the corresponding part of the radius. The medial flange is the larger one and is directed dorsomedially, whereas the lateral one extends dorsolaterally. The proximal part of the ulna and most of the shaft length show a triangular cross section. The ulna thins progressively distally, but it is slightly expanded at the distal end. The olecranon process is located caudoventrally at the proximal end of the ulna. It is subconical, prominent, and projects caudally (PRIETO-MARQUEZ 2007).

The radius (Figure 17) is a straight, slender bone with only a slightly expanded proximal and distal end and is nearly as long as the ulna. The proximal end of the bone is squarish in cross section, the lateral and medial side fit into the angular excavation of the ulna. The distal end is externally rounded and thickened in the area of contact with the ulna (LULL & WRIGHT 1942; HORNER et al. 2004; PRIETO-MARQUEZ 2007).

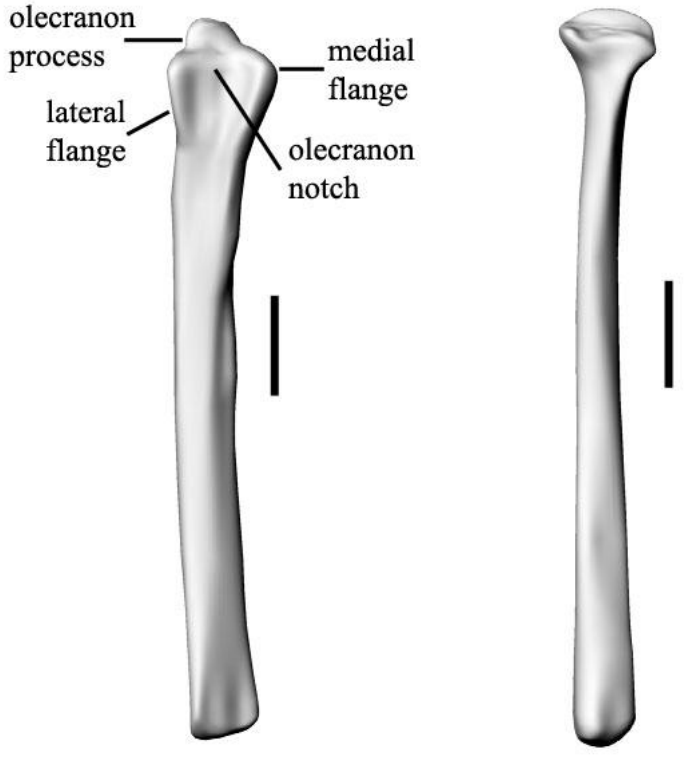

Figure 17: Digitized right ulna from cranial view (left) and right radius from caudal view (right); scale bars = 10 cm.

In *Brachylophosaurus* two carpals can be observed. The first carpal (the distal one after HARTMAN 2004) is a very small bone, which shows a pebblelike and spherical shape (not to be seen in Figure 18 as missing). The second carpal (the proximal one after HARTMAN 2004 / see Figure 18) is the larger one and is tetrahedral in shape. It is wedged between the distal ends of the radius and ulna (PRIETO-MARQUEZ 2007).

The manus (Figure 18) consists of four digits, corresponding to II-V. Metacarpals II, III, and IV are elongated and form a tight and compact unit. Metacarpal III is the longest and most robust bone, metacarpal IV is slightly shorter, but nearly as solid as metacarpal III. Metacarpal II is the shortest and most slender of the three bones. All metacarpals are expanded at their proximal and distal ends. Metacarpal V is a short and robust element that is laterally offset (PRIETO-MARQUEZ 2007).

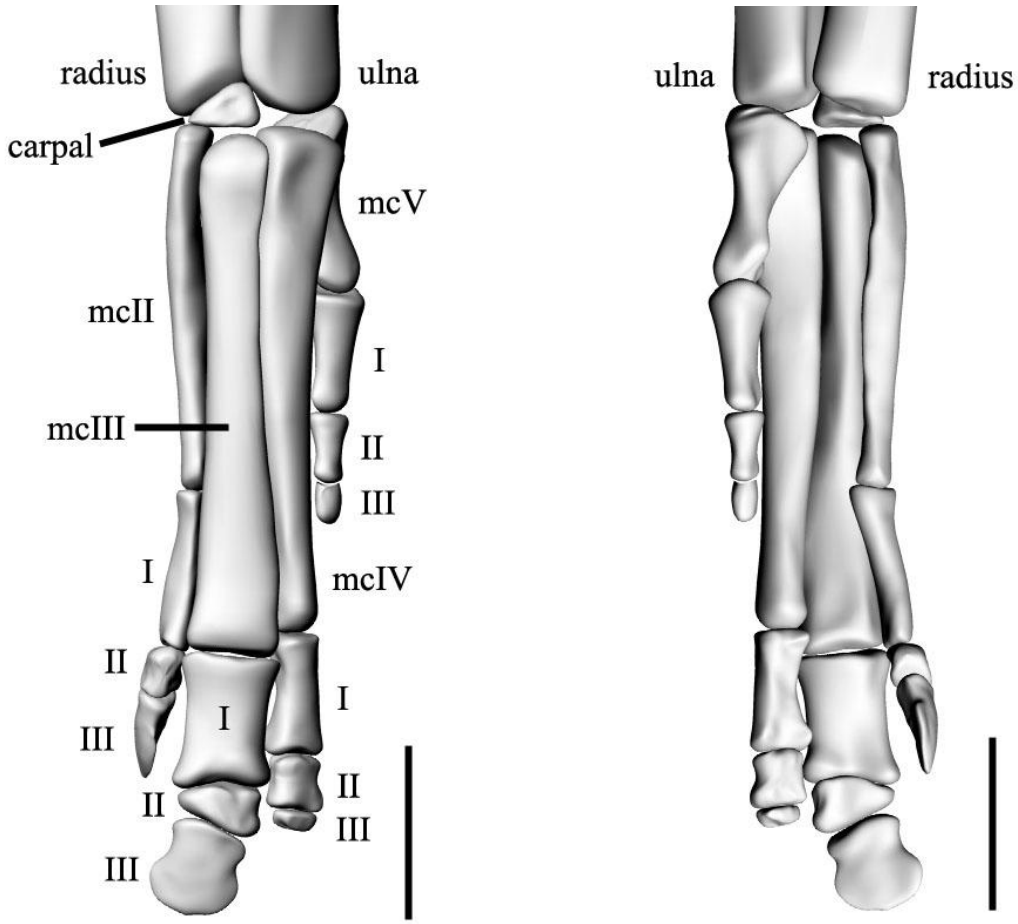

Figure 18: Digitized left manus from cranial (left) and caudal view (right) (the supposed fourth phalange on digit IV is missing); scale bars = 10 cm.

The phalangeal formula is 3-3-3-4. In contrast to digits II-IV, digit V is relatively small and short and follows the lateral offset of metacarpal V. The phalanges of digit V get progressively smaller and resemble truncated cones. Both digits II and III start proximally with a subrectangular, slightly hourglass-shaped first phalange (II-1 and III-1). These are followed by characteristic, wedge-shaped phalanges (II-2 and III-2). Both digits end distally in hoof-shaped unguals (II-3 and III-3). Phalange IV-1 of digit IV is a mediolaterally twisted subrectangular bone, followed by a stocky, relatively small subrectangular phalange IV-2, different to the wedge-shaped phalanges II-2 and III-2 (PRIETO-MARQUEZ 2007). Phalanges IV-3 and IV-4 are small bones, also of roughly rectangular shape.

After PRIETO-MARQUEZ (2007), the phalangeal formula of *Brachylophosaurus* is not 0-3-3-3-3, as has been postulated for the Hadrosauridae, but 0-3-3-3-4. A fourth phalange on digit IV might be also found in other hadrosaurids, since this bone could be easily removed by taphonomic processes and/or overlooked during or after the collection of bones. Otherwise it could be an autapomorphy of *Brachylophosaurus canadensis*.

3.3 Pelvic girdle

The ilium (Figure 19) is an elongated and mediolaterally compressed bone. The long preacetabular process is ventrally deflected and projects anteroventrally. Near its anterior end the process shows a slight thickening, whereas on its medial side a large ridge continues caudally into the anterior part of the central body of the ilium. This ridge is indented for attachment of the sacral vertebrae. The dorsal margin of the central part of the ilium shows a convex lateral profile cranial to the supraacetabular process and a concave outline along its caudal portion (PRIETO-MARQUEZ 2007).

The supraacetabular process is relatively large and projects lateroventrally from the dorsal edge of the central body. The pubic peduncle is cranioventrally directed and sharp and forms the anteroventral corner of the central part of the ilium. Compared to the robust ischial peduncle it is more slender. Its anterior surface builds up the cranial half of the arch of the acetabulum. In caudoventrally direction that arch connects with the caudal end of the ischial peduncle and the ventral border of the postacetabular process, into which the central part of the ilium extends caudally (PRIETO-MARQUEZ 2007).

The pubis (Figure 19) is composed of an anterior expanded prepubic blade and caudally by three bone projections: the iliac and ischial peduncles and an elongated postpubic process.

The iliac peduncle is larger than the ischial peduncle, is laterally offset and projects caudodorsally. The ischial peduncle is more slender, mediolaterally compressed, and projects caudally. The prepubic blade forms cranially a subellipsoidal sheet of bone and narrows caudally. The postpubic process is a long, rodlike, and thin process that projects caudoventrally. It is medially offset from the central part of the pubis, ventral to the ischial peduncle. The process thins gradually in caudoventral direction until it tapers into a rounded end (PRIETO-MARQUEZ 2007).

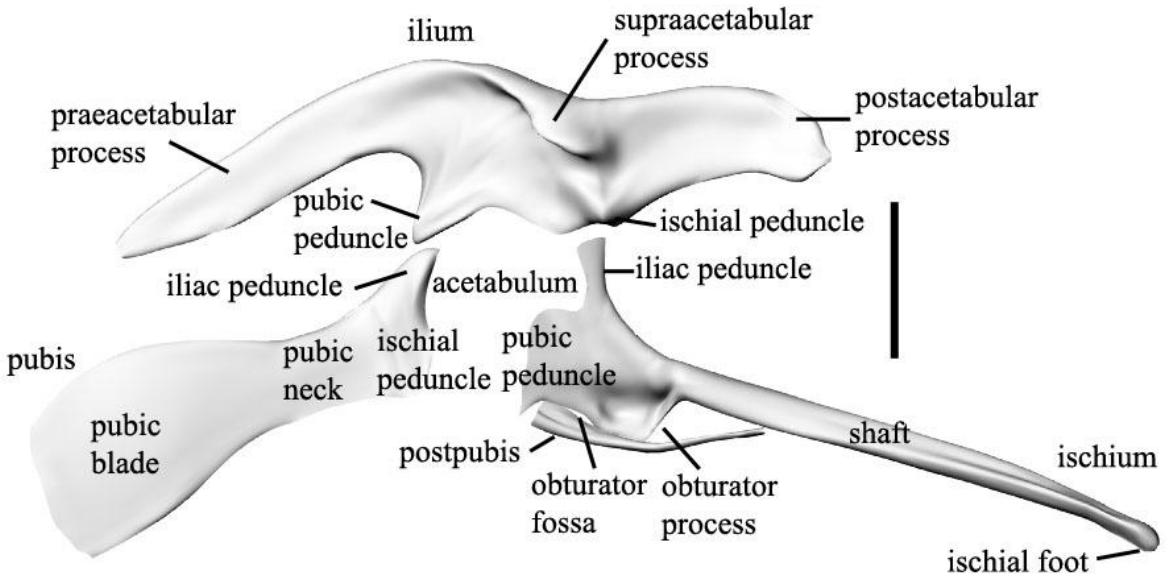

Figure 19: Digitized left pelvic girdle from lateral view; scale bar = 25 cm.

The ischium (Figure 19) is made of a long subcylindrical shaft that expands cranially into an irregular blade that contains the iliac and pubic processes. When the two ischia are joined, the dorsal margins of the anterior blades diverge laterally from each other, whereas caudally the shafts contact each other. The posteriorly located obturator process is displaced medially from the parasagittal plane of the ischium. The expanded anterior region of the bone arches dorsally to form the iliac process and ventrally to form the pubic process (PRIETO-MARQUEZ 2007).

The iliac process shows a subrectangular shape and projects anterodorsally. The pubic peduncle, which projects anteriorly, is slender and more compressed mediolaterally. Cranioventral to the shaft is a large foramen, build up by the obturator process caudally and a caudoventrally projecting process on the ventral border of the ischial blade (PRIETO-MARQUEZ 2007).

3.4 Hindlimb

The femur (Figure 20) is a massive element, which is straight in lateral view and slightly convex outwardly in cranial view. The upper part of the shaft, which expands into the femoral head, shows a more convex and cylindrical form, separated by a shallow longitudinal groove that connects proximally with the lesser trochanter (HORNER et al. 2004; PRIETO-MARQUEZ 2007).

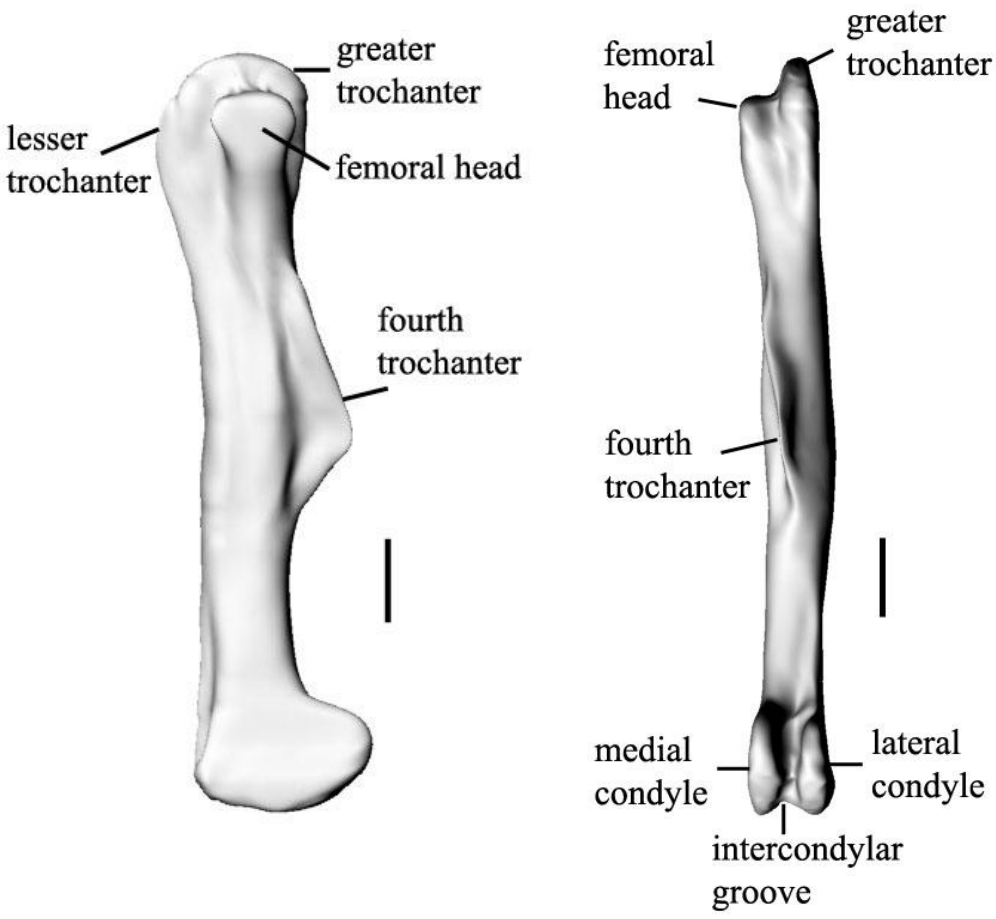

Figure 20: Digitized and reworked (see chapter 4.2) right femur from medial (left) and caudal view (right) (femoral head is incomplete); scale bars = 15 cm.

The femoral head is of subcylindrical shape and projects medially from the proximal end of the shaft. It is rather isolated by a lateral constriction, which separates the head from the medial surface of the greater trochanter. The latter forms the lateral side of the proximal end of the femur. Anteriorly and proximally to the greater trochanter there is a deep cleft that separates it from the lesser trochanter. The wedge-shaped lesser trochanter is elongated, thickens distally, and curves toward the proximal end of the greater trochanter (PRIETO-MARQUEZ 2007).

The fourth trochanter is located on the posterior surface of the femur and comprises nearly one-third of the total length of the bone. The fourth trochanter shows a triangular profile with a gentle outline proximally, followed distally by a deeper and more D-shaped curvature (PRIETO-MARQUEZ 2007).

The distal end of the femur expands into two condyles, which describe an H-shaped outline in distal view. Both condyles are mediolaterally compressed and expand caudally, but the medial condyle is the larger one (PRIETO-MARQUEZ 2007).

The tibia (Figure 21) is a robust bone, consisting of a straight and cylindrical central shaft that expands proximally and distally. The proximal end is more expanded than the distal one and is twice the diameter of the central shaft. Proximally, the tibia shows two condyles, which are oriented caudally. They are relatively small compared to the prominent cnemial crest that is located anterior to the two condyles and forms the anterolateral side of the proximal end of the tibia. This is slightly arched laterally and embraces partially the proximal portion of the fibula. In its medial two-thirds the distal end of the tibia articulates with the astragalus. Anterolaterally, it is excavated for the reception of the ascending process of the astragalus. Laterally, it articulates with the calcaneum (PRIETO-MARQUEZ 2007).

The fibula (Figure 21) is a long and slender bone, situated along the lateral side of the tibia. Mediolaterally, it is compressed, particularly on its proximal part. The fibula is expanded proximally and distally and articulates with the tibia medially and the calcaneum distally. It is elongated and oriented parallel to the parasagittal plane until it twists medially along its distal third. The proximal end is expanded anterocaudally and slightly arched, the distal end is much less expanded and shows a flat surface on the caudal side (PRIETO-MARQUEZ 2007).

The astragalus (no figure as missing) is subtriangular in anterior view and articulates laterally with the calcaneum to form the proximal tarsus. Proximally it articulates with a

recessed border on the tibia. With its long axis the astragalus is oriented anterolaterally, parallel to the distal end of the tibia. It is rather shallow, convex on its distal side, and concave on the proximal side. The ascending process forms the lateral border and the apex of the element and projects proximally, covering the distal end of the tibia along its medial section. The medial face of the astragalus is flattened and directed parallel to the medial side of the distal tibia. The distal side shows a broad saddle-shaped surface and in distal view the bone is subrectangular and narrows toward the medial side (PRIETO-MARQUEZ 2007).

The calcaneum (no figure as missing) is a crescent-shaped and compact bone, which covers one-third of the total mediolateral width of the tibia and fibula. Located in the ankle, it articulates with the astragalus medially, the fibula proximally, and the tibia caudally. Thus the proximal surface of the calcaneum borders on the distal end of the fibula. It is a strongly concave facet and D shaped in proximal view. The lateral side is flat and the anterodistal surface is convex and rounded. A sharp ridge with a narrow border separates two strongly concave proximocaudal surfaces medially. Both the lateral and medial side of the calcaneum is subparallel (PRIETO-MARQUEZ 2007).

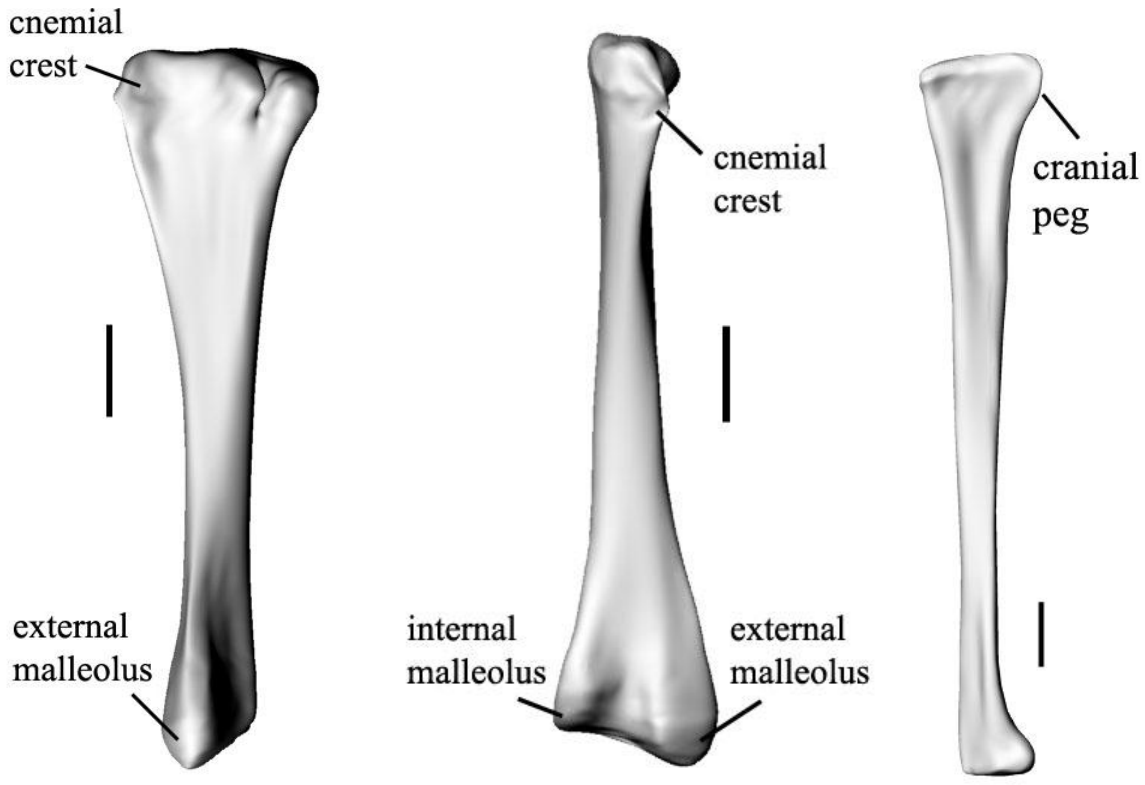

Figure 21: Digitized and reworked (see chapter 4.2) left tibia from lateral (left) and cranial view (center) and left fibula from medial view (right); scale bars = 10 cm.

Only one distal tarsal (no figure as missing) is known from *Brachylophosaurus*. The element is discoidal and slightly concave on its proximal side. It is attached to the proximal surface of metatarsal IV and abuts the lateroventral border of the proximal side of metatarsal III (PRIETO-MARQUEZ 2007).

The pes (Figure 22) is a robust and compact structure. There are three digits: II, III, and IV, which have a phalangeal formula of 3-4-5, respectively.

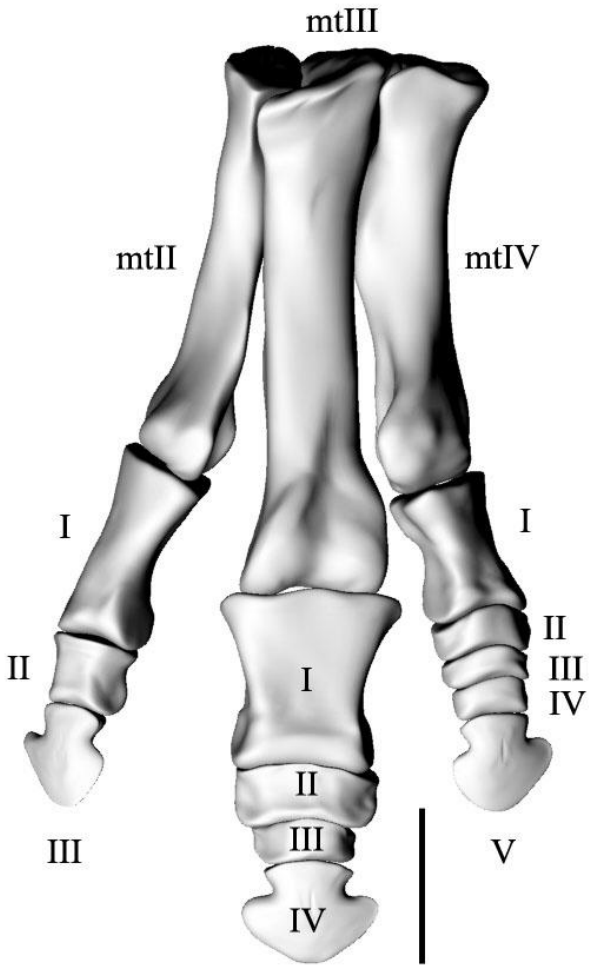

Figure 22: Digitized left pes from dorsal view; scale bar = 15 cm.

The metatarsals are large, stout, and elongated elements with expansions at its distal and proximal ends. They are tightly articulated and form a solid unit. Metatarsal II is shorter than metatarsal III but longer than metatarsal IV. Metatarsal III is the longest and most robust of the metatarsals. Metatarsals II and III show a strongly articulation. The morphology of metatarsal IV is close to a mirror image of metatarsal II. The proximal surface of metatarsal IV does not articulate at the same level as the one of metatarsal III, as metatarsal

IV is slightly displaced distally. This arrangement provides space for the distal tarsal, which fits on the concave proximal surface of metatarsal IV. The addition of the tarsal fills that space up to the level of the proximal border of metatarsals II and III (PRIETO-MARQUEZ 2007).

The pedal digits are proximally supported by a large, robust, and broad phalange. The largest of them is phalange III-1, which is subrectangular and dorsoventrally compressed. Phalanges II-1 and IV-1 are similar in morphology, but the latter one is shorter. They show triangular proximal profiles. In contrast to phalange III-1, which has a bilateral symmetry, phalanges II-1 and IV-1 are symmetrical and slope toward the medial and lateral sides of the foot, respectively. The other phalanges are compact and proximodistally compressed bones. This compression increases from digit II to digit IV. So, phalange II-2 is almost twice as proximodistally wide as phalange III-2, and the latter one is thicker than phalange IV-2. Successive, more distal phalanges become also shorter proximodistally within each digit, which terminates all in an arrowhead-shaped ungual (PRIETO-MARQUEZ 2007).

Ungual III-4 has a bilateral symmetry, while unguals II-3 and IV-5 are asymmetrical and are morphological images of each other. Pedal unguals differ from the manual ones in being much more expanded distally. Pedal digit III is projecting more dorsally, while digits II and IV surround it at a slightly lower level (PRIETO-MARQUEZ 2007).

Due to the limited working time in Malta it was not possible to digitize more bone material, e.g. vertebras or ribs, but for this project the bones of the locomotory parts of the skeleton were essential and sufficient.

The more important fact is the high completeness of the *Brachylophosaurus canadensis* specimens of the Malta collections, which provided the possibility to digitize many bones from the same individual. This made it a lot easier to build up a 3D-reconstruction of the digitized skeletal parts, as only a few bones have to be scaled (see chapter 4.3). Further, the digitized bones made it possible to construct the extremities of the model with a high accuracy, e.g. concerning the overall shape and the relation of length and size of fore- and hindlimb. However, in the simulations the bones were not used, as this would have increased computing time considerably and would also require the modeling of muscles and tendons, which is too time-consuming as to be done within this project.

In the next chapter the digitizing process and the working steps from the single digital bones to the finished *Brachylophosaurus* model are described.

4. Methods

Different working steps were necessary to get from single digitized bones to a hadrosaur model, which is able to walk or carry out other movements.

In the following these different working steps are described, including the digitizing procedure, the creation of the skeleton and body, and the making of the simulations. For further and more detailed information about these topics see MALLISON (2007) and MALLISON et al. (2009).

In this project the following three computer programs were used:

1. Preprocessing: McNeel Associates 'Rhinoceros® 3.0 NURBS modeling for Windows®';
   Rhinoceros 3.0® is a NURBS (non-uniform rational B-Spline) based CAD (computer aided design) program
   ►this program was used to digitize the bones, building up the skeleton, and generating the hadrosaur model
2. Postprocessing: Geomagic Corporation 'Geomagic Qualify 8.0®';
   Geomagic Qualify 8.0® is a CAQ (computer aided quality assurance) program
   ►this program was used to transform the model as NURBS object into a polygon body and to cut the polygon model into separate body sections
3. Simulations: MSC Corporation™ 'MSC.visualNastran 4D®';
   MSC.visualNastran 4D® is a rigid body modeling software for FEA (finite element analysis) and kinetic/dynamic modeling
   ►this program was used to connect the body sections via joints, to create a flexible model, and to prepare and work out the simulations

4.1 Digitizing hadrosaur bones

For digitizing the bones of *Brachylophosaurus* a mechanical Immersion MicroScribe-3D® point digitizer was used (Figures 23 & 24). The input from the digitizer to the connected computer was controlled with the provided foot pedal (Figure 23). To obtain and process digital data the computer program Rhinoceros® 3.0 NURBS modeling for Windows® was

used. Adhesive masking tape allowed marking the bones with points and curves, that is auxiliary lines, providing also a visual aid during digitizing. Finally, a specially constructed variable holder (Figures 23 & 24) was applied to stabilize mainly the medium-sized bones during digitizing, while small bones were stabilized with plasticine (MALLISON 2007; MALLISON et al. 2009).

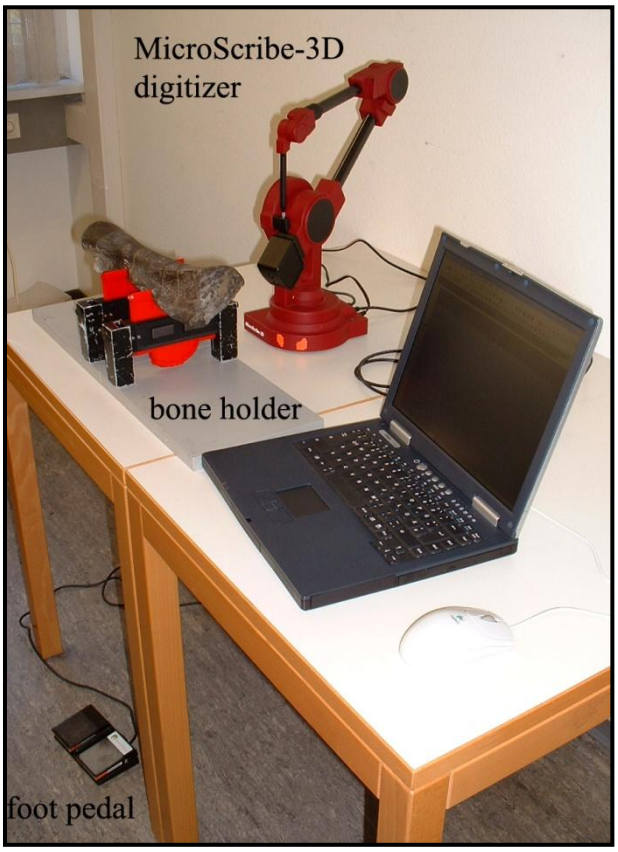

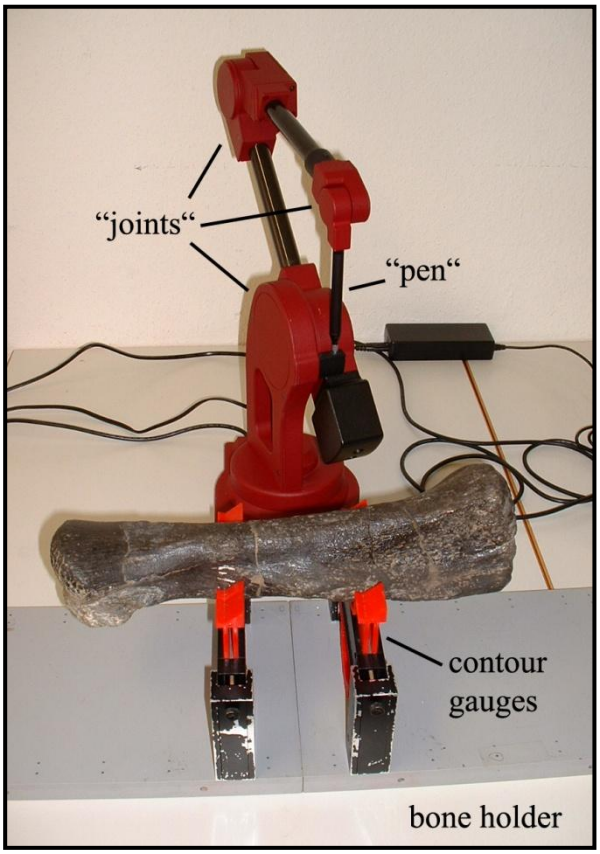

Figure 23 (left): The Immersion MicroScribe-3D® point digitizer, which is connected to a laptop computer, the specially constructed variable bone holder, and the foot pedal used to control digitizer data transfer to the computer (photo by the author).
Figure 24 (right): The Immersion MicroScribe-3D® point digitizer and the specially constructed variable bone holder in detail (photo by the author).

The digital images of the bones should be highly accurate, e.g. for assembling them to a digital image of the skeleton, which is a lot easier if the digitized bones are as realistic as possible. Therefore, the bones should be selected carefully for digitizing. Ideally, they should be complete and not deformed. However, they can derive from different skeletons of one specimen, as complete skeletons are not always available. In this case the bones have to be scaled in Rhinoceros® so that they have the right proportions, as if they belong to one skeleton. Also, the bones can be mirrored if necessary, which can be easily done in

Rhinoceros® as well. For example, if only a right humerus is available the bone can be mirrored to get the left one. Also, a bilaterally symmetrical bone needs only to be complete in one half, since it can be mirrored to get the complete one (MALLISON 2007; MALLISON et al. 2009).

Accuracy is essential when digitizing bones, because even slight aberrations of the curves can lead to significant shifts on volume or appearance. Beside slight unnoticed rotations of the bone during digitizing, which may lead to misinterpretations, significant movements of the bone are possible due to instable placement or physical contact. To avoid these problems a variable bone support was designed. It can be taken apart into smaller pieces, which makes it easy to stow and transport. The support consists of a basal plate, custom made metal holders, which can be placed at variable intervals on the basal plate, and commercially available plastic contour gauges supported by the metal holders (Figure 25). The bones can be mounted stably on the contour gauges and resist shifting and turning much better as without support. Further, using the smooth plastic gauges instead of metal holders there is no risk of scratching the bone (MALLISON 2007; MALLISON et al. 2009).

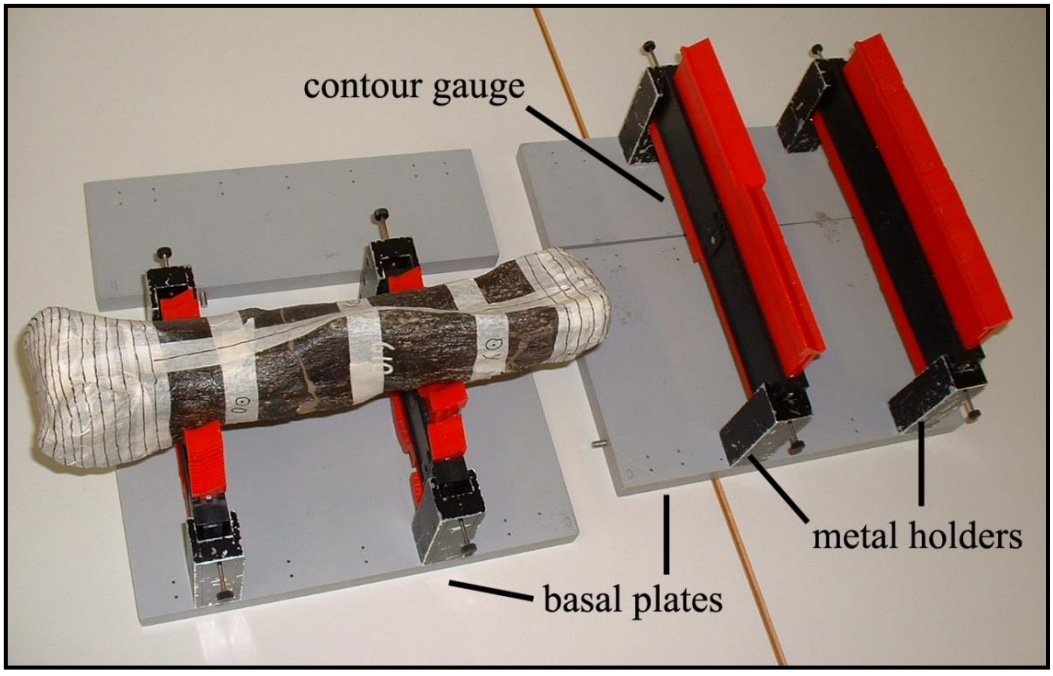

Figure 25: The variable bone support in detail view; on the left, the holder in minimum configuration carries a metacarpal of *Diplodocus* from the Institute for Geosciences, which is marked for digitizing; on the top and right are the extension parts of the holder for larger bones; the width of the contour gauges can be doubled for broad bones (photo by the author).

In the case of smaller bones, e.g. phalanges, the holder is too large so that the bones cannot be placed stably on it. To digitize these small bones of relatively simple shape plasticine was used, to fix the bones and avoid movements. However, using this method it is necessary to wrap the bone completely in adhesive masking tape, to avoid direct contact between plasticine and bone. On the other hand allows the masking tape to mark the complete bone with auxiliary guiding lines, which makes it a lot easier to digitize bones of minor size (Figures 26 & 27) (MALLISON 2007; MALLISON et al. 2009).

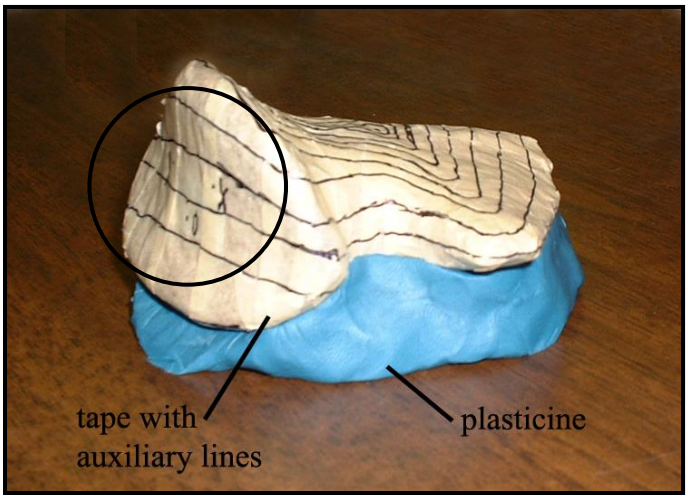

Figure 26 (left): Phalanx III dextral (JRF 200W specimen) of metatarsal II from ventral view ready for digitizing. The ungual is wrapped in adhesive masking tape, marked completely with auxiliary lines, and embedded in plasticine (photo by the author).
Figure 27 (right): The same phalanx from caudolateral view, showing also the three coordinates necessary for digitizing (on the left within the circle) (photo by the author).

Before starting to digitize, coordinates for recalibration must be marked on the bone as well as a seam line (Figure 28), an imaginary line connecting all curve starts and ends, which must not be digitized. In the case of small and medium sized bones, a single set of coordinates located roughly halfway down the length of the bone is sufficient. Three coordinates are needed: an origin point (O1) for the origin of the coordinate system and two points (X1, Y1) to determine the direction of the x- and y-axis respectively (Figure 28). The coordinates can be placed in any relation to each other except for a straight line, as Rhinoceros® translates into a Cartesian coordinate system internally. Thus, the coordinates have not to be placed in a right triangle (MALLISON 2007; MALLISON et al. 2009).

Multiple coordinate sets allow digitizing larger bones. Coordinates should be placed in a way that one set (Cset1=O1, X1, Y1) is accessible in all positions the bone will have to be

placed in during digitizing. If this is not possible, a second set (Cset2=O2, X2, Y2) must be placed so that it can be reached with the digitizer after calibration through Cset1. Therefore, the two sets of coordinates should be placed at approximately 1/4 and 3/4 of the length of the bone to allow maximum range for the digitizer. Some bones may require more sets of coordinates. In this case, Cset2, Cset3, and so on should all be accessible from Cset1, which should be placed roughly halfway down the bone (MALLISON 2007; MALLISON et al. 2009).

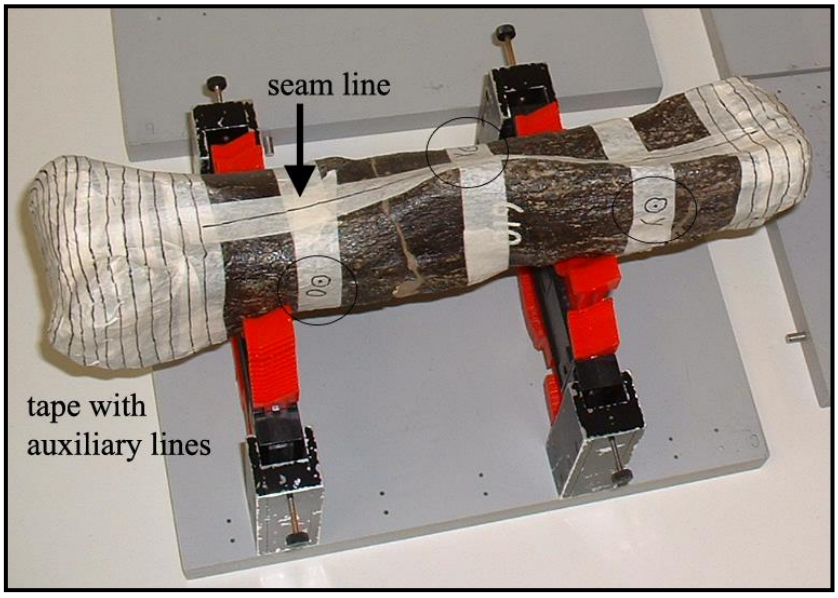

Figure 28: A closer view of the *Diplodocus* metacarpal, which is prepared for digitizing with closed curves. The three coordinates are marked by a circled dot and a letter (0/X/Y). The ends of the bone have been wrapped with tape and marked with auxiliary lines to alleviate digitizing (photo by the author).

The best way to obtain 3D data of bones with the digitizer is by storing curves. To construct a surface the 'loft' function on curves can be used, but a 'closed loft' is more practical, as it leads directly to a closed 3D body. Both curves and surfaces in Rhinoceros® are created as NURBS objects. This process is best described as the electronic equivalent of wrapping sub-parallel wires around a bone, and then pulling a cloth tight around the wires (Figures 29 & 30) (MALLISON 2007; MALLISON et al. 2009).

To obtain the curves it is necessary to enter the 'digsketch' command into Rhinoceros® and to place the tip of the digitizer on the bone at the start point of the intended curve. The next steps are to press the foot pedal down and to move the digitizer tip over the bone until the desired end point of the curve is reached. Finally, the foot pedal must be released. It is important that neighboring curves are of similar length and are

roughly parallel, as large differences in length or separation can create artifacts in the final surface. Further, the curves may not cross each other. The curves should be more closely spaced where the morphology of the bone shows important details or when the topology changes abruptly, e.g. at the articular ends. In contrast, rather simple surface areas, like shafts of long bones or scapular blades, require fewer curves. In contrast to open curves, the use of closed curves is an important improvement in digitizing bones. Closed curves mean that each curve reaches 360° around the bone as an infinite loop, which allows a closed loft over the entire bone in one step. Thus, there is no need to assemble two surfaces into one body, as with open curves, a process which is quite difficult in using Rhinoceros®. A closed loft requires, in addition to closed curves, a start and an end point at each end of the loft. This will result in a closed body instead of an open surface (Figure 29) (MALLISON 2007; MALLISON et al. 2009).

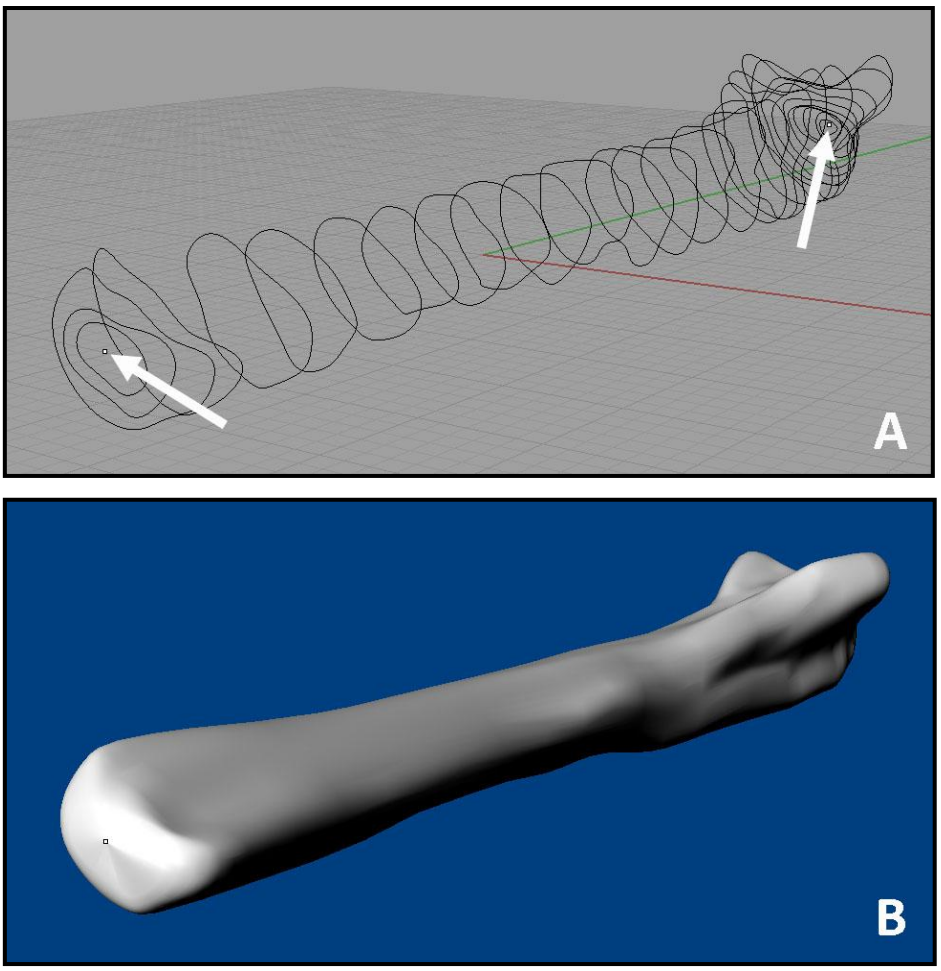

Figure 29: Digital file of the right ulna of *Brachylophosaurus* (JRF 200W). **A**: Closed curves digitized on the bone. Note the start and end points (arrows) for the closed loft. **B**: Lofted surface based on the curves in A.

To get a surface with minimum artificial distortion, all curve ends must meet the respective curve starting points with minimum overlap and shift along the seam line and point in roughly the same direction. To achieve this, it is useful to mark starting points on the bone by taping a strip of adhesive masking tape along the intended seam line (usually the long axis of the bone) and mark curve starts by a lengthwise line with cross marks. This reduces also wriggling of the seam line, which often causes considerable lofting artifacts. To minimize distortion at the bone ends, it is advisable to cover a small circle at each end with masking tape and draw the first and last few curves onto the tape prior to digitizing. The endpoints should also be marked here (Figure 28) (MALLISON 2007; MALLISON et al. 2009).

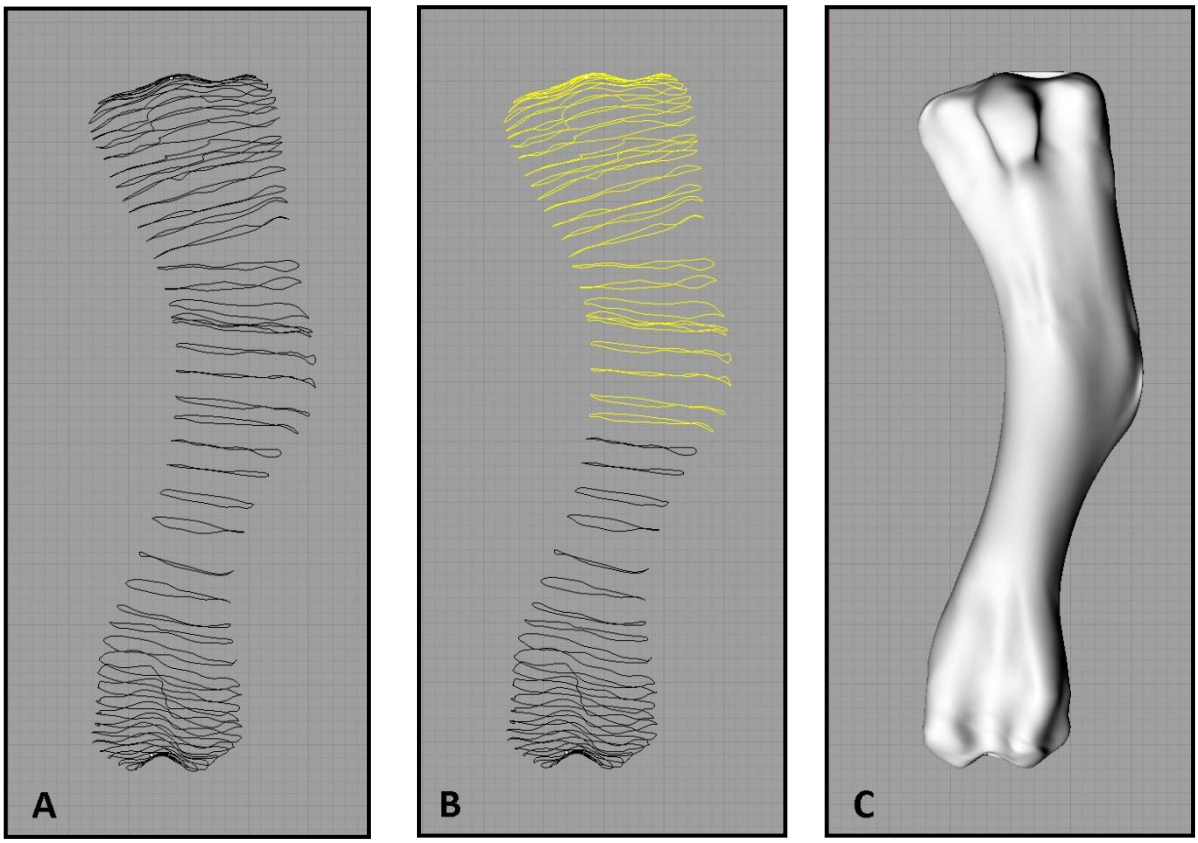

Figure 30: Digital file of the right humerus of *Brachylophosaurus* (JRF 200W). **A**: Closed curves digitized on the bone. **B:** To loft the surface each point/curve must be selected one by one. **C**: Lofted surface based on the curves.

Lofting a surface over closed curves (command 'loft') is the easiest way to create surfaces for digitized bones in Rhinoceros®. A loft that has a point object at one end, in addition to the closed curves, is closed at that end. However, it still remains a surface and is not changed into a body. In contrast, a loft that both starts and ends with a point will create a body. In order to loft, the respective curves must be selected and the proper loft option

chosen. Then, each point/curve must be selected by hand in the proper order, starting with one endpoint, then the nearest curve, then the next etc. to the other end of the bone (Figure 30) (MALLISON 2007; MALLISON et al. 2009).

4.2 Rework digitized bones

As the dinosaur model, which is used in the simulations, bases upon a virtual skeleton, it is of great importance to have complete and undamaged bones for digitizing, as they ensure the correctness of the skeleton and hence of the model. However, some of the required bones may be not available, damaged, or incomplete. In the two latter cases, this would demand to rework the digitized images of the bones, because damaged or incomplete bones can complicate the assembling of the skeleton, as they may lead to incorrect positioning of adjacent bones or to incorrect lengths of arm or leg.

Reworking a digitized bone has to be done carefully, e.g. by using images of the respective bone from the same specimen or from closely related taxa. In case of *Brachylophosaurus*, bones from other hadrosaurine hadrosaurs can also be easily used as samples, because the bones a very similar among different species. Of course, it is not possible to rework a digitized bone image to a one-to-one copy of the real bone in a complete or undamaged condition. Nevertheless, a carefully reworked bone image is quite more useful in assembling a skeleton than that of a damaged or incomplete bone. Therefore, slight deviations between the reworked image and the real bone are negligible.

The closed curves which build up a digitized bone image in Rhinoceros® (see chapter 4.1) can be edited by their control points (Figure 31). To edit a curve, it must be marked and then the control points must be activated (command '_PointsOn'). A control point can be moved by marking it and then move it with the computer mouse. This can also be done simultaneously with several marked points. It is essential to loft consistently to control the changes of the bone surface caused by the edited curves. This process has to be repeated until the bone surface has the favored shape. Finally, the control points can be deactivated (command '_PointsOff').

The following example demonstrates the process of editing closed curves using their control points: phalanx III of metacarpal II dextral, belonging to the JRF 200W specimen.

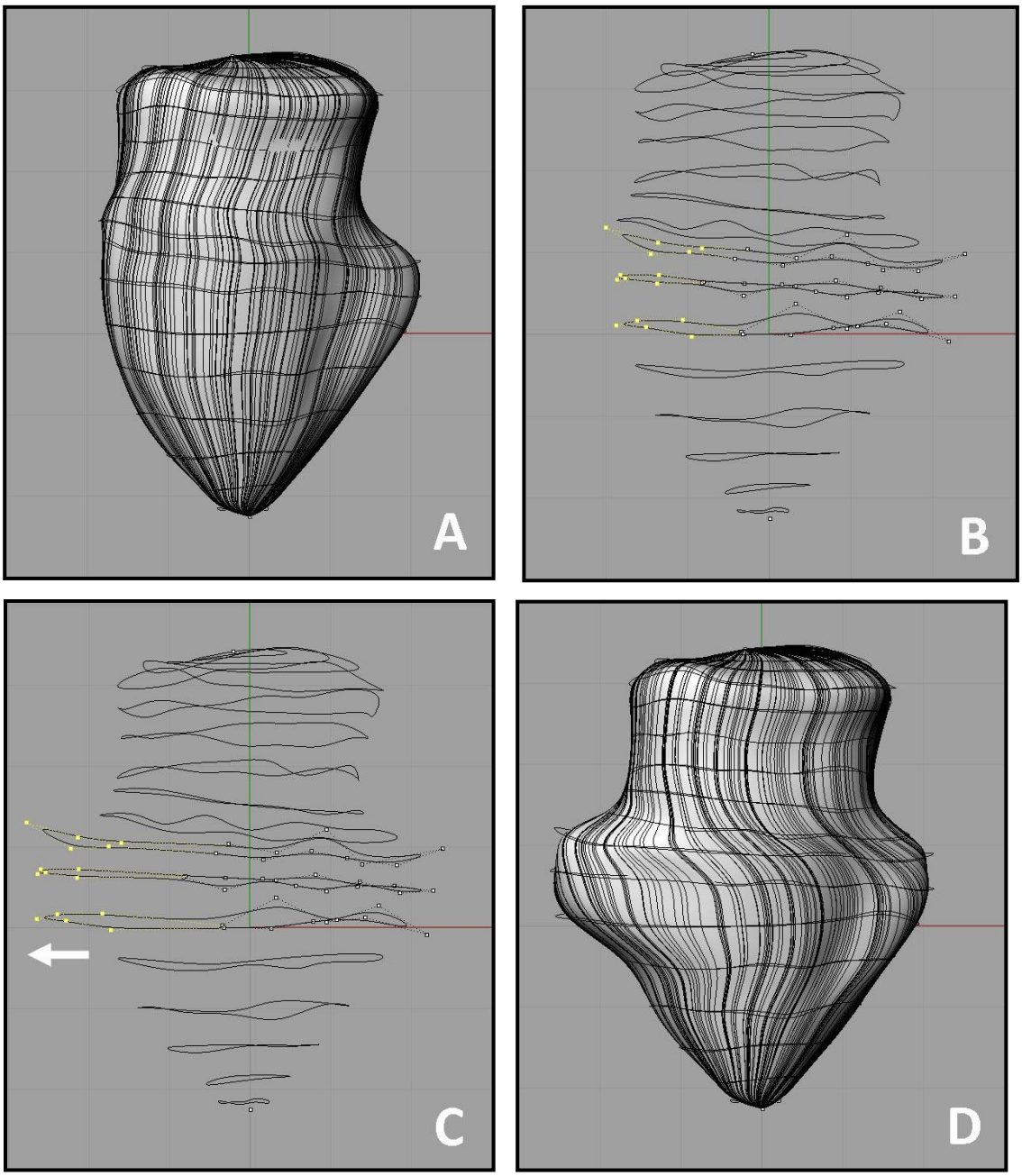

Figure 31: Digital file of the right phalanx III of metacarpal II of *Brachylophosaurus* (JRF 200W) from dorsal view.
A: Digital image of the phalanx in dorsal view, showing the closed curves and the lofted surface.
B: The lofted surface is deleted, control points of three curves are activated, and the points which shall be moved are marked. **C:** The marked points of the three curves are moved with the computer mouse in direction of the white arrow. **D:** The control points are deactivated and a new lofted surface was generated, showing the modification of the surface on the left side of the bone.

The following digitized *Brachylophosaurus* bones were reworked:

- Right femur cast of the MOR 794 specimen
- Left scapula and metatarsal III of the JRF 200W specimen
- Single left tibia

The digitized cast of the right femur of MOR 794 was reworked, because the cast based on a bone which is rather crushed, mostly along its longitudinal axis (Figures 32 & 33). To avoid later problems in modeling the upper leg, especially concerning the estimation of its cross-section, it was necessary to restore the original bone surface in order to get a more precise volume of the femur (Figures 34 & 35). However, the incomplete femoral head of the cast was not complemented, as it is not essential for assembling the skeleton and would have been too much interpretative.

Figure 32: Right femur cast of *Brachylophosaurus* (MOR 794) from lateral view (photo by the author).

Figure 33: Detailed view of the medial part of the femur cast from lateral view, showing the crushed surface and the damaged fourth trochanter (photo by the author).

Figure 34 (left): Digital file of the right femur cast of *Brachylophosaurus* (MOR 794) from medial view. On the left the original, on the right the reworked digitized bone.
Figure 35 (right): The same file from lateral view. On the left the reworked, on the right the original digitized bone.

The left scapula of the *Brachylophosaurus* JRF 200W specimen shows an incomplete distal part (Figures 36 & 37), affecting the articulation surfaces with coracoid and humerus, which complicates the assembling of the shoulder girdle skeleton. Also, the scapula is deformed as the ribcage was smashed due to the embedding process. As the scapula follows the contour of the rib cage, it is no longer convex to the lateral side of the body but rather concave. This would lead to a wrong body cross-section and body shape in the range of the shoulder girdle. Therefore, the scapula was partly complemented in its distal part for a better assembling of the skeleton and its convex shape was rebuilt to compensate the deformed rib cage (Figures 38 & 39). Although these corrections are more interpretative as in the case of the femur described above, they were essential for a more accurate shoulder girdle skeleton and a more precise modeling of this body segment (Figure 40). The MOR 794 specimen has a complete left scapula, but it was not possible to digitize this one, because the risk to damage the bone was too high in that case, due to its difficult accessibility with the digitizer based on the articulated condition of the skeleton.

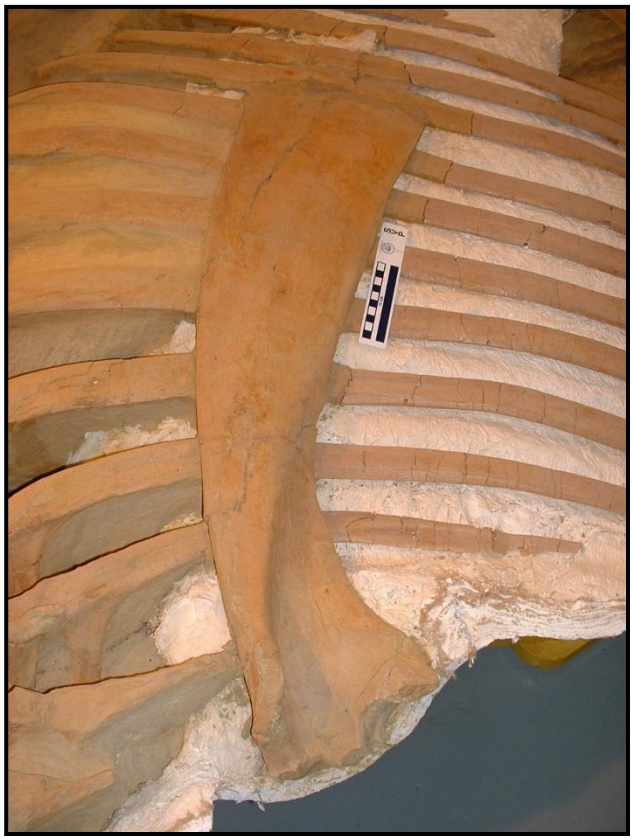

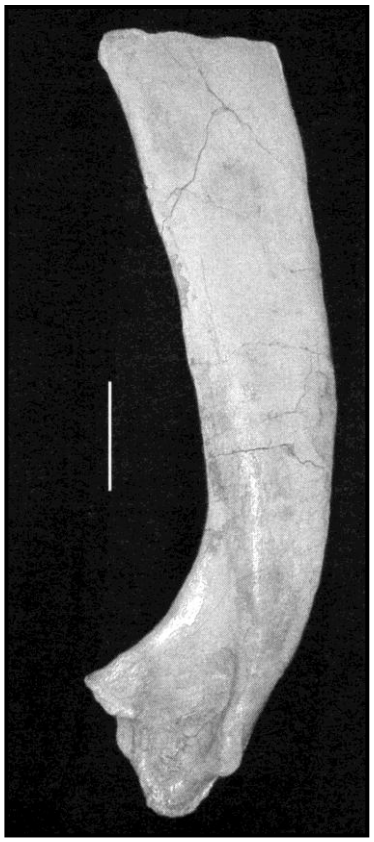

Figure 36 (left): Incomplete left scapula of *Brachylophosaurus* (JRF 200W) in lateral view (photo by the author).

Figure 37 (right): Complete right scapula of *Brachylophosaurus* (MOR 1071-7-18-98-298) in lateral view; scale bar = 10 cm (PRIETO-MARQUEZ 2007).

Figure 38: Comparison of the complete left scapula of *Brachylophosaurus* specimen MOR 794 (below / from ventral view) and the reworked digitized left scapula of *Brachylophosaurus* specimen JRF 200W (above). Note the rebuild convex shape of the digitized scapula, which can also be seen in the original one below (photo by the author).

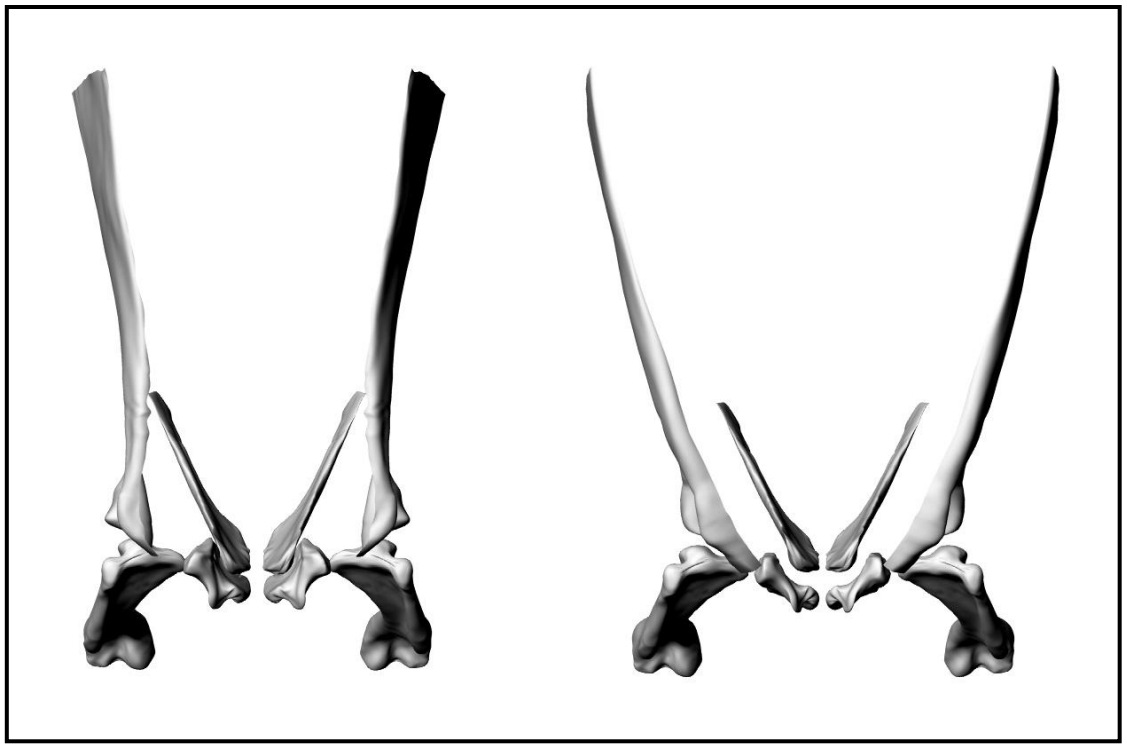

Figure 39: Comparison of the two possible shoulder girdles of the digital skeleton from dorsal view. On the left the shoulder girdle with the original digitized scapulae (one digitized, the other one mirrored), one the right the modified shoulder girdle with the reworked scapulae.

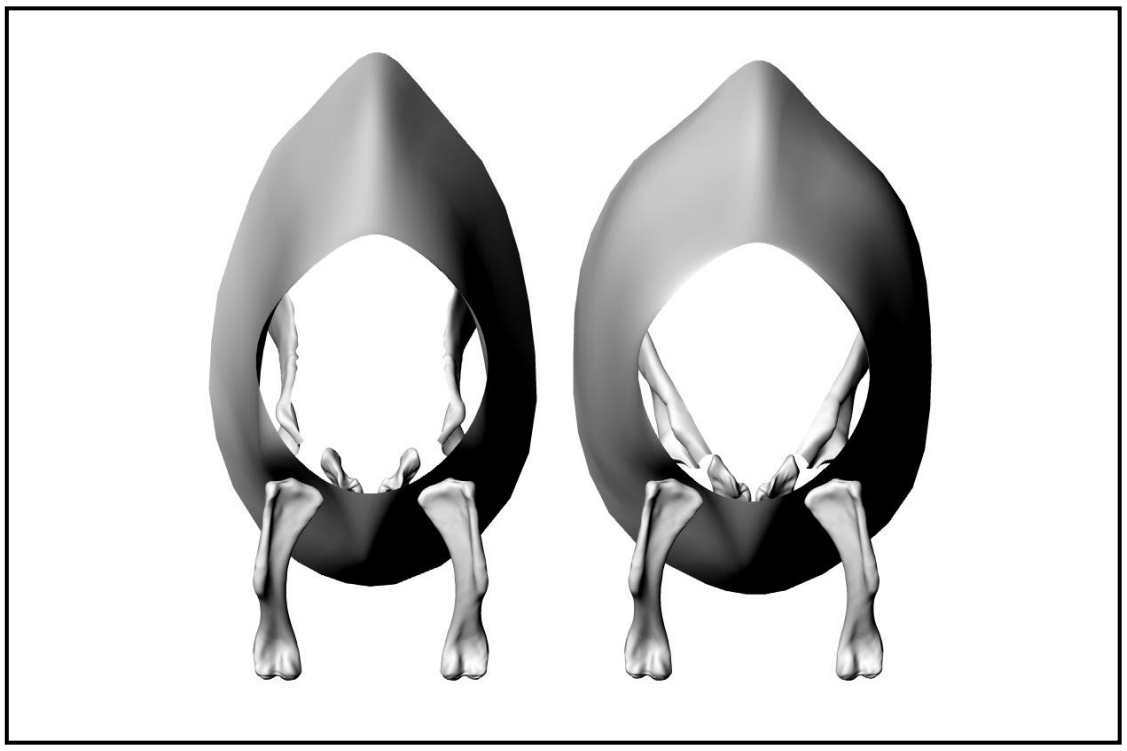

Figure 40: Comparison of the two possible body shapes depending on the two different shoulder girdles from cranial view. Left body with the original digitized scapulae, right body with the reworked scapulae. With the latter one the body becomes broader and the humeri are in a greater distance to each other.

The left third metatarsal of the JRF 200W *Brachylophosaurus* specimen is crushed in the proximal part of its medial side (Figure 41). Therefore, articulation with the second metatarsal and a correct arrangement of the metatarsus in the digital skeleton would have been hindered. To avoid this, the third metatarsal was reworked to restore the original surface (Figure 42).

Figure 41: Third metatarsal of *Brachylophosaurus* specimen JRF 200W from medial view. Note the crushed area on the right half of the bone (photo by the author).

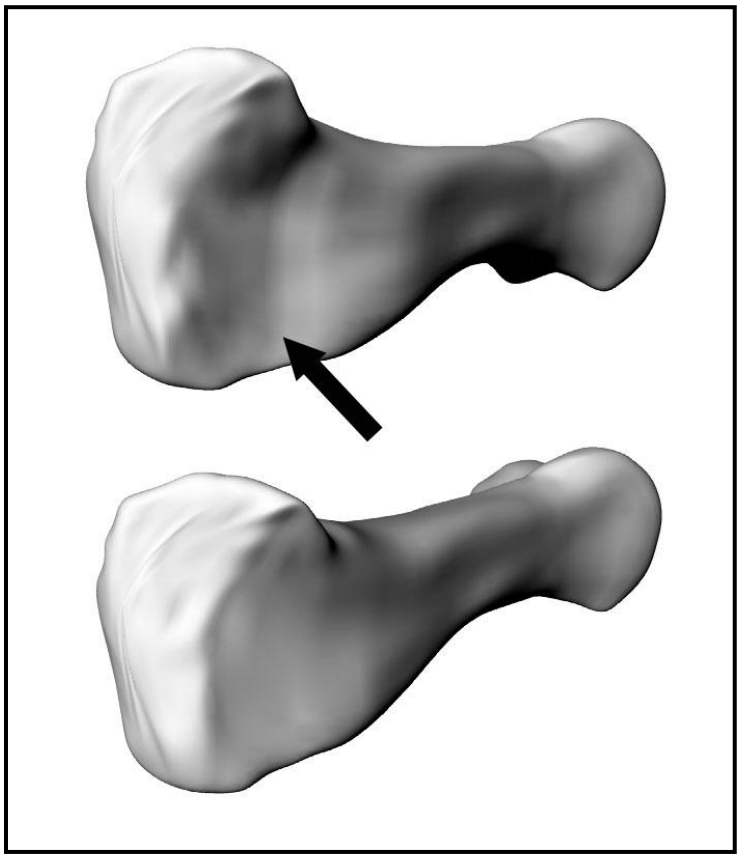

Figure 42: Digital file of the third metatarsal of *Brachylophosaurus* specimen JRF 200W from medio-proximal view. Above the original digitized bone, below the reworked one. The black arrow shows the crushed area in the proximal part of the metatarsal.

The single left *Brachylophosaurus* tibia is damaged and incomplete in its distal part (Figure 43). However, as no other disarticulated tibia was available this one had to be digitized. It was indispensable to rework the digital file (Figures 44 & 45 & 46) of this bone as otherwise the assembling of the whole lower leg would have been impossible. The fibula, astragalus, and calcaneus cannot be placed correctly without a complete tibia.

Figure 43: Left tibia from mediodistal view. The black arrow shows the incomplete part of the distal end (photo by the author).

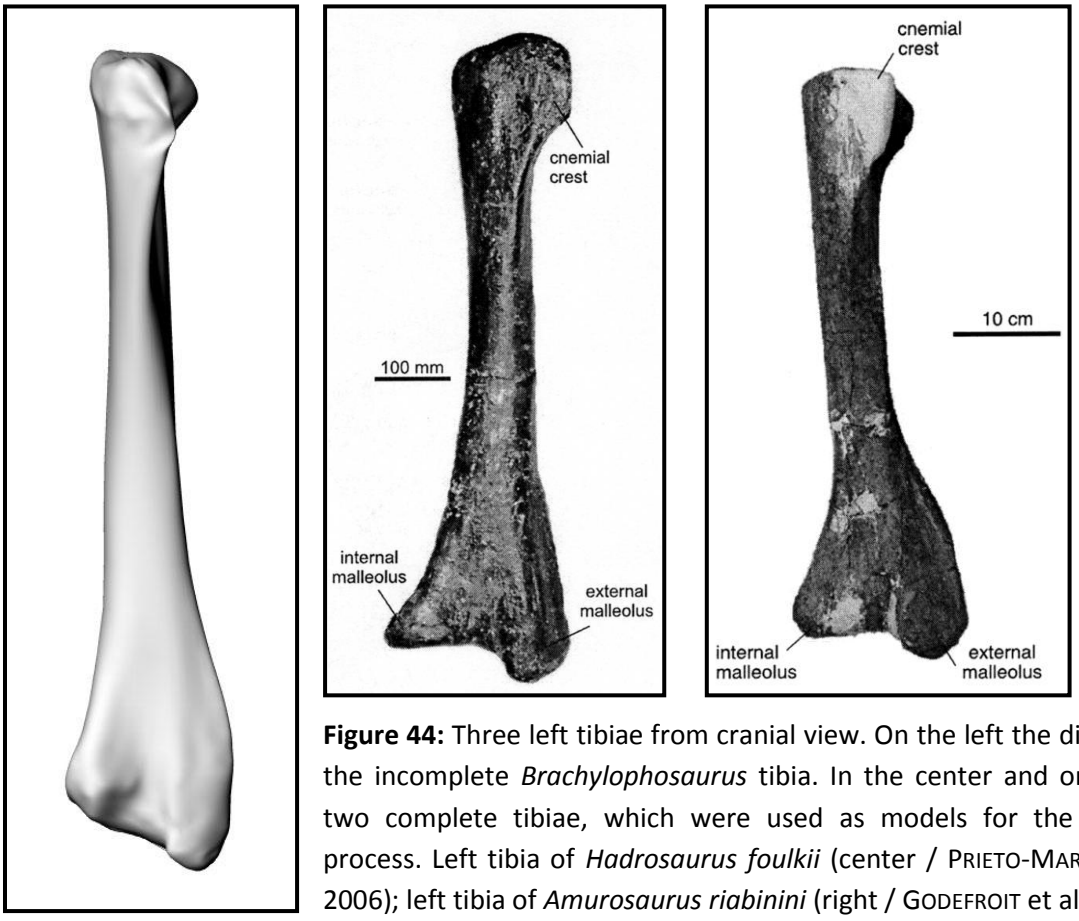

Figure 44: Three left tibiae from cranial view. On the left the digital file of the incomplete *Brachylophosaurus* tibia. In the center and on the right two complete tibiae, which were used as models for the reworking process. Left tibia of *Hadrosaurus foulkii* (center / PRIETO-MARQUEZ et al. 2006); left tibia of *Amurosaurus riabinini* (right / GODEFROIT et al. 2004).

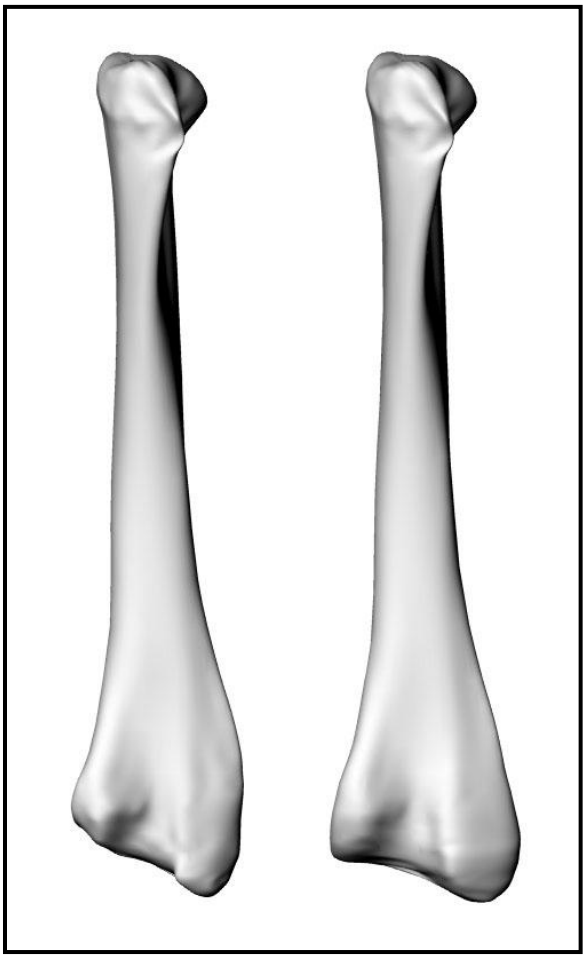

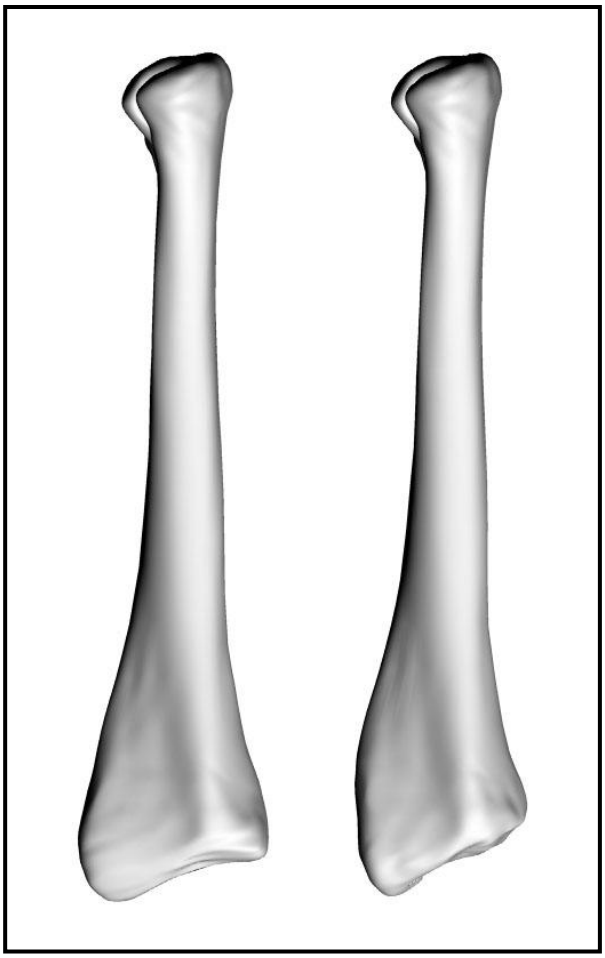

Figure 45 (left): Digital file of the left *Brachylophosaurus* tibia from cranial view. On the left the original, on the right the reworked digitized bone.
Figure 46 (right): The same file from caudal view. On the left the reworked, on the right the original digitized bone.

Beside the tibia, another problem had to be solved to assemble the lower leg of the digital *Brachylophosaurus* skeleton. Unfortunately, no disarticulated astragalus or calcaneus was available and the articulated ones of the displayed skeletons were not accessible for digitizing. Without these proximal tarsalia it is not possible to determine the correct distance between the lower leg and the metatarsalia and to bring the articulation surfaces of the ankle joint in the correct position. To solve this problem an astragalus and calcaneus of the ornithopod dinosaur *Dryosaurus lettowvorbecki* (see chapter 3) were digitized (Figures 47 & 48 & 51) and transformed to replace the missing hadrosaur bones. Certainly, the transformed *Dryosaurus* bones are not real copies of the *Brachylophosaurus* bones, but they are the best available alternatives (Figures 49 & 50 & 51). Therefore, slight differences between the original hadrosaur bones and the transformed *Dryosaurus* bones are less important than the possibility to create the ankle joint in a reasonable manner.

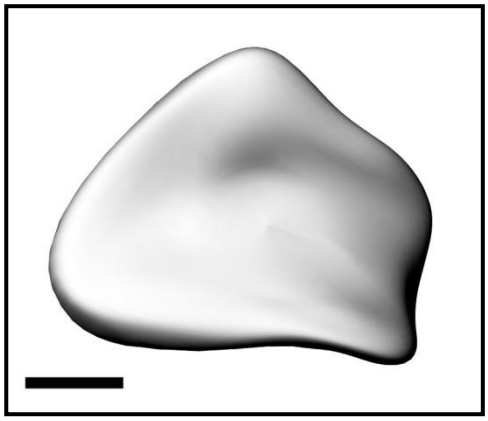

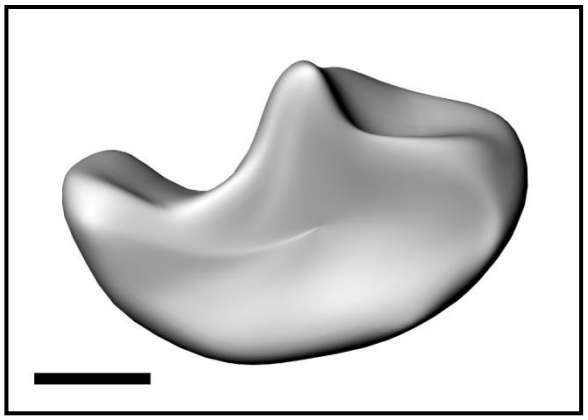

Figure 47 (left): Digital file of the left *Dryosaurus* astragalus (GPIT/RE/6421) from dorsal view; scale bar = 1 cm.

Figure 48 (right): Digital file of the right *Dryosaurus* calcaneus (GPIT/RE/5248) from dorsolateral view; scale bar = 1 cm.

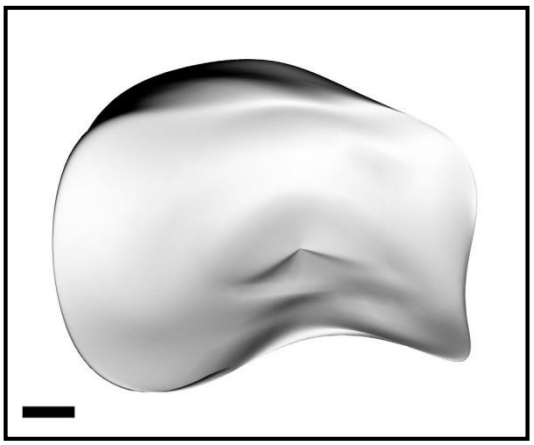

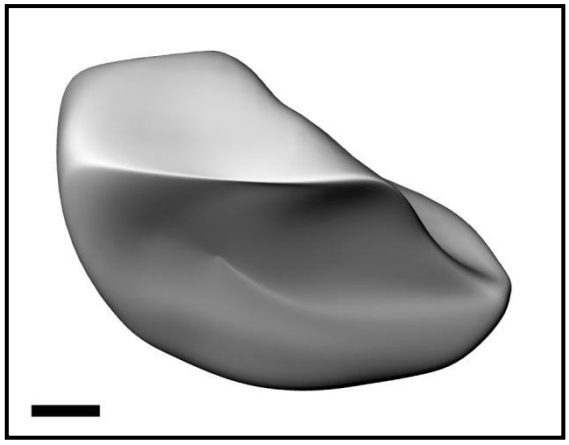

Figure 49 (left): Digital file of the transformed left *Dryosaurus* astragalus from dorsal view; scale bar = 2 cm.

Figure 50 (right): Digital file of the transformed and mirrored right (now left) *Dryosaurus* calcaneus from dorsolateral view; scale bar = 2 cm.

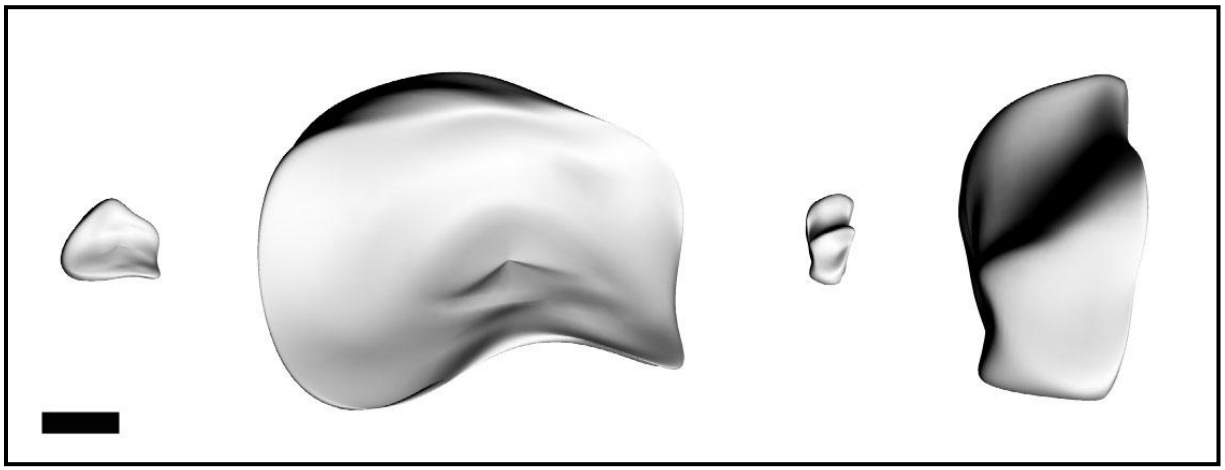

Figure 51: Size comparison of the original and transformed *Dryosaurus* astragali and calcanei from dorsal view; scale bar = 3 cm.

In contrast to the reworking of the tibia, the use of images to transform the two bones of *Dryosaurus* was not practical. Either, no images were available, as in case of the calcaneus, or the few ones which were available, as in case of the astragalus, show not all different views, which were necessary for a correct transformation. Also, concerning the astragalus, the images are too different to be used as models for the transforming process, as the shape of this bone seems to be more variable among hadrosaur species (Figures 52 & 53). Because of this, the two bones were mainly transformed by adapting them to the shapes of the distal ends of tibia and fibula, and to the proximal articulation surfaces of the three metatarsalia (see chapter 4.3).

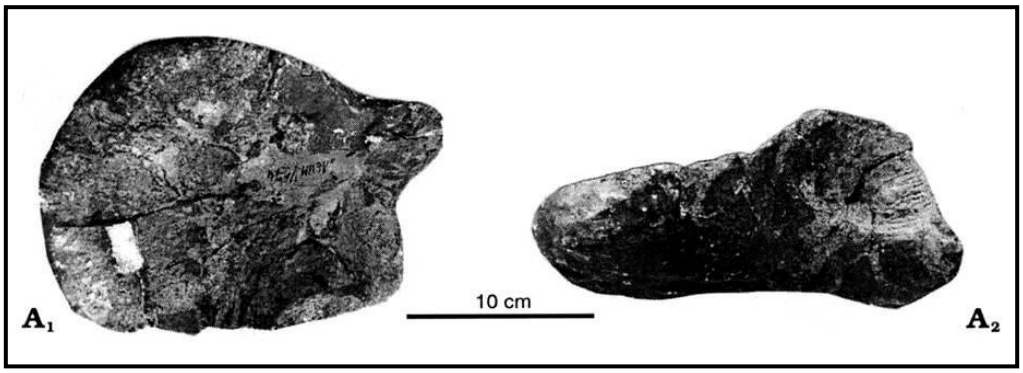

Figure 52: Left astragalus of *Amurosaurus riabinini* from dorsal (A1) and cranial (A2) view (GODEFROIT et al. 2004).

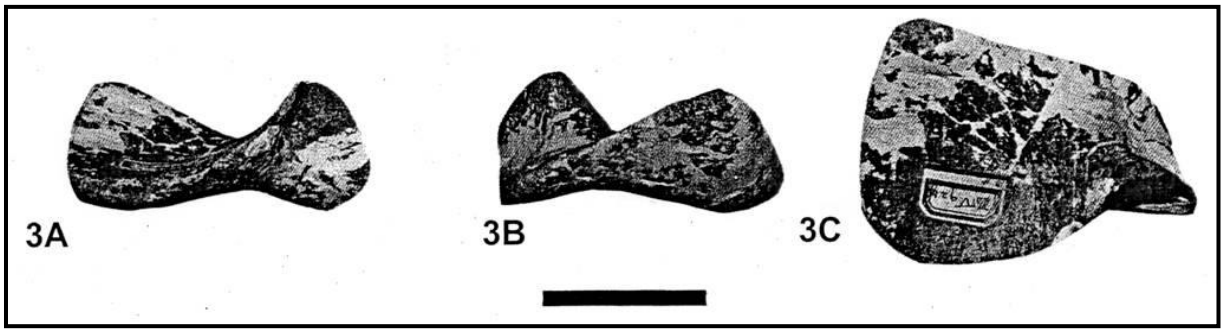

Figure 53: Left astragalus of *Charonosaurus jiayinensis* from cranial (3A), caudal (3B), and dorsal (3C) view; scale bar = 5 cm (GODEFROIT et al. 2001).

4.3 Creating the hadrosaur model - the skeleton

After reworking the digitized bones, another working step has to be done before the construction of the skeleton can start. As the bones belong to three individuals of *Brachylophosaurus* of different body size, their digital images had to be scaled before assembling them. Since most of the digitized bones belong to the JRF 200W specimen, their scale was used in Rhinoceros® for calibration of the digital bones belonging to the two other specimens. This concerned the pelvic girdle and the femur in case of the MOR 794 specimen, and the five manus phalanges in case of the JRF 116H specimen. Further, the single tibia had to be scaled. In contrast, it was not necessary to scale the *Dryosaurus* astragalus and calcaneus, as these two bones had to be transformed, which was done after the bones of the lower leg and the pes were assembled. Therefore, they were adapted to the right size during the transformation process.

The pelvic girdle and the femur of the MOR 794 specimen as well as the single tibia were scaled in Rhinoceros® by using a skeletal drawing of *Brachylophosaurus* specimen JRF 200W from lateral view made by Scott Hartman [www.skeletaldrawing.com].

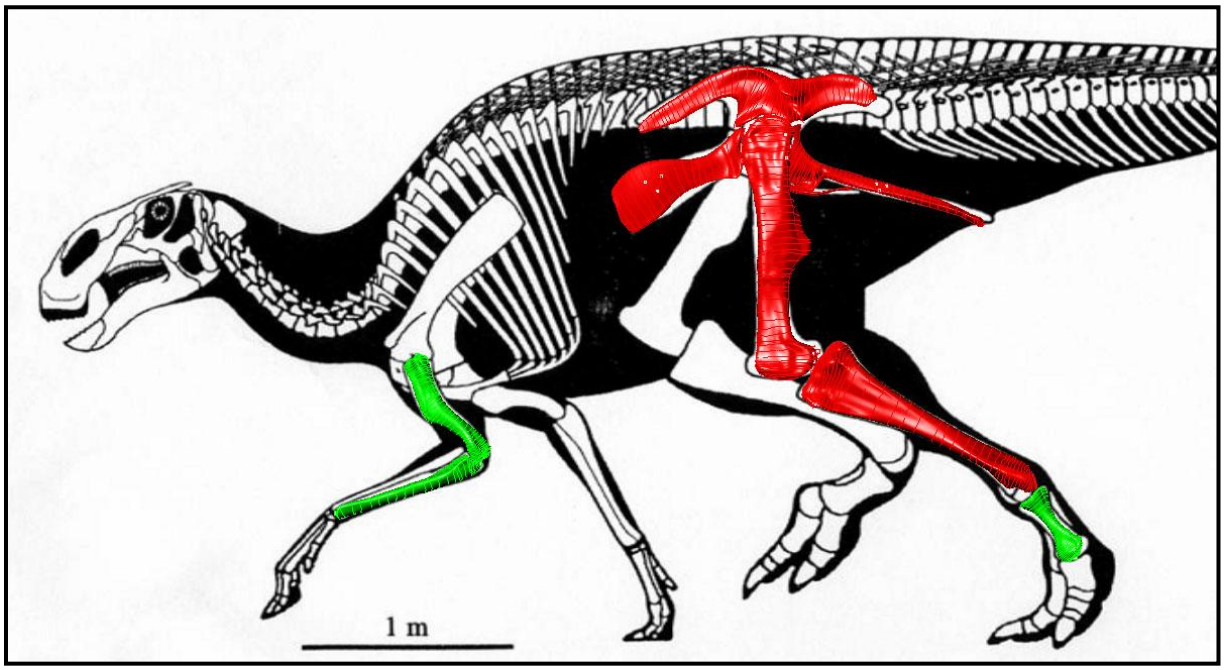

Figure 54: Skeletal drawing of *Brachylophosaurus* specimen JRF 200W from lateral view [www.skeletaldrawing.com]. The green colored bones belong to this specimen and were used to scale the image in Rhinoceros®. After that, the red colored bones (from MOR 794 and the single tibia) were adjusted to this scale respectively size.

For the scaling process (Figure 54) some digitized bones of the JRF 200W specimen were selected. These bones were used to scale the skeletal drawing to that size which is in accordance to the bones. As soon as bones and skeletal image match, which means that they now have the same scale, the MOR 794 pelvic girdle and femur, and also the single tibia, were included and adjusted to this scale respectively size. Figure 54 shows that the pelvic girdle does not match perfectly to the skeletal drawing, but enough for scaling.

However, the five manus phalanges of the JRF 116H specimen are too small to scale it with the aid of this skeletal drawing. In their case the adjustment to the scale of the manus phalanges belonging to the JRF 200W specimen was made by using photos, calculating the correct size. As no three-dimensional manus of *Brachylophosaurus* was available, the manus of a mounted *Edmontosaurus annectens* skeleton was used for that purpose (Figure 55).

Figure 55: Right manus (cast) of *Edmontosaurus annectens* in the collection of the Black Hills Institute in Hill City from cranial view (South Dakota / USA) (photo by the author).

Now, with the reworked and scaled bones the preparations for the construction of the skeleton are finished. For building up the skeleton in Rhinoceros® it is sufficient to assemble only the bones of one side, as the other half of the skeleton can be created by mirroring the assembled one. This makes the construction easier and avoids also differences between the right and left side of the skeleton.

As samples for the skeletal construction mainly photos and images were used. Skeletal drawings (as in Figure 54) are not really useful, as the animals are shown usually in a forward motion, which is not suitable for the construction of the digital skeleton, as the model should base on a neutral standing pose. Also, the skeletal drawings show not enough details, e.g. of the hand skeleton, and miss the three-dimensionality of a mounted skeleton.

Further, it is not clear if the skeletal drawings consider the unpreserved epiphyseal (articular) cartilage of the bones. HOLLIDAY et al. (2001a, 2001b, 2002, 2010) suggest that the amount of missing cartilage can be potentially large in dinosaurs. They estimate that 10 to 20% of limb bone size, as well as major articular surface features, are severely truncated or lost during skeletonization in extant archosaurs (alligators and birds). Therefore, an appreciable amount of morphological data may be absent in dinosaur skeletons as well, although birds showed less dramatic changes than alligators. SCHWARZ et al. (2007a) examined the first fossil evidence for articular cartilage in a sauropodomorph dinosaur (*Cetiosauriscus greppini*), which indicates the presence of a large articular capsule on sauropod forelimbs, showing that the forelimb length of sauropods might have been larger than previously assumed.

Concerning the *Brachylophosaurus* digital skeleton, it is difficult if not impossible to estimate the amount of cartilage and therefore also the correct space between the limb bones. It was tried to take the cartilage into account when building up the skeleton, assembling especially the larger bones not close-packed, but rather with a certain space between them. Despite this, it is possible that the fore- and hindlimbs are too short as the estimated amount of cartilage might be too small.

The construction of the shoulder girdle (Figures 56 & 57) was rather difficult. On the one hand it was hard to define the correct positions of the individual bones, and on the other hand due to the reworked scapula (see chapter 4.2). As it was not possible to complement the distal part of the scapula completely, the articulation with the coracoid and a correct placement of coracoid and sternal was hindered. Despite these inaccuracies, the reworked scapula was quite more useful than the original one. Skeletal drawings show often a cartilage (?) plate (Figure 58) between the two coracoids (e.g. PAUL 2010), which seems to be not documented in the fossil record. In contrast, after HORNER et al. (2004), the coracoids meet along their rostrodorsal surfaces. As information about this plate can also not be found in the literature, it was decided to follow the description of Horner et al. (2004), placing the coracoids side by side. The sternals were joined to one another by cartilage at their proximomedial ends (HORNER et al. 2004). This can also be seen in the JRF 116H *Brachylophosaurus* specimen, where the two sternals are still articulated (Figure 59).

As sample for the construction of the shoulder girdle mainly photos from displayed skeletons were used, e.g. Figures 60 & 61.

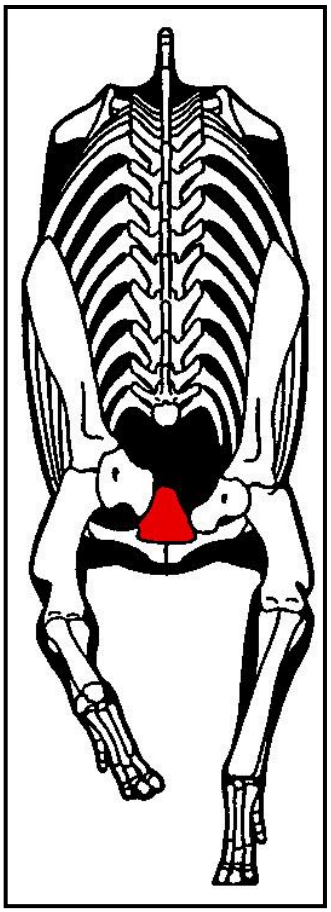

Figure 58: *Corythosaurus* postcranial skeleton from cranial view, showing the cartilage (?) plate between the coracoids (colored red) (modified after PAUL 2010).

Figure 56 (above): Shoulder girdle of the digital *Brachylophosaurus* skeleton from cranial view; scale bar = 20 cm.
Figure 57 (below): Shoulder girdle of the digital *Brachylophosaurus* skeleton in craniolateral view; scale bar = 20 cm.

Figure 59: The articulated sternals of the JRF 116H *Brachylophosaurus* specimen from dorsal view (photo by the author).

Figure 60: Shoulder girdle of a mounted *Edmontosaurus annectens* skeleton from craniolateral view, on display in the Denver Museum of Nature & Science (Colorado / USA) (photo by the author).

Figure 61: Shoulder girdle of a mounted *Edmontosaurus annectens* skeleton (cast) from craniolateral view, on display in the Black Hills Institute in Hill City (South Dakota / USA) (photo by the author).

The assembling of the forelimb (Figures 62 & 63) was quite less complicated than that of the shoulder girdle, as none of the bones had to be reworked, which increases the fitting accuracy to a high degree. Again photos of mounted hadrosaur skeletons were mainly used for the overall shape of the forelimb (Figures 64 & 65), added by photos of the Malta specimens for details, especially in case of wrist and hand (Figures 66 & 69).

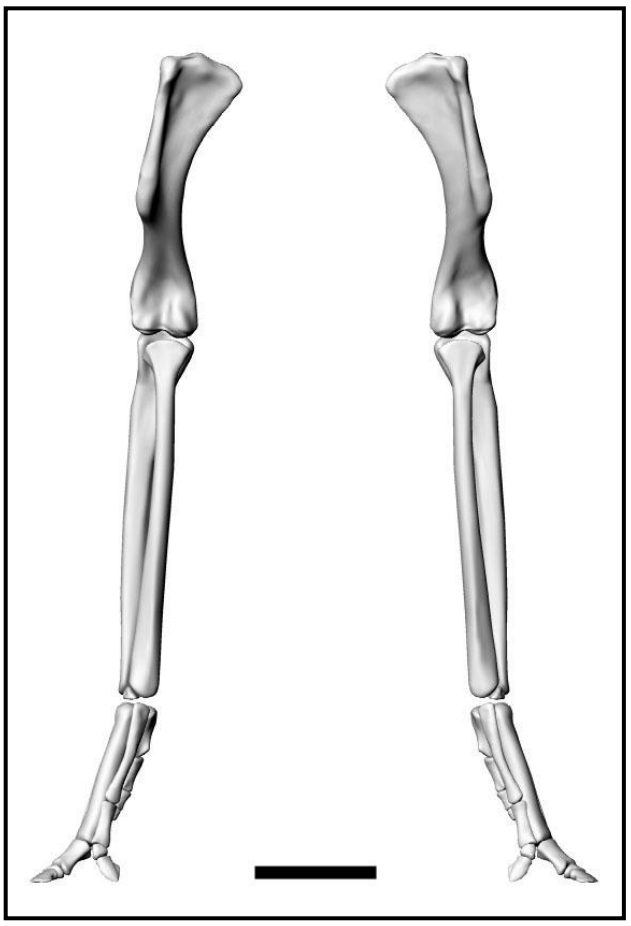

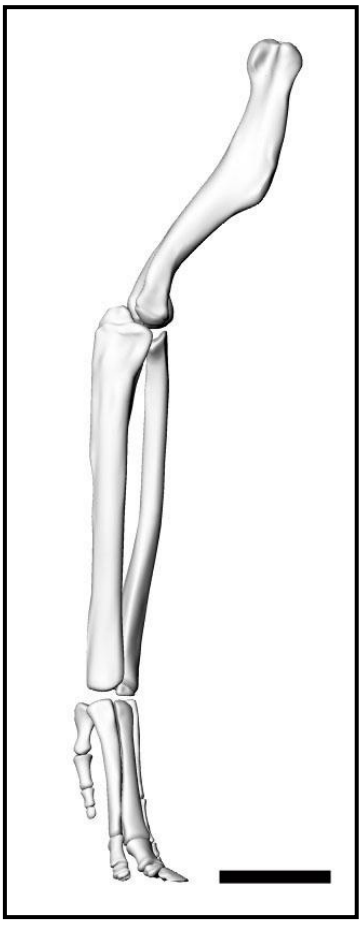

Figure 62 (left): Forelimbs of the digital skeleton from cranial view; scale bar = 25 cm.
Figure 63 (right): Right forelimb of the digital skeleton from lateral view; scale bar = 20 cm.

Although one carpal was missing and could therefore not be digitized, the wrist construction described by HARTMAN (2004) can be comprehended. When articulated, the proximal carpal sits firmly between the distal ends of ulna and radius, preventing rotation around the long axis (Figures 66 & 67). The distal carpal (the missing one) is firmly affixed to the proximal one and to radius and ulna and protrudes distally beyond the forearm. When the manus is extended, the distal carpal forms a peg and socket joint with a notch in the metacarpal row, as metacarpal III is slightly displaced distally in relation to metacarpals II and IV. Therefore, during manual extension the wrist is limited to movement in the parasagittal plane.

Figure 64 (left): Forelimbs of the mounted *Edmontosaurus annectens* skeleton from cranial view, on display in the Denver Museum of Nature & Science (Colorado / USA) (photo by the author).
Figure 65 (right): Right forelimb of the mounted *Edmontosaurus annectens* skeleton (cast) from craniolateral view, on display in the Black Hills Institute in Hill City (South Dakota / USA) (photo by the author).

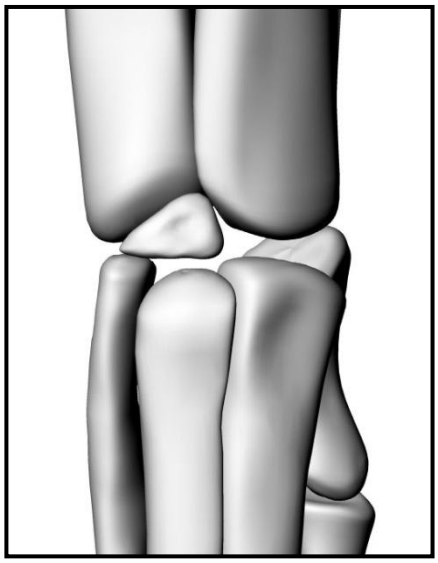

Figure 66 (left): Left proximal carpal of the JRF 200W *Brachylophosaurus* specimen from cranial view, fitting perfectly between radius and ulna (photo by H.Mallison).
Figure 67 (right): Left wrist of the digital skeleton from cranial view (without distal carpal).

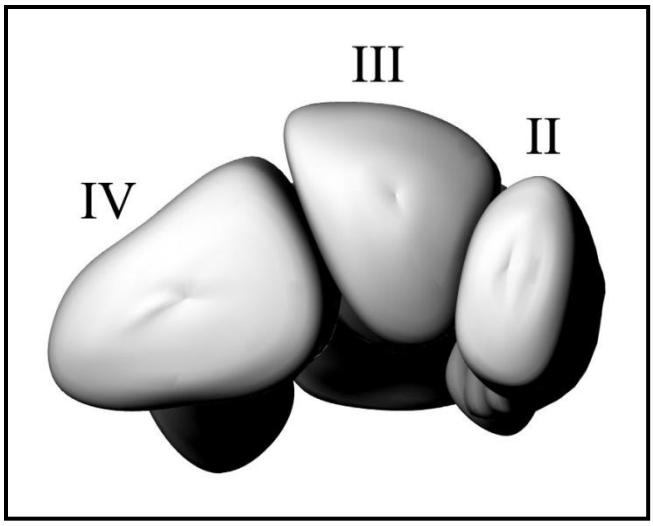

As DILKES (2001) described, are the metacarpals II-IV firmly united and articulated in an arc configuration, which was more resistant to bending than if the metacarpals were aligned in a transverse row (Figure 68).

Figure 68: Digital image of metacarpals II-IV of the left manus from dorsal view.

For the correct placement of the metacarpals the so-called mummified *Brachylophosaurus* specimen JRF 115 (called "Leonardo"), which is also displayed in Malta, was of great use, as here the metacarpals of the right hand are still articulated (Figure 69). However, for digitizing this specimen was not suitable, as the bones are mainly articulated and especially not exposed enough.

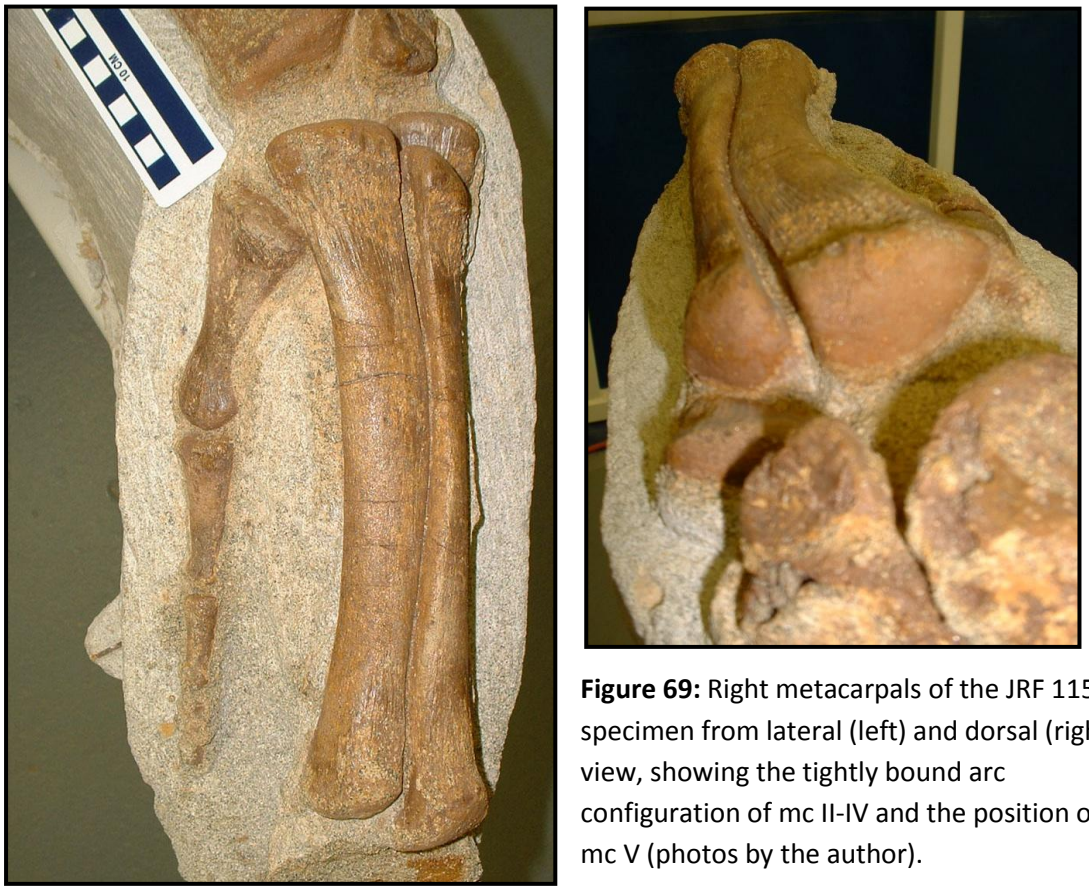

Figure 69: Right metacarpals of the JRF 115 specimen from lateral (left) and dorsal (right) view, showing the tightly bound arc configuration of mc II-IV and the position of the mc V (photos by the author).

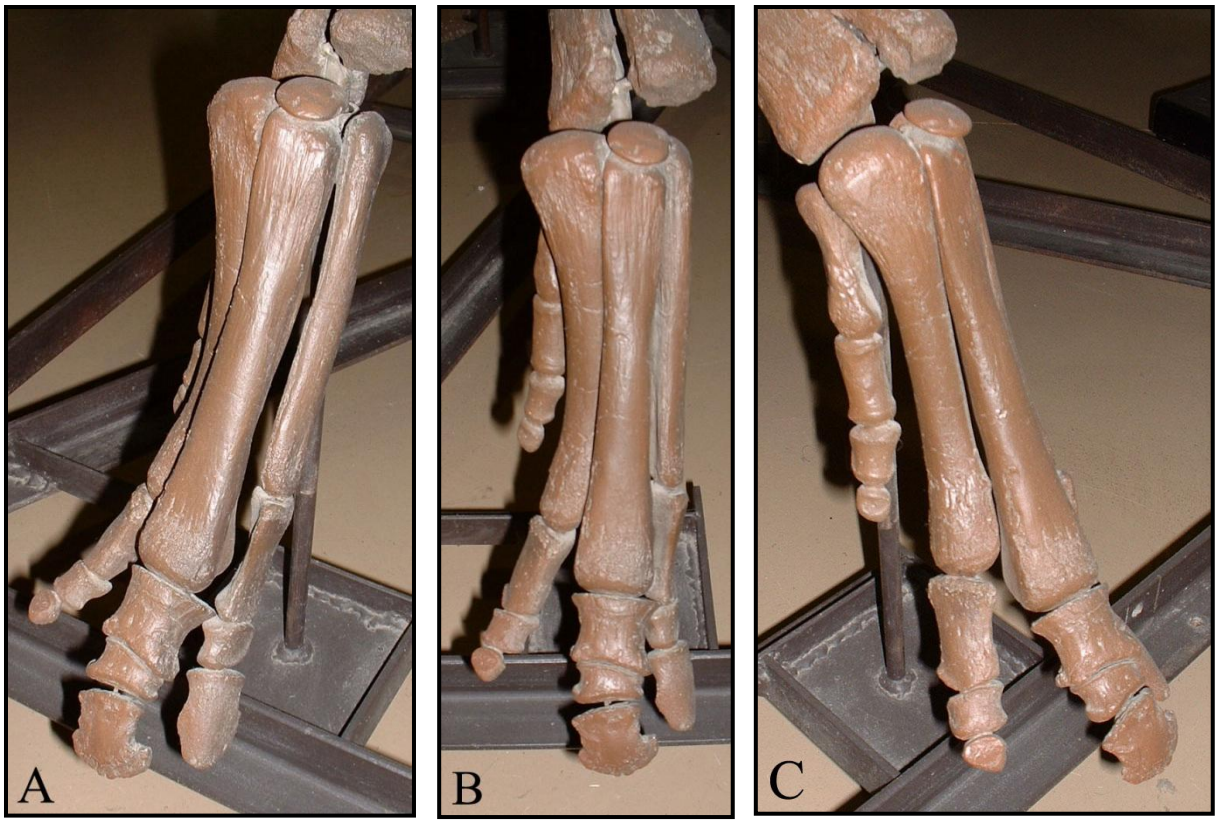

Figure 70: Right manus of the mounted *Edmontosaurus annectens* skeleton (cast) from craniomedial (A), frontal (B), and craniolateral (C) view, on display in the Black Hills Institute in Hill City (South Dakota / USA) (photos by the author). The shown carpal on top of metacarpal III might be the distal one, missing in the Malta material.

For the arrangement of the phalanges none of the Malta specimens was suitable, as no complete articulated hand skeleton was available. Therefore mounted hands from displayed skeletons had to be used (Figure 70). In addition, the articular surfaces of the phalanges allow usually a visual best fit assembling of the bones. According to the mounted skeletal hands and images (e.g. BAKKER 1986 (Figure 71); DILKES 2000) it was decided to place the metacarpals in a steeply posture, when the hand has contact to the ground.

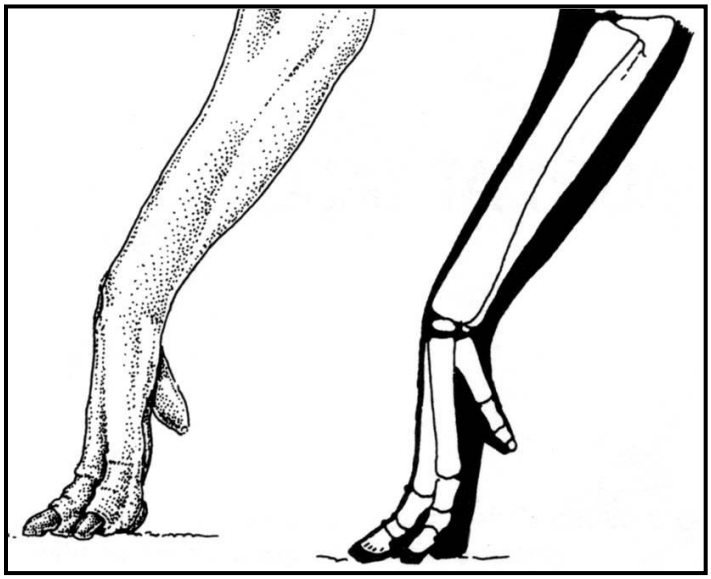

Figure 71: Hadrosaurian right lower arm and hand skeleton (right) with flesh reconstruction (left), showing the steeply posture of the metacarpals, respectively the hand (BAKKER 1986).

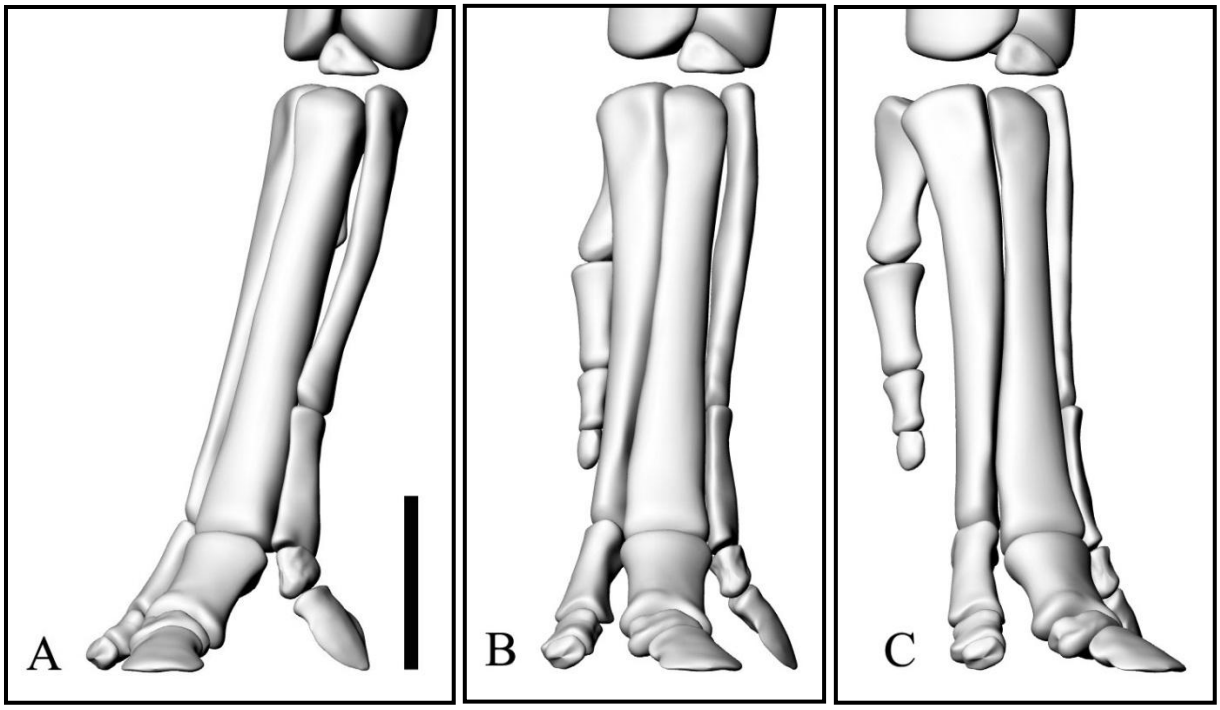

Figure 72: Digital image of the right manus of *Brachylophosaurus* from craniomedial (A), frontal (B), and craniolateral (C) view in standing pose; scale bar = 10 cm.

Concerning the *Brachylophosaurus* hand (Figure 72), the abducted posture of digit II is rather unusual. This posture bases on the wedge-shaped second phalanx, which turns the third phalanx to a more medial position. However, that this orientation of the second phalanx should be correct can be seen in the right hand of the MOR 794 specimen (Figure 73). The broader edge of the wedge-shaped bone is oriented towards digit III. Although the hand is slightly disarticulated, the orientation of the phalanx seems not to have changed during fossilization.

Figure 73: Right hand of the *Brachylophosaurus* specimen MOR 794 from medial view, showing the orientation of the second phalanx of digit II (black arrow) (photo by the author).

Since it was possible to digitize the left part of the pelvic girdle of the MOR 794 specimen (Figure 74) as a whole, its bones are already articulated. As the femur covered parts of the pelvic girdle, the pubis and ischium are incomplete in their proximal parts. However, this has no effect on the construction of the hind limb.

Figure 74: Left pelvic girdle of the *Brachylophosaurus* specimen MOR 794 from lateral view (photo by H.Mallison).

The only modification of the pelvic girdle which had to be done was to bring the distal ends of the ischia in contact (Figures 75 & 76), after mirroring the digitized left part.

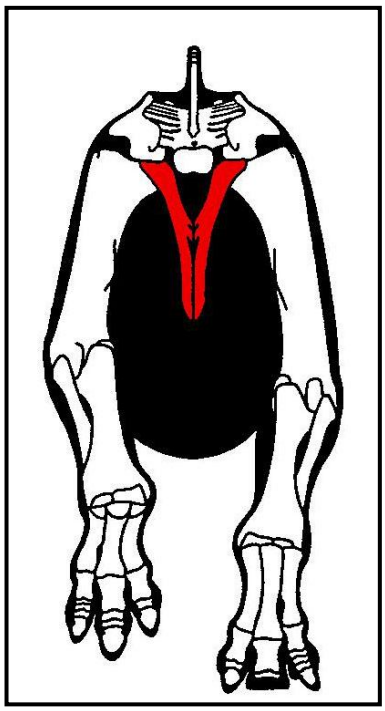

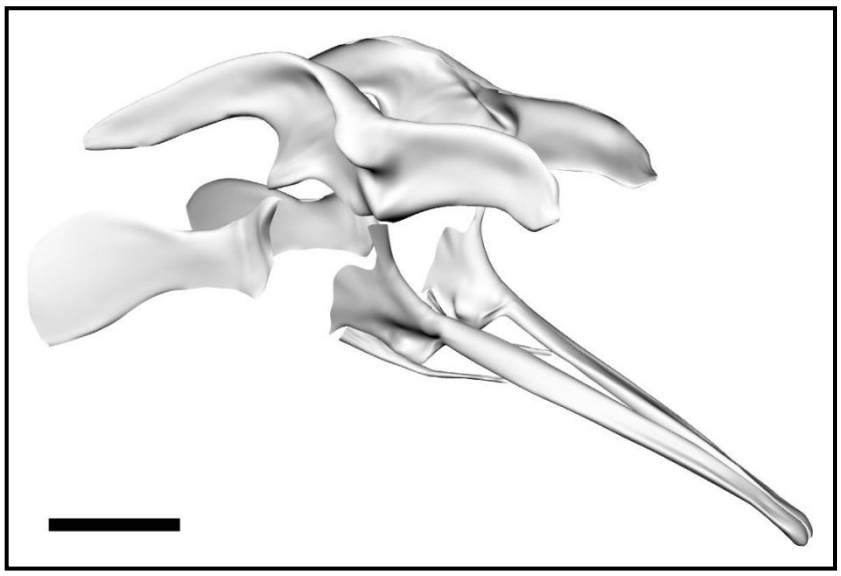

Figure 75 (above): Digital image of the pelvic girdle of *Brachylophosaurus* from caudolateral view; scale bar = 25 cm.
Figure 76 (left): *Corythosaurus* postcranial skeleton from caudal view, showing the ischia in contact (colored red) (modified after PAUL 2010).

The most difficult part in assembling the hindlimb (Figure 77) was the lower leg, due to the reworked tibia and the transformed astragalus and calcaneus (see chapter 4.2).

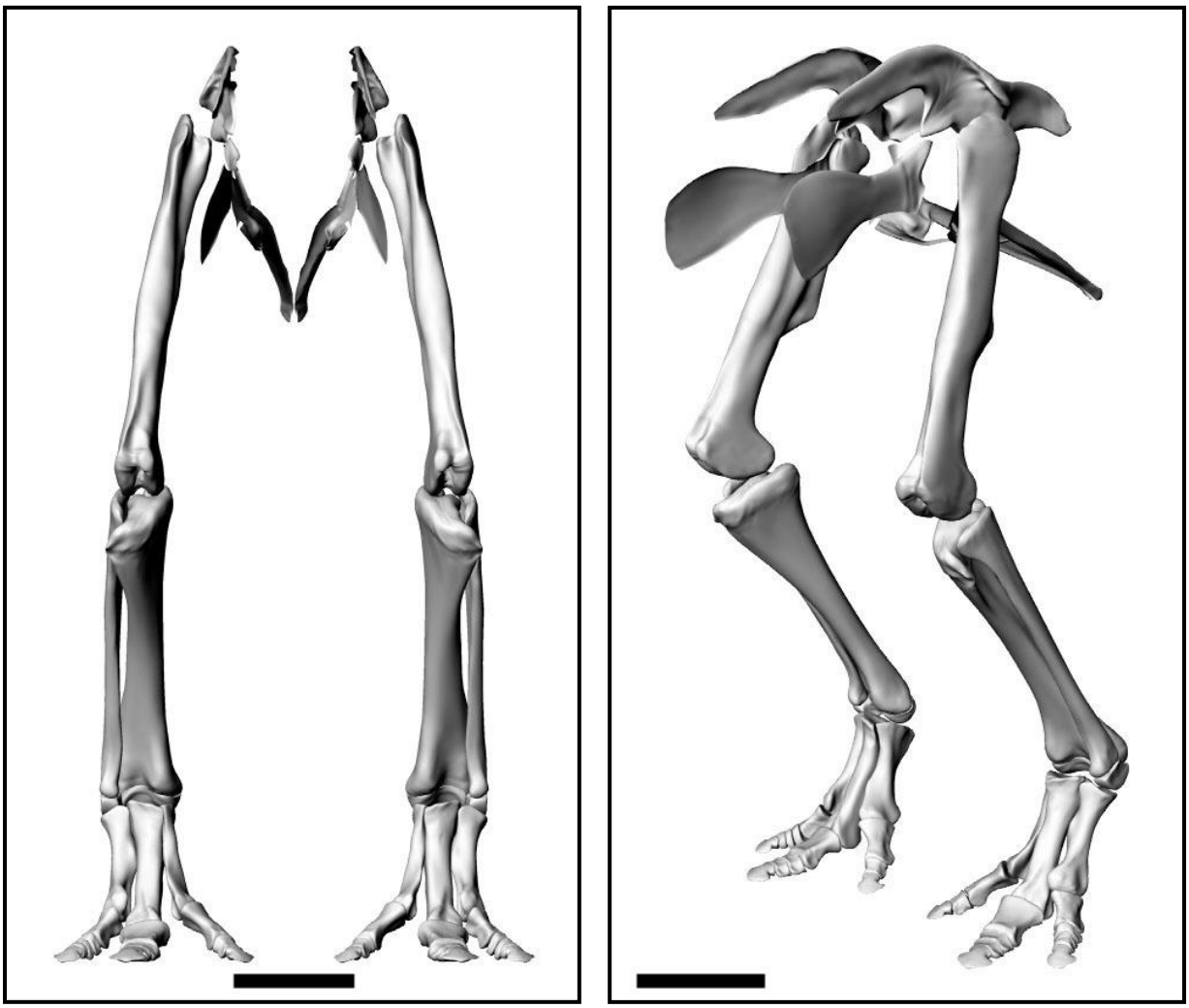

Figure 77: Hindlimbs of the digital *Brachylophosaurus* skeleton from cranial (left) and craniolateral (right) view in standing pose; scale bars = 40 cm.

Since the digitized femur cast had an incomplete femoral head, the digital copy cannot join in the acetabulum. Therefore, the position of the femoral head in relation to the acetabulum had to be estimated. In the neutral standing pose the hindlimb was assembled in a bent posture (Figure 77), as otherwise the straight forelimbs get no contact to the ground (Figures 87 & 88) and the head of the model would not looking forward, but rather be directed downwards to the ground (Figure 98). As the left lower leg of the MOR 794 specimen is still articulated (Figures 78 & 80), it provides a perfect sample for the position of the fibula in relation to the tibia in the digital skeleton (Figures 79 & 81). Astragalus and calcaneus were adapted to the shapes of the distal ends of tibia and fibula during their

transformation process, and also to the proximal ends of the three metatarsalia, using again the MOR 794 specimen and images, e.g. from BRETT-SURMAN and WAGNER (2007) (Figure 82), as samples for a correct adjustment of the two bones (Figure 83).

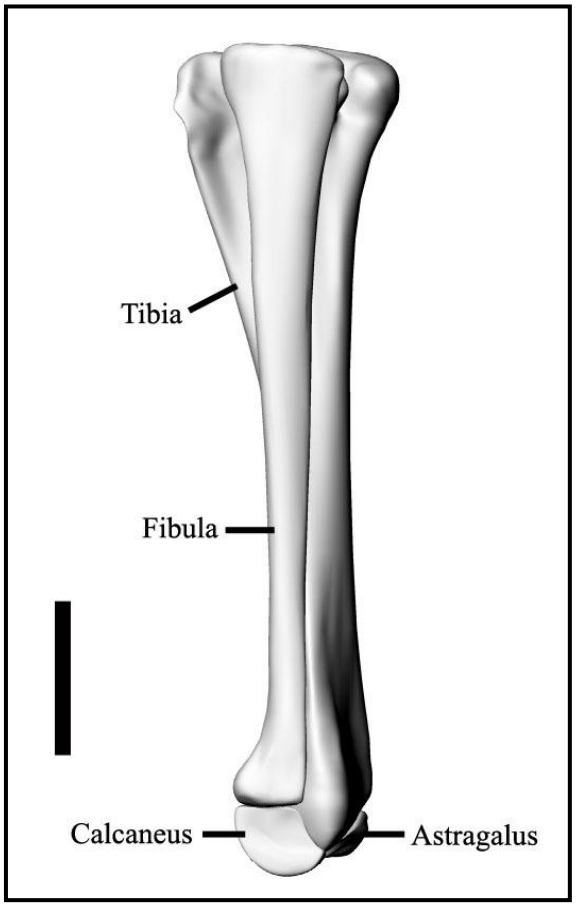

Figure 78 (left): Left lower leg of the MOR 794 *Brachylophosaurus* specimen from ventrolateral view (photo by the author).
Figure 79 (right): Digital image of the left lower leg from lateral view; scale bar = 20 cm.

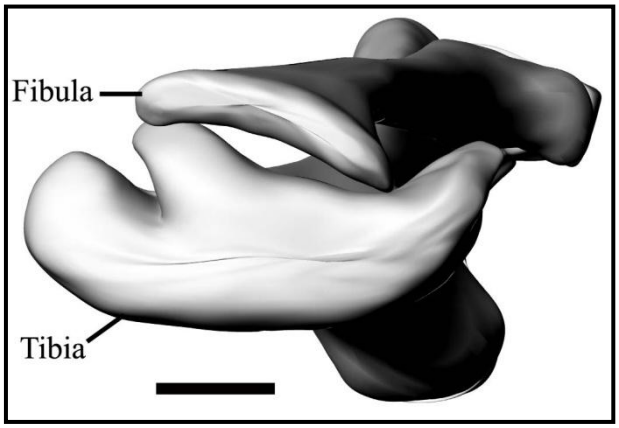

Figure 80 (left): Left lower leg of the MOR 794 *Brachylophosaurus* specimen from dorsal view (photo by the author).
Figure 81 (right): Digital image of the left lower leg from dorsal view; scale bar = 8 cm.

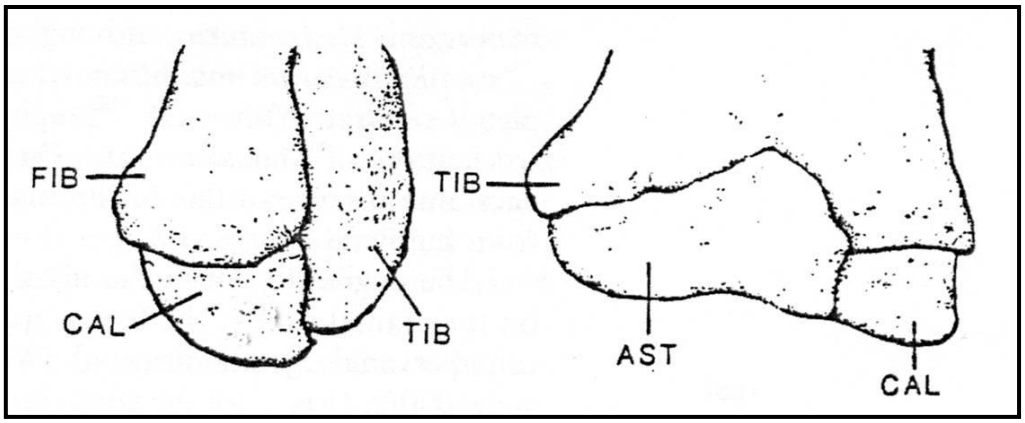

Figure 82: Distal end of the left lower leg of *Anatotitan* AMNH 5730 in lateral (left) and anterior (right) view (in the latter without fibula): TIB = tibia, FIB = fibula, AST = astragalus, CAL = calcaneus (modified after BRETT-SURMAN and WAGNER (2007)).

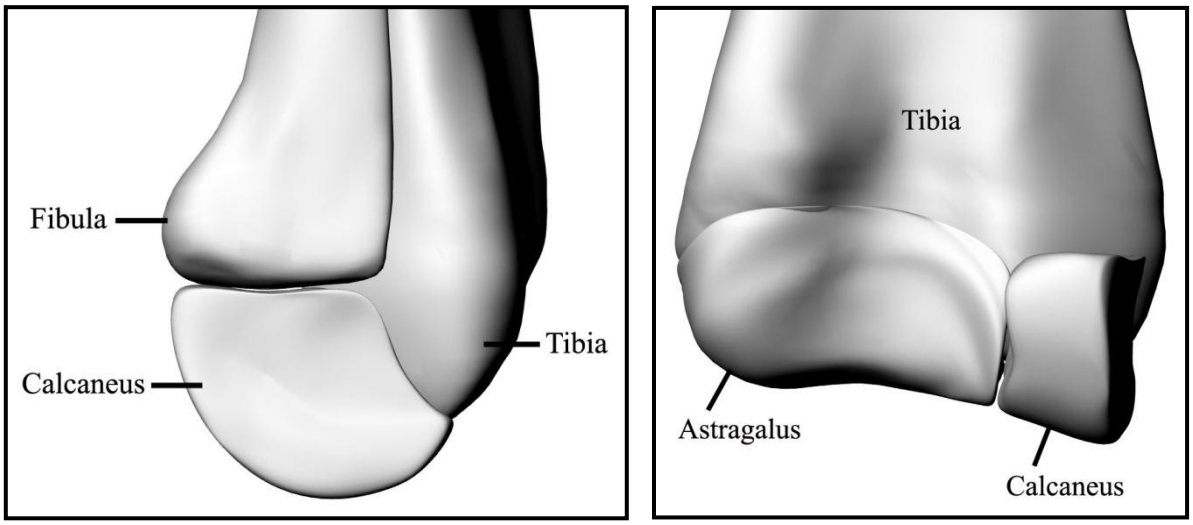

Figure 83: Digital image of the distal end of the left lower leg of *Brachylophosaurus* from lateral (left) and cranial (right) view (in the latter without fibula).

Regarding the lower leg of the digital skeleton the figures show that despite the reworked and transformed bones (tibia, astragalus, and calcaneus) the accordance with the real conditions is largely achieved.

The assembling of the pes (Figure 84) was the less complicated part of the hindlimb, as the JRF 200W *Brachylophosaurus* specimen provided the complete bone material in a good state of preservation (Figure 85). Thus, no bones have to be scaled or reworked, with exception of metatarsal III (see chapter 4.2).

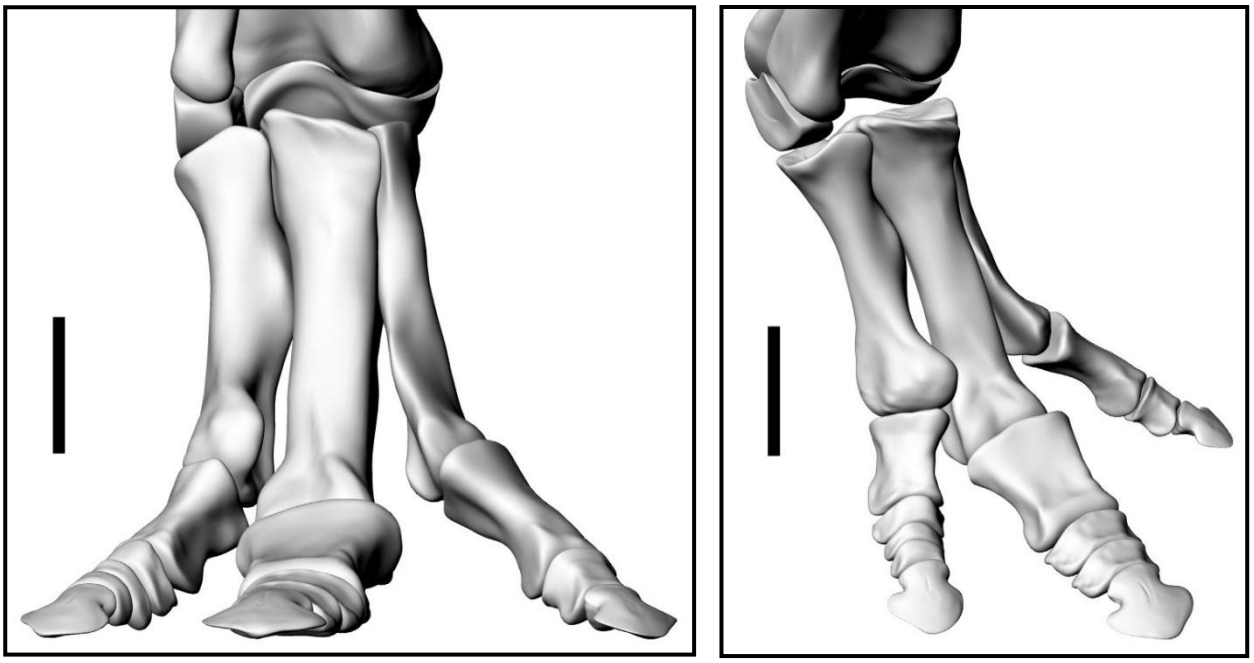

Figure 84: Right pes of the digital *Brachylophosaurus* skeleton from cranial (left / scale bar = 12 cm) and dorsolateral (right / scale bar = 15 cm) view in standing pose.

Figure 85 (left): Most bones of the right pes of the JRF 200W *Brachylophosaurus* specimen from dorsal view; phalanx I of toe III and the metatarsals are missing (photo by the author).
Figure 86 (right): Digital image of the left ankle joint from cranial view.

It can be noticed that the ankle joint of the digital skeleton seems to be inaccurate, as the proximal tarsals and the metatarsalia fit not perfectly (Figure 86). However, as it was not possible to transform the shape of the *Dryosaurus* bones to that of the original hadrosaur bones completely, and since the distal tarsal is missing, these inaccuracies were to be expected, but they are no handicap for the creation of the model or the simulations.

Finally, shoulder- and pelvic girdles as well as fore- and hindlimbs were taken together, finishing the digital skeleton (Figures 87 & 88)

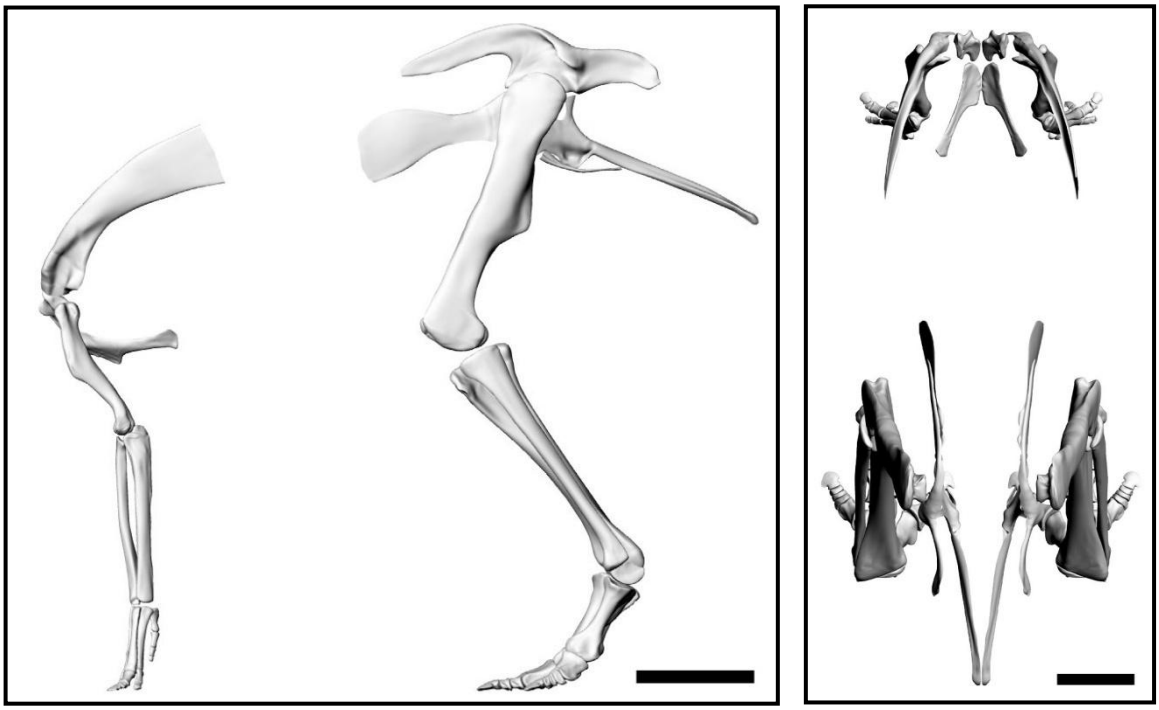

Figure 87: The digital *Brachylophosaurus* skeleton from lateral (left / scale bar = 50 cm) and dorsal (right / scale bar = 30 cm) view in standing pose.

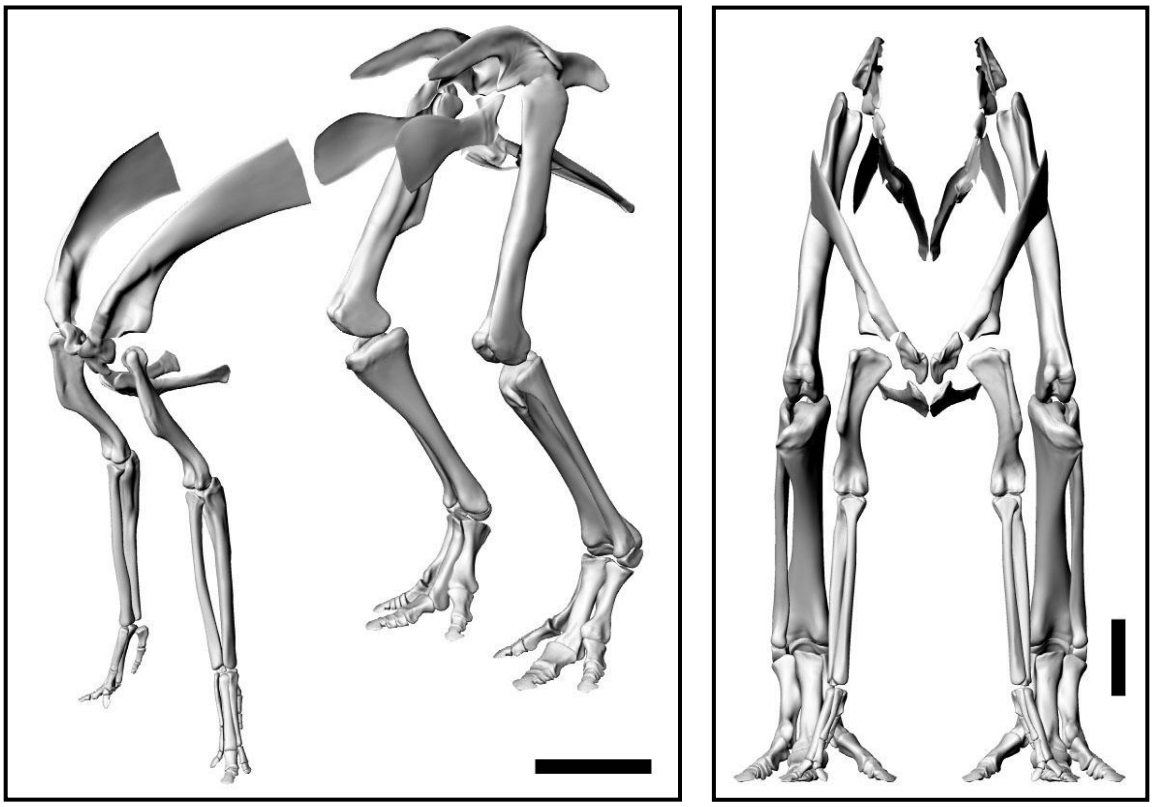

Figure 88: The digital *Brachylophosaurus* skeleton from dorsolateral (left / scale bar = 50 cm) and cranial (right / scale bar = 30 cm) view in standing pose.

4.4 Creating the hadrosaur model - the body

After the construction of the skeleton, the next working step was to create the hadrosaur body. In theory, it is possible to create the body on the basis of the digital skeleton alone, but this is rather difficult and provides a higher risk of error in soft tissue reconstruction. The use of skeletal drawings (Figures 12 & 54) alone is also not practical, as only two cross sections (Figures 58 & 76) are available, which are insufficient to build the whole body, even when they are combined with lateral and dorsal views. Here, the inaccuracies would be too high. However, in contrast to the digital skeleton, the drawings include the reconstruction of soft tissues as black outlines.

Therefore, in this work a buyable and widely detailed *Parasaurolophus* desk model (Figure 89) was digitized to get a preliminary body. Although this *Parasaurolophus* model is more accurate than a simple toy model, the use of such models is problematical (CHRISTIANSEN 2000; PAUL 1997b), and of course the model represents not the correct hadrosaur species. To get the correct species and to avoid possible inaccuracies of the digitized desk model the available skeletal drawings and the digital skeleton of *Brachylophosaurus* were used to transform the *Parasaurolophus* into a *Brachylophosaurus.* Through the combination of the digitized desk model, the skeletal drawings, and the digital skeleton the *Brachylophosaurus* model could be made quite realistic.

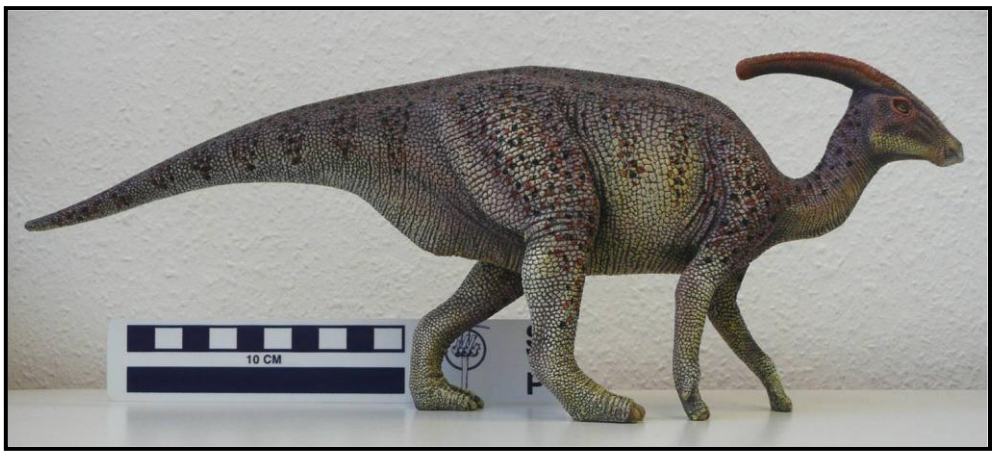

Figure 89: The *Parasaurolophus* desk model, which was digitized (photo by the author).

The *Parasaurolophus* model (Figure 90) was digitized in the same way as the bones, by 'lofting' a NURBS surface over a set of closed curves in Rhinoceros 3.0®. As the digitizing of the model was rather difficult, and cannot be repeated easily, arms and legs were also

digitized separately. Then, they were removed, as arms and legs of the *Brachylophosaurus* model were built later, according to the digital skeleton for a higher correctness.

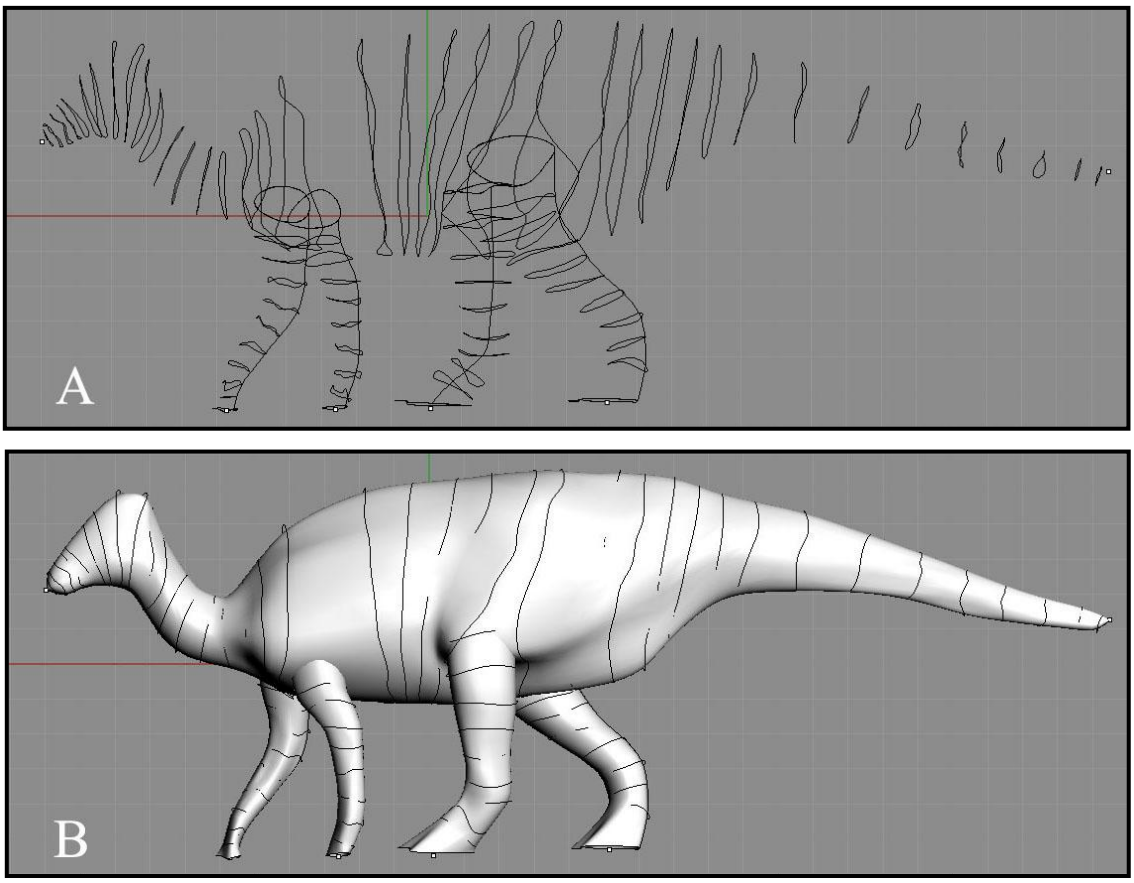

Figure 90: The digitized *Parasaurolophus* model from lateral view, showing the set of closed curves (A) and the lofted surface (B).

Now, the *Parasaurolophus* body had to be transformed into the *Brachylophosaurus* body, first by adapting its closed curves to the body outline of the skeletal drawing of *Brachylophosaurus* MOR 794 from lateral view (Scott Hartman [www.skeletaldrawing.com]) (Figure 91), which can be placed as background image in Rhinoceros 3.0®. Ideally, also skeletal drawings from other views should be considered, but for *Brachylophosaurus* no other ones are available. Therefore, the trunk width had to be adapted to the bones alone, whereas the width of head, neck, and tail was mainly retained from the *Parasaurolophus* model. The curves were edited by their control points (see chapter 4.1 and chapter 4.2).

Despite the fact that most of the digitized bones belong to the JRF 200W specimen, and that the other bones were scaled to that size, it was decided to use the skeletal drawing of the MOR 794 specimen for the transformation of the *Parasaurolophus* body, as this reconstruction bases on a more complete skeleton as in the case of the JRF 200W specimen.

It is advisable to arrange the input data in Rhinoceros 3.0® in a way that the long axis of the model is parallel to one of the axes of the coordinate system. This makes one of the program's construction planes perpendicular to the long axis, which is helpful for creating the model (Figures 92 & 93) (MALLISON 2007).

It is possible to create separate objects for separate body parts. It must be decided whether the arms and legs are to be created as separate objects or together with the trunk. Creating separate legs is advisable, as curves perpendicular to the long axis of the created element give the best control over the shape of the object. The trunk can also be created as several objects, but this is usually not recommendable. Separate objects can lead to kinks at the contact lines, which require further time consuming editing to remove them. An exception can be the head, especially in those cases where a large head is connected to the trunk by a narrow neck. Here, lofting may produce artifacts due to the strong change of shape respectively geometry (MALLISON 2007).

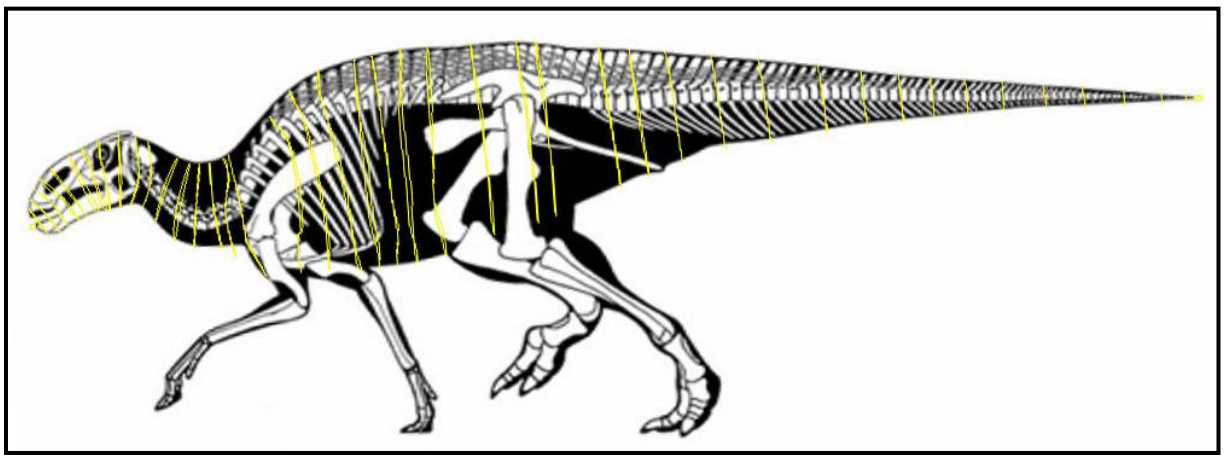

Figure 91: The skeletal drawing of *Brachylophosaurus* MOR 794 with soft tissue reconstruction from lateral view [www.skeletaldrawing.com]. The closed curves of the *Parasaurolophus* model are already adapted and colored yellow for better visibility.

After adapting the closed curves to the skeletal drawing of *Brachylophosaurus*, the curves had to be scaled to the scale of the bones, to allow the combination of the curves, respectively the body surface, with the digital skeleton in Rhinoceros 3.0®. First, the skeletal drawing (as background image) is scaled up to the digital skeleton and then the closed curves are scaled to the image (Figure 92). After finishing this process, the background image can be deleted (Figure 93).

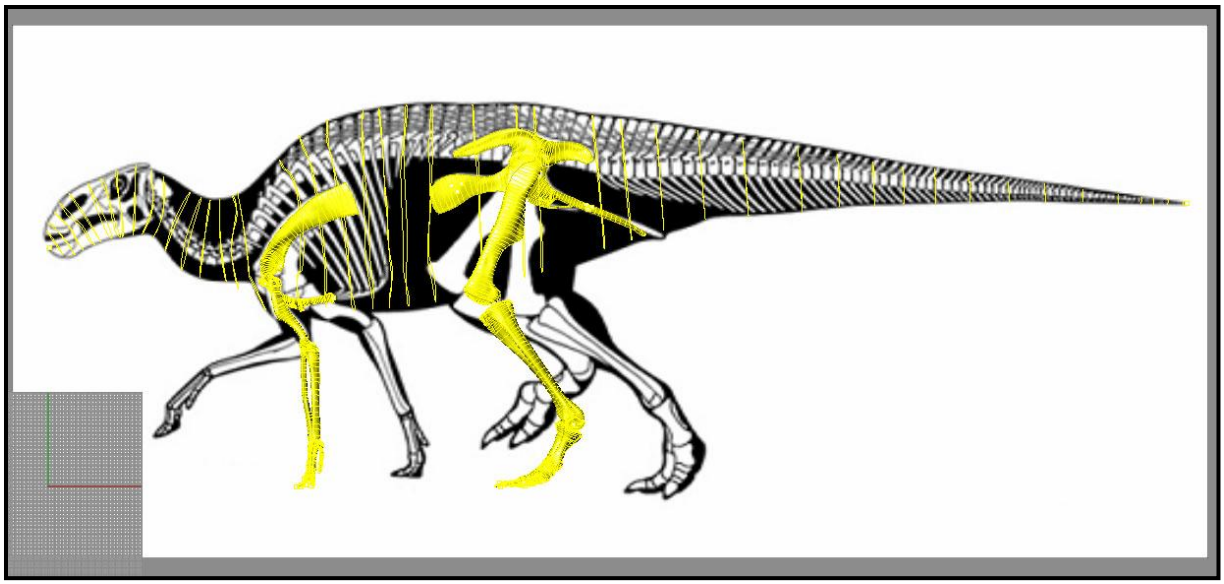

Figure 92: The combination of the closed curves, respectively the body surface, with the digital skeleton from lateral view. Compared to Figure 91 the background image was slightly rotated to match to the neutral standing pose of the skeleton.

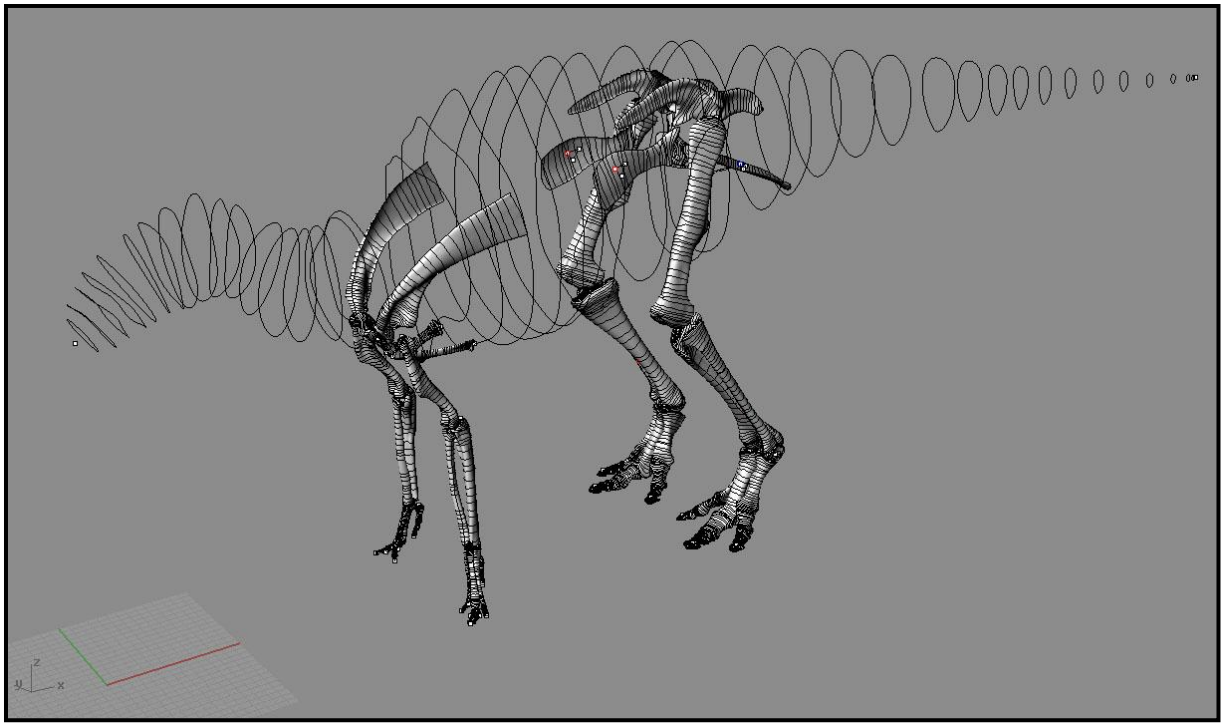

Figure 93: The closed curves together with the digital skeleton from dorsolateral view. Note that the long axis of the model is placed parallel to the x-axis of the coordinate system in Rhinoceros 3.0®.

When the adaptation and scaling of the closed curves were finished, they were lofted to generate the body surface (Figure 94). It was possible to loft the complete body as a whole. The long axis of the generated body surface shows the seam line, where the surface

starts and ends, as well as several auxiliary lines, which were generated by Rhinoceros 3.0® for lofting, due to the size and complexity of the model surface.

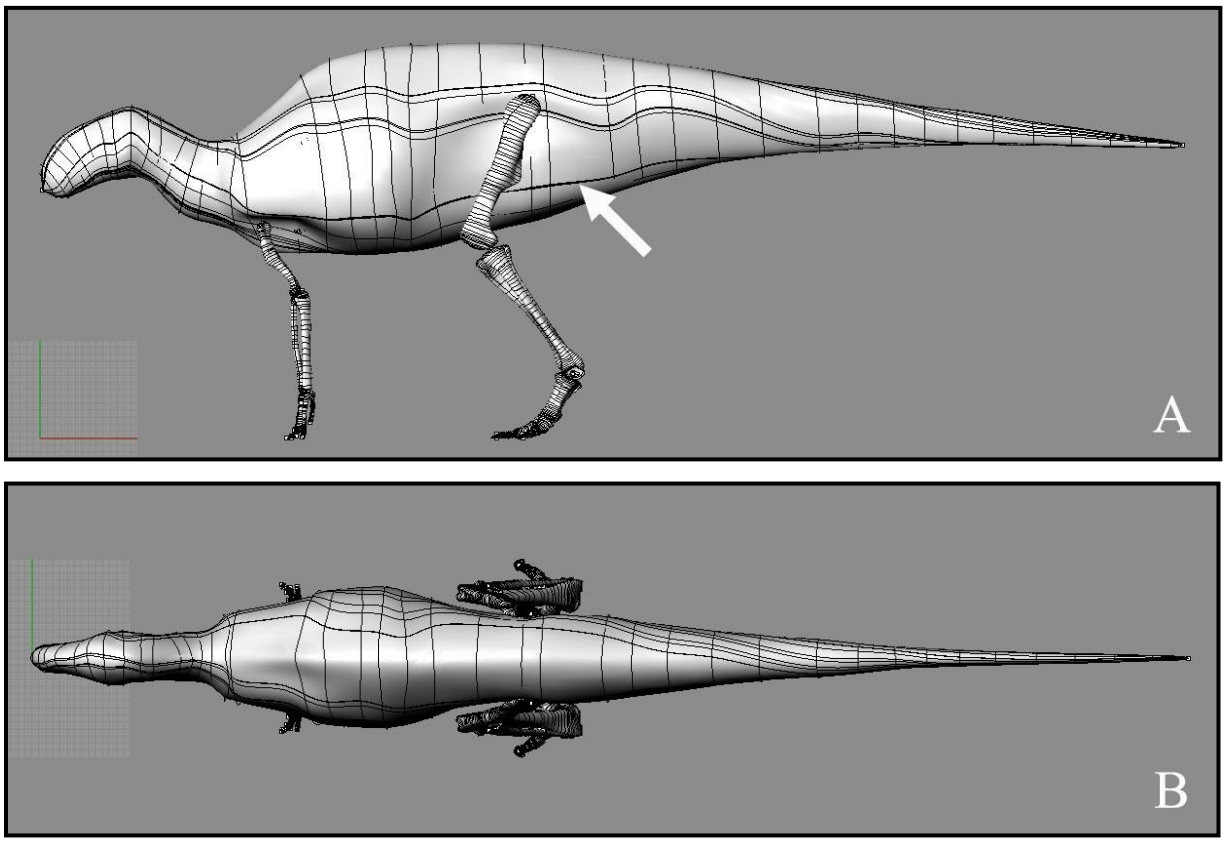

Figure 94: The *Brachylophosaurus* model from lateral (A) and dorsal (B) view, showing the lofted body surface. The white arrow marks the seam line of the generated surface; the other lines which run along the body are auxiliary lines, generated for lofting by the program.

The next working step was to construct the surfaces of arms and legs, also by using closed curves (Figure 95 A). However, these curves based not on digitized ones as in case of the body, but were generated in Rhinoceros 3.0® and edited by their control points. The creation of arms and legs was made mainly according to the bones, but also with the help of available muscle reconstructions of hadrosaurs (e.g. LULL and WRIGHT 1942; PAUL 1987). However, freehand body modeling using closed curves is rather limited, so that the shape of arms and legs is kept more basic. Also, a detailed study and modeling of hadrosaur musculature was beyond the scope of this work. After generating and editing the closed curves of arms and legs, they were lofted to get the surfaces (Figure 95 B).

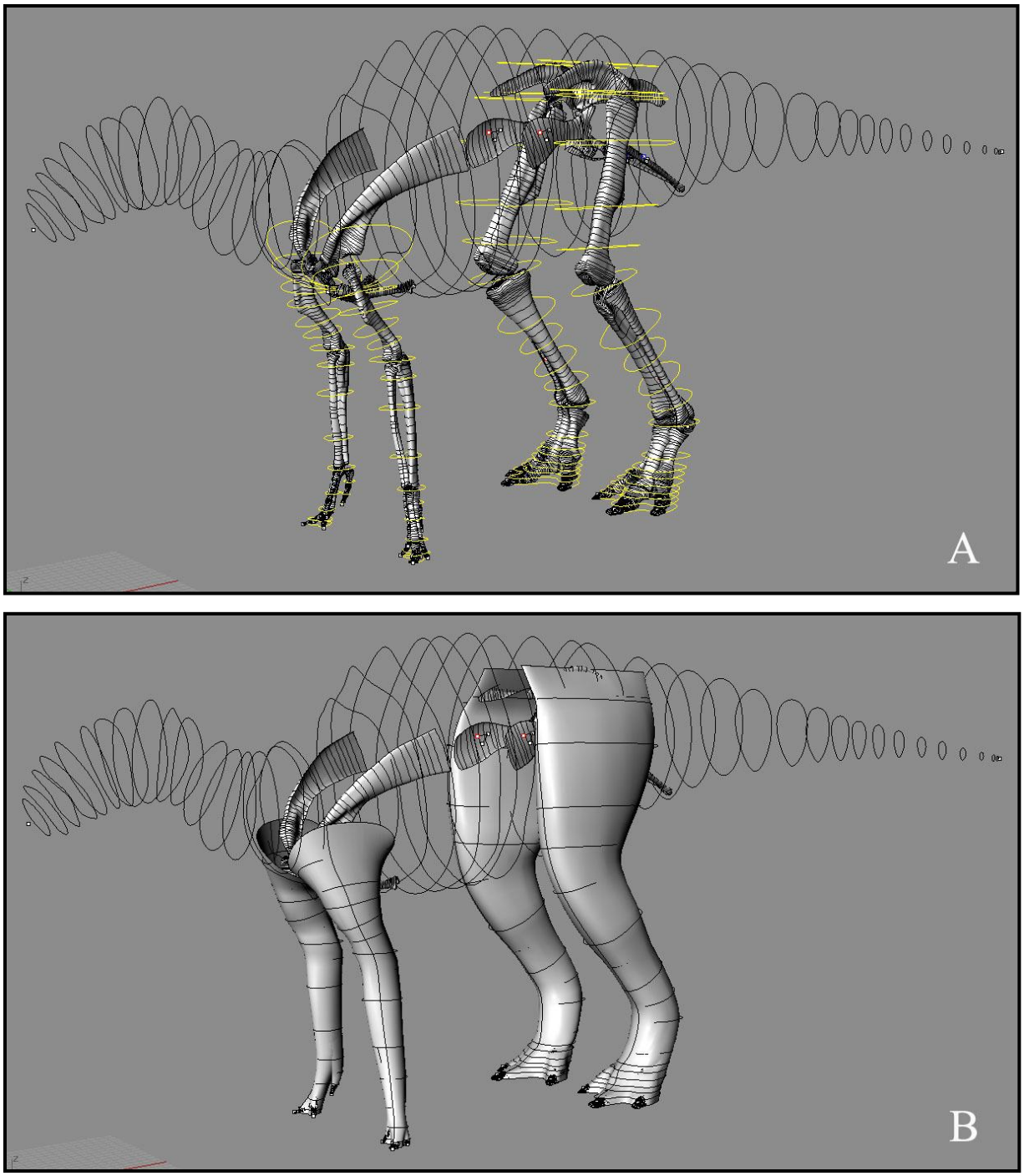

Figure 95: The closed curves (marked yellow), which build up the surfaces of arms and legs (A); the finished arms and legs after lofting the closed curves (B). Both images from craniolateral view.

Concerning the hand, it was not possible to include digit V when lofting the arm surface, as this digit is too much separated from the other ones. Therefore, it got a surface on its own (Figure 96). Through this separation it was necessary to omit digit V when replacing the NURBS surface with a rigid polygon body and cutting the arm into functional units. However, as digit V of the hand plays no role in locomotion, this exclusion has no influence on the simulations.

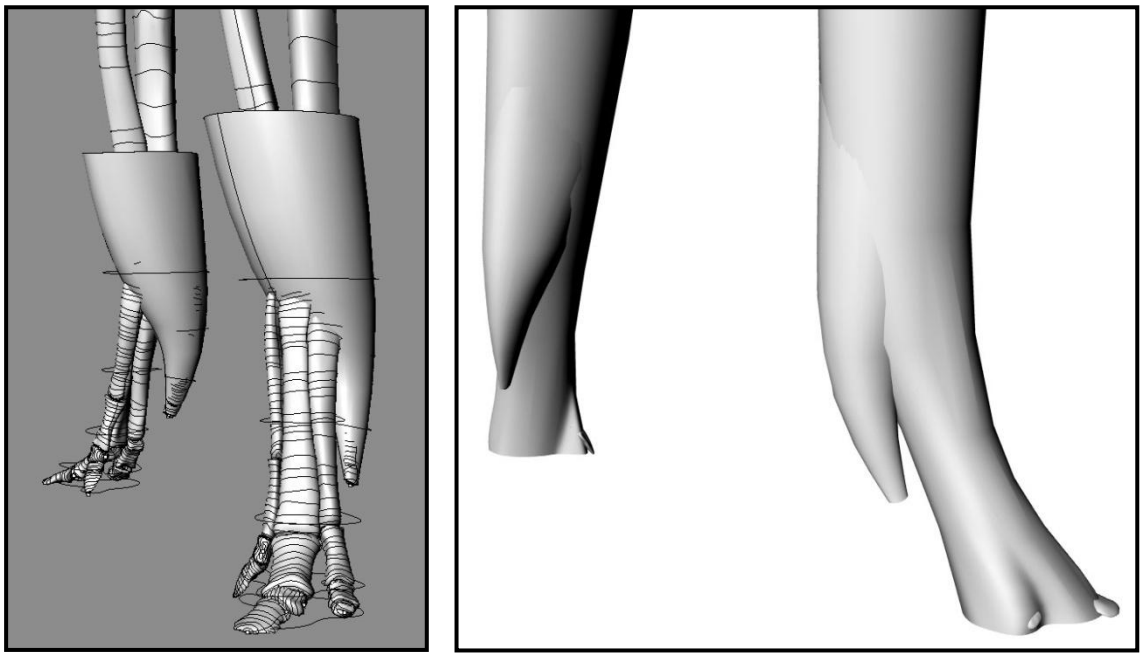

Figure 96: The separate lofted surfaces of digits V of the hands: without lofted arm surfaces (left) from craniolateral view and with lofted arm surfaces (right) from caudolateral view.

With the surface lofting of arms and legs the creation of the NURBS model in Rhinoceros 3.0® was finished (Figures 97 & 98).

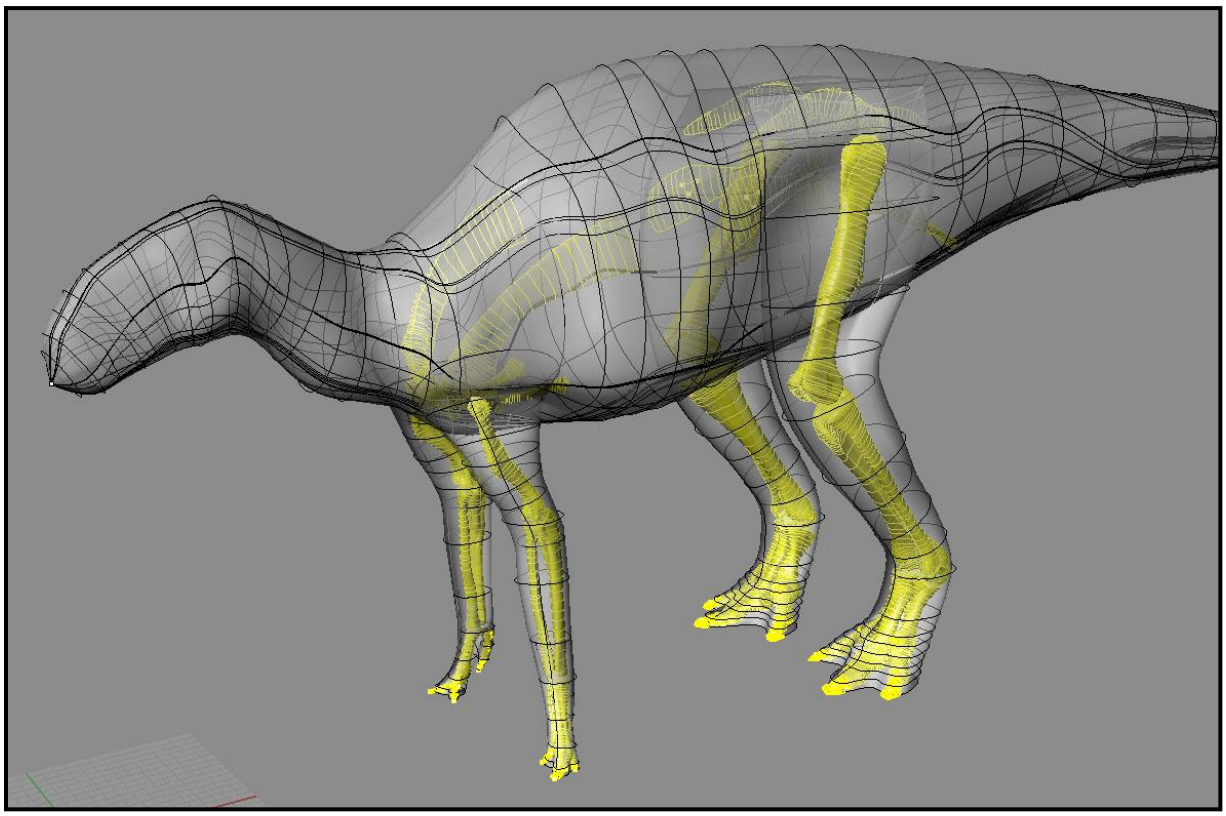

Figure 97: The finished *Brachylophosaurus* NURBS model in semi-transparent view from dorsolateral view.

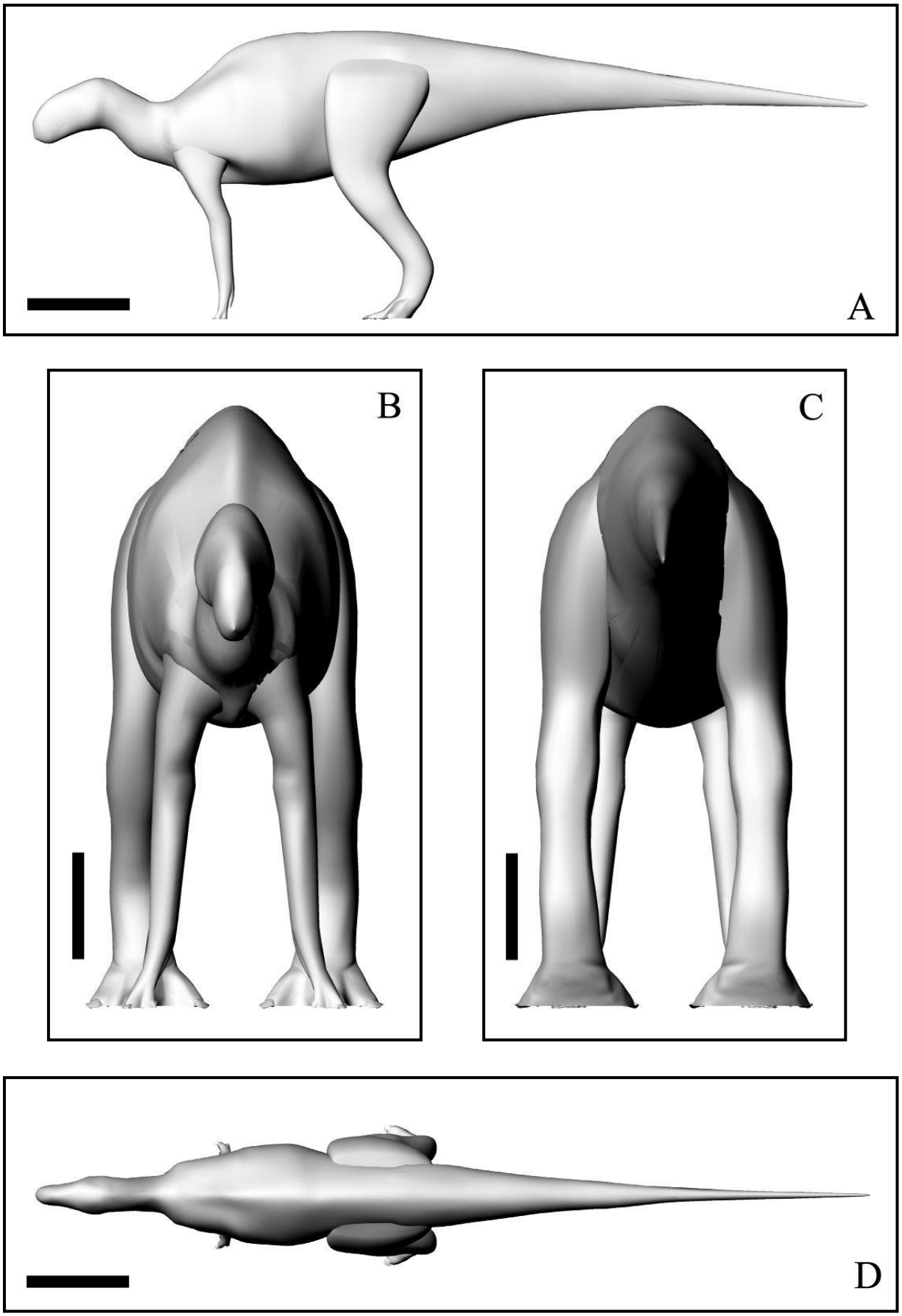

Figure 98: The finished *Brachylophosaurus* NURBS model from lateral (A), cranial (B), caudal (C), and dorsal (D) view; scale bars A & D = 100 cm, scale bars B & C = 50 cm.

When the creation of the *Brachylophosaurus* model as NURBS object was finished, the bones were removed and the following working steps were done with the NURBS model alone. A further use of the bones in the simulations, e.g. in combination with muscles and tendons, was not possible, as the required computing time and power would have been too high and the realization would have been too time-consuming.

Since the NURBS object respectively model is no solid body, it cannot be used in MSC.visualNastran 4D®. Therefore, it had to be transformed into a polygon body, which was done using the Geomagic Qualify 8.0® program. First, the complete NURBS object / model (including arms and legs) was exported as stereolithography binary file (*.stl) and imported in Geomagic Qualify 8.0®. Through this transfer the NURBS object can be changed into a polygon body. Now, the polygon body can be reworked in Geomagic Qualify 8.0®. The reworking includes for example the fill of holes, polygon reducing, or polygon smoothing. After that, the model was cut along its long axis in two halves and one half was deleted. The remaining one was ex- and imported as polygon body from Geomagic Qualify 8.0® back in Rhinoceros 3.0® (as *.stl file). Here, the model half was mirrored to get again a complete polygon body (Figure 99). This procedure is necessary to ensure that right and left half of the model are actually uniform, as otherwise problems in the simulations can arise. The cutting of the polygon body was done in Geomagic Qualify 8.0®, as the process here is less complicated than in Rhinoceros 3.0®.

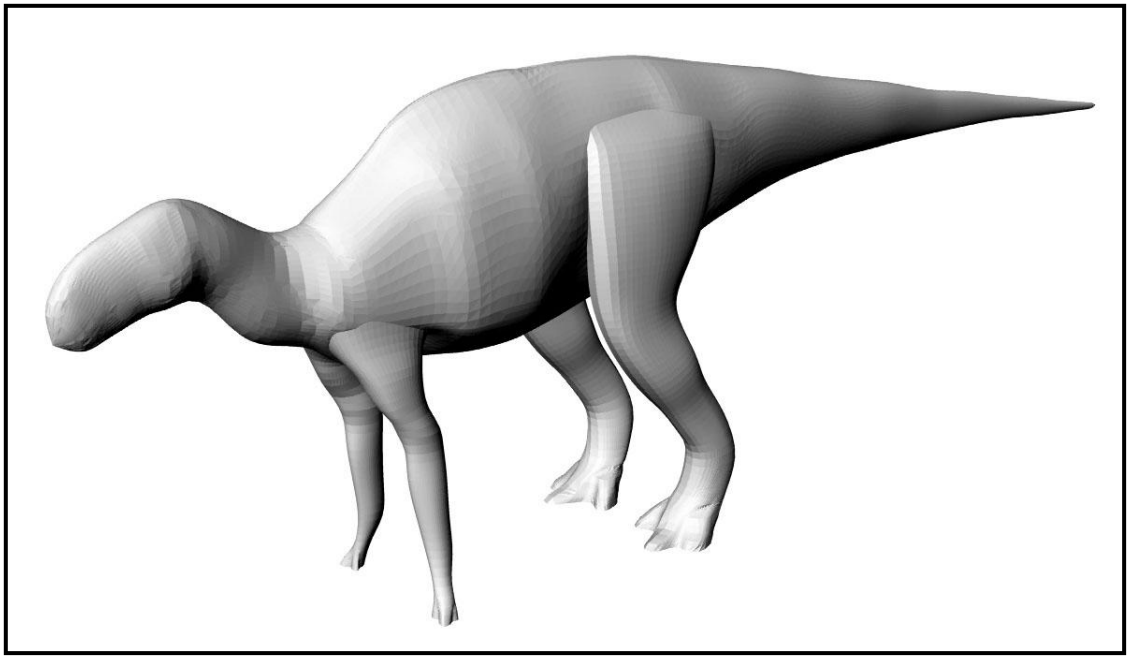

Figure 99: The symmetrical *Brachylophosaurus* polygon model from dorsolateral view; digits V are already omitted.

To allow motion, the symmetrical polygon model can now be sectioned into separate body parts respectively functional units. It is advisable to limit the number of body segments with regard to computing time and power, but as the vertebral column of back, sacrum, and especially the tail of hadrosaurs is stiffened by ossified tendons (see chapter 2.1), the range of motion of trunk and tail is rather limited anyway. Therefore, higher numbers of body sections are not needed so that head and neck as well as the trunk consist of only three segments each and the tail was not sectioned at all. The segmentation of the trunk was actually not necessary, but has been done as precaution, because at a later time sectioning would have been cumbersome.

The body sections of head, trunk, and tail (Figure 100) are named 'head' (A), 'anterior neck' (B), 'posterior neck' (C), 'shoulder' (D), 'body' (E), 'hips' (F), and 'tail' (G). Again, the body sections were cut and reworked in Geomagic Qualify 8.0®. When filling the holes of the separate body sections, each body is also closed on its front and back side, which transforms it from a tube to a solid body. The same process was done with the sections of arms and legs, in which the open dorsal and ventral sides of each body were closed.

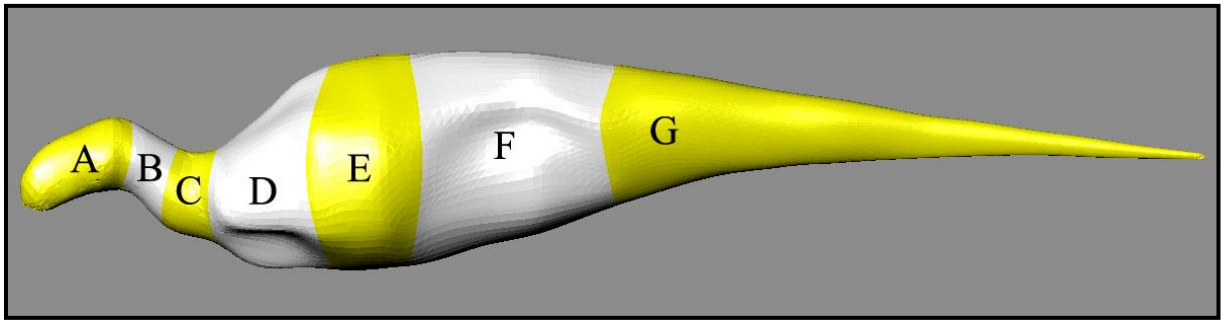

Figure 100: The polygon body from lateral view, showing the body sections.

For arms and legs the sectioning is predetermined by the articulation surfaces. The sections are named 'upper arm' (H), 'forearm' (I), 'hand' (J), 'upper leg' (K), 'lower leg' (L), and 'foot' (M) (Figure 101). In most simulations hand and foot were not more separated, as for example the grasping function of the hand was not needed here. Also, it was expected that a more detailed sectioning of hand and foot would increase simulation complexity and computing time. However, the foot was more sectioned in some simulations with the parts 'foot' (N), 'Mt II'(O), 'Mt III'(P), and 'Mt IV'(Q) (Figure 102), to allow retraction of the toes when moving the foot forward.

Arm and leg of one body side were cut in Geomagic Qualify 8.0®, and afterwards they were mirrored in Rhinoceros 3.0® to achieve also uniformity of the extremities of both body sides. After that, the *Brachylophosaurus* polygon model with its separated solid body parts (Figure 103) was finished and ready for use in MSC.visualNastran 4D®.

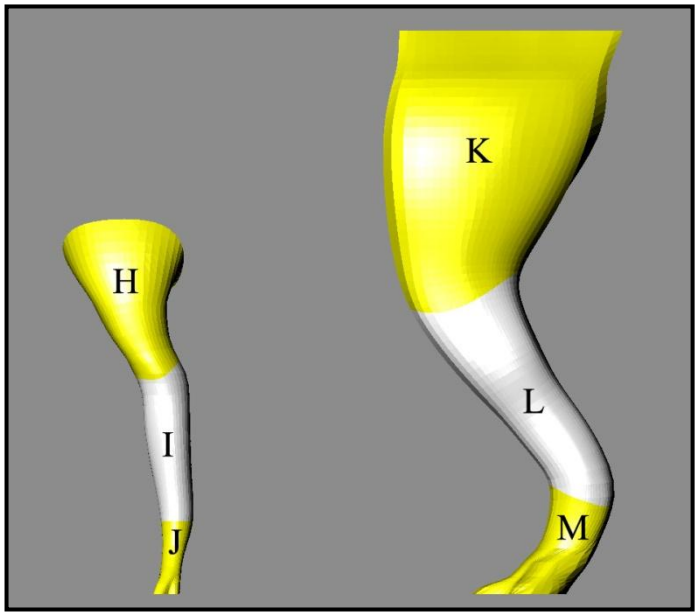

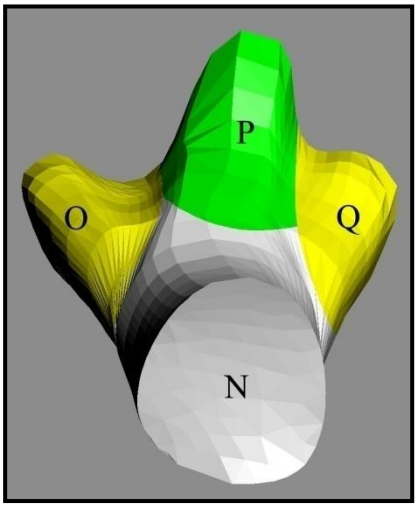

Figure 101 (left): Left arm and leg of the polygon model from lateral view, showing the different sections.
Figure 102 (right): Right foot of the polygon model from dorsal view, showing the sectioning which was used in some of the simulations to allow retraction of the three toes.

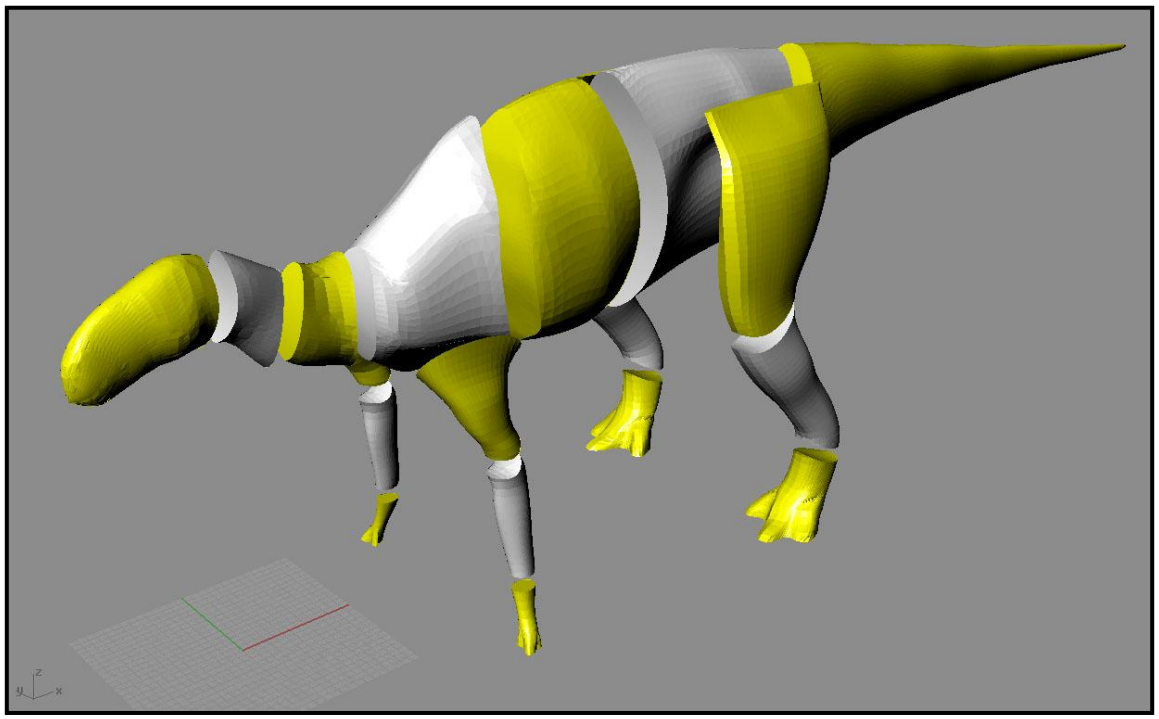

Figure 103: The polygon model from dorsolateral view, showing the separated solid body parts.

4.5 Running simulations

The software NASTRAN is a general purpose finite element analysis (FEA) program, which was originally produced by NASA and mainly written in FORTRAN. NASTRAN provides a variety of engineering problem-solving requirements, in contrast to other more specialized programs, which concentrate on particular types of analysis (MALLISON 2007).

MSC.visualNastran 4D® is a commercially available software package based on NASTRAN that can be used for kinetic/dynamic modeling for 3D body assemblages and finite element analysis (FEA). As all other NASTRAN versions, the program handles only rigid bodies. Rigid bodies will not deform or break apart during a simulation, even though a physical object, that is the subject of simulation, may actually do so (MALLISON 2007).

MSC.visualNastran 4D® solves problems by using a variety of sophisticated numerical methods. Problems are time-discretized so that MSC.visualNastran 4D® computes motion and forces, while making sure that all the constraints are satisfied. With its systematic approach MSC.visualNastran 4D® is able to model a huge variety of problems, using numerical integration. Both the fast and simple Euler integration with fixed integration intervals and the more accurate Kutta-Merson integration, that allows variable time steps, are available in MSC.visualNastran 4D®. In this work only Kutta-Merson was used, which requires significantly more computing power than the Euler integration (MALLISON 2007).

In MSC.visualNastran 4D® a model is build up by a set of 3D objects or bodies, which are referred to in the program as bodies. They can be imported into MSC.visualNastran 4D® from any CAD program, here from Rhinoceros 3.0®. Again stereolithography binary files (*.stl) were used as transfer format (MALLISON 2007).

To an imported body values for a large number of physical properties can be assigned. In the following, these values are described which were either used in this work, or could potentially influence locomotion analyses, but were not changed from the default settings:

- Central inertia: ‘uniform’, the default value, was selected for all bodies in the model.
- Contact: the user can define how the program handles collisions between bodies. The default model is based on an impulse/momentum model, for which the user can define the coefficient of friction and restitution.

- Material: material properties can be assigned. MSC.visualNastran 4D® offers a wide range of presets for materials that are used in industrial applications. From the values that can be set only density was adjusted in this work.
- World position: the relative position of a body can be defined in x, y, z and rx, ry and rz (rotation around x, y and z axes).

Each body has a specific coordinate system. The relative position of this coordinate system versus the general 'world' coordinate system of the program is defined by the position of the body in the CAD program (MALLISON 2007).

In MSC.visualNastran 4D® bodies can be connected to one another with constraints, and meters can be attached to their center of mass. In addition, inputs can be defined for various values such as position, speed etc. To define where exactly a constraint or meter is to attach to the body, a coordinate must be placed on the body (Figure 104).

A coordinate is positioned via values for the position on the object (x, y, z) and its rotation versus the object coordinate system (rx, ry, rz), or by the same values in the 'world' coordinate system (Figure 104).

Forces can be applied at any desired point via a coordinate. The direction is controlled by defining force values for each axis. The applied force for each axis itself can be controlled by a formula.

An input allows to enter numerical data into MSC.visualNastran 4D®. The input type 'table' allows the user to define time steps and the input variable at each time step. In addition to tables, it is possible for many features in MSC.visualNastran 4D® to specify mathematical formulae as input.

While a simulation is in progress, many values can be measured in meters. A meter is attached either to a body or constraint. In the first case it refers to the center of gravity of the body, in the second to the 'base' coordinate of the constraint. The data of a meter is displayed in a separate window as a digital value for each measured parameter or as graph (MALLISON 2007).

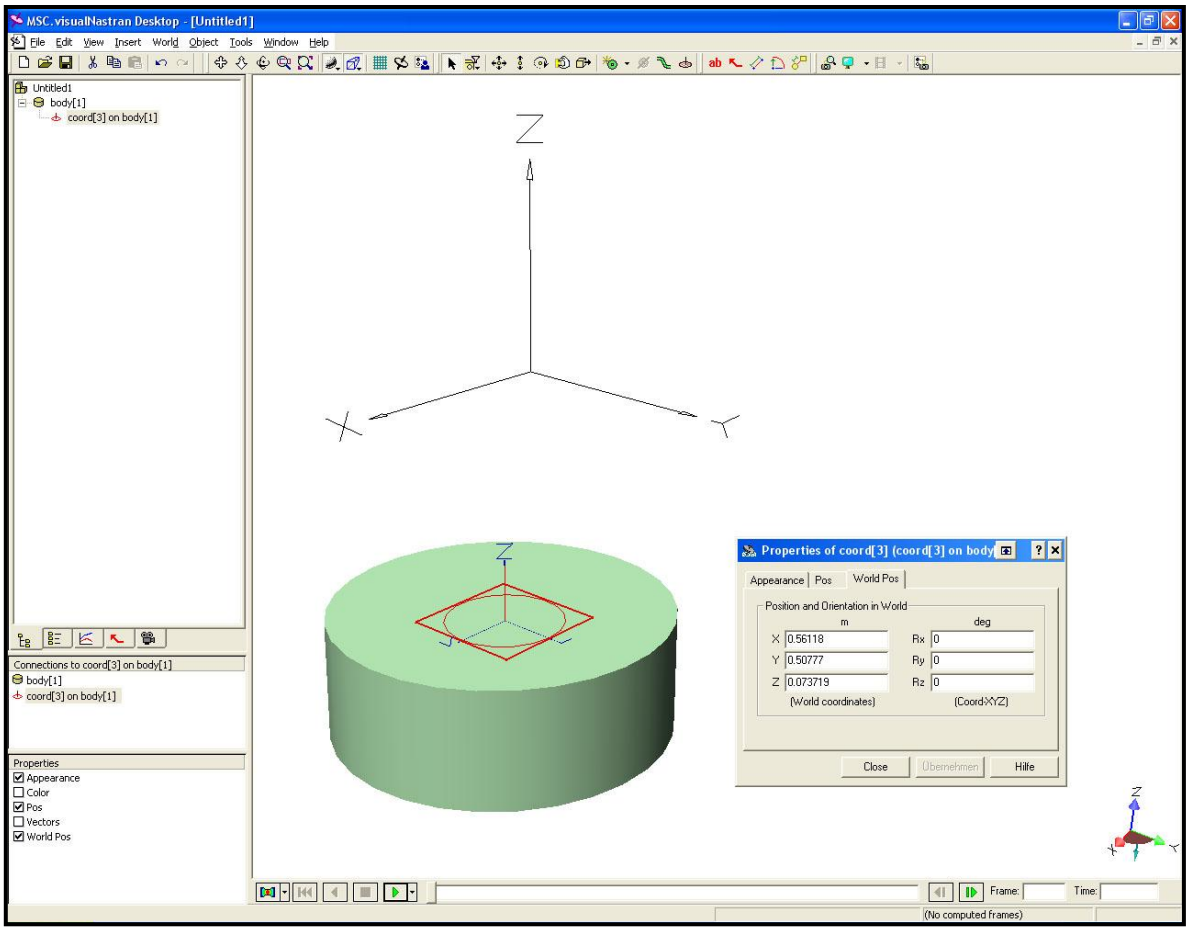

Figure 104: Screenshot from the MSC.visualNastran 4D® program, showing a coordinate attached to a body with opened properties window and positioning values in the 'world' coordinate system.

Constraints are connections between two coordinates. One coordinate on one of the two bodies is the 'base' coordinate, defining the axes of the constraint. The other coordinate on the second body may be aligned to the 'base' by the program at the creation of the constraint. This is necessary if the constraint limits rotation or shift around or along axes. A variety of constraint types are available as presets. In this work the following constraints were mainly used:

- Rigid joint (Figure 105A): connects two bodies so that no motion is possible. Although it is not necessary in all cases, it is advisable to place the coordinates of the joint at the intended points, as this later allows the creation of a correctly aligned mobile joint, simply by changing the constraint type instead of creating a new joint. Also, any joint, which is not active during a given simulation run, can be set to 'rigid' to save calculation time. Later, it can be changed back at any time if needed.
- Revolute joint (Figure 105B): this constraint has one rotary degree of freedom, which is not controlled in any respect, except for setting a certain value before simulation

start. Therefore, the two connected bodies can rotate freely if external forces (e.g. gravity) accelerate them. If one of the two connected bodies is 'fixed', this joint can be used for example to re-pose the other body by changing the position value of the constraint.

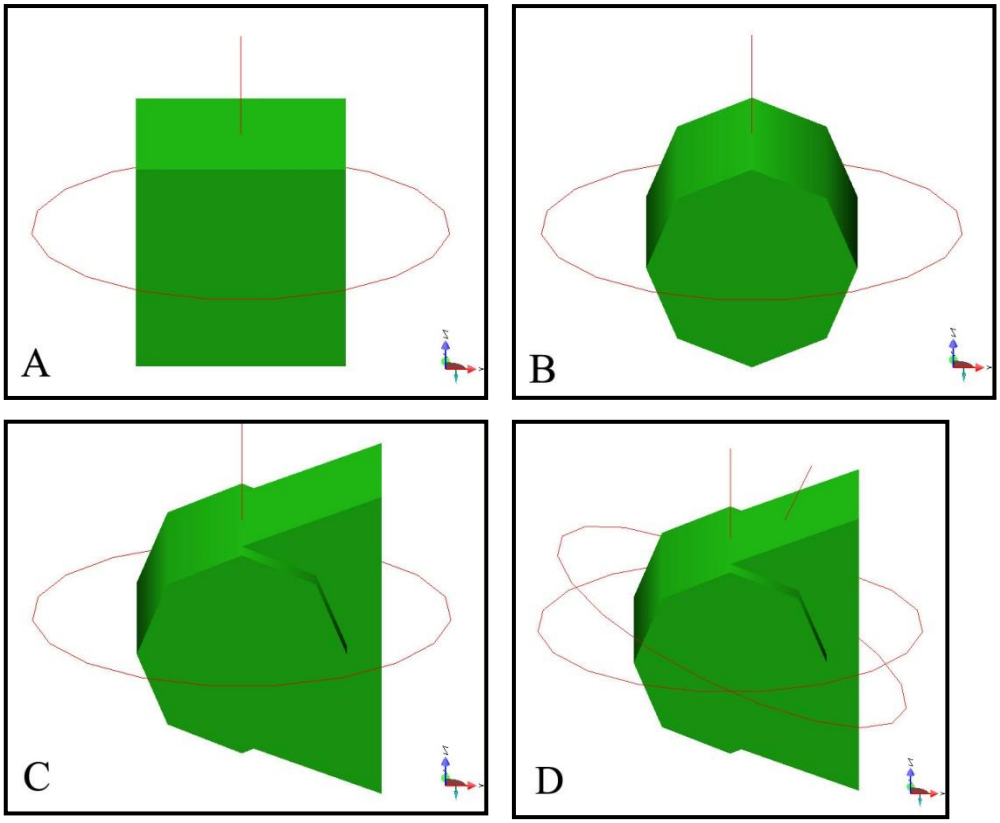

Figure 105: The three joint types, which were mainly used in the simulations:
A: Rigid joint; B: Revolute joint (with rotation around the y-axis); C: Revolute motor (with rotation around the y-axis); D: Revolute motor with rotation of 25 degrees around the y-axis, showing the two coordinates which are not both visible at 0 degree.

- Revolute motor (Figures 105C & 105D): this is a 'revolute joint' in which the sole degree of freedom can be controlled throughout the simulation. MSC.visualNastran 4D® offers different options for applying this joint. From these only the orientation option was used in this work (Figure 113), which determines the angle between the base coordinate and the second coordinate. The options can be determined by any type of input, e.g. table or formula. Also, on a 'revolute motor' any property can be measured with meters. This type of constraint was extensively used for checks on posture stability and for walking cycles, because of the possibility to dictate positions at certain time points. Complex joints with more than one degree of freedom, e.g.

shoulder and hip joint, were simulated by combining several revolute motor joints and auxiliary bodies at right angles (Figures 110A & 110B) (MALLISON 2007).

To prepare a model for the simulations, it is necessary to import the body objects, to set their properties, to place coordinates on them, to connect these with the desired constraint types, and to create and customize all meter objects and data input for the simulation run, such as tables and formulae of all input types. MSC.visualNastran 4D® regards bodies, which are connected by rigid constraints, as one object. Also, any degree of freedom that is set fixed is regarded as rigid connection. Further, as MSC.visualNastran 4D® is a rigid body simulation, bodies do not deform upon collision, their contacts are always elastic collisions (MALLISON 2007).

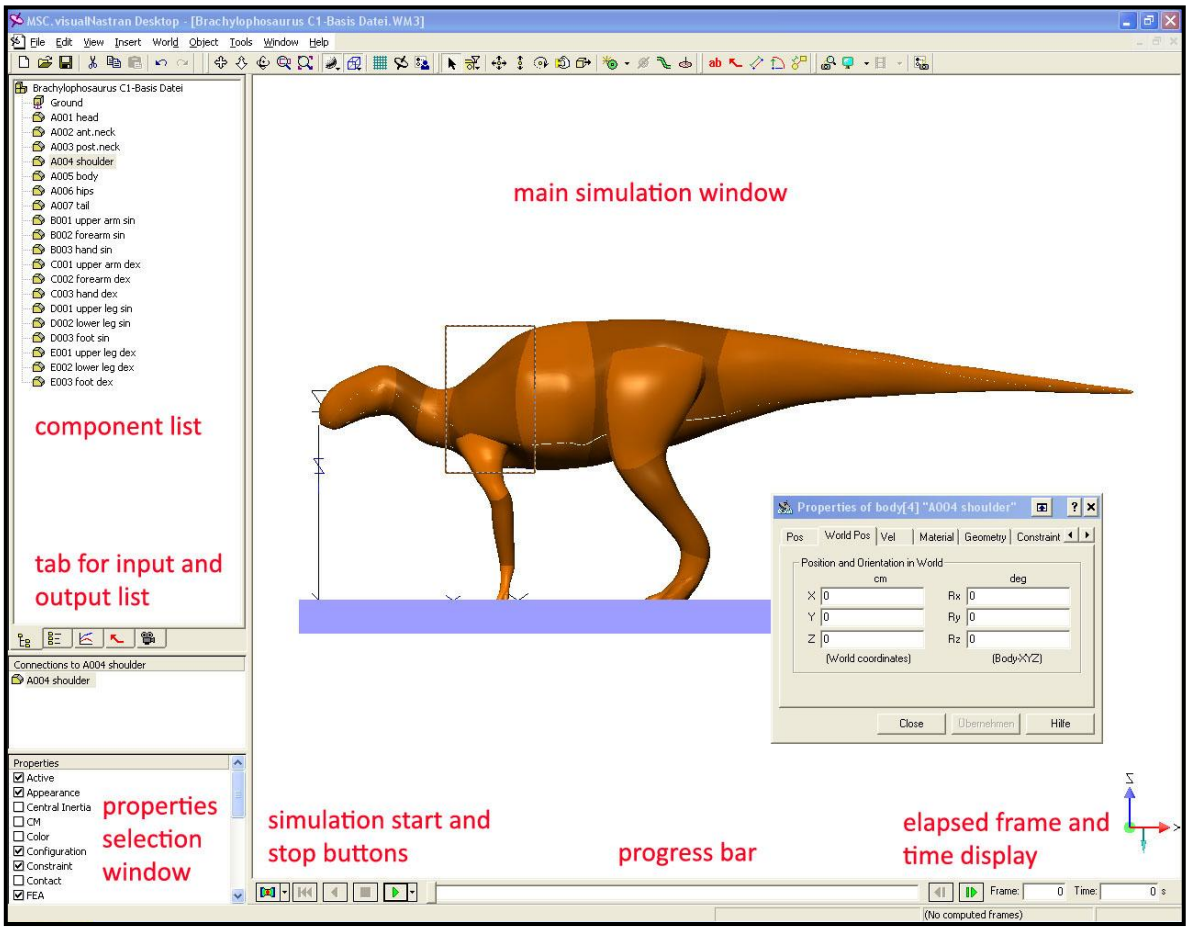

Figure 106: Screenshot from the MSC.visualNastran 4D® program, showing the bodies of the model after importing them from Rhinoceros 3.0® in anatomically correct positions, according to their positions in the CAD program. The world coordinate system position of an imported body is always (0,0,0), as can be seen in the properties window of the shoulder body. The tip of the snout of the model coincides with the world origin. A box shaped generic body serves as ground.

When a body is imported into MSC.visualNastran 4D® (as stereolithography binary file), it will be positioned automatically in the same relation to the world coordinate system of this program, as it has to the comparable coordinate system in the CAD software used (here Rhinoceros 3.0®). It is also important that the world coordinate system position of an imported body will always be (0,0,0) for all axes after import, independent of the position of the center of the body. Therefore, the model should be placed in the CAD program in a way that a point, which is easily measurable and meaningful (e.g. the tip of the snout), coincides with the origin of the world coordinate system, because any measurement of position in MSC.visualNastran 4D® is always relative to this point. In addition, one of the axes (in this work the x-axis) should be placed along the medial axis of the model so that symmetrical points will have the identical position value amounts on the axis (in this work the y-axis), which is perpendicular to this medial axis (Figure 106) (MALLISON 2007).

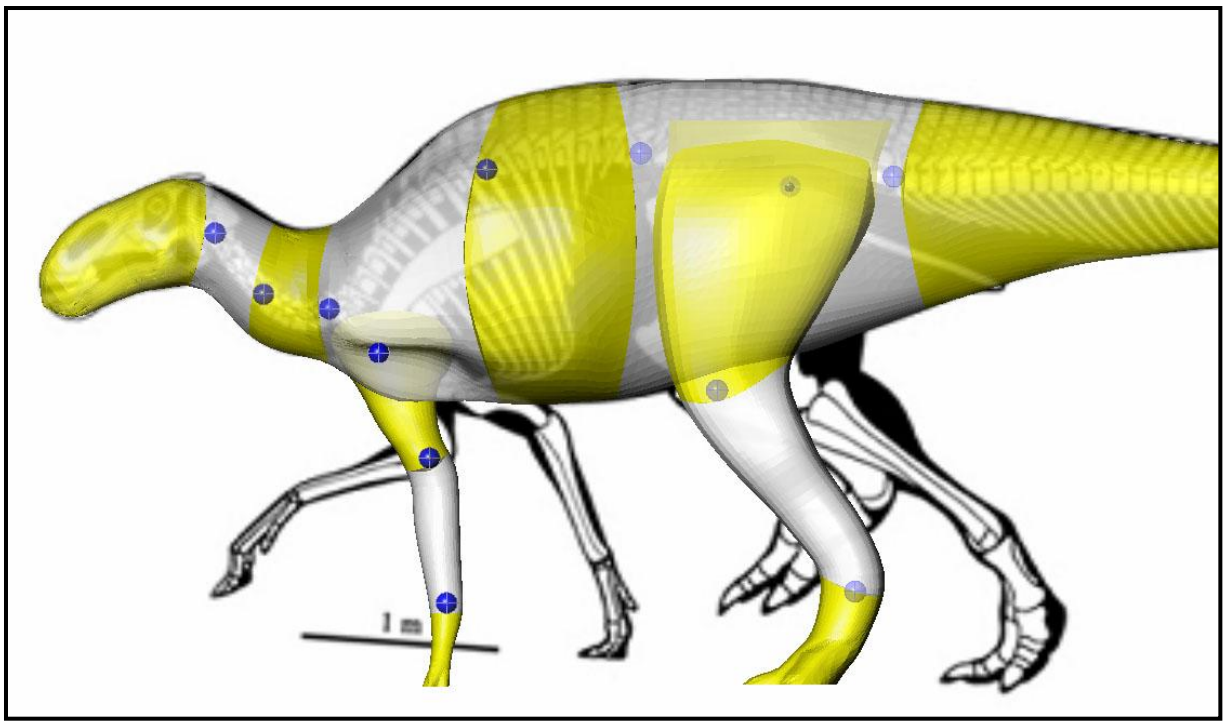

Figure 107: The sectioned polygon model in Rhinoceros 3.0® from lateral view with the skeletal drawing of the MOR 794 specimen as background image, showing the auxiliary bodies (spheres), which were used for positioning the joints. For better visibility of the spheres the skeleton was omitted here.

To simulate vertebrate motions correctly, the bodies have to be connected in anatomically correct locations. As each constraint is created between two coordinates, their placement determines the accuracy of the simulation model. Although it is possible to place

the coordinates in MSC.visualNastran 4D® directly, e.g. by using measurements from a skeleton, it is easier to mark the exact positions of the joints with auxiliary bodies (spheres) in Rhinoceros 3.0® (Figure 107). These bodies should be placed correctly, preferably by using a virtual skeleton or a skeletal drawing as background image, and then imported as *.stl files in MSC.visualNastran 4D® (Figure 108). Here, the two coordinates can be set and the resulting joint can be located in the center of mass of the auxiliary body. In the case of one-axis joints the auxiliary bodies can be deleted after constructing the joints (MALLISON 2007).

In the *Brachylophosaurus* model all joints along the vertebral column consist of only one constraint each, as the ossified tendons limit strongly the range of motion of back, sacrum, and tail. Theoretically, the joints of the neck, which is not stiffened by the tendons, could have been built using two constraints each, but in order to reduce the number of constraints due to computing time and power this solution was not realized. Also, concerning locomotion, one constraint each was regarded as sufficient when connecting these body parts. Therefore, after constructing the constraints of the vertebral column, the auxiliary bodies were deleted. In case of elbow, knee, and Mt III joints also one constraint each was constructed (one degree of freedom), and no auxiliary bodies were needed beyond constraint positioning (Figure 109).

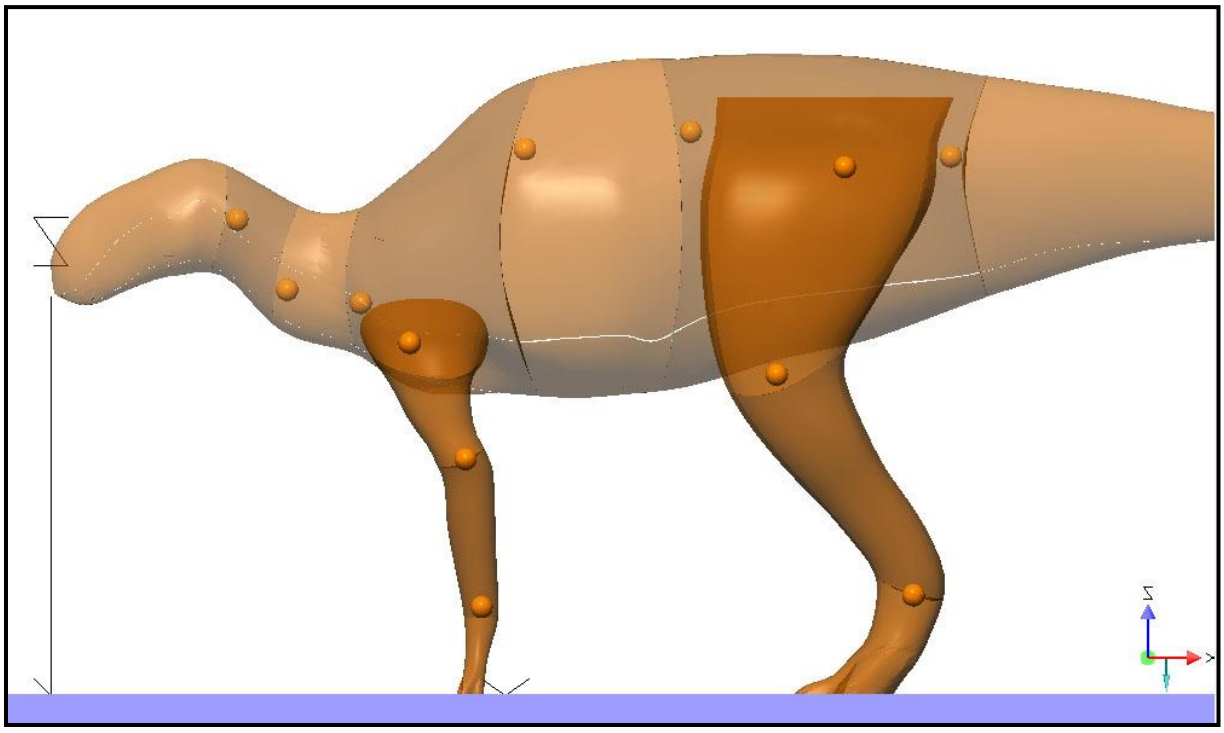

Figure 108: The model in MSC.visualNastran 4D® from lateral view after importing the auxiliary bodies (spheres) from the CAD program (as *.stl files).

While joints like the knee joint can be represented by one rotary joint, the hip joint for example requires more than one degree of freedom. These joint types are best represented by two or more rotary joints with perpendicular axes, which are located in the same place. To achieve this, an auxiliary body can be used, e.g. a sphere, which is located at the place of the intended joint. The sphere should then be connected to one of the two bodies (at best the proximal one) by a rotary joint (e.g. for transverse motion, that is adduction and abduction), while a second constraint with a different rotary axis (e.g. for sagittal motions, that is pro- and retraction) can be used to connect the sphere to the second body. The base coordinates for both joints should have the same position, ideally at the center of mass of the auxiliary object (the sphere), which should coincide with the (averaged) center of rotation of both axes. Simple geometric bodies are most suitable for auxiliary bodies, as their mass is easy to determine and subtract from the CAD-based bodies. Further, spheres have the advantage that no rotation around their geometric center will move their center of mass. In the case of a two axes joint, one auxiliary body is sufficient, three degrees of freedom require two bodies (MALLISON 2007).

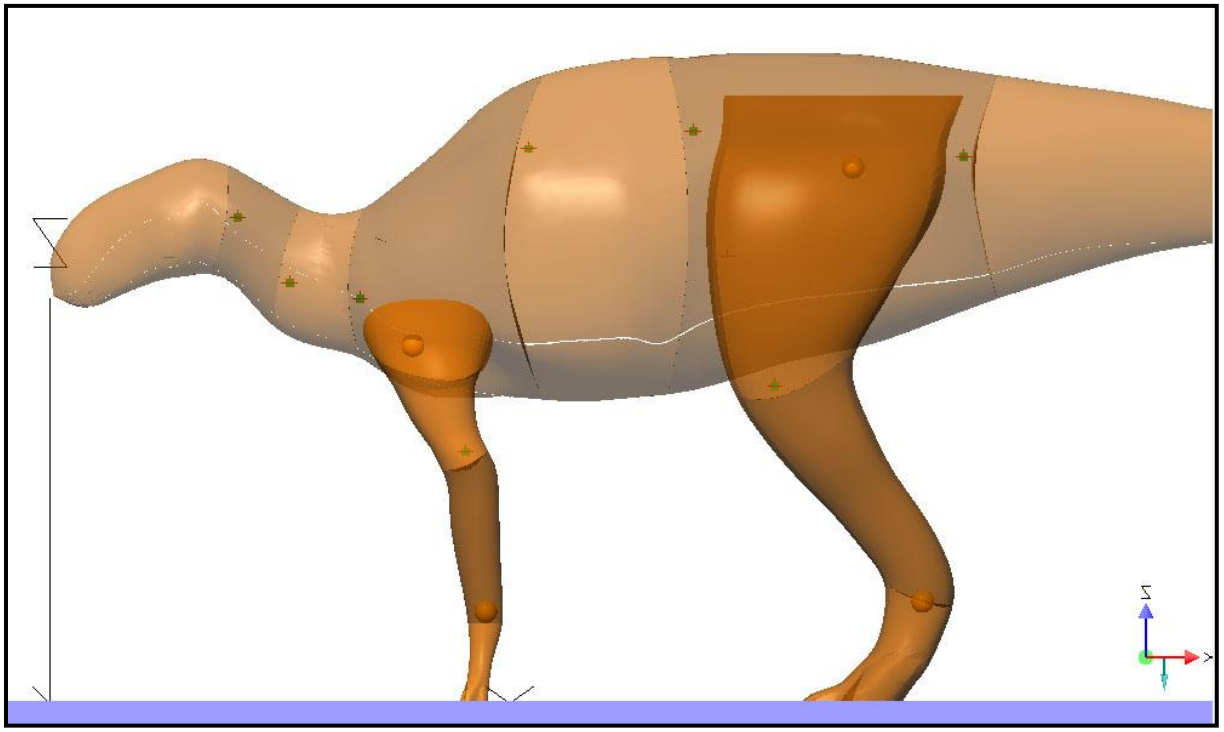

Figure 109: The model in MSC.visualNastran 4D® from lateral view after constructing the joints and deleting those auxiliary bodies which belong to joints with only one degree of freedom.

In the hadrosaur model wrist, ankle, Mt II, and Mt IV joints were built as two axes joints (rotation around the x- and y-axes), shoulder and hip joints as three axes joints (rotation around x-, y-, and z-axes).

- In a two axes joint (Figure 110A) with one auxiliary body the order from proximal to distal would be: body – joint - auxiliary body – joint - body
- In a three axes joint (Figure 110B) with two auxiliary bodies the order from proximal to distal would be: body – joint - auxiliary body – joint - auxiliary body – joint - body

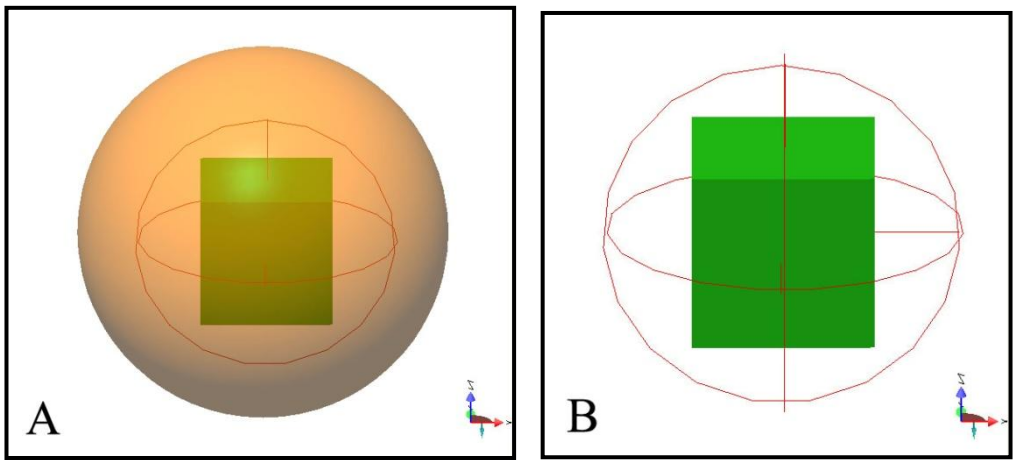

Figure 110: The two axes joint type (A) and the three axes joint type (B). In (B) the two auxiliary bodies were omitted for better visibility of the joint.

A coordinate can be connected to a body in the simulation or to the 'background', but the latter is usually not advisable. The coordinate can be placed at any point on the body. After that, the 'World Position' tab of the 'Properties' window can be used to move the coordinate to the favored position. A source of error is the accidental use of the 'Position' tab instead of the 'World Position' tab, which gives the location in relation to the 'body' coordinate system instead of the 'world' coordinate system. Although this is not relevant if both coincide, this can change during the simulation model building phase, e.g. if the position of the model is altered at a later time (MALLISON 2007).

In MSC.visualNastran 4D® symmetrically paired joints should always be exactly symmetrically arranged. Asymmetrical constraints can generate problems in controlling complex model motions, as it would be difficult to determine the exact angles at which they must be rotated to achieve similar (mirrored) motions for the right and left model side. This

can result in extremely high artificial forces and even in a breakdown of simulation calculation (MALLISON 2007).

There are also constraint types that can be employed between the model and the surroundings. In principle, an ideal model would be as accurate as possible, and therefore not require any artificial connection between the model and its surrounding (usually the ground), but MSC.visualNastran 4D® cannot model ground reaction forces reliably. To solve this problem, 'generic' joints were used (Figure 111 / Videos 1A & 1B). A 'generic' constraint has no predefined conditions so that the user can define any formula for different control features, e.g. position or velocity. These can be assigned to sliding or rotational motions around one axis (MALLISON 2007).

- **Video 1A** shows what happens in a motion simulation without using 'generic' joints and without using the 'collide' function between ground and hands and feet.
- **Video 1B** shows what happens in a motion simulation without using 'generic' joints and with active 'collide' function between ground and hands and feet.

The use of 'generic' joints in combination with the 'collide' function is not possible.

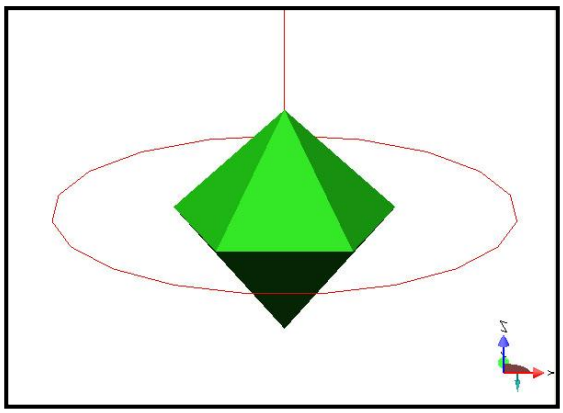

Figure 111: The 'generic' joint.

The generic joint was the only constraint type, which was used in this work for interactions between parts of the simulated animal (hands and feet) and the ground (Figure 112). The 'base' coordinate was placed on the moving element, e.g. the hand, and then the simulation was calculated until visual inspection indicated contact with the ground. In the next step, the 'world position' of the 'base' coordinate at this time step and the elapsed simulation time were written down. After this, the simulation was reset to t=0 s, a new coordinate created on the 'ground' body with the same 'world position' as just determined,

and a ‘generic’ constraint attached between the two. MSC.visualNastran 4D® offers various options for creating the constraint, but to avoid unwanted movements of simulation elements, ‘split constraint (do not move anything)’ was chosen. A formula or simple time reference was entered, ensuring that the constraint would not become active, respectively would be ignored, before the time step at which contact happens. Through the formula or time reference it is not only possible to determine the activation of the constraint, but also its deactivation, which would be the time step when the hand respectively foot lifts off the ground. The goals were defined in a way that either the generic joint mimicked a rigid joint, which means that no rotation or sliding motion along any axis was allowed, or by allowing rotation around certain axes (MALLISON 2007).

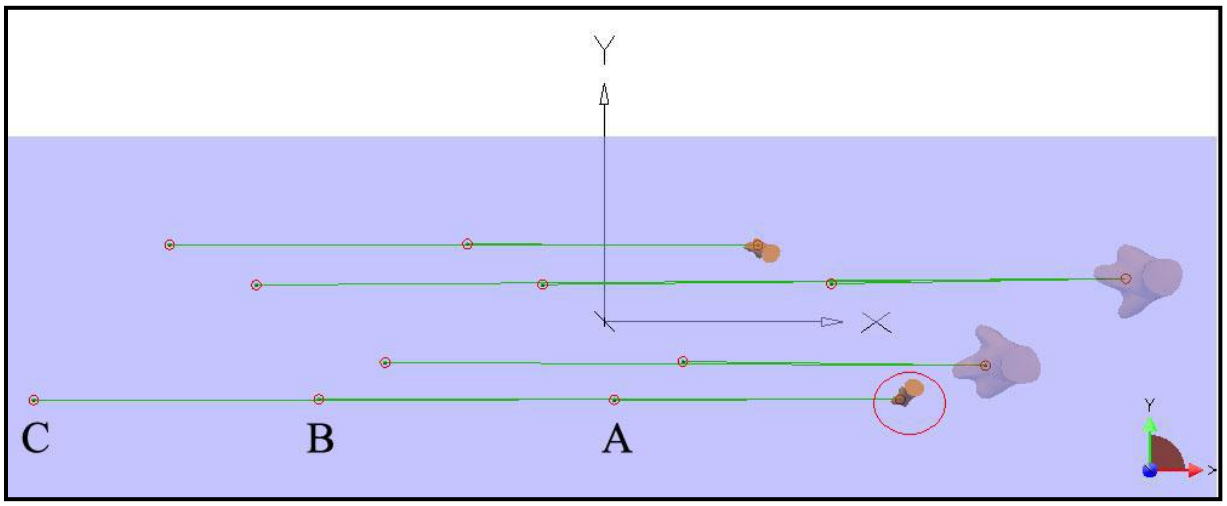

Figure 112: The use of generic constraints in the simulation of the quadruped cross gait. In case of the left hand for example (red circle), three generic constraints were built. The base coordinate of each constraint is placed on the hand, while each associated coordinate is placed on the ground at that point where the hand will touch down to a certain time step. The hand will be at point (A) after 1s, at point (B) after 3s, and at point (C) after 5s. When the hand reaches point (A) this generic constraint becomes active in the interval between 1s and 2s. Generic constraint (B) will be active between 3s and 4s, and generic constraint (C) between 5s and 6s.

This type of constraint, with formulae to control the motions, exactly mimics the rigid, revolute and revolute motor joints, but with a different way of building the constraint between the two coordinates. Using a generic joint makes it possible to create a joint in ‘split’ state. Normally, MSC.visualNastran 4D® forces the two coordinates to rest in the same place at simulation start and then moves the coordinates with the bodies. However, a ‘split’ constraint leaves each coordinate where it is placed. The other constraint types must be in ‘joined’ state at simulation start to become effective. The use of generic constraints is the

only way to create a point-to-point constraint, which connects two bodies at a time step different from t=0 and does not move them artificially when becoming 'active' (MALLISON 2007).

To serve as 'ground' a box shaped generic MSC.visualNastran 4D® body was created and set to 'fixed'. No collisions were set to occur, not even between the feet and the ground, as these slow down the simulation and can be turned on at will whenever required for the investigation at hand (MALLISON 2007).

In the research of locomotion aspects, the most important parameters are the position, orientation, and speed of body parts, and the forces and accelerations they experience. These parameters describe the animal motion and can be used to control a simulation of a moving animal. In the ideal case, each separate muscle, tendon, and ligament should be simulated, but this would demand high efforts of time, computer power, and the need to exactly reconstruct large amounts of soft tissue. Therefore, the limits imposed on this work mean that muscle forces cannot be used to control the simulations. Rather, parameters, which were effective on the main articulations, must be used as proxies. Here, the motion is defined by entering certain values for torques or positions at certain time steps, via a simple function of time or an input table (MALLISON 2007).

'Table' inputs were only used to enter time discretized values. A table can be copied to and pasted from the MS Windows® clipboard, which allows creating, editing, and importing tables into other programs, e.g. MS Excel®. Table data points serve as anchor points for a function that determines the values for each integration time step. Therefore, it is not necessary to define a y value for each time step. Four different types of functions are available: 'piecewise constant', where the function is constant at the given y value from one x value to the next, 'piecewise linear', for which each interval between two defined y values is represented by a linear function between the two given y values, 'quadratic spline', for which the program places a second order function through the given y values, and 'cubic spline', for which a third order spline is calculated. In principle, MSC.visualNastran 4D® does not calculate a function, but rather approximates it in an iterative process. Because of that, the apparent 'function' is in fact just a value table with infinitesimally small steps, and cannot be displayed as a mathematical formula. In the simulations the 'piecewise linear' option was usually chosen (Figure 113), as a simulation is much easier to control through linear functions, saving time and effort (MALLISON 2007).

To create a sequence of motions, which are not determined by factors inherent to the simulation, e.g. gravity and fixed rotational or sliding speeds, inputs must be used. Complex sequences can be created by using them, such as an animal standing up or walking cycles. In this work all motions were controlled by 'tables' that defined the orientation of a revolute motor joint in time.

The best way to create a motion sequence is to define so-called 'cornerstone positions'. These are the start and end positions of a motion sequence, between which motion is linear, without reversals of the direction of rotation. The data for the 'cornerstone positions' are achieved by posing the complete model by entering varying values of the orientation for all constraints. As MSC.visualNastran 4D® usually moves that body to which the second coordinate of the constraint is attached, it is often necessary to set one body to 'fixed' (that is immobile) before adjusting constraint orientation values. Has the model the desired pose, all values can be copied to a MS Excel® sheet. Then, the next position of the model must be arranged, copying again all values. In case of a walking cycle, these two initial positions are the points of greatest pro- and retraction of the limbs and its contralateral copy, in which the previously protracted limb is now fully retracted. If the model displays an animal which gets up from a resting pose on the ground for example, this resting pose would be the first position and a stable standing posture would be the endpoint (MALLISON 2007).

After the start and end positions have been defined, intermediate time points must be selected and more precise values for all joint orientations determined. The intermediate points should divide the previous time intervals into roughly equidistant segments. To work on the intermediate positions the simulation must be run with the two initial positions. Then, the time step for the intermediate position is chosen and the simulation display shifted to it. Now, the file should be saved under a different name. After this, the simulation data is deleted, setting the start (t=0s) of the simulation to the current time step. The model is now in the position which is defined by the two starting positions and can be rearranged by the various constraints. To work on an intermediate position without deleting simulation data is impossible, as each change (of a constraint for example) causes the return of the model to the original starting position.

To integrate the new position into the simulation, all constraint positions have to be copied to a MS Excel® data sheet together with the correct time. In the next step, the original simulation file can be opened again and the new tables copied into the inputs. This

process of creating intermediate positions should be repeated until a smooth motion has been achieved, which can then be checked for its plausibility (MALLISON 2007).

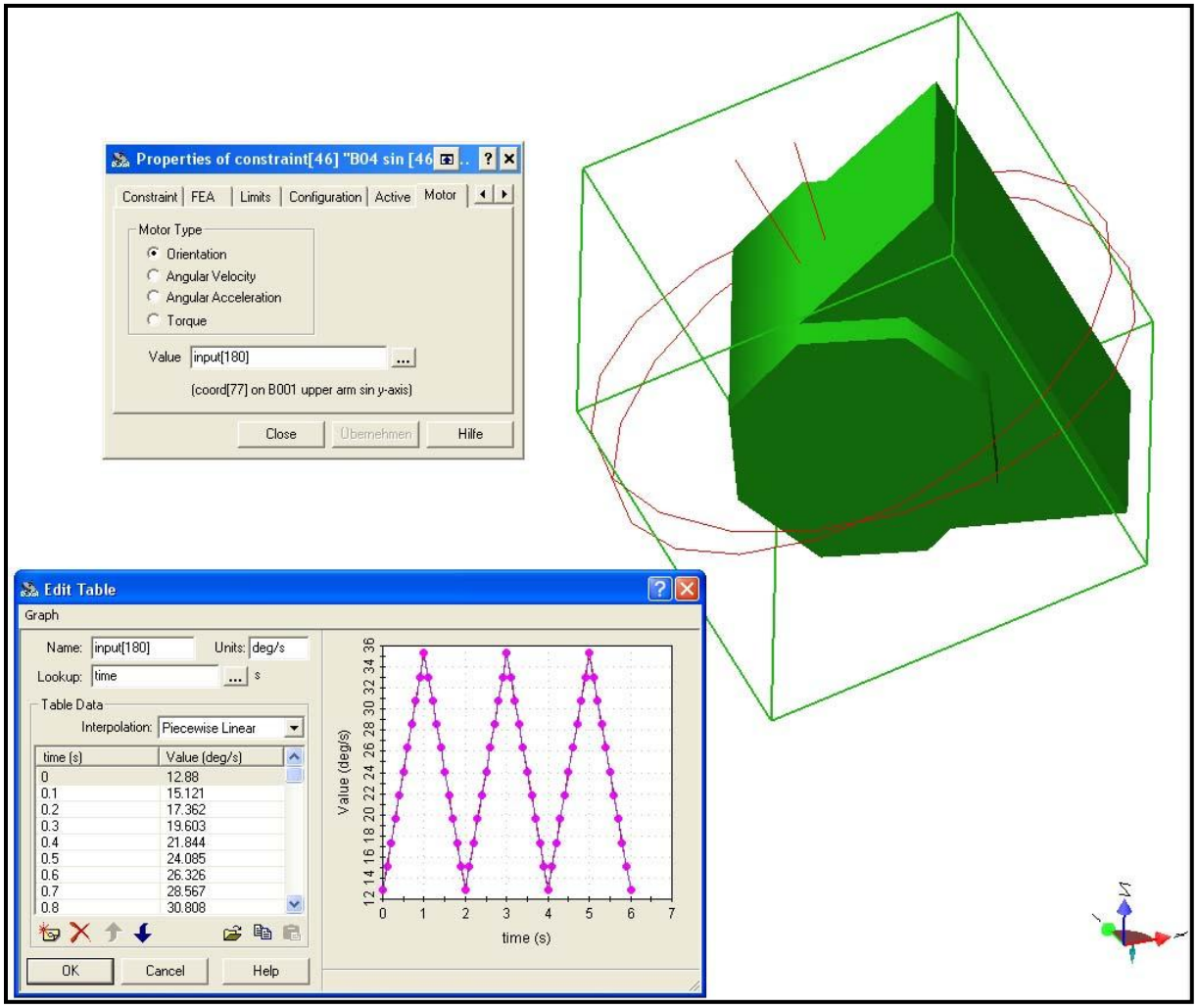

Figure 113: Revolute motor joint of the left elbow (rotation around the y-axis), showing the input type 'table', which allows defining time steps and the input variable at each time step. The diagram in the right half of the 'edit table' shows the time steps according to the 'piecewise linear' function and the cycle repeating of the motion sequence. However, such a symmetrical repetition is not possible in most cases, e.g. due to rounding errors in MSC.visualNastran 4D®.

As example to illustrate the development of a motion simulation, the different working steps which have to be done for the interval between 0s to 2s of the quadrupedal cross gait, which was simulated in this work, are described here:

At the beginning, the model is arranged in the neutral standing pose with all constraints set as rigid. Those constraints which are used to rearrange the model and to make the simulation are changed from the rigid to the revolute motor type, each with its corresponding rotation axis. Using the revolute motor joints, the model is rearranged to the

desired body posture; in this case to a quadrupedal cross gait posture. The bodies are moved by changing the degree values of the constraints. Although it would be possible to use revolute joints for this purpose, it is easier to change the rigid joints directly into revolute motor joints so that the joints have not to be changed twice. In the ‘properties’ window of each constraint the motor type ‘orientation’ has to be chosen. Then, the input table can be opened and the time steps with their corresponding degree values can be entered (Figure 113). First, each table has only two values: the value for 0.0s and for 1.0s.

At 1.0s the left arm and leg should have those postures, which the right arm and leg show at 0.0s and vice versa. That means for example, if D04 sinistral (left knee joint) has the value -3.0 degree and E04 dextral (right knee joint) the value 3.95 degree at 0.0s, D04 should have 3.95 degree and E04 -3.0 degree at 1.0s. In case of constraints with a rotation around the x- or z-axis, the signs of the values have to be changed. In the example of D04 and E04 this is not necessary, as these constraints rotate around the y-axis. Concerning the interpolation the ‘piecewise linear’ function was chosen. Further, all revolute motor joints were set to be ‘always active’.

After preparing the revolute motor joints, the generic joints have to be constructed. In the quadrupedal cross gait the right hand and the left foot are provided with generic joints first, as they maintain contact with the ground during the first step. The left hand and the right foot, which lift off the ground, are both provided with a base coordinate only. The corresponding second coordinates are placed when their positions are determined by the touchdown points of the base coordinates after the step has been done. These two generic joints are needed for the second step between 1.0s and 2.0s. The two generic joints, which were built first, are set ‘active’ for the time span between 0.0s and 1.0s. The goals of the generic joints are usually defined in a way that no rotation or sliding motion along any axis was allowed, with the exception of the quadrupedal cross and pace gaits, where a rotation of the hands around the z-axis was allowed.

Finally, the simulation is able to start and the first step is run. Regarding the quadrupedal cross gait, left arm / right leg and right arm / left leg should now interchange their postures and degree values. However, in all gaits slight deviations can arise, which means for example that the constraints achieve the correct values, but the corresponding extremity does not touch the ground or sinks into it. In the beginning of the simulations these deviations are mainly caused by the fact that the model stands in a straight position at

0.0s, but moves to the side during the forward motion, resulting in a diagonal model posture (Figure 114). This sideward movement of the model can be observed in all simulated gaits (see chapter 5), but it is not intended at the beginning of the simulations. It depends on the posture of the extremities, which are arranged in the different gaits considering research results, e.g. THULBORN (1989), and tracks. Hence, it is usually not predictable how the model will react actually when starting a simulation.

To ensure a correct contact with the ground, the postures of the extremities have to be reworked. Therefore, model position at time step 1.0s is saved under a different name and simulation data are deleted, allowing the correction of the degree values of the constraints. When the correct posture is adjusted, the new values are entered at time step 0.0s in the original file and the simulation can start again. Are the modifications correct, and all extremities are now in contact with the ground, the cornerstone positions of the first step are determined. Now, the intermediate positions, at time steps 0.1s, 0.2s, and so on, have to be reworked to achieve a fluent motion between 0.0s and 1.0s. After that the first step is finished.

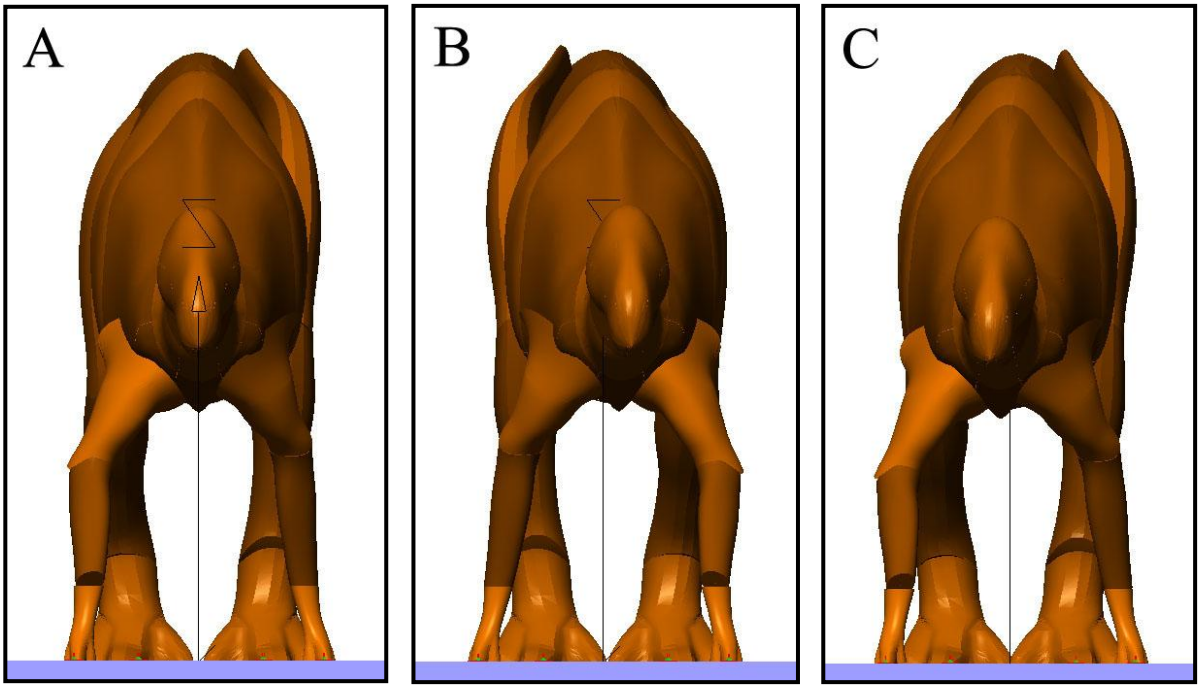

Figure 114: The *Brachylophosaurus* model in the motion simulation of the quadrupedal cross gait from cranial view. Starting position at time step 0.0s, showing the straight model posture (A); model position at time step 1.0s, showing the diagonal model posture (B); model position at time step 2.0s, after moving from the one side to the other (C).

The procedure for the second step, the interval between 1.0s and 2.0s, is basically the same as for the first step. The degree values are changed again and also corrected if necessary. The main difference is that the model moves now not from a straight position to a diagonal one, but from the left to the right side or vice versa (Figure 114). Therefore, some degree values have to be adapted to this changed conditions, but this new ones can then be used for the next steps. As this movement from one side to the other is more complex to simulate than a straight forward motion still deviations can appear in the following steps, particularly as now the effect of rounding errors in MSC.visualNastran 4D® becomes more and more recognizable, especially in the simulations of the quadrupedal gaits.

The second pair of generic joints is constructed after placing the two coordinates on the ground, whose positions were determined by the first step. These two constraints are set 'active' for the time span between 1.0s and 2.0s. Although the first step is already calculated, the simulation has to start again from 0.0s.

4.6 Model review

Before using the finished *Brachylophosaurus* model in the simulations, it has to be checked concerning its body length and weight, the position of the center of gravity, and the shape of hand and foot in comparison with tracks.

It is possible to measure the body length of the model in Rhinoceros 3.0®, resulting in a length of 8.2 meters. This value was compared with the length of the skeletal drawing of the JRF 200W specimen (Figure 54) stated by Scott Hartman. The length of his "Roberta" amounts 8.3 meters. Therefore, although the skeletal drawing of the MOR 794 specimen was used for building the model body, the scaling to the size of the JRF 200W specimen and hence to the digital skeleton was successful.

In MSC.visualNastran 4D® the material of each body can be defined, and so also its mass. For that purpose different materials are listed in the properties window of each body, e.g. steel or copper. However, no "animal" material is available, but since the volume of each body is given, its density has to be defined to get the mass (mass = density x volume).

Studies, which examined the body mass of dinosaurs, used often the density of water to calculate the mass. Therefore, they used the value of 1000 kg/m^3 or 1 kg/l (e.g. ALEXANDER 1985, 1989; MOTANI 2001; SEEBACHER 2001). However, especially the discovery of air-sac systems in dinosaurs, together with the consideration of the lungs, made it necessary to differentiate density according to the different body parts (e.g. PAUL 1997b; HENDERSON 2006; BATES et al. 2009). PAUL (1997b) assigned early theropods a value of 0.9 kg/l and more advanced theropods with more extensive air-sacs 0.85 kg/l. In sauropods it has to be differentiated between the body and the neck, because the intensely pneumatic neck vertebrae (e.g. WEDEL 2003; SCHWARZ et al. 2007b) would decrease density of the neck in relation to the trunk. After PAUL (1997b) the value for the main body of sauropods can be set at 0.9 kg/l and for their necks at 0.6 kg/l. Both values were also used by HENDERSON (2006) for the body and neck density of the prosauropod *Plateosaurus engelhardti*, and also by MALLISON (2007), who used the value of 0.9 kg/l for the complete *Plateosaurus* body including the neck. For sauropods HENDERSON (2006) set the density of the bodies at 0.8 respectively 0.85 kg/l and for the necks at 0.3 respectively 0.6 kg/l.

In this project, the *Plateosaurus* density of 0.9 kg/l was adopted for the *Brachylophosaurus* body parts, as when building the model no density value for hadrosaurs was available. In case of *Plateosaurus* as well as *Brachylophosaurus* the lungs have to be considered, but no air-sac system. After WEDEL (2003) show most prosauropoda and the ornithischia no postcranial skeletal pneumaticity, although in prosauropods this was under discussion (e.g. GUNGA 2007). A recent study of YATES et al. (2012) shows that the postcranial skeletal pneumaticity of *Plateosaurus* is apparently sporadic in its occurrence and has only been observed in very few specimens, in which it is of very limited extent, affecting only the posterior cervical vertebrae and possibly the mid dorsals in one specimen. Therefore, it was arguable to assume a similar density in *Plateosaurus* and *Brachylophosaurus*. Further, it was not necessary to differentiate between the hadrosaur neck and body.

In 2009 BATES et al. published their results about body mass reconstructions in four dinosaur species. One of the dinosaurs examined was a sub-adult *Edmontosaurus annectens*. Concerning the density of its different body parts, they used also the value of 1 kg/l, except for head and thorax, which show lesser densities due to the single lung cavity and an additional air sac in the skull. Finally, they calculate for the whole *Edmontosaurus* body a

density of 0.93 kg/l. This value almost matches the assumed density for the *Brachylophosaurus* body.

When using the density value of 0.9 kg/l for the different *Brachylophosaurus* body parts, the complete body mass of the hadrosaur is 3032 kg (3031.8412 kg). Table 1 shows the masses of the individual body parts and Figures 100 & 101 show their position and shape.

Body part	Mass (kg)	Body part	Mass (kg)
Head	68.647	Upper leg sinistral	191.38
Anterior neck	30.558	Lower leg sinistral	75.912
Posterior neck	41.883	Foot sinistral	32.173
Shoulder	337.58	Upper leg dextral	191.38
Body	698.52	Lower leg dextral	75.912
Hips	774.68	Foot dextral	32.173
Tail	369.44		
Upper arm sinistral	37.325		
Forearm sinistral	15.502		
Hand sinistral	2.9746		
Upper arm dextral	37.325		
Forearm dextral	15.502		
Hand dextral	2.9746		

Table 1: The individual body parts of the *Brachylophosaurus* model with their respective body masses.

The later introduced sectioning of the foot, which was used in some of the simulations (Figure 102), changed the complete body mass to 3031.8619 kg because of slight inaccuracies when cutting the foot into different parts.

The auxiliary bodies, which were used for joints with more than one degree of freedom, possess different masses. The four bodies of the shoulder joints and the two of the wrist joints have a mass of 0.5 kg each. The four bodies of the hip joints and the two of the ankle joints have a mass of 2 kg each. The heavier mass of the auxiliary bodies of the legs was necessary for a higher stability of the leg joints during locomotion, especially in the bipedal gaits (Video 2A). All together the auxiliary bodies have a mass of 15 kg, which was

not added to the complete mass as the bodies are only used for technical support and are no parts of the hadrosaur body. Further, in relation to the 3032 kg of the complete hadrosaur, the 15 kg of the auxiliary bodies are insignificant as they represent only 0.5 % of the complete body mass and have therefore no influence on the simulations.

- **Video 2A** shows what happens in a motion simulation when the auxiliary bodies of the legs have no heavier mass.

How realistic is the weight of the *Brachylophosaurus* model in relation to its length? After PAUL (1997b) most American hadrosaurs weighed about 2500 – 3000 kg or more. In PAUL (2010) the author stated values of length and weight for most known hadrosaur species. His values are a general figure for the size of the largest known adults of a species. However, for dinosaurs without air-sacs he used a density value of 0.95 kg/l.

Table 2 shows a comparison of the *Brachylophosaurus* model using different densities and a comparison of the model with hadrosaurine hadrosaur species from PAUL (2010), which belong to the similar size range.

	Length (m)	**Weight (kg)**
Brachylophosaurus model with density 0.9 kg/l	8.2	3032
Brachylophosaurus model with density 0.93 kg/l after BATES (2009)	8.2	3133
Brachylophosaurus model with density 0.95 kg/l after PAUL (2010)	8.2	3200
Hadrosaurine hadrosaur species after PAUL (2010)		
Brachylophosaurus canadensis	11	7000
Edmontosaurus (*Anatosaurus*) *annectens*	9	3200
Kritosaurus (or *Gryposaurus*) *incurvimanus*	7	2200
Kritosaurus (or *Gryposaurus*) *latidens*	7.5	2500
Kritosaurus (or *Gryposaurus*) *monumentensis*	8	3000
Maiasaura peeblesorum	7	2500
Saurolophus (=*Prosaurolophus*) *maximus*	8.5	3000
Saurolophus osborni	8.5	3000

Table 2: Comparison of the *Brachylophosaurus* model using different densities, and comparison of the model with hadrosaurine hadrosaur species, which belong to the similar size range.

When using the density of BATES (2009) (0.93 kg/l), the complete body mass of the *Brachylophosaurus* model amounts 3133 kg. The density used by PAUL (2010) (0.95 kg/l) increases the body mass to 3200 kg (Table 2). Therefore, the difference between the body masses amounts 101 kg (this work compared with BATES (2009)), respectively 168 kg (this work compared with PAUL (2010)). This would represent a 3 % bigger body mass after BATES (2009), and a 6 % bigger body mass after PAUL (2010), in comparison with the original model.

Each of these three different densities was tested successively in a motion simulation (Videos 3A, 3B, 3C). The results show that a slightly higher body mass has no influence on the simulation. Therefore, the initially used density of 0.9 kg/l was maintained.

- **Video 3A** shows bipedal gait A IS3 (intermediate steps reworked and feet sectioned) from lateral view with a body density of 0.9 kg/l.
- **Video 3B** shows bipedal gait A IS3 from lateral view with a body density of 0.93 kg/l.
- **Video 3C** shows bipedal gait A IS3 from lateral view with a body density of 0.95 kg/l.

The comparison of the *Brachylophosaurus* model used in this work with the hadrosaurine hadrosaur species after PAUL (2010) (Table 2) shows that the length / weight relation of the model coincides with other hadrosaur species of similar size range, but not with his values for *Brachylophosaurus canadensis*. However, a weight of 7000 kg for a *Brachylophosaurus* with a length of 11 m is questionable, because this would require a distinct higher body volume in relation to the other species, as body density of course does not change. After PAUL (1997b) are hadrosaurs unusually uniform and isometric in body design and proportions regardless of size. Such a discrepancy in the length / weight relation between *Brachylophosaurus* and the other species is therefore rather unlikely. Finally, based on the comparison of the used *Brachylophosaurus* model with the other hadrosaurine species, a complete body mass of 3032 kg for the model seems to be realistic.

ALEXANDER (1989) argued that in case of a bipedally walking dinosaur with its long heavy tail the center of mass lies close to the hips and that the average position of the feet, while on the ground, must be under the center of mass. HENDERSON (1999) estimated the centers of mass of extinct animals by 3D mathematical slicing. One of the dinosaur species he examined was *Iguanodon bernissartensis* (Figure 115). Although not specified, but after visual comparison with a skeletal reconstruction of *Iguanodon bernissartensis* (PAUL 2010), it

can be estimated that the center of mass in the shown quadrupedal body posture seems to be located close to the pubes in front of the pelvic girdle.

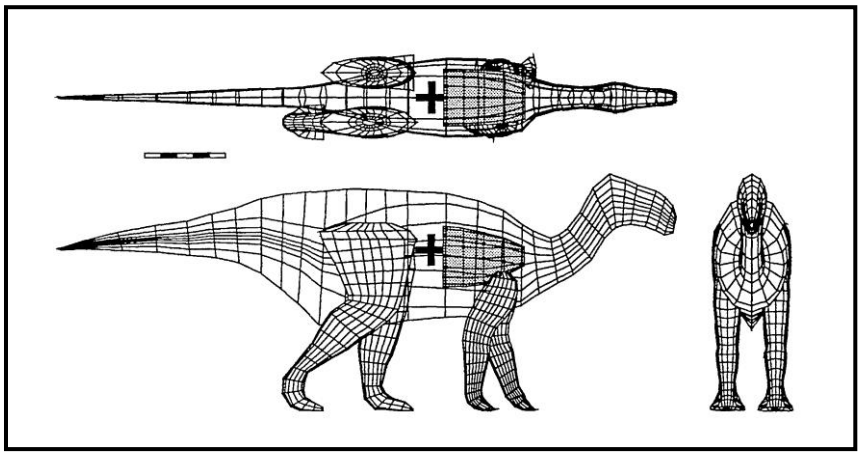

Figure 115: Dorsal, lateral, and anterior views of *Iguanodon* body form, lung cavity (gray cylinder in anterior trunk region), and center of mass (large black cross); scale bar = 1 m HENDERSON (1999).

BATES et al. (2009) calculated the center of mass of the examined *Edmontosaurus annectens* for 6 different models, in which the volumes of body segments and respiratory organs were varied. However, their sensitivity analysis consistently placed the center of mass well below and in front of the hip joint, regardless of the chosen combination of body and respiratory structure volumes (Figure 116).

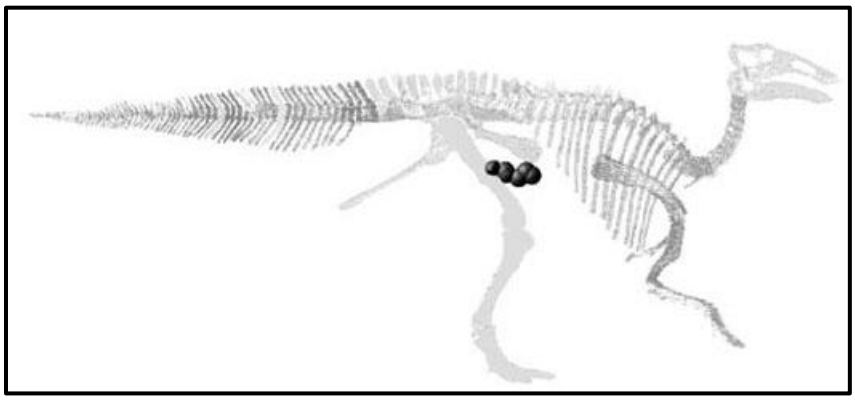

Figure 116: Centers of mass (black spheres) of the different *Edmontosaurus* models (BATES et al. 2009).

Concerning the *Brachylophosaurus* model, MSC.visualNastran 4D® shows the center of mass on demand. However, the model parts must be fused for that purpose, otherwise only the centers of mass of the different body parts are shown. To achieve this, the polygon bodies are grouped in Rhinoceros 3.0® and the whole model (as *.stl file) is ex- and imported in MSC.visualNastran 4D®. In the quadrupedal standing posture (Figure 117) the center of mass is placed below the pubes and in front of the hip joints. This seems to be a lower

position as in case of *Iguanodon bernissartensis*, but a comparison is difficult as HENDERSON (1999) shows no skeletal image.

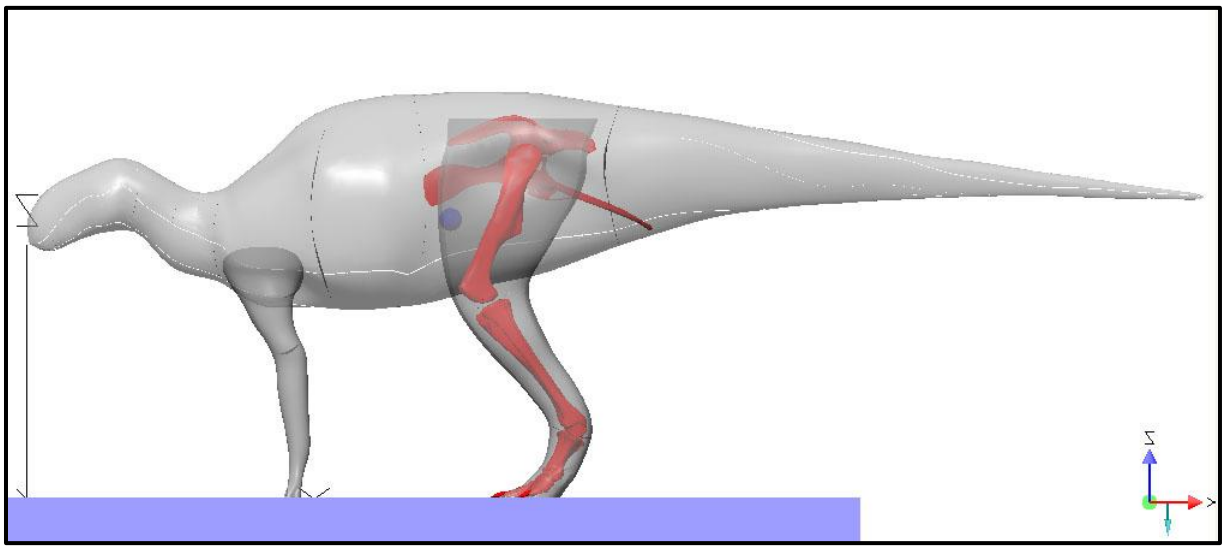

Figure 117: The *Brachylophosaurus* model in quadrupedal standing posture from lateral view, showing the position of the center of mass (blue sphere) calculated by MSC.visualNastran 4D®.

In the later simulated bipedal standing posture (Figure 118) the position of the center of mass correlates with the positions calculated by BATES et al. (2009). Further, the feet are placed under the center of mass as described by ALEXANDER (1989).

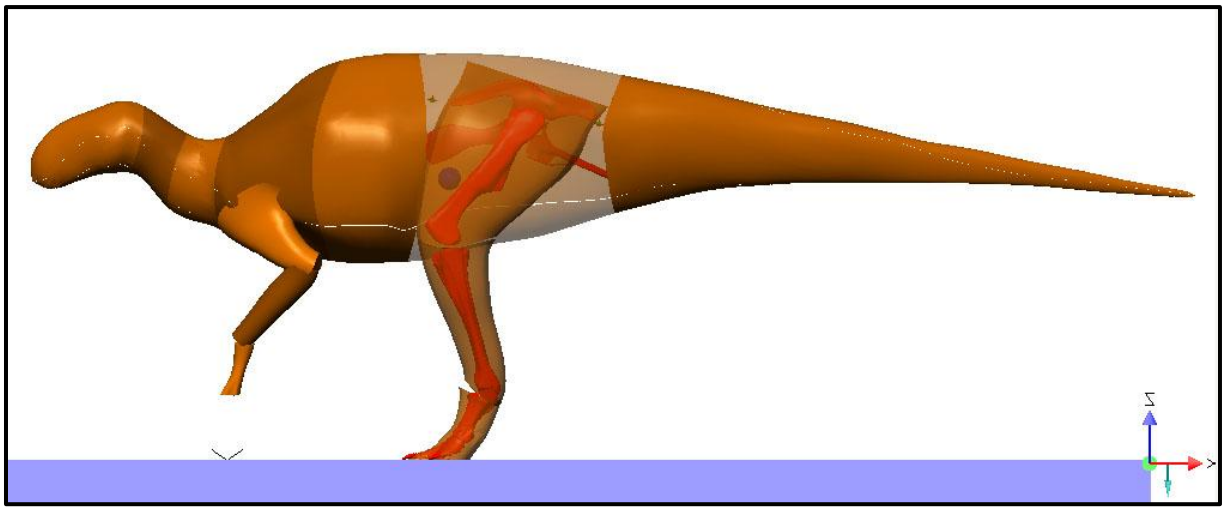

Figure 118: The *Brachylophosaurus* model in bipedal standing posture from lateral view, showing the position of the center of mass (blue sphere) according to BATES et al. (2009).

In the sectioned model it is not possible to display the center of mass by MSC.visualNastran 4D®. However, it can be replaced by a coordinate, which is attached to the hips body, using its positioning values. Through the coordinate the position of the center of mass can always be visualized, but a meter cannot be attached to a coordinate, which allows no measurements. Therefore, it was necessary to create a movable body as center of mass, which allows to measuring its movements by an attached meter. As body a blue sphere was used, as in Figures 117 & 118. Usually, this body would fall down according to the gravity when starting the simulation, but connecting it to the hips body would fix the sphere to the model body. To avoid this, a 'Prescribed motion' (Figure 119) was given to the sphere. This function can be found in the 'Position' tab of the properties window.

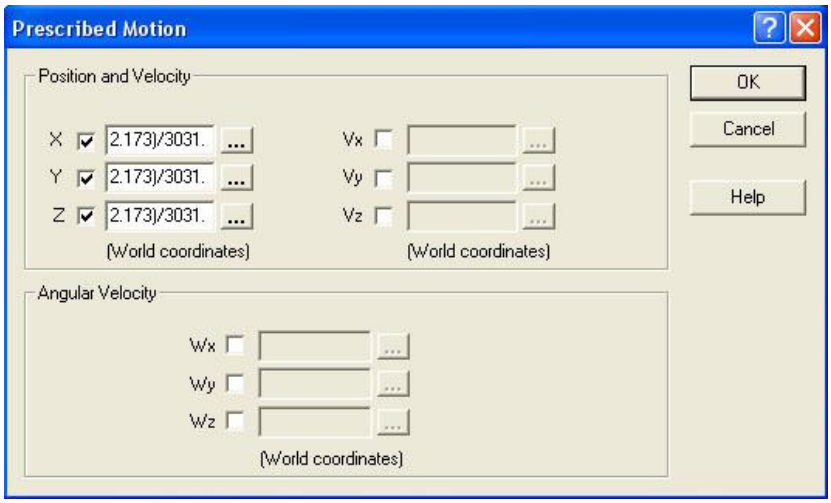

Figure 119: The 'Prescribed motion' window.

Here, formulas can be edited for the position of the body. To determine the center of mass the following formula was used (after ÖZKAYA and NORDIN 1999):

$$m_1 * r_1 = m_2 * r_2$$

$$m_1 * (x_s - x_1) = m_2 * (x_2 - x_s)$$

$$m_1 * x_s - m_1 * x_1 = m_2 * x_2 - m_2 * x_s$$

$$m_1 * x_s + m_2 * x_s = m_2 * x_2 + m_1 * x_1$$

$$x_s * (m_1 + m_2) = m_1 * x_1 + m_2 * x_2$$

$$x_s = \frac{m_1 x_1 + m_2 x_2}{m_1 + m_2} = \frac{m_i x_i}{M}$$

Based on this formula the following three formulas were edited (cm = center of mass / p = position):

- (body[1].cm.p.x*68.6470+body[2].cm.p.x*30.5580+body[3].cm.p.x*41.8830+body[4].cm.p.x*337.58+body[5].cm.p.x*698.52+body[6].cm.p.x*774.68+body[7].cm.p.x*369.44+body[13].cm.p.x*37.325+body[17].cm.p.x*15.502+body[11].cm.p.x*2.9746+body[12].cm.p.x*37.325+body[16].cm.p.x*15.502+body[10].cm.p.x*2.9746+body[15].cm.p.x*191.38+body[19].cm.p.x*75.912+body[9].cm.p.x*32.173+body[14].cm.p.x*191.38+body[18].cm.p.x*75.912+body[8].cm.p.x*32.173)/3031.8412
- (body[1].cm.p.y*68.6470+body[2].cm.p.y*30.5580+body[3].cm.p.y*41.8830+body[4].cm.p.y*337.58+body[5].cm.p.y*698.52+body[6].cm.p.y*774.68+body[7].cm.p.y*369.44+body[13].cm.p.y*37.325+body[17].cm.p.y*15.502+body[11].cm.p.y*2.9746+body[12].cm.p.y*37.325+body[16].cm.p.y*15.502+body[10].cm.p.y*2.9746+body[15].cm.p.y*191.38+body[19].cm.p.y*75.912+body[9].cm.p.y*32.173+body[14].cm.p.y*191.38+body[18].cm.p.y*75.912+body[8].cm.p.y*32.173)/3031.8412
- (body[1].cm.p.z*68.6470+body[2].cm.p.z*30.5580+body[3].cm.p.z*41.8830+body[4].cm.p.z*337.58+body[5].cm.p.z*698.52+body[6].cm.p.z*774.68+body[7].cm.p.z*369.44+body[13].cm.p.z*37.325+body[17].cm.p.z*15.502+body[11].cm.p.z*2.9746+body[12].cm.p.z*37.325+body[16].cm.p.z*15.502+body[10].cm.p.z*2.9746+body[15].cm.p.z*191.38+body[19].cm.p.z*75.912+body[9].cm.p.z*32.173+body[14].cm.p.z*191.38+body[18].cm.p.z*75.912+body[8].cm.p.z*32.173)/3031.8412

In case of the simulations with the sectioned feet the formulas were adapted accordingly:

- (body[1].cm.p.x*68.6470+body[2].cm.p.x*30.5580+body[3].cm.p.x*41.8830+body[4].cm.p.x*337.58+body[5].cm.p.x*698.52+body[6].cm.p.x*774.68+body[7].cm.p.x*369.44+body[13].cm.p.x*37.325+body[17].cm.p.x*15.502+body[11].cm.p.x*2.9746+body[12].cm.p.x*37.325+body[16].cm.p.x*15.502+body[10].cm.p.x*2.9746+body[15].cm.p.x*191.38+body[19].cm.p.x*75.912+body[14].cm.p.x*191.38+body[18].cm.p.x*75.912+body[8].cm.p.x*23.924+body[20].cm.p.x*3.4037+body[21].cm.p.x*2.6709+body[22].cm.p.x*2.1998+body[9].cm.p.x*24.262+body[23].cm.p.x*3.0345+body[24].cm.p.x*2.8193+body[25].cm.p.x*2.0525)/3031.8619
- (body[1].cm.p.y*68.6470+body[2].cm.p.y*30.5580+body[3].cm.p.y*41.8830+body[4].cm.p.y*337.58+body[5].cm.p.y*698.52+body[6].cm.p.y*774.68+body[7].cm.p.y*369.44+body[13].cm.p.y*37.325+body[17].cm.p.y*15.502+body[11].cm.p.y*2.9746+body[12].cm.p.y*37.325+body[16].cm.p.y*15.502+body[10].cm.p.y*2.9746+body[15].cm.p.y*191.38+body[19].cm.p.y*75.912+body[14].cm.p.y*191.38+body[18].cm.p.y*75.912+body[8].cm.p.y*23.924+body[20].cm.p.y*3.4037+body[21].cm.p.y*2.6709+body[22].cm.p.y*2.1998+body[9].cm.p.y*24.262+body[23].cm.p.y*3.0345+body[24].cm.p.y*2.8193+body[25].cm.p.y*2.0525)/3031.8619
- (body[1].cm.p.z*68.6470+body[2].cm.p.z*30.5580+body[3].cm.p.z*41.8830+body[4].cm.p.z*337.58+body[5].cm.p.z*698.52+body[6].cm.p.z*774.68+body[7].cm.p.z*369.44+body[13].cm.p.z*37.325+body[17].cm.p.z*15.502+body[11].cm.p.z*2.9746+body[12].cm.p.z*37.325+body[16].cm.p.z*15.502+body[10].cm.p.z*2.9746+body[15].cm.p.z*191.38+body[19].cm.p.z*75.912+body[14].cm.p.z*191.38+body[18].cm.p.z*75.912+body[8].cm.p.z*23.924+body[20].cm.p.z*3.4037+body[21].cm.p.z*2.6709+body[22].cm.p.z*2.1998+body[9].cm.p.z*24.262+body[23].cm.p.z*3.0345+body[24].cm.p.z*2.8193+body[25].cm.p.z*2.0525)/3031.8619

- **Video 4A** shows bipedal gait A IS1 (intermediate steps not reworked and feet not sectioned) from lateral view with movable center of mass.

The data of the meter, which was attached to the center of mass body, are displayed as graph in Figure 120, which shows the 'Position' meter.

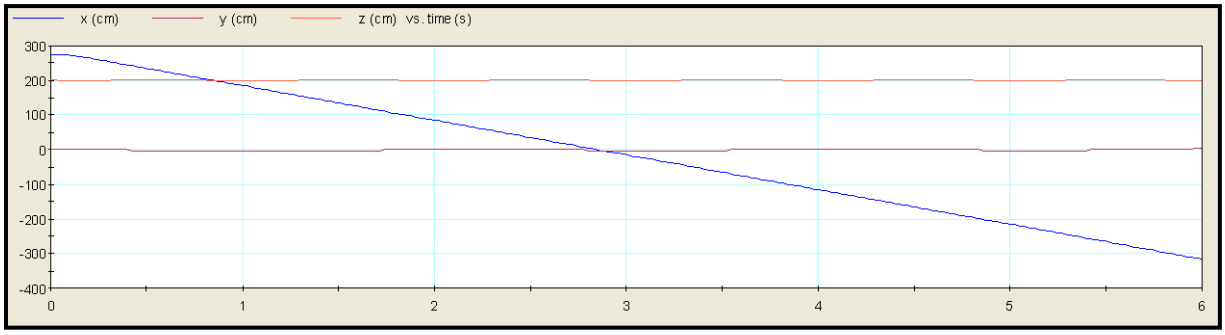

Figure 120: The data of a 'Position' meter displayed as graph.

Further, Video 4A shows that the center of mass position, which was calculated with the formula, slightly differs from that calculated by MSC.visualNastran 4D® (Figure 121). However, both positions are in accordance with those calculated by BATES et al. (2009).

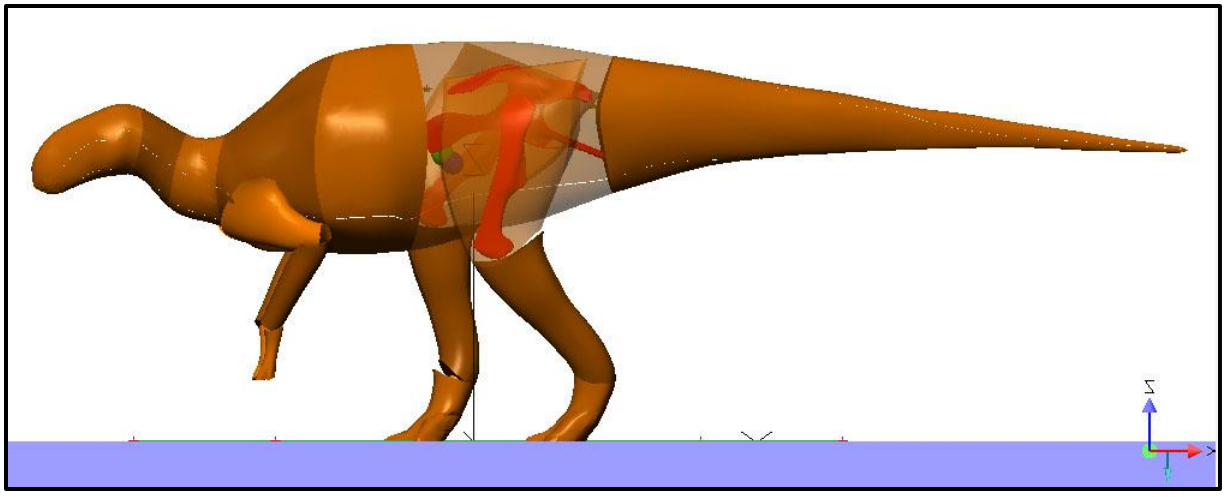

Figure 121: Bipedal gait A from lateral view, showing the position of the center of mass after MSC.visualNastran 4D® (green sphere) and its position after the calculated formula (blue sphere).

Finally, the question arises if the hand and foot of the *Brachylophosaurus* model are in accordance with hadrosaur tracks. Ornithopod manus prints show a variety of different shapes (MORATALLA et al. 1992; LOCKLEY and WRIGHT 2001) and even in the same trackway manus prints can differ from each other (MORATALLA et al. 1992). Hadrosaur manus prints are often described as crescent or semilunate (CURRIE 1983, 1991), but Figure 122 shows that the

hand print of the model is rather subtriangular in shape. However, when modeling the hadrosaur hand it was not determinable how the skin or a web of skin actually covered the hand skeleton. Also, even if the webbing is interpreted as fossilized digital pad as be done by BAKKER (1986), its reconstruction would not have been possible due to its unknown shape and size. Therefore, the assumed disparity between the model hand print and the field tracks could be expected.

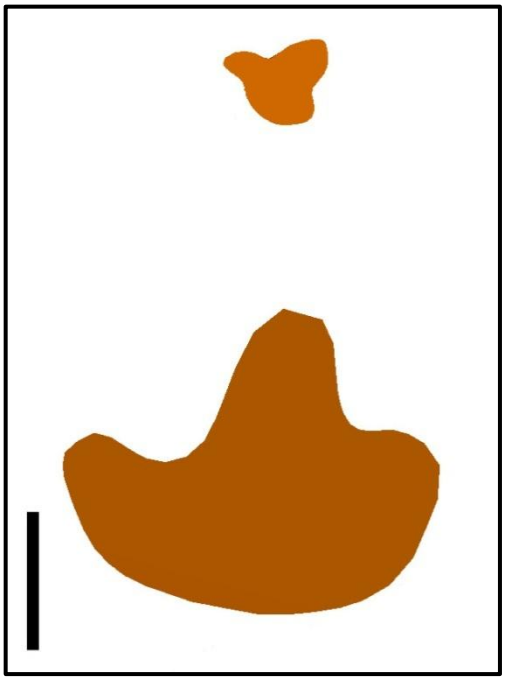

Figure 122: Right hand and foot print of the *Brachylophosaurus* model from dorsal view, according to the quadrupedal standing pose, but with shortened distance between them, scale bar = 20 cm.

The foot print of the model is tridactyl and mesaxonic, as described by THULBORN (1990), but the variety of hadrosaur foot print types is quite large (Figure 123). As in case of the hand, the flesh reconstruction of the foot was difficult, because it was not possible to determine how the skin or the supposed interdigital webbing (Figure 123 (b) & (l)) are arranged.

In summary, regarding body length, body mass, center of mass, and the hand and foot prints the *Brachylophosaurus* model seems to be quite realistic and coincides with the results of other researchers. This is an important precondition before using the model in the simulations, which are described in the next chapter.

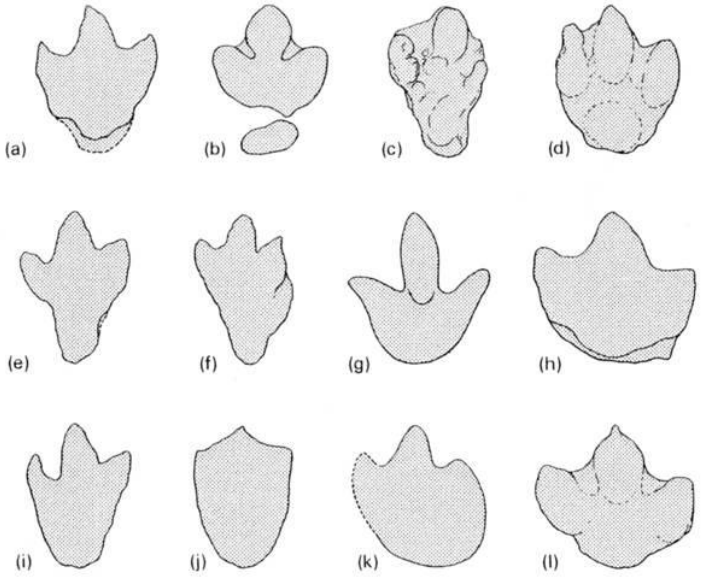

Pes prints attributed to hadrosaurs. (a) *Amblydactylus gethingi*, from the Lower Cretaceous of British Columbia, Canada; about 64 cm long. (b) Unnamed footprint, from the Upper Cretaceous of Alberta, Canada; about 62.5 cm long, excluding 'heel pad'. (c) Unnamed footprint, from the Upper Cretaceous of Utah, USA; about 140 cm long, including metatarsus. (d) *Amblydactylus gethingi*, from the Lower Cretaceous of British Columbia, Canada; about 62 cm long. (e) *Dinosauropodes bransfordii*, from the Upper Cretaceous of Utah, USA; about 73 cm long, including metatarsus. (f) *Dinosauropodes magrawii*, from the Upper Cretaceous of Utah, USA; about 136 cm long, including metatarsus. (g) *Gypsichnites pacensis*, from the Lower Cretaceous of British Columbia, Canada; about 29 cm long. (h) *Amblydactylus kortmeyeri*, from the Lower Cretaceous of British Columbia, Canada; about 11 cm long. (i) *Hadrosaurichnus australis*, from the Upper Cretaceous of Argentina; about 37 cm long. (j) *Taponichnus donottoi*, from the Upper Cretaceous of Argentina; about 57 cm long. (k) *Telosichnus saltensis*, from the Upper Cretaceous of Argentina; about 52 cm long. (l) *Amblydactylus kortmeyeri*, from the Lower Cretaceous of British Columbia, Canada; about 42 cm long. Footprints of early Cretaceous age (a,d,g,h,l) are questionably attributed to hadrosaurs.

Figure 123: Pes prints attributed to hadrosaurs from THULBORN (1990).

5. Simulations

Before starting the simulations, it had to be decided which gaits or motions should be examined using the hadrosaur model. In case of hadrosaurs, it was necessary to consider their ability to walk bipedally and quadrupedally. The descriptions of tracks and trackways (e.g. THULBORN 1989, 1990; WRIGHT 1999) as well as considerations about hadrosaur body postures and locomotion (e.g. GALTON 1970; MARYANSKA and OSMOLSKA 1984) were used as guidelines to develop different motion simulations and body postures.

In the beginning of a simulation its most important control factor is the gravity, which affects the model in all simulations. It defines if a certain body posture or motion is possible or not, and therefore if it is likely or not. This kind of control is especially important in simulations which cannot be controlled by tracks, e.g. the erecting of the hadrosaur body. In gait simulations the trackways of the model were compared with trackways and their descriptions from the literature, when the simulations were finished. Through the wide occurrence of iguanodontian and hadrosaurian tracks and trackways characteristics could be determined (e.g. LOCKLEY and WRIGHT 2001), resulting in a high amount of information. This makes them to the most important control factor of the gait simulation results.

In the simulation videos the gaits are classified as follows (on the example of bipedal gait A):

- Bipedal gait A IS1: the intermediate steps (IS) (aerial phase of hands (quadrupedal gait) and feet during a stride) are not reworked.
- Bipedal gait A IS2: the intermediate steps are reworked, but the feet are not sectioned.
- Bipedal gait A IS3: the intermediate steps are reworked and the feet are sectioned.

Since it is not possible to draw conclusions about the intermediate steps from tracks and trackways, the simulations can only provide possible alternatives. Two of them are shown in the simulations, one with the feet not sectioned, which means that each foot moves as solid unit, and the other one with sectioned feet, which means that each foot possess movable toes. The latter alternative was used predominantly in simulations were the feet are placed close to the midline, leading to a wide overlapping of the feet.

5.1 Quadrupedal locomotion

The first quadrupedal gaits examined are the cross and pace gait. A gallop as shown by SELLERS et al. (2009) was not simulated, as the realization of the aerial phase of the gallop (all 4 limbs have no contact with the ground) would not have been possible due to the generic constraints.

In addition to these 'regular' quadrupedal gaits different so-called 'semibipedal' gaits were simulated. The term 'semibipedal' was originally used by THULBORN (1989) for the ability of ornithopods to switch between bipedal and quadrupedal gait. In this work the term is used for quadrupedal motion without rotation of the arm around the shoulder joint. In this kind of locomotion the arms were used instead like 'hiking sticks', which were extended and retracted alternately in a repeating interval.

5.1.1 Results

It was decided to simulate first the **cross gait**, following the quadrupedal gait descriptions of THULBORN (1989) (Figure 124) when defining an initial posture of the limbs:

- The hindfeet took strides of moderate length.
- They produced a broad trackway with reduced pace angulation and consistent step length.
- The forefeet often left a wider trackway than the hindfeet.
- Step length of the forefeet often exceeds step length of the hindfeet.

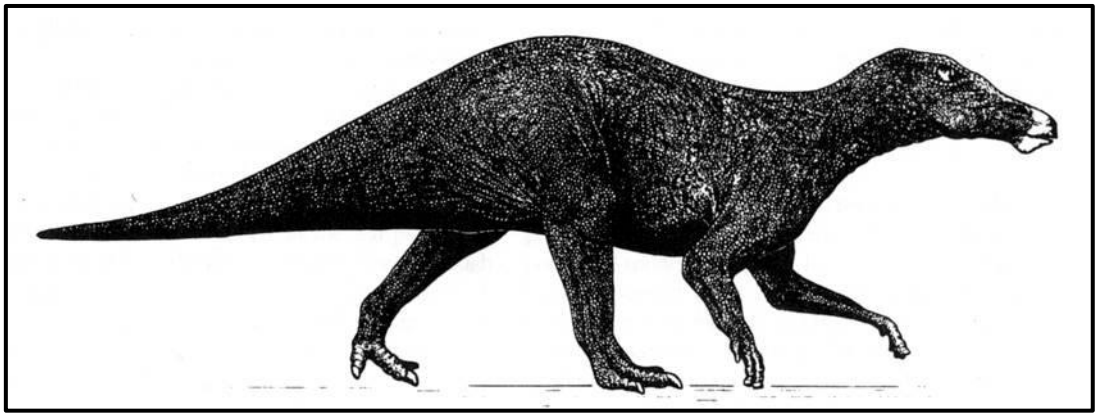

Figure 124: Restoration of an advanced ornithopod dinosaur in its quadrupedal gait (THULBORN 1989).

Further, the manus prints show that the dorsal surface of the hand is usually oriented forwards or anterolaterally (MORATALLA et al. 1992; LOCKLEY and WRIGHT 2001).

After MORATALLA et al. (1992) seems the inward rotation of the pes prints also to be typical of ornithopod quadrupedal trackways.

When arranging the initial cross gait body posture, it was tried to consider all these features resulting in the model posture shown in Figures 125A & B.

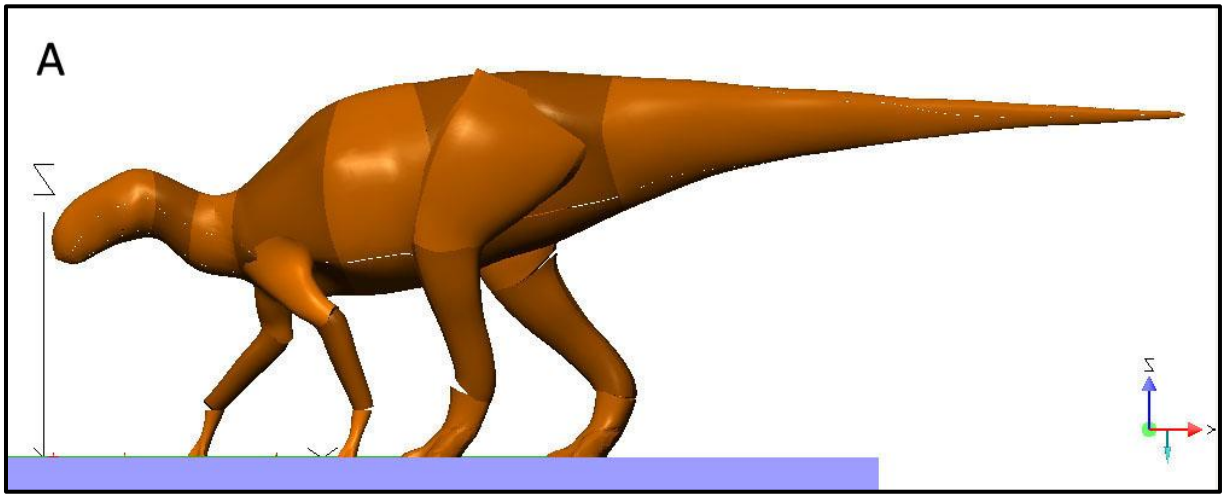

Figure 125: The *Brachylophosaurus* model in cross gait body posture from lateral (A) and cranial (B) view.

To achieve a moderate stride length of the hindfeet, they were placed in a moderate distance to each other along the x-axis (long axis of the model). Compared to the neutral standing pose the hindfeet were placed closer to the midline to increase stability, but without overlapping, to get a broad trackway with reduced pace angulation.

Due to their shorter length, the only way to attain a wider trackway of the forefeet, and to become an adequate step length of the forefeet compared to the hindfeet, is to shift the shoulder region closer to the ground below the level of the hips. Additionally, in this posture a forward orientation of the dorsal surface of the hand is only possible if the elbow is rotated outwards (right arm in Figure 125B).

A flexible tail was not included in the simulations due to the stiffened vertebral column caused by the ossified tendons (see chapter 2.1). Therefore, the model body moves as unit without an independent movement of the tail.

The following videos show the results of the **cross gait** simulation:

- **Video 5A** shows cross gait IS1 from lateral view.
- **Video 5B** shows cross gait IS1 from dorsal view.
- **Video 5C** shows cross gait IS2 from lateral view.
- **Video 5D** shows cross gait IS2 from cranial view.
- **Video 5E** shows cross gait IS2 from dorsocranial view.
- **Video 5F** shows cross gait IS2 from dorsocraniolateral view.
- **Video 5G** shows cross gait IS2 from caudal view.
- **Video 5H** shows cross gait IS2 from dorsocaudolateral view.

The second quadrupedal gait, the **pace gait**, was simulated using the same body posture as in the cross gait, but with inverted positions of the arms (Figure 126).

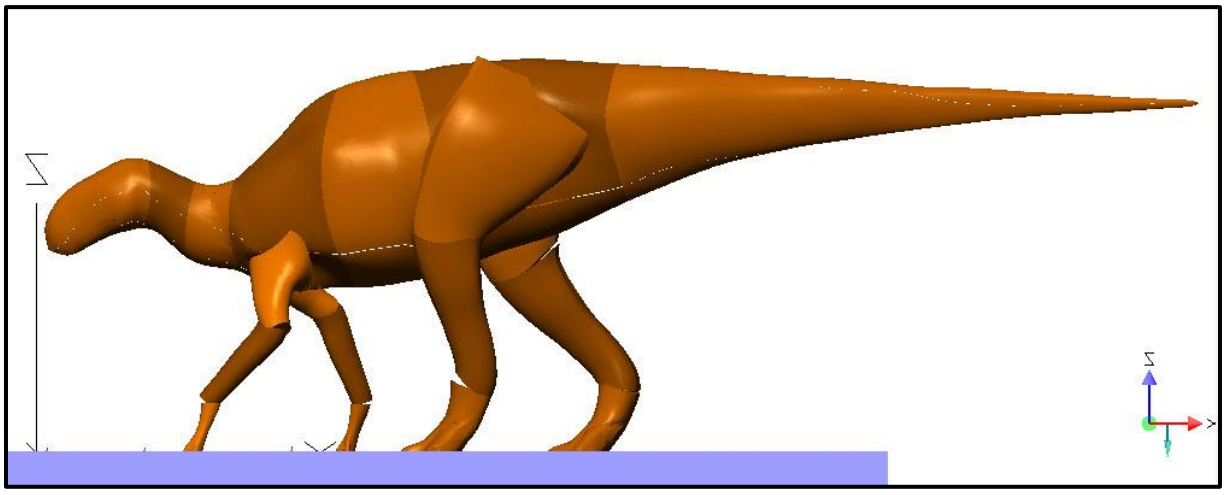

Figure 126: The *Brachylophosaurus* model in pace gait body posture from lateral view.

The following videos show the results of the **pace gait** simulation:

- **Video 6A** shows pace gait IS1 from lateral view.
- **Video 6B** shows pace gait IS1 from dorsal view.
- **Video 6C** shows pace gait IS1 from cranial view.
- **Video 6D** shows pace gait IS1 from dorsocranial view.
- **Video 6E** shows pace gait IS1 from caudal view.

Semibipedal gait A was developed on basis of the descriptions by WRIGHT (1999) (see chapter 2.2), concerning an ornithopod trackway from the Purbeck Limestone Group (Upper Jurassic-Lower Cretaceous, UK) attributed to an iguanodontid dinosaur.

In this trackway (left trackway in Figure 127) the foot prints are arranged in a single line and the hand prints were placed in two lines on either side of the line formed by the foot tracks. Therefore, they show a lateral position in relation to the foot prints instead of an anterolateral position. Further, the hand prints show that the dorsal surface of the hand is not oriented forwards or anterolaterally, but facing outwards parallel to the trackway midline with digit I directed anteriorly rather than medially (WRIGHT 1999).

The model body posture which was used for the simulations of semibipedal gait A is shown in Figures 128A & B.

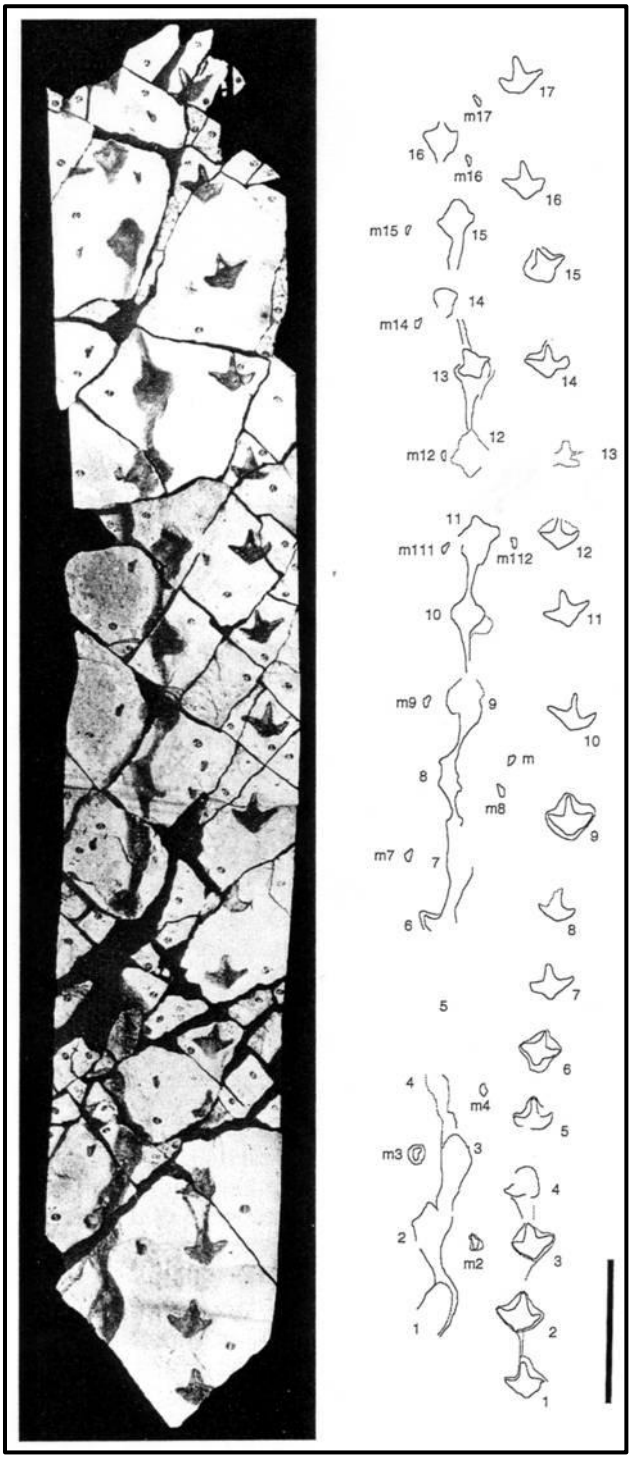

Figure 127: Two ornithopod trackways (picture (left) / drawing (right)), attributed to iguanodontid dinosaurs, from the Purbeck Limestone Group (Upper Jurassic-Lower Cretaceous, UK). The trackway on the left, showing manus (m) impressions, was used as guideline for the development of semibipedal gait A; scale bar = 1 m (WRIGHT 1999).

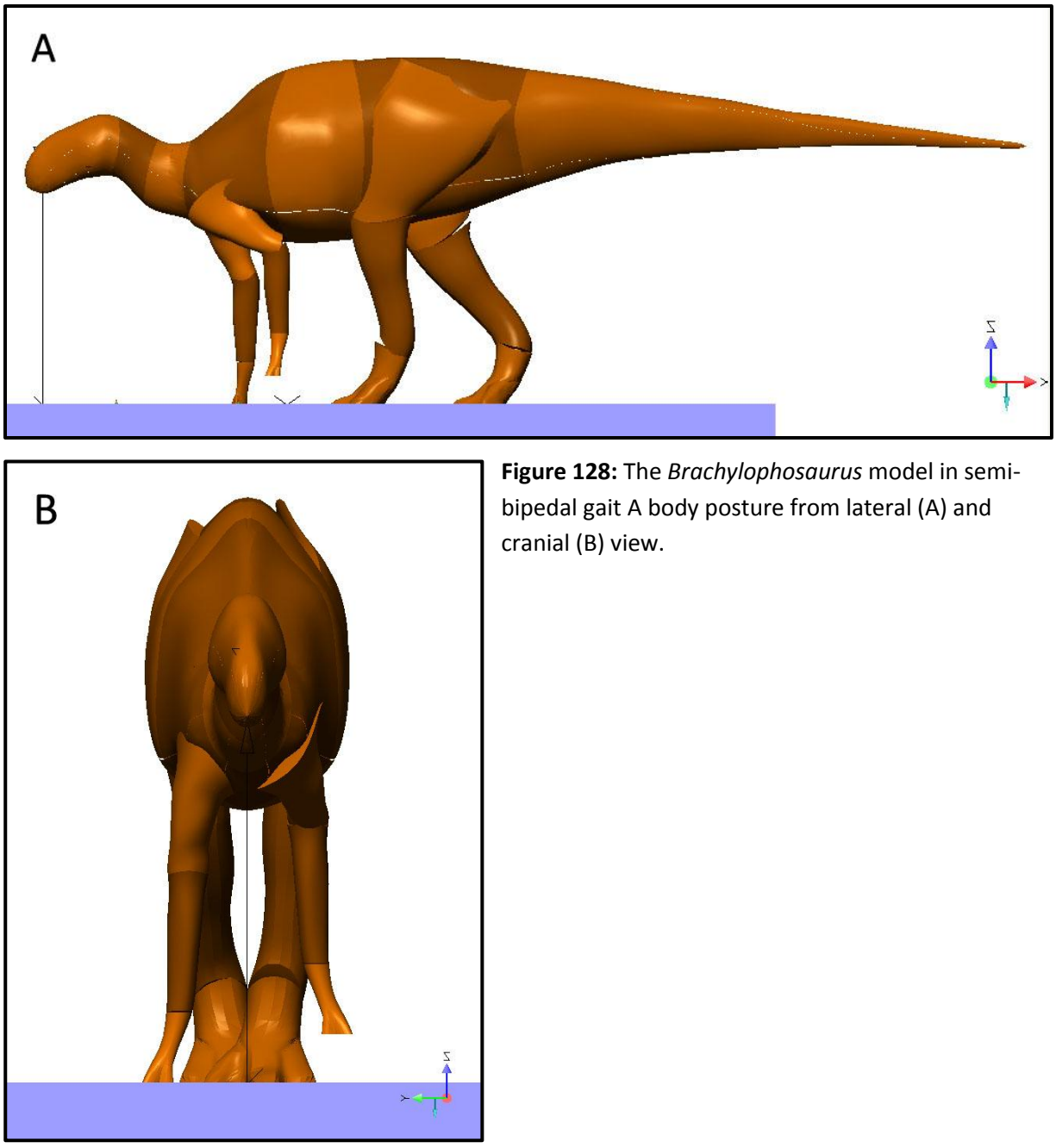

Figure 128: The *Brachylophosaurus* model in semi-bipedal gait A body posture from lateral (A) and cranial (B) view.

The following videos show the results of the **semibipedal gait A** simulation:

- **Video 7A** shows semibipedal gait A IS1 from lateral view.
- **Video 7B** shows semibipedal gait A IS1 from dorsal view.
- **Video 7C** shows semibipedal gait A IS2 from lateral view.
- **Video 7D** shows semibipedal gait A IS2 from dorsocranial view.
- **Video 7E** shows semibipedal gait A IS3 from cranial view.
- **Video 7F** shows semibipedal gait A IS3 from dorsocraniolateral view.
- **Video 7G** shows semibipedal gait A IS3 from caudal view.
- **Video 7H** shows semibipedal gait A IS3 from dorsocaudolateral view.

After semibipedal gait A has shown that the arms can be used in a different way, which means without rotation around the shoulder joints, the question arises if this kind of locomotion would also be possible in the simulations of cross and pace gait. To transform the cross gait in **semibipedal gait B** the generic constraints of the hands were removed and the motion of the arms was changed. In contrast, the body posture as well as the motion of the legs were not modified (Figure 129).

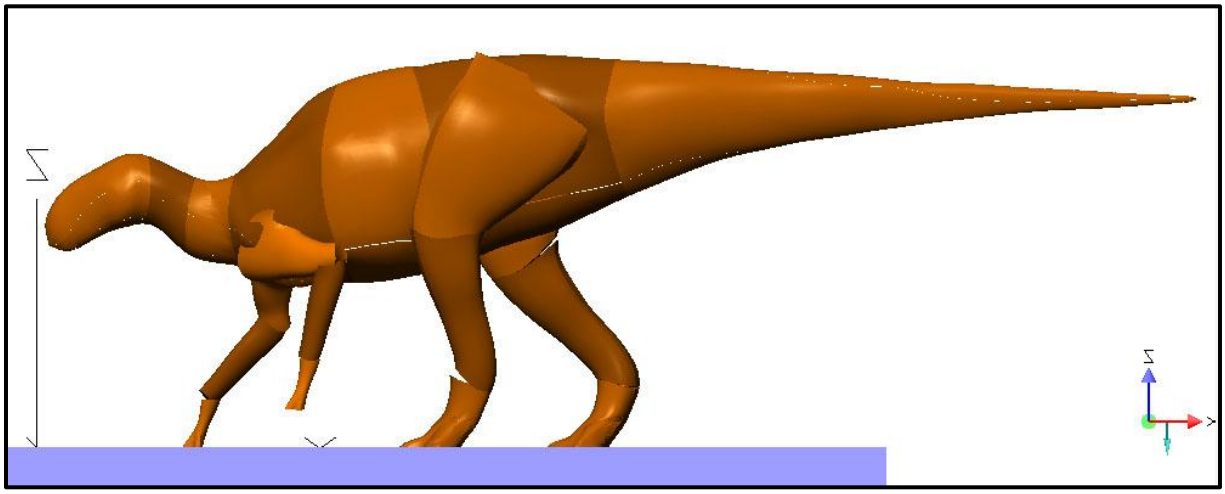

Figure 129: The *Brachylophosaurus* model in semibipedal gait B body posture from lateral view.

The following videos show the results of the **semibipedal gait B** simulation:

- **Video 8A** shows semibipedal gait B IS2 from lateral view.
- **Video 8B** shows semibipedal gait B IS2 from dorsocranial view.
- **Video 8C** shows semibipedal gait B IS2 from dorsocraniolateral view.
- **Video 8D** shows semibipedal gait B IS2 from dorsocaudolateral view.

When the simulation of semibipedal gait B was finished, the pace gait was also transformed in **semibipedal gait C** (Figure 130).

The following videos show the results of the **semibipedal gait C** simulation:

- **Video 9A** shows semibipedal gait C IS2 from lateral view.
- **Video 9B** shows semibipedal gait C IS2 from dorsocranial view.
- **Video 9C** shows semibipedal gait C IS2 from dorsocraniolateral view.
- **Video 9D** shows semibipedal gait C IS2 from dorsocaudolateral view.

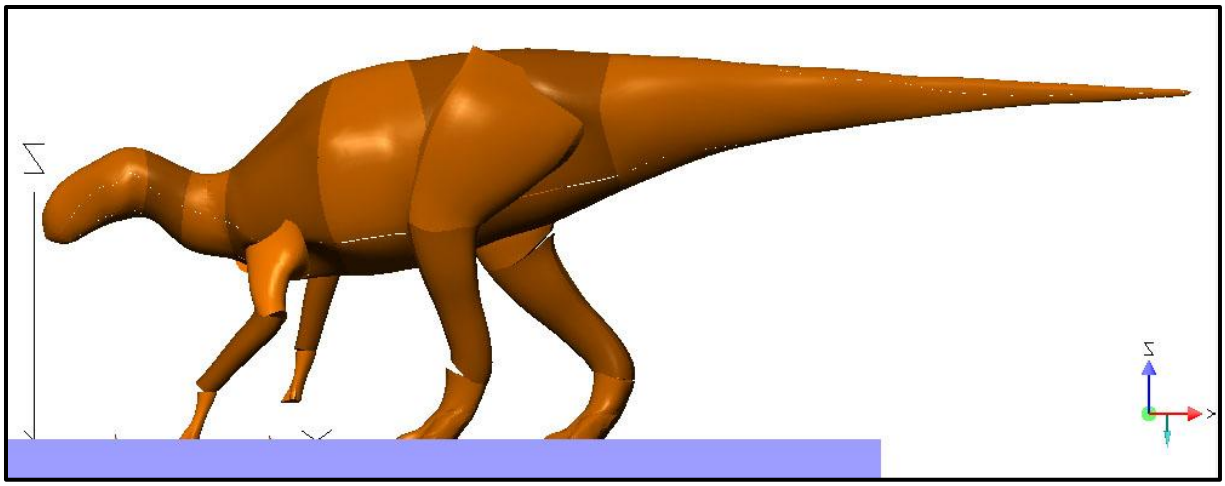

Figure 130: The *Brachylophosaurus* model in semibipedal gait C body posture from lateral view.

Semibipedal gait D (Figures 132A & B) and **semibipedal gait E** (Figures 133A & B) were developed on basis of two ornithopod trackways with manus impressions from the Lower Cretaceous of British Columbia (Figure 131 (A)) (LOCKLEY and WRIGHT 2001). The two trackways differ in their width, in the step length of the foot prints, and in the stride length and position of the hand prints. Semibipedal gait D bases on the left trackway (A), semibipedal gait E on the right trackway (A). **Semibipedal gait F** (Figures 134A & B) bases on an ornithopod trackway from the Lower Cretaceous of South Dakota (Figure 131 (B)) (LOCKLEY and WRIGHT 2001).

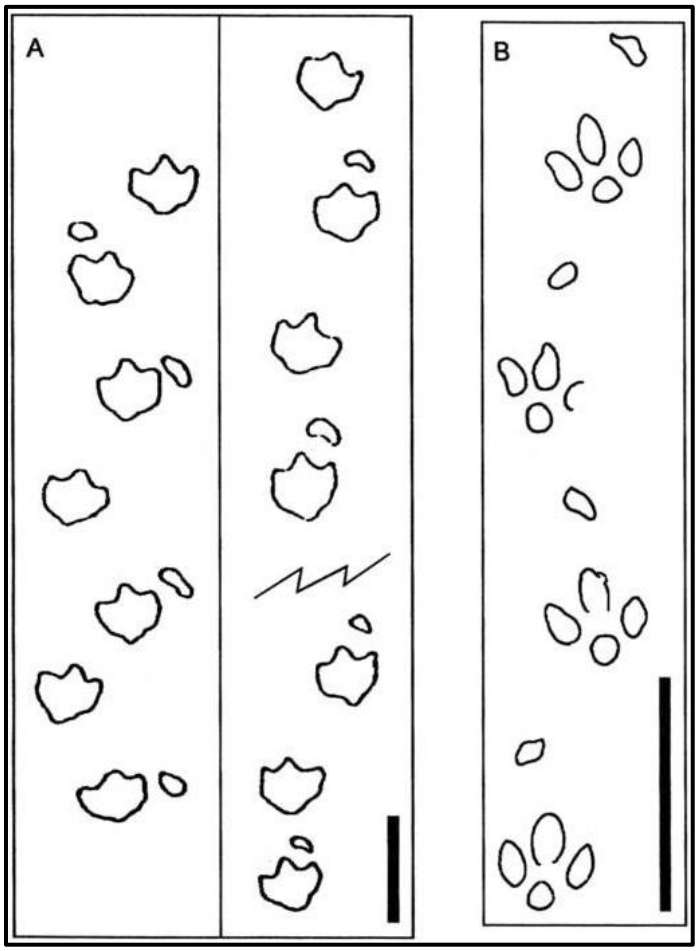

Figure 131: Lower Cretaceous trackways from British Columbia (A) and South Dakota (B). Tracks are attributed to large quadrupedal ornithopod dinosaurs; scale bar = 1 m (LOCKLEY and WRIGHT 2001). Semibipedal gait D bases on left trackway (A), semibipedal gait E on right trackway (A). Semibipedal gait F bases on trackway (B).

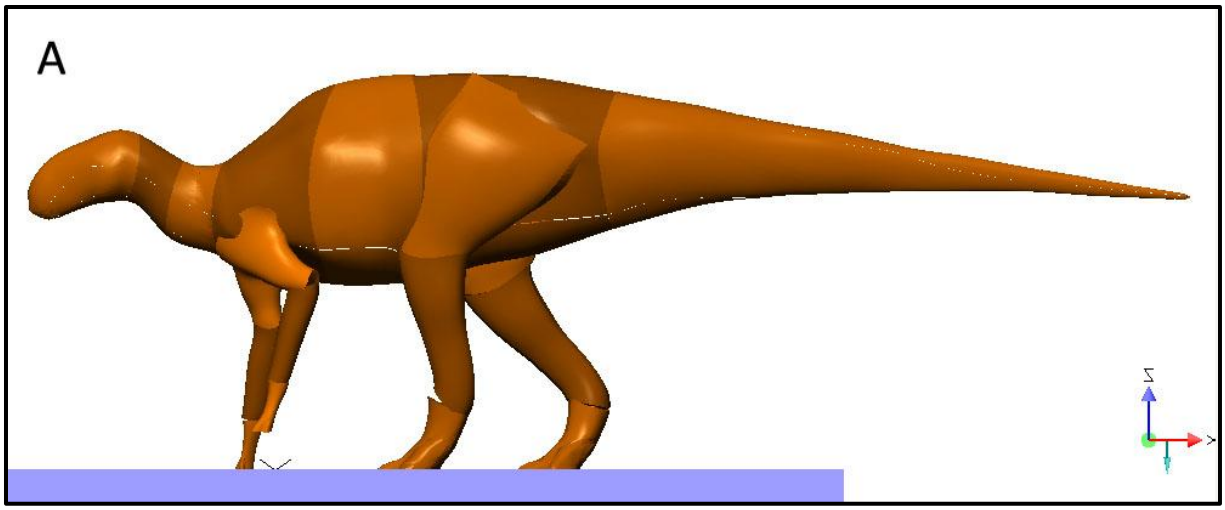

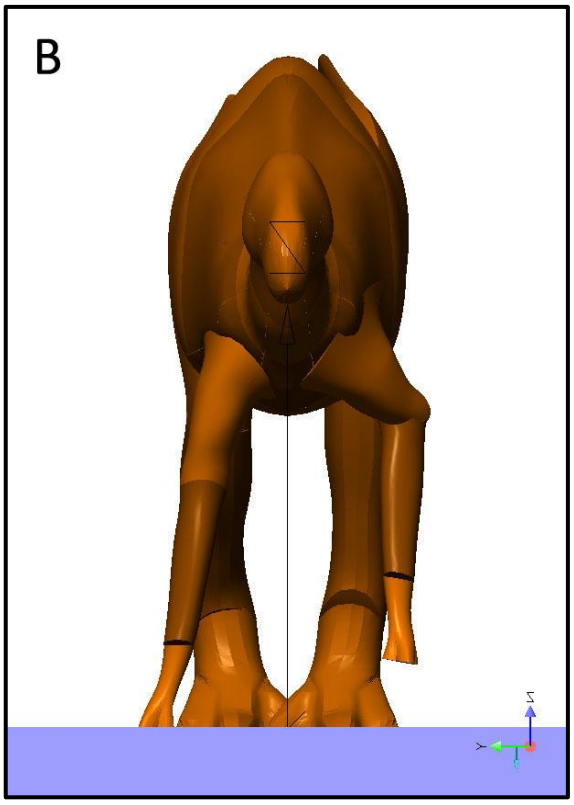

Figure 132: The *Brachylophosaurus* model in semi-bipedal gait D body posture from lateral (A) and cranial (B) view.

The following videos show the results of the **semibipedal gait D** simulation:

- **Video 10A** shows semibipedal gait D IS2 from lateral view.
- **Video 10B** shows semibipedal gait D IS2 from dorsal view.
- **Video 10C** shows semibipedal gait D IS2 from cranial view.
- **Video 10D** shows semibipedal gait D IS2 from dorsocraniolateral view.
- **Video 10E** shows semibipedal gait D IS2 from caudal view.
- **Video 10F** shows semibipedal gait D IS2 from dorsocaudolateral view.

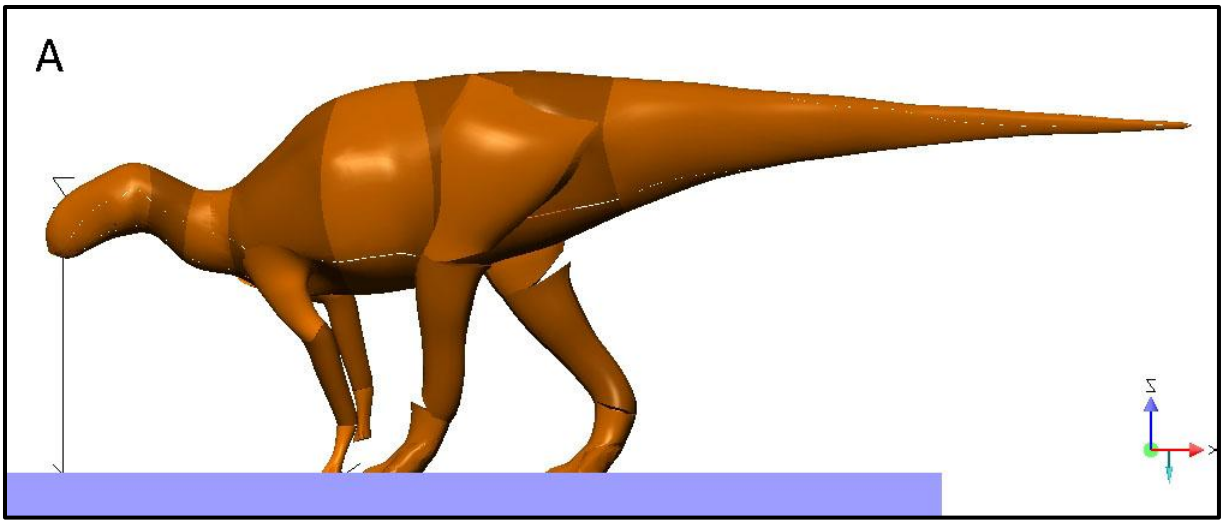

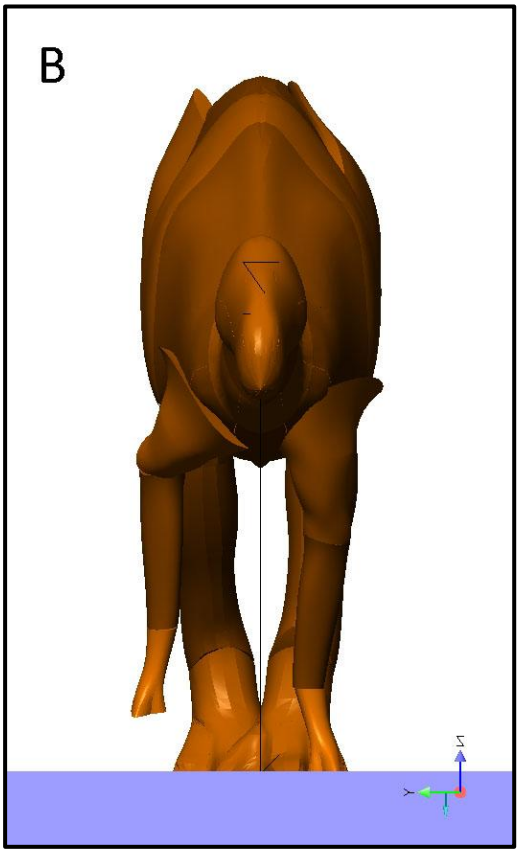

Figure 133: The *Brachylophosaurus* model in semi-bipedal gait E body posture from lateral (A) and cranial (B) view.

The following videos show the results of the **semibipedal gait E** simulation:

- **Video 11A** shows semibipedal gait E IS3 from lateral view.
- **Video 11B** shows semibipedal gait E IS3 from dorsal view.
- **Video 11C** shows semibipedal gait E IS3 from cranial view.
- **Video 11D** shows semibipedal gait E IS3 from dorsocraniolateral view.
- **Video 11E** shows semibipedal gait E IS3 from caudal view.
- **Video 11F** shows semibipedal gait E IS3 from dorsocaudolateral view.

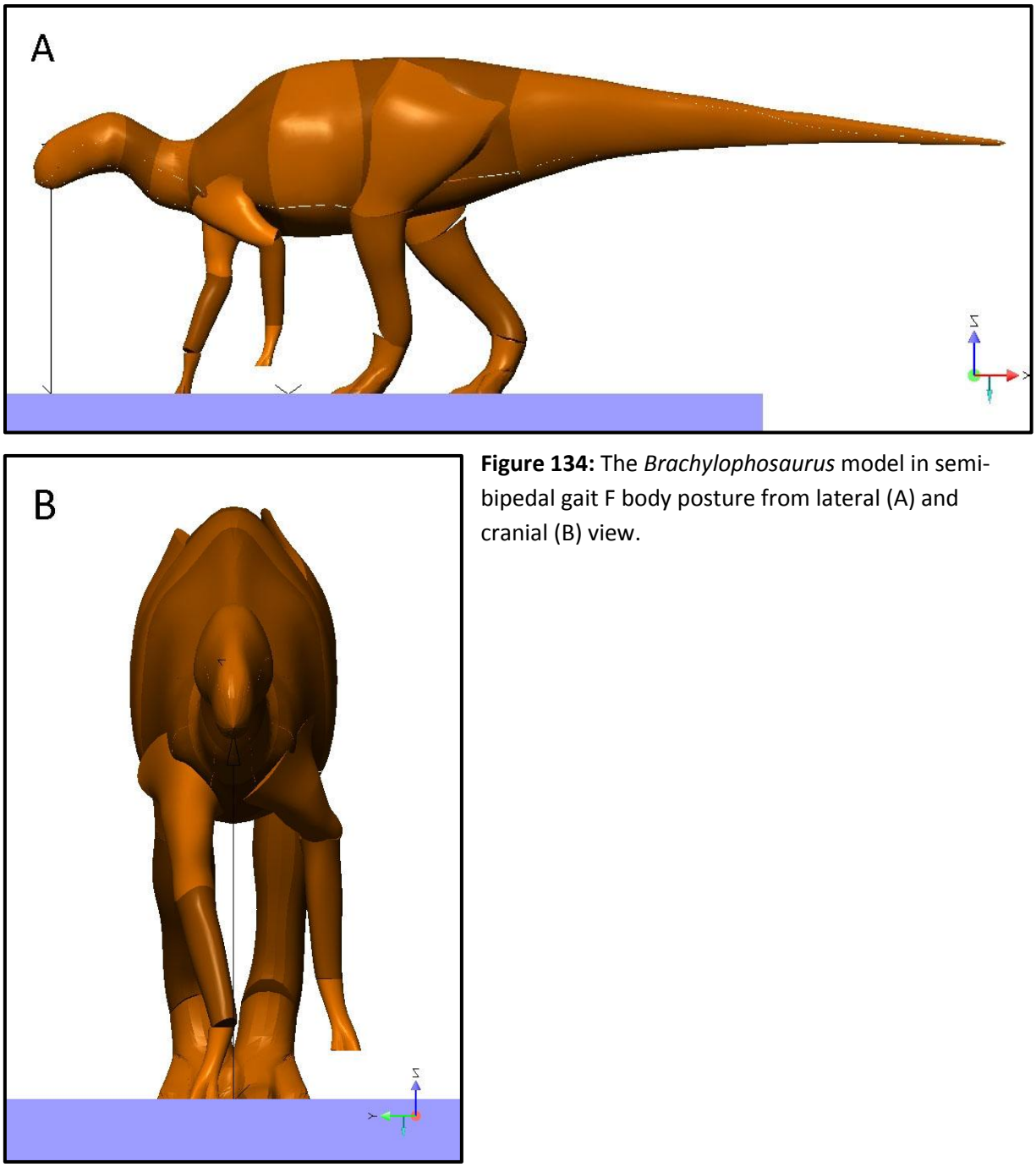

Figure 134: The *Brachylophosaurus* model in semi-bipedal gait F body posture from lateral (A) and cranial (B) view.

The following videos show the results of the **semibipedal gait F** simulation:

- **Video 12A** shows semibipedal gait F IS3 from lateral view.
- **Video 12B** shows semibipedal gait F IS3 from dorsal view.
- **Video 12C** shows semibipedal gait F IS3 from cranial view.
- **Video 12D** shows semibipedal gait F IS3 from dorsocraniolateral view.
- **Video 12E** shows semibipedal gait F IS3 from caudal view.
- **Video 12F** shows semibipedal gait F IS3 from dorsocaudolateral view.

The simulated quadrupedal gaits imply the question, if a gait change from quadrupedal to bipedal locomotion during progression would be possible. In case of the semibipedal gaits, this transition can be carried out easily by retracting both arms simultaneously. Concerning the cross gait, transition is more complex, as the arm is full included in the motion sequence.

The following videos show **motion change from semibipedal gait D to bipedal gait**:

- **Video 13A** shows gait change IS2 from lateral view.
- **Video 13B** shows gait change IS2 from cranial view.

In the motion change from cross gait to bipedal gait the generic constraints were hided in the videos for better visibility.

The following videos show **motion change from cross gait to bipedal gait**:

- **Video 14A** shows gait change IS2 from lateral view with unhidden generic constraints.
- **Video 14B** shows gait change IS2 from lateral view.
- **Video 14C** shows gait change IS2 from cranial view.
- **Video 14D** shows gait change IS2 from dorsocranial view.
- **Video 14E** shows gait change IS2 from caudal view.

5.1.2 Discussion

When regarding quadrupedal ornithopod trackways (Figure 135), it is obvious that they show no uniformity, but several differences in their appearance.

These differences are for example:

- The distance between the foot prints and the distance between the hand prints
- The position of the hand print in relation to the foot print
- The distance between hand and foot print
- The overlapping of the foot prints
- The orientation of the hand print: the dorsal surface of the hand is oriented in different ways
- The shape of hand and foot prints; only the tridactyl foot shape is uniform

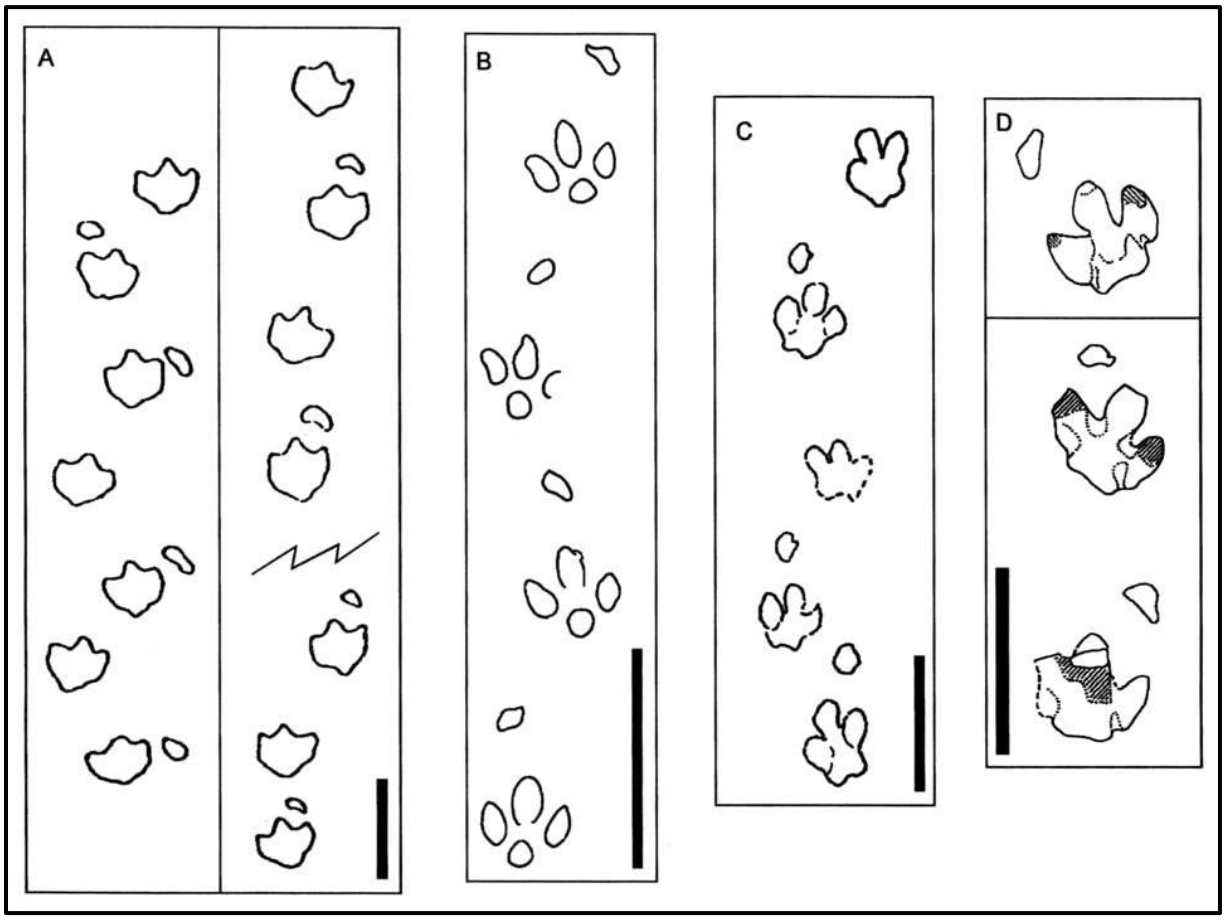

Figure 135: Trackways from large quadrupedal ornithopods from the Cretaceous of North America (from LOCKLEY and WRIGHT 2001): (A) Lower Cretaceous trackways from British Columbia; (B) Lower Cretaceous trackway from South Dakota; (C) *Caririchnium leonardii* from the Cenomanian of Colorado; (D) hadrosaur tracks from the Maastrichtian of Canada. Scale: 1m. ((A) after CURRIE 1983; (B) after LOCKLEY et al. 2001; (C) & (D) after CURRIE et al. 1991).

The variety of quadrupedal ornithopod trackways had to be considered in the simulations, making it impossible to simulate only one quadrupedal gait.

As Figures 127 & 135 show, are some trackways attributed to iguanodontids and not to hadrosaurs. However, as advanced iguanodontid dinosaurs, such as *Iguanodon*, and hadrosaurs are closely related (e.g. McDONALD et al. 2010, McDONALD 2012), there are only minor differences between their trackways (THULBORN 1990). Therefore, it was of importance to include also the iguanodontid trackways in the simulations to reflect the variety of quadrupedal locomotion in advanced ornithopod dinosaurs.

The **cross gait** (Videos 5A–H) trackway of the model (Figure 137) shows the characteristics described by THULBORN (1989), as the moderate stride length of the hindfeet, the broad trackway of the hindfeet including reduced pace angulation and consistent step length, and the wider trackway of the forefeet, which leads to a larger step length compared to the hindfeet. In addition, the hand print shows the required forward respectively anterolaterally orientation of its dorsal surface (e.g. LOCKLEY and WRIGHT 2001) and a position anterolateral to digits III and IV of the foot print (CURRIE et al. 1991; LOCKLEY and WRIGHT 2001; XING et al. 2012, see Figure 136). The inward rotation of the foot prints, which was described by MORATALLA et al. (1992), is also shown by most of the foot prints in Figure 135. Therefore, it was tried to include this feature in all simulations showing quadrupedal locomotion by inward rotation of the legs. However, in case of cross and pace gait the chosen rotation degree was not high enough so that the model trackways show only minor inward rotation of the foot prints (Figures 137 & 138). As a model trackway can be controlled first when the simulation is finished, the rotation degree was not corrected in the cross and pace gait simulations but in the following ones.

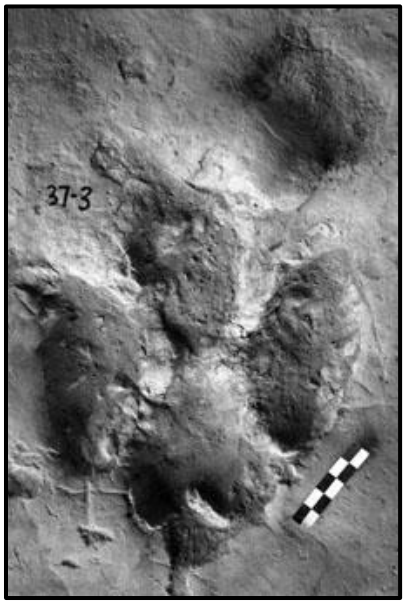

Figure 136: Left manus and pes track (from ventral) from the 'mid'-Cretaceous Lotus track site of south-central China attributed to *Caririchnium lotus*; scale bar = 10 cm (XING et al. 2012).

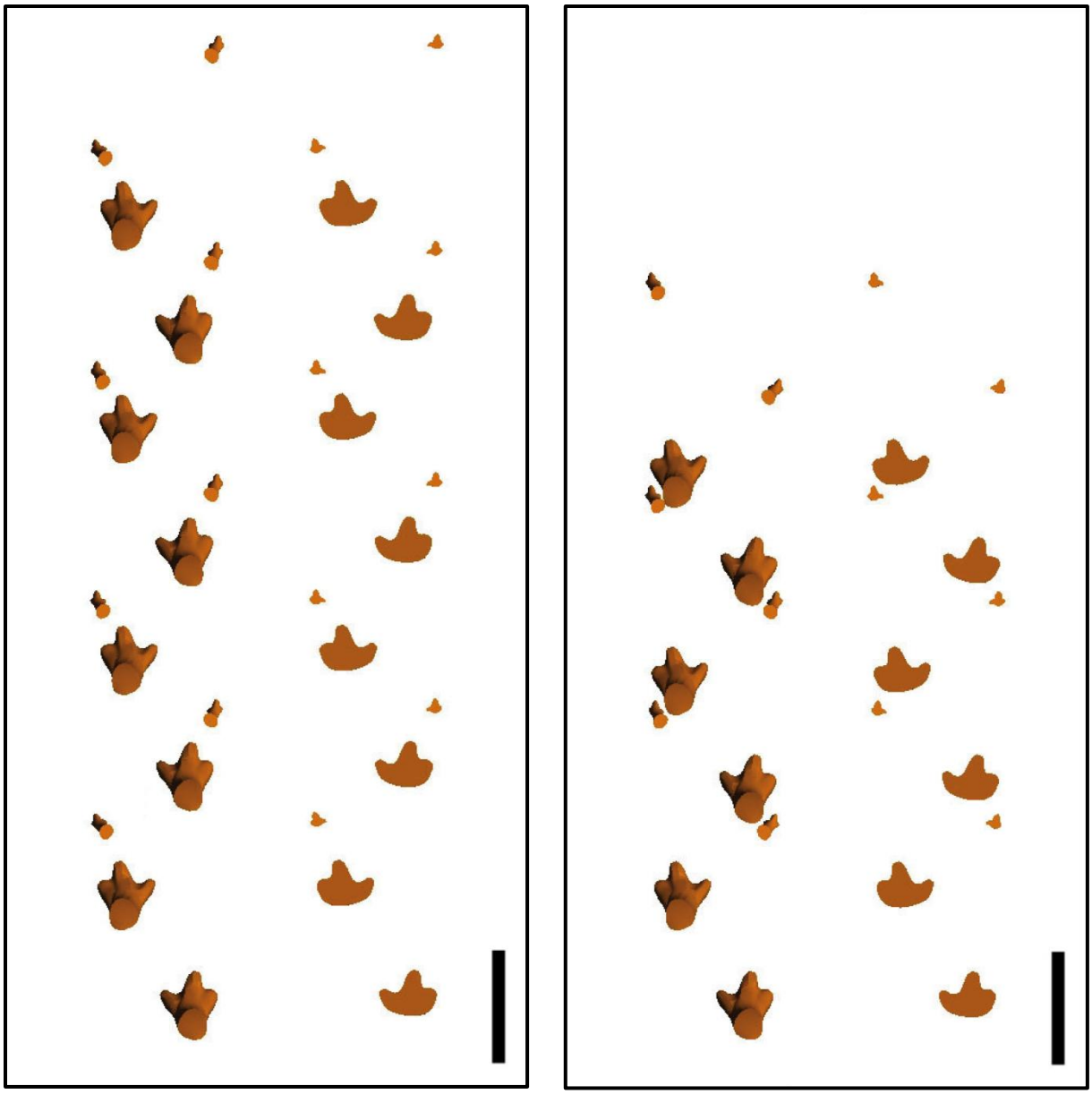

Figure 137 (left): Model trackway of the cross gait from dorsal view. The left trackway shows the position and orientation of hands and feet. The right trackway shows the corresponding hand and foot prints; scale bar = 1 m.

Figure 138 (right): Model trackway of the pace gait from dorsal view. The left trackway shows the position and orientation of hands and feet. The right trackway shows the corresponding hand and foot prints; scale bar = 1 m.

In contrast to the cross gait shows the **pace gait** (Videos 6A-E) model trackway (Figure 138) not the required characteristics. This trackway shows a posterolaterally position of the hand print in relation to the foot print and a wider space between the foot prints, which are also slightly rotated outwards.

As described in chapter 5.1 the simulation of a gallop (SELLERS et al. 2009) was not possible. However, the tracks of the simulated gallop have so far no analogy in the fossil

record, so that the use of a galloping gait in advanced ornithopods is rather unlikely, although not impossible.

In all simulations the tracks of the model are usually placed very regular, showing relatively constant stride and step lengths. Here, the question arises if a living animal would show more fluctuations in the placement of hands and feet, but to include such fluctuations in the walking simulations would be difficult and time consuming. Further, MORATALLA et al. (1992) examined a trackway with a regular distance between manus impressions, suggesting a 'harmonic' quadrupedal progression in which the limb movements are well coordinated. In addition, some of the hand and foot prints in Figure 135 show also such a distribution (e.g. left trackway A), which means that a regular arrangement of hand and foot prints in the model trackways is not in conflict with the fossil tracks.

The accordance of the cross gait model trackway with the literature (THULBORN 1989) seems to confirm Thulborn´s description of the hadrosaurian body posture while walking quadrupedally. The position of the shoulder region below the level of the hips, leading to a more downward directed anterior body, and the outward rotation of the elbows correspond with his implications and his assumed 'low-slung and somewhat sprawling gait' (THULBORN 1989).

While the arm rotates around the shoulder joint during forward motion, the scapula in quadrupedal ornithischians is rather rigid and probably does not move significantly during locomotion (MAIDMENT et al. 2012). As the simulation of the cross gait shows (Videos 5A-H), requires this arm rotation also a slight outward rotation of the hand on the ground (Figure 139). Since this hand rotation is not reported from tacks it was tried to avoid it, but the motion sequence did not work well without. This might be a result of technical constraints in the simulation, but the existence of such a slight hand rotation is nevertheless not impossible as it could be difficult to recognize it in the fossil record.

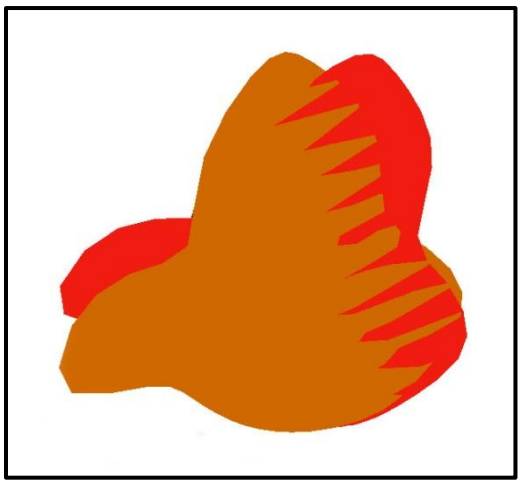

Figure 139: Right hand of the model from dorsal view, showing the position of the hand before the rotation (brown) and after it (red).

The model motion from one side to the other and back (zig-zag motion) during forward progression, which can be observed in all simulations showing quadrupedal locomotion, is caused by the inward rotation of the feet respectively legs, which is in accordance with the fossil tracks. In contrast, the arms are not involved here, as can be seen in semibipedal gait B, which is identical with the cross gait with the exception of the arms use. Semibipedal gait B shows that the body rotates from side to side even if the arm does not rotate around the shoulder joint.

The movement of the center of mass along the y-axis (Figure 140) is not regular, in contrast to its movement along the z-axis (Figure 141). Here, the up and down of the hips is clearly visible, showing a maximum nearly half of each step. The irregular movement along the y-axis is based most likely on the complex motion sequence of the cross gait. However, both curves show that the center of mass is hardly influenced by the rotation of the body, as the range of motion is rather limited.

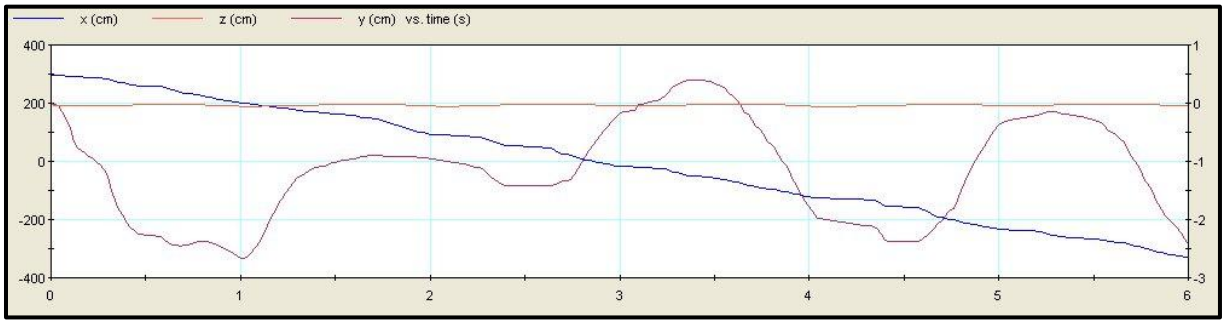

Figure 140: The diagram displays the position of the center of mass along the y-axis during the cross gait simulation (distance (cm) vs. time (s)). The scale on the left axis of the diagram belongs to the x- and z-axis, the reduced scale on the right belongs to the y-axis.

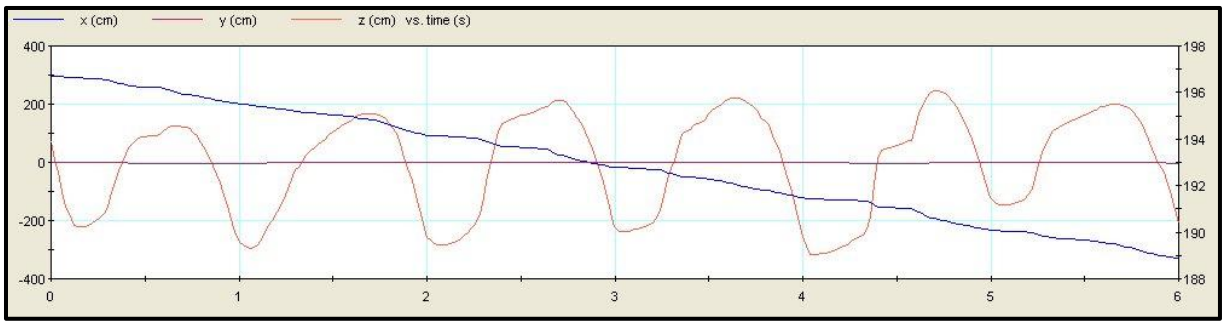

Figure 141: The diagram displays the position of the center of mass along the z-axis during the cross gait simulation. The scale on the left axis of the diagram belongs to the x- and y-axis, the reduced scale on the right belongs to the z-axis.

MORATALLA et al. (1992) supposed that the inward rotation of foot prints, which can be recognized in bipedal and quadrupedal locomotion, is caused by a slight rotation of the pelvic girdle and the swinging of the tail as a counterbalance during progression. Pelvic rotation and swinging of the tail are also connected with an inward rotation of the legs in the simulations, which seems to confirm the authors' assumption. According to Figure 140, the center of mass is obviously affected only to a minor degree by this pelvic rotation and tail swinging.

When simulating quadrupedal locomotion in hadrosaurs, the question arises to which extent the forelimbs supported the animal´s body mass. Based for example on the position of the center of mass, different authors were of the opinion that the forelimbs played no major supportive role and carried only a small percentage of the body mass (e.g. DILKES 2001; MORATALLA et al. 1992; THULBORN 1989, 1990). In the simulations the cross gait body posture was used to test this assumption. However, as the model should not move forward in this simulation, the generic constraints were deleted and all revolute motor joints were changed into rigid joints. Then, between ground and feet the 'collide' function was set, whereas the ground below the arms was deleted (Figure 142). Through this the distribution of the body mass can be demonstrated by using the influence of gravity.

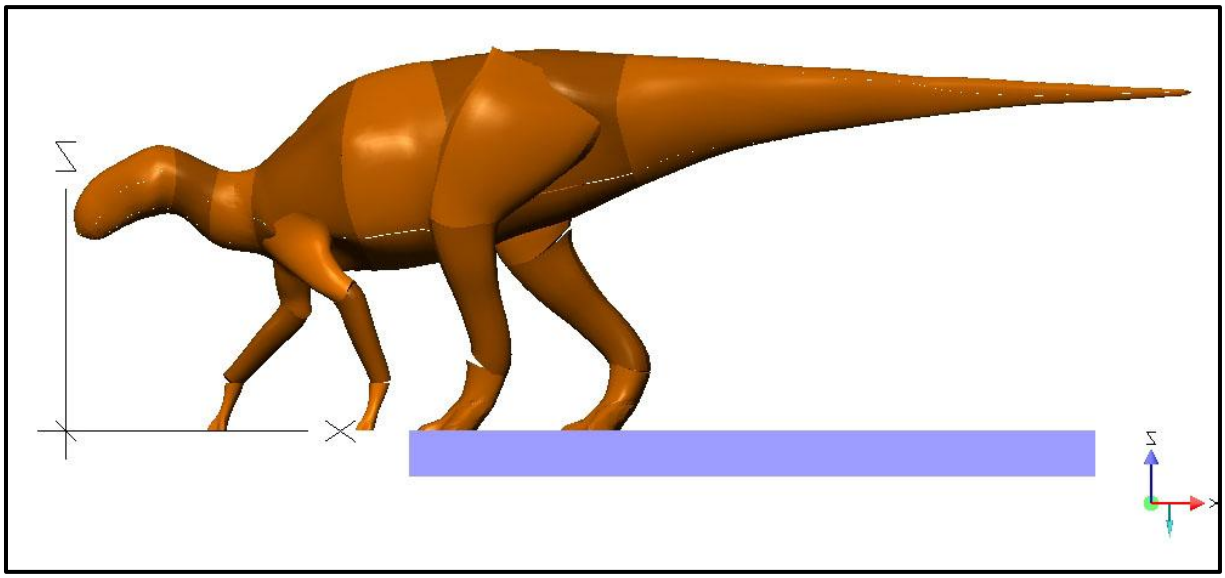

Figure 142: The *Brachylophosaurus* model in cross gait body posture from lateral view, ready for testing the supportive role of the forelimbs together with the distribution of the body mass.

- **Video 15A** shows the gravity test to define the supportive role of the forelimbs to bear the body mass.

The sequence shows that the model does not overturn forward when starting the simulation, indicating that the forelimbs are not loaded and therefore do not bear the body mass. This result could be expected due to the calculated position of the center of mass (see chapter 4.6) and the higher mass of the caudal body parts (see Table 1 / chapter 4.6), but the gravity test is nevertheless a good possibility to illustrate the potential supportive role of the forelimbs more clearly.

Finally, although the simulated cross gait and the associated model trackway are in accordance with the description by Thulborn, the tracks on which his description is based seem to be arguable. THULBORN (1989, 1990) used for his description the trace fossil *Moyenisauropus natator* (ELLENBERGER 1974) (now *Anomoepus natator* (OLSEN and GALTON 1984)), an ichnogenus from the Lower Jurassic of southern Africa, as example of an ornithopod walking on all fours. However, after LOCKLEY and WRIGHT (2001) are these tracks fundamentally different from the trackways of large quadrupedally walking ornithopods from the Cretaceous. The pes digits often show a clear hallux and the tracks often display manus prints that are pentadactyl, or at least tetradactyl when not fully impressed (Figure 143).

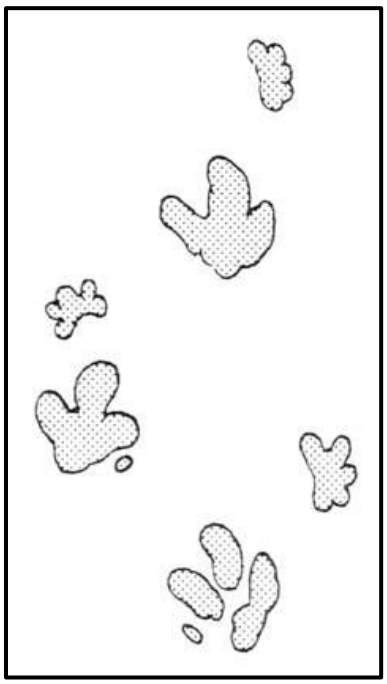

Figure 143: Ichnogenus *Moyenisauropus* (*Anomoepus*) *natator* from the Lower Jurassic of southern Africa (THULBORN 1989, after ELLENBERGER 1974).

Despite the arguments of LOCKLEY and WRIGHT (2001), shows the *Moyenisauropus (Anomoepus) natator* trackway some characteristics which occur also in the trackways shown in Figure 135, as the inward rotation of the foot prints, the wider trackway of the hand prints, and the position of the hand print anterolateral to digits III and IV of the foot print. However, to apply the characteristics of the *Moyenisauropus* trackway to quadrupedal ornithopod motion in general, as suggested by THULBORN (1989, 1990), is not possible like the trackways in Figure 135 show. Nevertheless, regarding this variety of trackways, the motion sequence of the cross gait simulation could be part of the wide range of quadrupedal locomotion shown by advanced ornithopod dinosaurs.

In those simulations which base on a fossil trackway, as semibipedal gaits A, D, E, and F, a wide accordance between the model trackways and the original ones should be achieved. Therefore, each model trackway should illustrate the essential characteristics of the respective fossil one, especially the correct position and orientation of hand and foot prints. It has to be considered that body size of the original track-maker and the model can be different, but it can be supposed that a comparison of body size is possible by comparing foot size of the fossil trackway with that of the model. However, as the actual size of the *Brachylophosaurus* foot is unknown, and the size of the modeled foot is only estimated, only a rough comparison of body size is possible. Concerning specific measures, like trackway width, step length of hand and foot prints, stride length of hand and foot prints, and distance between hand and foot print, it is difficult to transfer them correctly from the fossil trackway into a simulation, which was therefore not successful in all cases (Table 3).

	Semibiped A (1)		**Semibiped D**		**Semibiped E**		**Semibiped F**	
	Fossil trackway	**Modell trackway**	**Fossil trackway**	**Modell trackway**	**Fossil trackway**	**Modell trackway**	**Fossil trackway**	**Modell trackway**
Trackway width	33 cm	60 cm	111 cm	87 cm	82 cm	68 cm	64 cm	70 cm
Foot length	29 cm	40 cm	52 cm	40 cm	52 cm	40 cm	39 cm	40 cm
Foot width	24 cm	50 cm	60 cm	50 cm	60 cm	50 cm	41 cm	50 cm
Stride length foot prints	111 cm	187 cm	194 cm	187 cm	237 cm	247 cm	198 cm	190 cm
Step length foot prints	56 cm	93 cm	109 cm	103 cm	122 cm	125 cm	105 cm	97 cm
Stride length hand prints	91 cm	190 cm	193 cm	185 cm	237 cm	243 cm	200 cm	190 cm
Step length hand prints	75 cm	140 cm	85 cm **(2)**	140 cm	**(3)**	**(3)**	102 cm	100 cm
Distance hand and foot print	27 cm	45 cm	52 cm	37 cm	52 cm	43 cm	51 cm	47 cm

Table 3: Comparison of different measures from the fossil trackways and the respective model trackways of semibipedal gaits A, D, E, and F. Nearly all values display the average of the corresponding measures. All values were measured accurately as possible, but slight inaccuracies cannot be excluded. **(1)** The foot prints of the fossil trackway are not well preserved, which hindered precise measures; **(2)** Only one measure could be taken; **(3)** Step length of the hand prints could not be measured in the fossil trackway, therefore no measure was taken in the model trackway.

The model trackway (Figure 144) of **semibipedal gait A** (Videos 7A-H) shows most of the characteristics of the ornithopod trackway from the Purbeck Limestone Group described by WRIGHT (1999) (Figure 127). In both trackways the foot prints are arranged in a single line and the hand prints were placed in two lines on either side of the line formed by the foot tracks. As in the fossil trackway, the dorsal surface of the hand is oriented outwards in the model trackway, but to a minor extent. Therefore, the hand print is not fully parallel to the trackway midline with digit I directed anteriorly. The foot prints show also an inward rotation like in other quadrupedal trackways, which correlates again with pelvic rotation and swinging of the tail as can be seen in the simulation.

The comparison of the measures taken from the fossil trackway with those from the model trackway (Table 3) shows that the correct measures were not achieved in the simulation of semibipedal gait A.

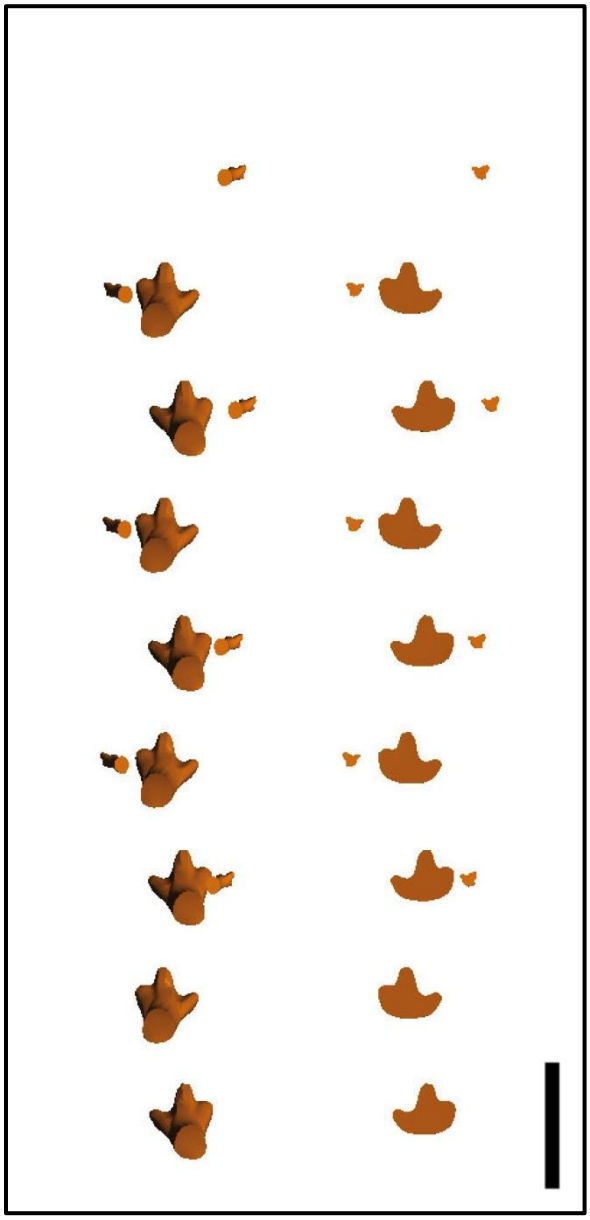

Figure 144: Model trackway of semibipedal gait A from dorsal view. The left trackway shows the position and orientation of hands and feet. The right trackway shows the corresponding hand and foot prints; scale bar = 1 m.

However, comparing length and width of the foot prints, which are obviously not well preserved in the fossil trackway, the track-maker seems to have a smaller body size than *Brachylophosaurus*. This would make the larger measures of the model trackway maintainable, but they are rather too high. However, the influence of a larger or smaller body size on these trackway measures can only be estimated. Nevertheless, it was tried to achieve a higher accordance between the different measures from the fossil and model trackways in the other semibipedal gaits.

The curves which display the position of the center of mass along the y-axis (Figure 145) and the z-axis (Figure 146) in semibipedal gait A show a more regular progression than those of the cross gait (Figures 140 & 141). Especially the movement of the body from one side to the other and back (along the y-axis) is visible more clearly in semibipedal gait A, and along the z-axis the curve reaches a maximum more exactly at each half step. However, along the y-axis the center of mass shows an opposite motion to that of the model, as the anterior body moves opposite to the posterior part. Hence, when the body turns to the left (positive numbers in the diagram) the center of mass turns to the right (negative numbers in the diagram) and vice versa. The reversal takes place not exactly at every full second but with a minor delay, presumably caused by the inertia effect. This delay can also be observed in the motion curve of the z-axis.

During progression the center of mass shows no symmetrical movement along the y-axis (Figure 145), but a lesser movement to the right and a stronger one to the left. This means that the model moves more and more to the right during the simulation, but of course only to a minor degree which has no influence on the simulation. This asymmetrical movement of the center of mass shows that it is difficult to generate symmetrical steps, as mirroring the values of one step to the other is usually not possible.

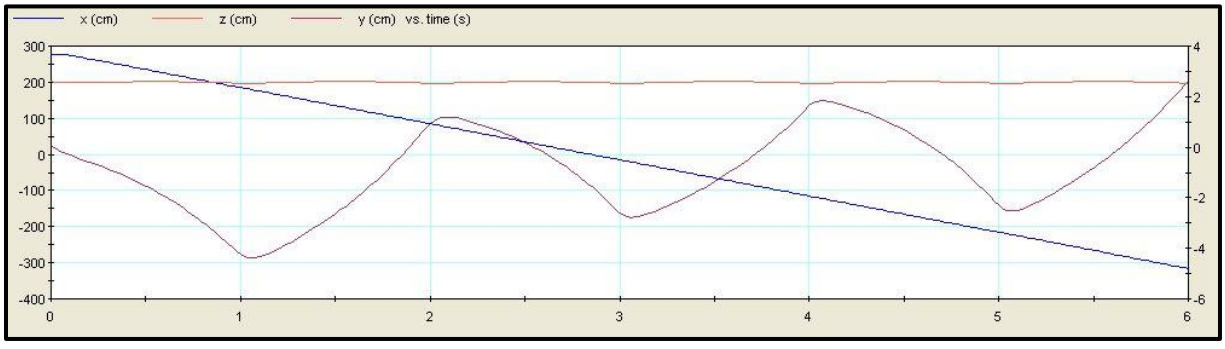

Figure 145: The diagram displays the position of the center of mass along the y-axis during the semibipedal gait A simulation.

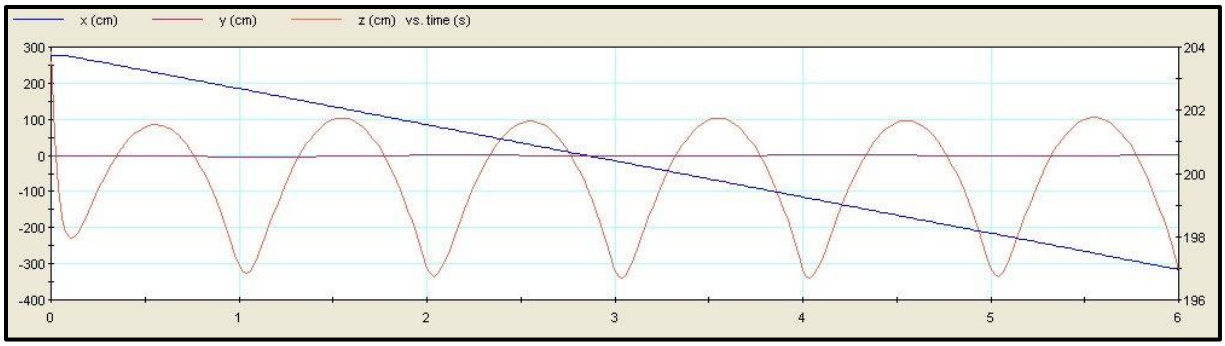

Figure 146: The diagram displays the position of the center of mass along the z-axis during the semibipedal gait A simulation.

In the cross gait the movement of the center of mass along the y-axis (Figure 140) differs considerably from semibipedal gait A. An opposite movement of the center of mass in comparison to the body motion can be recognized only at the beginning of the simulation (mainly between 0.0s and 1.0s), but later it moves in the same direction as the body. Further, the change from one side to the other and back is not synchronal with the transition from one step to the following one, and in the range between 1.0s and 2.8s its movement is relatively straight. It can be assumed that the more simple motion sequence of semibipedal gait A, without a rotation of the arm / body around the shoulder joint, caused the more regular movement of the center of mass along the y-axis in this simulation.

WRIGHT (1999) suggested that the track-maker held his arms in a vertical position when the hands were in contact with the ground, an assumption which is supported by the simulation. Regarding the skeletal anatomy of the wrist (Figures 67 & 72), a more straight posture of the forelimb seems to be essential when the back of the hand is facing outwards, as the bending of the wrist in the parasagittal plane is rather limited in that case (Figures 147 & 149). In contrast, when the dorsal surface of the hand is directed forwards, the bending of the wrist in the parasagittal plane is possible to a much greater extent (Figures 148 & 150). Hence, it seems that the more the back of the hand is directed outwards the more the arm must have a straight posture.

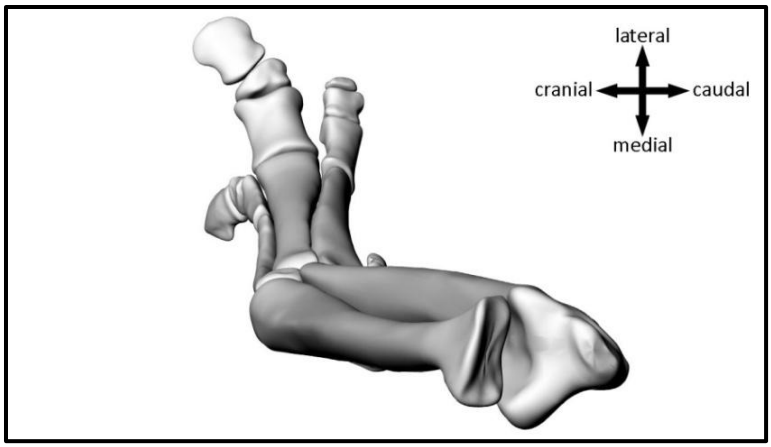

Figure 147: Right forearm and hand of the *Brachylophosaurus* skeleton from dorsal view, showing bending of the wrist in the parasagittal plane with dorsal surface of the hand directed outwards

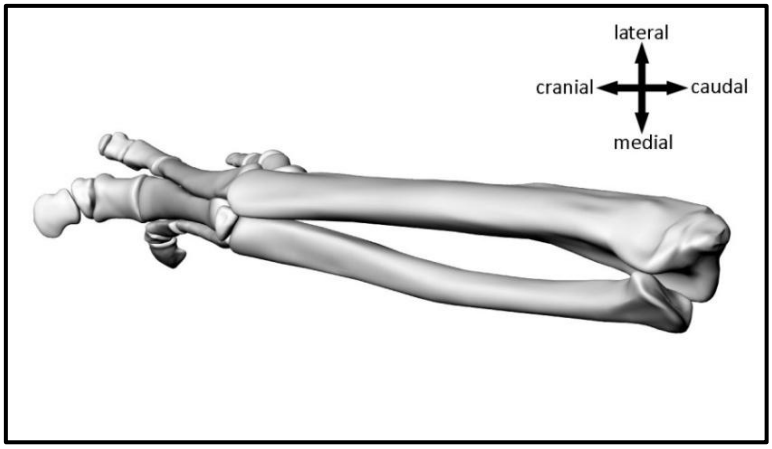

Figure 148: Right forearm and hand of the *Brachylophosaurus* skeleton from dorsal view, showing bending of the wrist in the parasagittal plane with dorsal surface of the hand directed forwards.

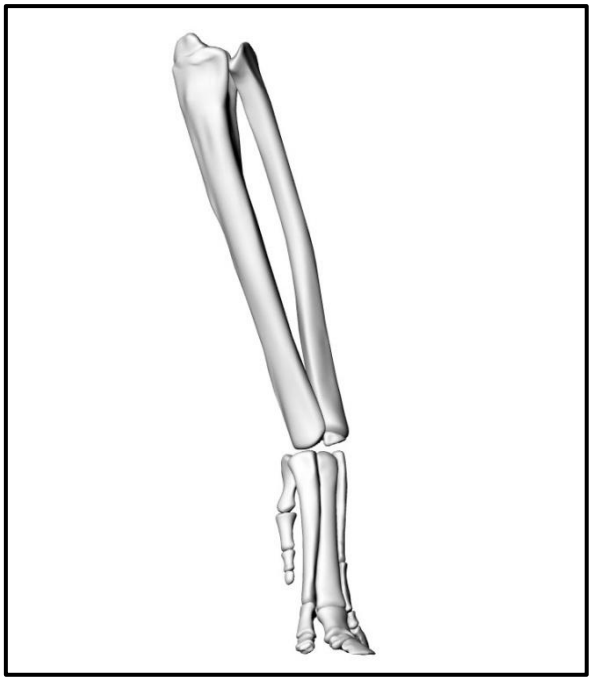

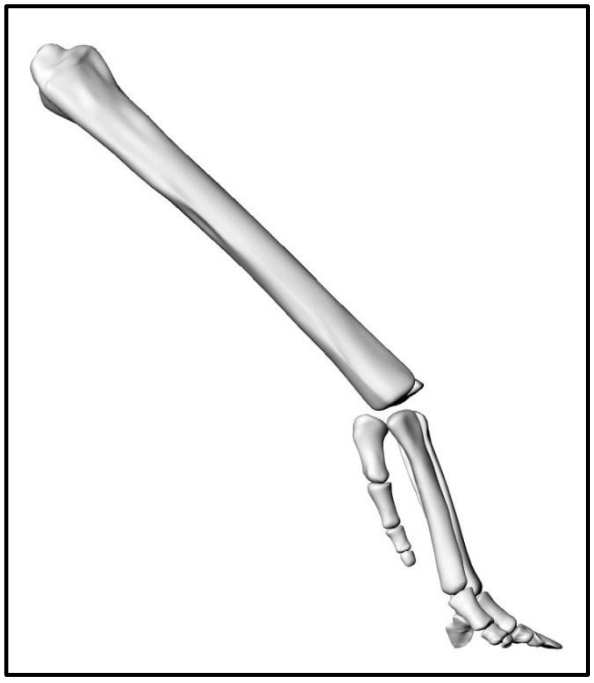

Figure 149 (left): Right forearm and hand of the *Brachylophosaurus* skeleton from lateral view, showing bending of the wrist in the parasagittal plane with dorsal surface of the hand directed outwards.

Figure 150 (right): Right forearm and hand of the *Brachylophosaurus* skeleton from lateral view, showing bending of the wrist in the parasagittal plane with dorsal surface of the hand directed forwards

Beside the correct posture of the arm, the semibipedal gait A simulation bears another problem. Regarding the interval from 0.0s to 1.0s for example, the right hand in the cross gait simulation (Figure 125A) could remain in contact with the ground during this whole first step (Figure 151). In semibipedal gait A this is not possible (Figure 152), since the right arm is too short to remain in contact with the ground during the first step. However, the position of the hand cannot be changed, as otherwise it would be no longer in accordance with the fossil tracks.

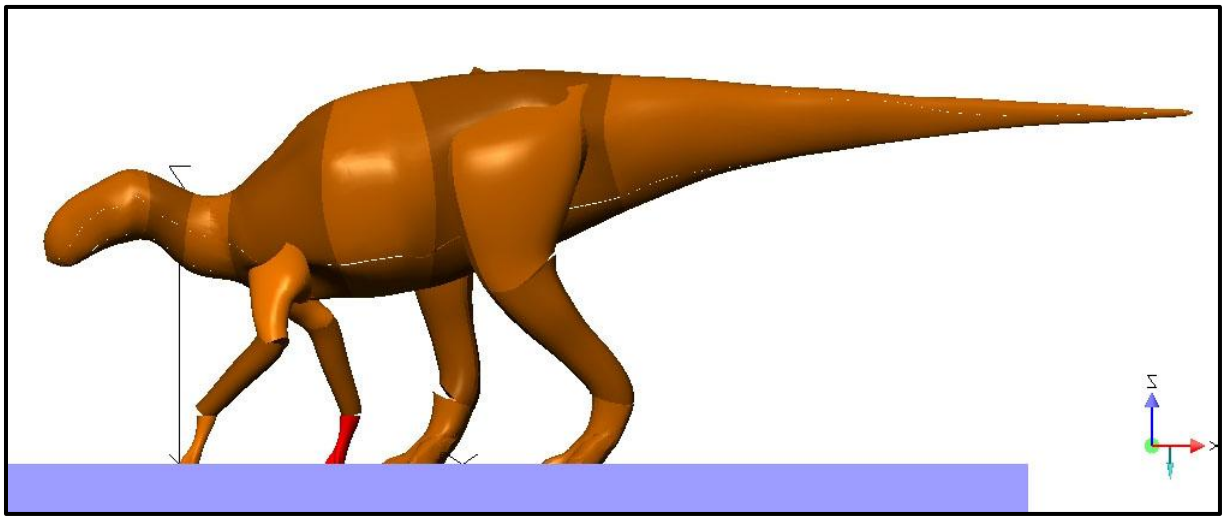

Figure 151: The *Brachylophosaurus* model in cross gait body posture from lateral view after the first step at 1.0s. The right hand (colored red) remains in contact with the ground during the whole first step from 0.0s to 1.0s.

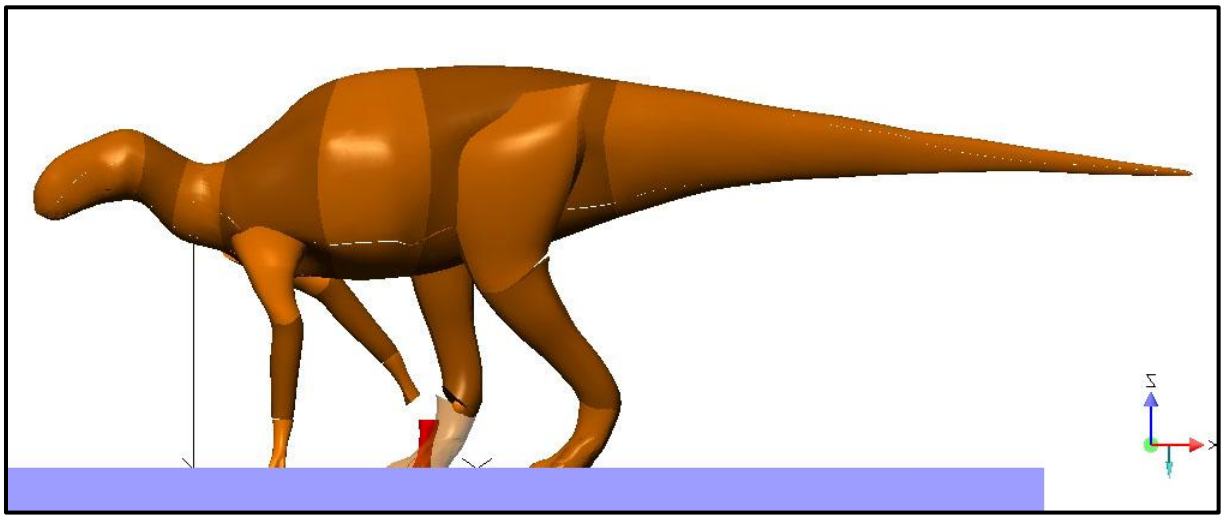

Figure 152: The *Brachylophosaurus* model in semibipedal gait A body posture from lateral view after the first step at 1.0s. In contrast to the cross gait, the right hand (position at 0.0s colored red) cannot remain in contact with the ground during the first step as the right arm is obviously too short. For better visibility the right foot was made translucent.

In contrast, in the starting posture of semibipedal gait A at 0.0s (Figure 128A), with the left leg in front and the right leg behind, ground contact was only possible using the right arm. This means that arms and legs are arranged according to the cross gait walking mode, although it is in the strict sense no 'regular' quadrupedal gait.

Therefore, since the use of the arms is not possible as in the cross or pace gait, the so-called 'semibipedal' locomotion was developed using the arms like 'hiking sticks'. In a repeating interval is one arm retracted and the other one extended in an alternate way so that during a step both arms have no contact with the ground, which is possible without difficulty due to the minor weight-bearing role of the forelimbs.

The non-supportive role of the forelimbs was also indicated by WRIGHT (1999), as the hand prints of the trackway were not placed beneath the body midline. Wright pointed out that the position of the hand prints and their orientation are in contrast to those reconstructions of quadrupedally walking iguanodontid dinosaurs where the forelimbs were placed slightly closer to the midline than the hindlimbs, and where the back of the hand is facing forwards. After her argumentation this would be problematical, since it would require rotation of the radius around the ulna leading to distortion and dislocation of the joints at the wrist or elbow. According to that, the posture of the forelimbs indicated by the Purbeck Limestone Group trackway would obviate this problem.

However, Wright´s assumption that a pronation of the manus is not possible in iguanodontid dinosaurs is arguable. After MAIDMENT et al. (2012) leads the medial movement of the radius in hadrosaurs and other quadrupedal ornithischians to pronation of the manus, whereas in bipedal ornithischians the radius was located anterior to the ulna, causing the manus to be supinated when articulated. This feature was probably required for manual manipulation of food and grasping. In contrast, in hadrosaurs a rotation of the distal end of the radius around the ulna is not possible, precluding supination of the manus. As hadrosaurs represent a clade of derived iguanodontian ornithopods (HORNER et al. 2004), it can be expected that pronation of the manus was also possible in related dinosaurs.

In addition, trackway B in Figure 135 shows hand prints placed closer to the trackway midline than the foot prints. Further, the orientation of hand prints with the back facing forwards or anterolaterally can be found in many trackways, as for example in trackways A, B, and D in Figure 135. As all these trackways are Cretaceous in age (LOCKLEY and WRIGHT 2001), they can be attributed to hadrosauriform dinosaurs, including also the iguanodontid

dinosaurs *Iguanodon bernissartensis* and *Iguanodon* (now *Mantellisaurus* (PAUL 2007)) *atherfieldensis* (MCDONALD et al. 2010, MCDONALD 2012), which were taken into account by WRIGHT (1999) concerning the Purbeck Limestone Group track-maker. A differentiation between these two species and other hadrosauriform dinosaurs concerning their locomotion is therefore rather unlikely. Therefore, the trackway of the Purbeck Limestone Group would represent one way, but not the only way, of quadrupedal locomotion in iguanodontid dinosaurs.

SENTER (2012) considers the orientation of the hadrosaurian manus with the back facing anterolaterally and the palm facing caudomedially as permanent. Therefore, accordant to MAIDMENT et al. (2012), he precludes supination of the hand, but in contrast to them he argues that active pronation is also not possible. Radius and ulna were fixed in position relative to each other, as the bone shapes do not allow the radius to cross over the ulna and concave surfaces on the ulna prevent the radius from moving out of position. In addition, the proximal and distal radio-ulnar joints lack rolling surfaces. After SENTER (2012) is his argumentation supported by the orientation of hadrosaurian manus tracks.

Regarding the digital arm skeleton (Figures 62 & 63), radius and ulna build in fact a solid unit showing an anterolateral orientation of the back of the hand in its neutral standing pose. It is noticeable that most of the manus tracks (e.g. Figure 135) differ not much from this neutral posture and are accordant with the orientation described by SENTER (2012). This could indicate that an active pronation is actually not possible.

In the simulations an orientation of the hand with the back facing forwards was achieved by rotation of the whole forelimb with the elbow rotating outwards (see cross and pace gait, semibipedal gaits B and C). In addition, in semibipedal gait A the orientation of the hand with its back facing outwards is also caused by rotation of the whole forelimb. An orientation of the hand with the back facing anterolaterally and the palm facing caudomedially would be problematical through the bending of the wrist along the parasagittal plane when the arm rotates around the shoulder joint during forward motion. Although in this orientation the back of the hand is not directed outwards, bending of the wrist should be more limited as if the back is directed forwards (see Figures 147-150). However, when using the semibipedal way of motion, this problem would be obviated as there is no rotation of the arm around the shoulder joint.

After finishing semibipedal gait A, the new developed semibipedal locomotion was also adopted for the cross and pace gait simulations. The cross gait simulation was transformed in **semibipedal gait B** (Videos 8A–D) and the pace gait simulation in **semibipedal gait C** (Videos 9A–D). Although the model trackway of the pace gait simulation shows not the required characteristics, e.g. concerning the position of the hand print in relation to the foot print, it was decided to test the semibipedal way of motion. The question was if it would be possible to achieve identical trackways of cross gait and semibipedal gait B (Figure 154) and also of pace gait and semibipedal gait C (Figure 155).

The comparison of the model trackways of cross gait (Figure 136) and semibipedal gait B (Figure 154) shows no difference in the positions of hand and foot prints. Hence, the arms could be used in both ways, either by rotation around the shoulder joint or using the semibipedal way of motion. However, the movement of the center of mass is more fluent in the semibipedal gait B simulation (Figures 154 & 155) as in the cross gait simulation (Figures 140 & 141), similar to semibipedal gait A (Figures 145 & 146).

This more fluent motion in semibipedal gait B was expectable, due to the missing rotation of the arm around the shoulder joint, which caused a more simple motion sequence. However, although the curves which display the movement of the center of mass along the y-axis and z-axis resemble those of semibipedal gait A, some differences exist. Along the y-axis (Figure 153) the center of mass moves first opposite to the body motion, but as in the cross gait the direction changes during the motion sequence, as there is no reversal between 1.0s and 3.0s. Therefore, from 2.0s to 6.0s the center of mass moves again accordant with the body motion. In contrast to the cross gait, in this interval direction change is more synchronal with the transition between two steps, as in semibipedal gait A.

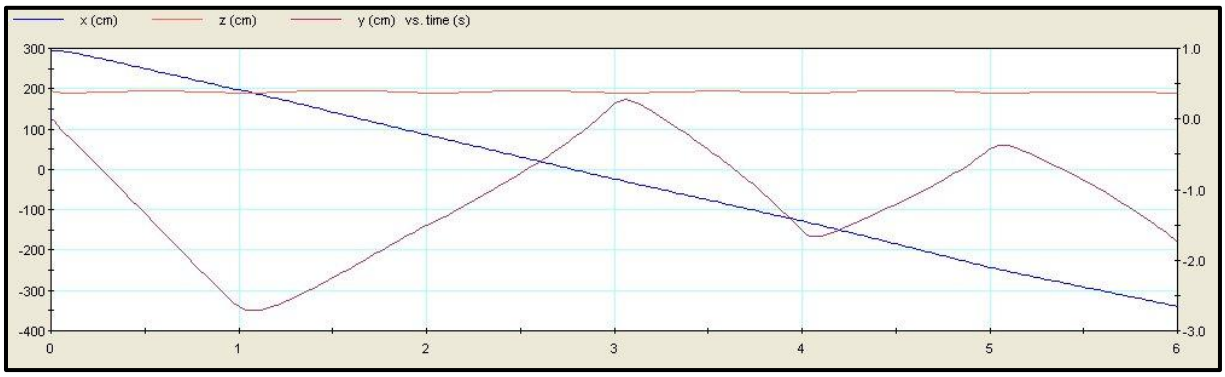

Figure 153: The diagram displays the position of the center of mass along the y-axis during the semibipedal gait B simulation.

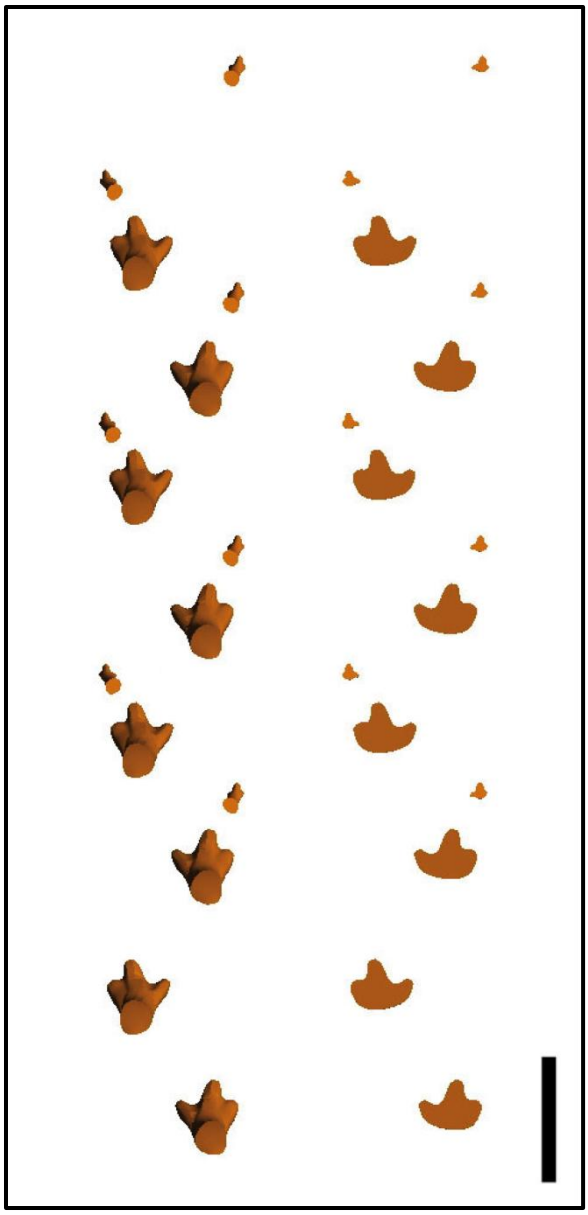

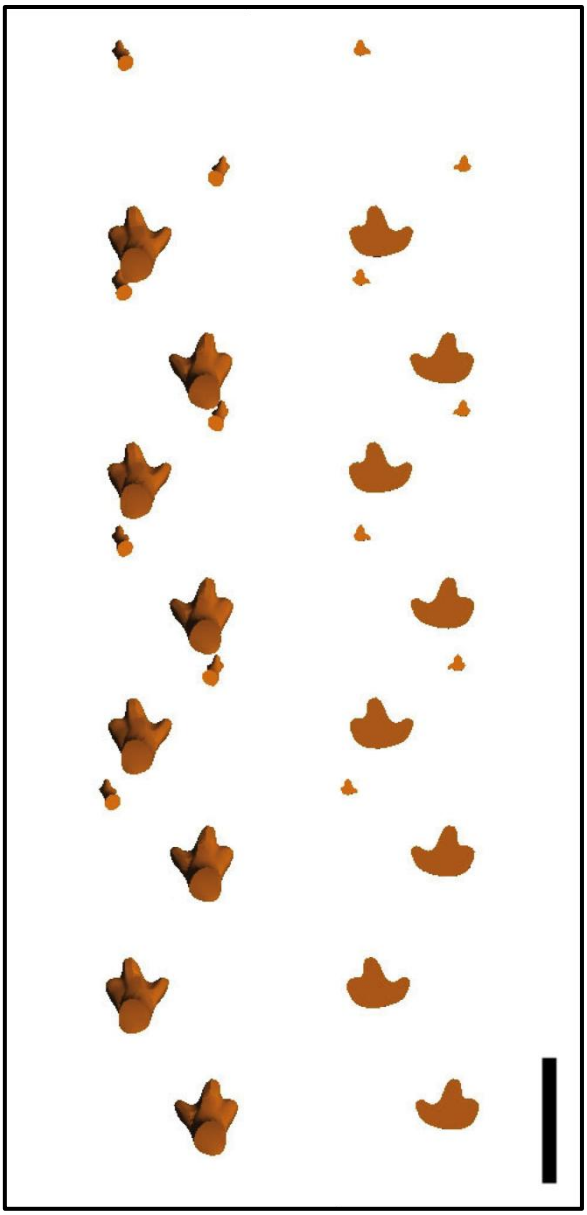

Figure 154 (left): Model trackway of semibipedal gait B from dorsal view. The left trackway shows the position and orientation of hands and feet. The right trackway shows the corresponding hand and foot prints; scale bar = 1 m.

Figure 155 (right): Model trackway of semibipedal gait C from dorsal view. The left trackway shows the position and orientation of hands and feet. The right trackway shows the corresponding hand and foot prints; scale bar = 1 m.

The movement of the center of mass along the z-axis (Figure 156) is also very similar to that of semibipedal gait A (Figure 146), but the maxima of the curve are clearly irregular. These differences between the curves of semibipedal gaits A and B show that despite the different use of the arms in cross gait and semibipedal gait B the similarity between these two simulations is maintained, as the motion of the legs was not changed.

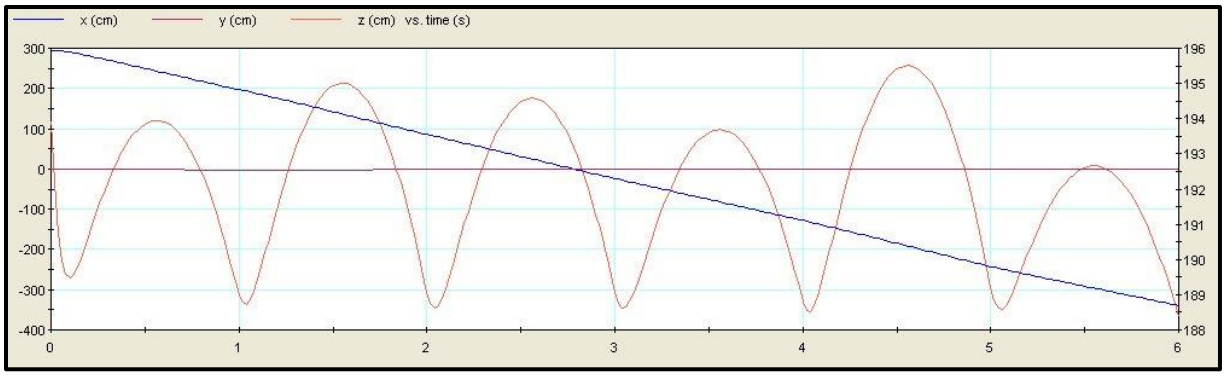

Figure 156: The diagram displays the position of the center of mass along the z-axis during the semibipedal gait B simulation.

Nevertheless, although the diagrams show a more regular progression in semibipedal gait B (Figures 153 & 156) than in the cross gait (Figures 140 & 141), and the slight outward rotation of the hand is also not necessary in the semibipedal way of motion, it is not clear which kind of locomotion should be preferred comparing these two simulations.

Comparing the model trackways of pace gait (Figure 138) and semibipedal gait C (Figure 155), it is obvious that the trackways are not accordant. Semibipedal gait C shows a minor distance between the hand prints and also between the foot prints, as both are closer to the midline as in the pace gait trackway. Whereas step length of the forefeet is larger in the pace gait trackway, step length of the hindfeet is virtually the same in both trackways. The latter bases on the increased pace angulation in semibipedal gait C, which equalizes the lower distance between the foot prints in this trackway. In addition, the foot prints are more rotated outwards in the pace gait than in semibipedal gait C. These observed differences between the two trackways are the result of the missing rotation of the arm around the shoulder joint in semibipedal gait C, as this rotation caused a larger shift of arm and leg away from the midline in the pace gait simulation.

In contrast to semibipedal gait A, the bending of the wrist is possible without difficulties in cross and pace gait as well as in semibipedal gaits B and C. In these simulations the back of the hand is facing forwards or anterolaterally so that a straight posture of the arm is not necessary and the head and the anterior body can be directed more downwards.

Semibipedal gait D (Videos 10A–F) bases on a trackway (left trackway Figure 131 (A) / see also Figure 135) which shows hand prints with the back of the hand oriented more outwards, but not parallel to the trackway midline as in semibipedal gait A. However, as in case of the latter, the orientation and position of the hand prints seem to require also a more elongated posture of the arm, leading to a lesser bending of the wrist. Further, concerning the first step, ground contact of the right arm is not possible as in semibipedal gait A (Figures 157 & 158), which requires again locomotion in the semibipedal way.

The model trackway of the semibipedal gait D simulation (Figure 159) is widely accordant with the fossil trackway concerning the position and orientation of hand and foot prints, and also regarding the step and stride length of the foot prints (see Table 3), which show the characteristic inward rotation in both trackways.

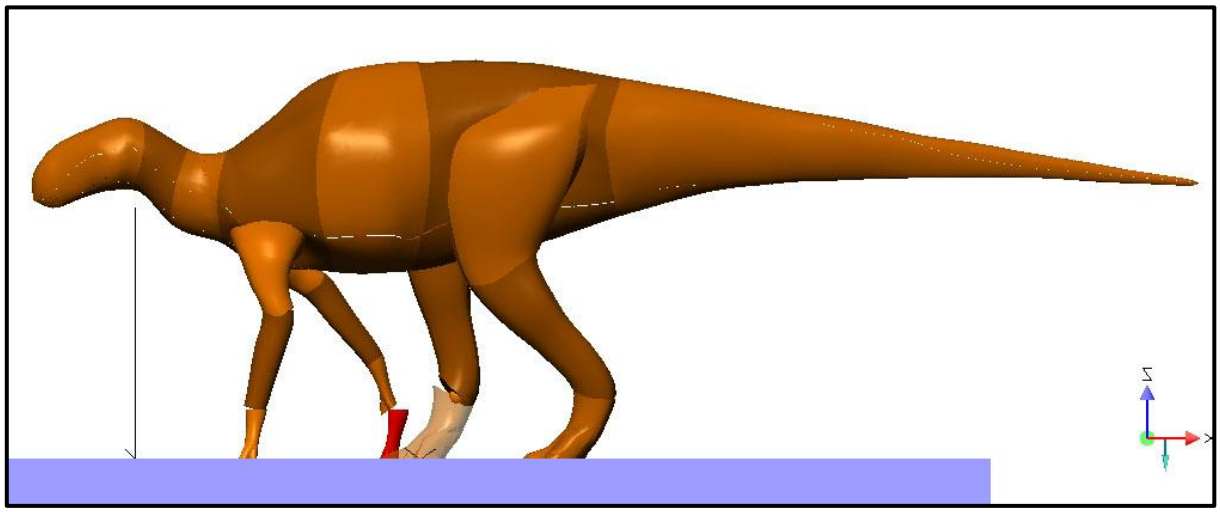

Figure 157: The *Brachylophosaurus* model in semibipedal gait D body posture from lateral view after the first step at 1.0s. As in semibipedal gait A the right hand (position at 0.0s colored red) cannot remain in contact with the ground during the first step. For better visibility the right foot was made translucent.

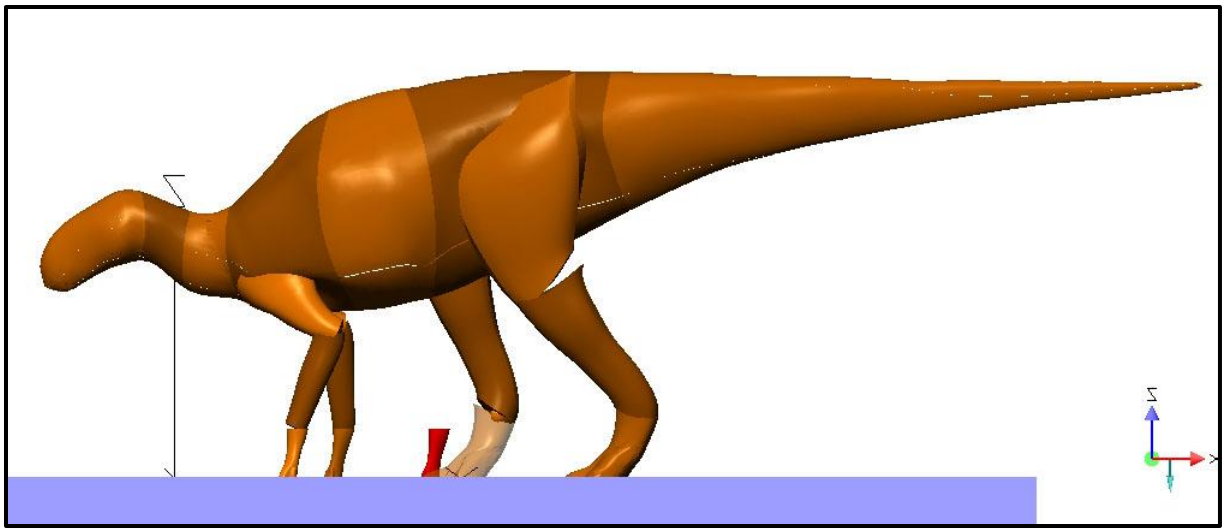

Figure 158: The *Brachylophosaurus* model in semibipedal gait D body posture from lateral view after the first step at 1.0s. In contrast to Figure 157 the body was slightly rotated downwards cranial and the right arm was set on the ground. However, the required position (red colored hand) is again out of reach. In addition, the bending of the left arm may be critical.

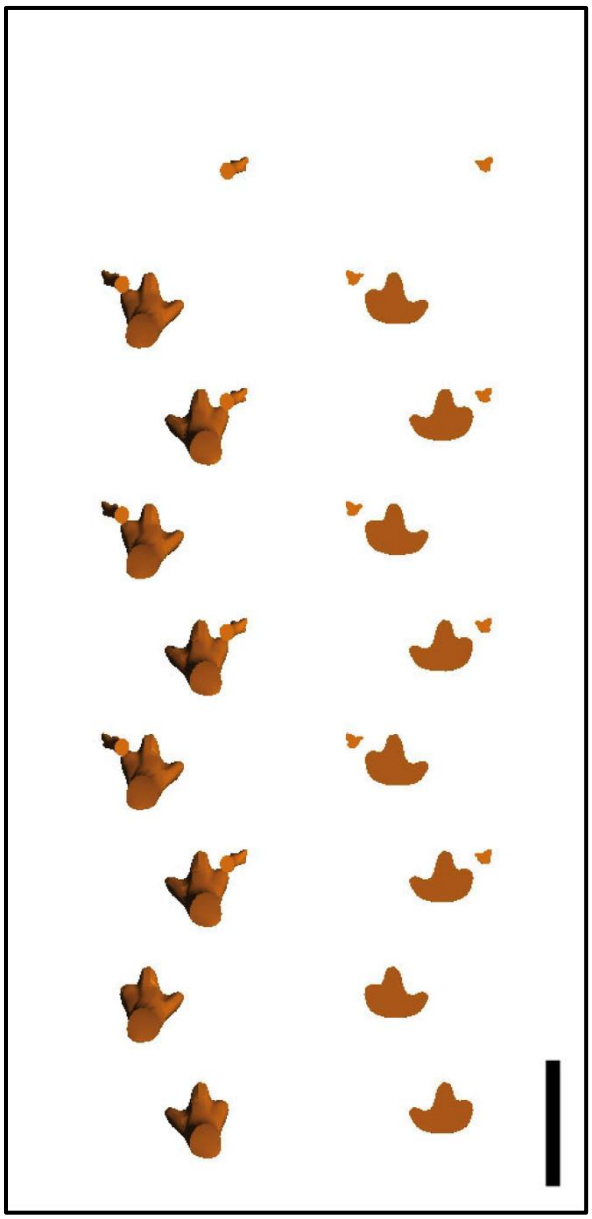

Figure 159: Model trackway of semibipedal gait D from dorsal view. The left trackway shows the position and orientation of hands and feet. The right trackway shows the corresponding hand and foot prints; scale bar = 1 m.

Step length of the forefeet is difficult to compare, as the left side of the fossil trackway shows only one hand print, which is closer to the trackway midline, indicating a shorter step length than in the model trackway. However, stride length of the hand prints on the right side of the trackway nearly coincides with the one of the model trackway (Table 3).

In contrast to semibipedal gait A, foot length of the track-maker is slightly larger as the modeled one of *Brachylophosaurus* (Table 3). Trackway width is larger in the fossil trackway, but if the original track-maker was in fact of larger body size this could be correct, as well as the slightly higher measures of the step and stride lengths of the fossil trackway and the shorter distance between hand and foot print in the model trackway.

Altogether, there is a higher accordance between the measures of fossil and model trackway in semibipedal gait D than in semibipedal gait A (Table 3). If the measures are compared considering body size their differences would match, but also without considering body size the measures from the model trackway are highly acceptable, as they show only minor deviations to those of the fossil trackway.

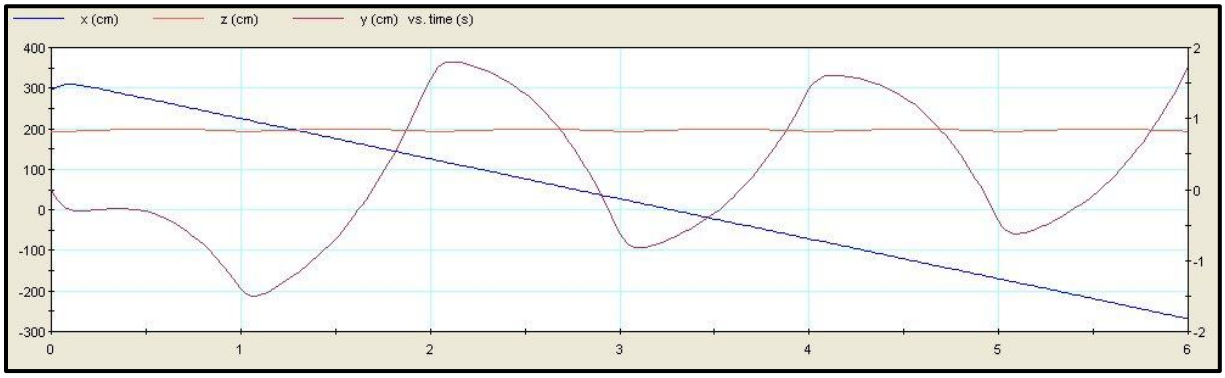

Figure 160: The diagram displays the position of the center of mass along the y-axis during the semibipedal gait D simulation.

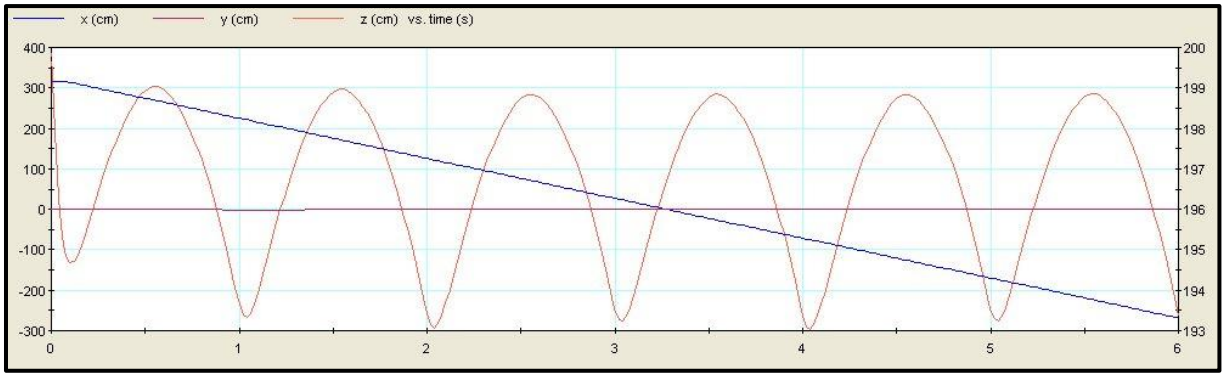

Figure 161: The diagram displays the position of the center of mass along the z-axis during the semibipedal gait D simulation.

The movement of the center of mass in semibipedal gait D (Figures 160 & 161) is similar to that of semibipedal gait A (Figures 145 & 146). Along the y-axis (Figure 160) it moves opposite to the body motion, again with a slight shift to the left during progression (i.e. the model moves to the right). Direction change takes place also with a minor delay after every full second according to step transition. However, the range of lateral movement of the center of mass is smaller in semibipedal gait D than in semibipedal gait A, as the scales on the right side of the diagrams show (Figures 145 & 160). This is based presumably on the minor overlapping of the feet (see Figures 128B & 132B), which corresponds with the broader trackway of semibipedal gait D. The wider distance of the feet seems to cause a lesser rotation of the body, and therefore of the center of mass, despite the inward rotation of the feet which is part of all motion sequences. Along the z-axis (Figure 161) the center of mass moves very regular, in contrast to semibipedal gait B (Figure 156), but in accordance with semibipedal gait A.

Like semibipedal gait D, **semibipedal gait E** (Videos 11A–F) is based on a trackway from the Gething Formation of British Columbia which is of Aptian age (CURRIE 1983; LOCKLEY and WRIGHT 2001). However, this trackway (right trackway Figure 131 (A) / Figure 135) differs clearly from the one of semibipedal gait D, as trackway width is smaller and step and stride length of the foot prints as well as stride length of the hand prints are larger (Table 3). In addition, the hand print is located closer to the midline, with an anterolaterally orientation of its dorsal surface and a position anterolateral to digits III and IV of the foot print. This orientation of the hand print resembles those in the cross gait and semibipedal gait B. In contrast, foot size of the track-maker is the same in both trackways. Also, as in the semibipedal gait D trackway, stride lengths of hand and foot prints are virtually the same in the semibipedal gait E trackway (Table 3).

The large step length of the foot prints and the more anterior placed hand prints made it difficult to determine the initial body posture of semibipedal gait E (Figures 133A & B). In contrast to the other semibipedal simulations, it was not possible to use again the cross gait-like posture with the right arm in contact with the ground at the beginning and the left arm and right leg moving forward during the first step. Although this posture was tested, the right arm is definitely too short to achieve the correct position, whereas in the other semibipedal simulations this was the case with the left arm.

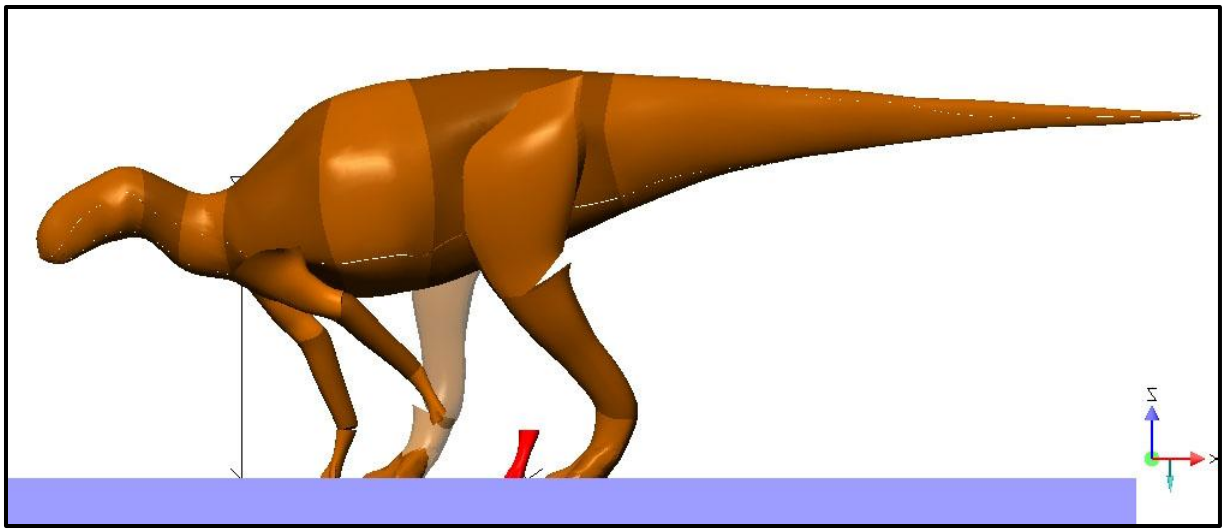

Figure 162: The *Brachylophosaurus* model in semibipedal gait E body posture from lateral view after the first step at 1.0s, showing that the left hand (position at 0.0s colored red) cannot remain in contact with the ground during the first step.

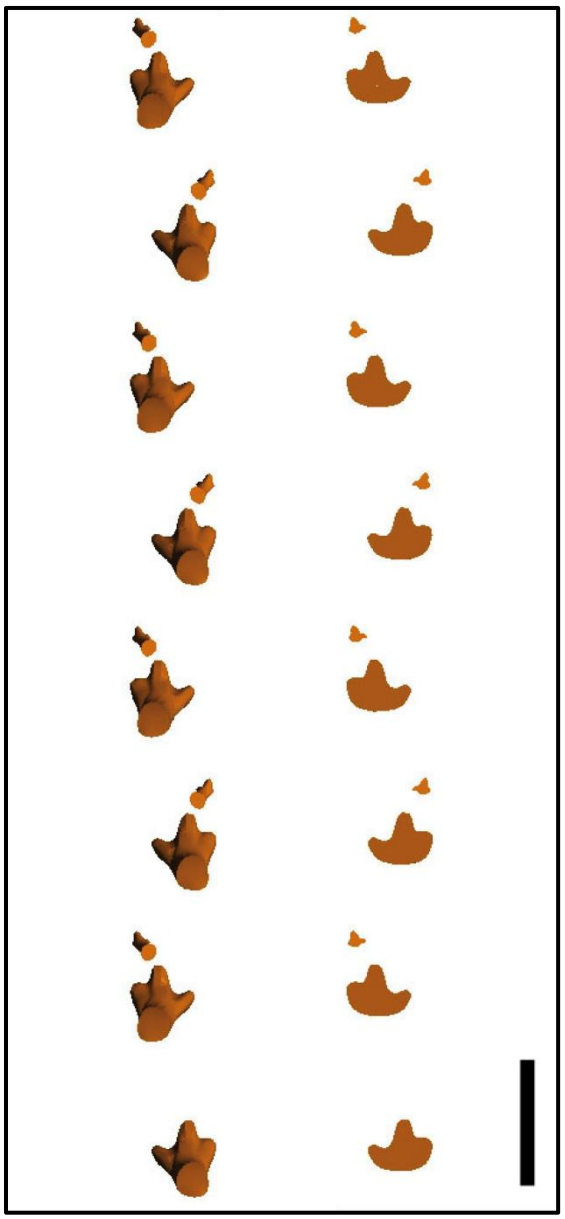

Figure 163: Model trackway of semibipedal gait E from dorsal view. The left trackway shows the position and orientation of hands and feet. The right trackway shows the corresponding hand and foot prints; scale bar = 1 m.

Hence, in semibipedal gait E a more pace gait-like posture was developed (Figure 133) with the left arm having contact with the ground when the simulation starts and the right arm and leg moving forward during the first step. Again, only the semibipedal way of motion is possible, since the left arm cannot stay in contact with the ground during the first step (Figure 162).

In contrast to semibipedal gait A (Figures 128A & B) and D (Figures 132A & B), the left arm in semibipedal gait E shows no straight posture, but in this case the bending of the wrist is possible to a higher degree due to the orientation of the hand like in the cross gait (Figures 125A & B) and semibipedal gait B (Figures 129A & B).

In semibipedal gait E foot length of the track-maker in the fossil trackway is the same as in the one of semibipedal gait D (Figure 131 (A)), and therefore it is also slightly larger as the modeled one of *Brachylophosaurus* (Table 3). Hence, the slightly smaller width of the model trackway could be correct again. In the model trackway (Figure 163) step and stride length of the foot prints are close to the original measures as well as stride length of the hand prints. The foot prints show also inward rotation as in the other motion sequences. In contrast to semibipedal gait D, the measures of the model trackway are a little higher than those of the fossil trackway (Table 3). This would be in contrast to a possibly larger body size of the original track-maker, but a high accordance of the measures of both trackways is achieved anyway. It was not possible to measure the step length of the hand prints, as the fossil trackway shows only prints of the right hand. Since it is not clear if the prints of the left hand have actually existed or were simply not fossilized, the model trackway is shown with prints of both hands. The distance between hand and foot print in the model trackway is shorter as in the fossil one, but would match considering the body size (Table 3).

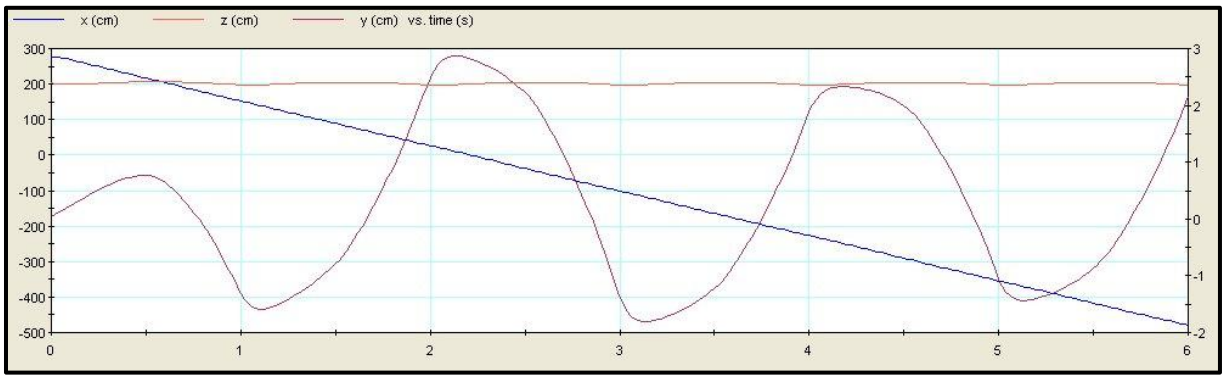

Figure 164: The diagram displays the position of the center of mass along the y-axis during the semibipedal gait E simulation.

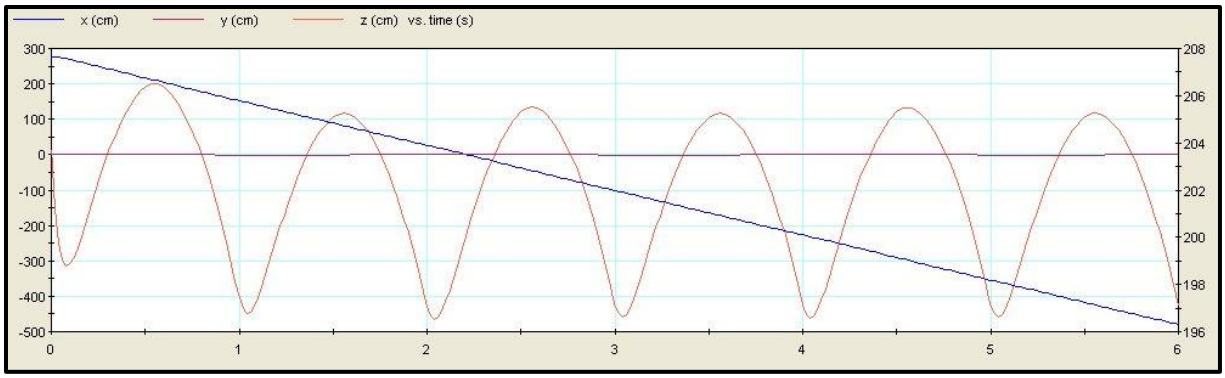

Figure 165: The diagram displays the position of the center of mass along the z-axis during the semibipedal gait E simulation.

The movement of the center of mass along the y-axis (Figure 164) and the z-axis (Figure 165) in semibipedal gait E shows only little differences to the motion curves of semibipedal gait A (Figures 145 & 146) and D (Figures 160 & 161). The range of lateral movement along the y-axis is smaller as in gait A, but larger than in gait D. This would coincide with the overlapping of the feet, which is larger in gait E (Figure 133B) than in gait D (Figure 132B), but smaller than in gait A (Figure 128B). Therefore, trackway width in gait E is smaller than in gait D, but broader than in gait A (Table 3). In addition, the curve of the y-axis is more symmetrical in semibipedal gait E, but along the z-axis the motion of the center of mass is as regular as in the two other simulations.

Semibipedal gait F (Videos 12A–F) bases on a trackway from the Lakota Formation, which is located near Rapid City, South Dakota, and is probably of Barremian age (LOCKLEY and WRIGHT 2001). The trackway (Figure 131 (B) / Figure 135) shows unusual quadripartite foot prints and hand prints placed anterior to the apex of pes digits III and IV (LOCKLEY and WRIGHT 2001). The dorsal surface of the hand print is oriented more laterally than in semibipedal gait E, but to a lesser extent than in semibipedal gait D (Figure 131 (B)).

The position of two hand prints close to the trackway midline anterior to pes digit III is different to hand print positions in the other fossil trackways. The position and orientation of the hand print cause a somewhat unusual posture of the arm (Figures 134A & B), including a bending of the wrist which requires again a straight arm posture like in semibipedal gaits A (Figures 128A & B) and D (Figures 132A & B). As in the other semibipedal simulations the right arm is too short to remain in contact with the ground during the first

step, so that semibipedal locomotion was used again (Figures 166 & 167). In addition, as in semibipedal gaits A and D, the cross gait-like initial posture could be used.

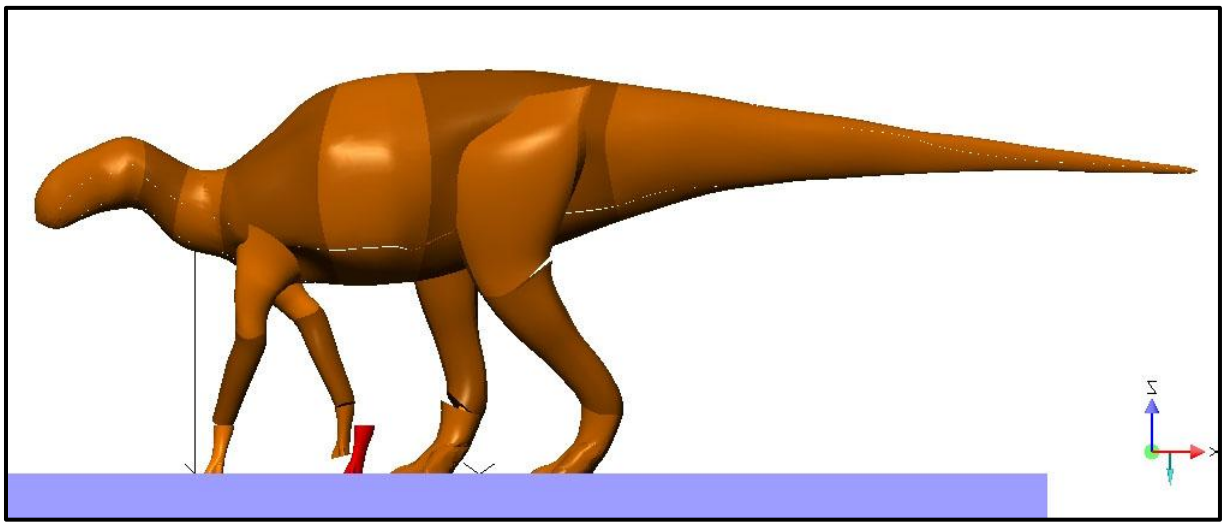

Figure 166: The *Brachylophosaurus* model in semibipedal gait F body posture from lateral view after the first step at 1.0s. As in semibipedal gaits A and D the right hand (position at 0.0s colored red) cannot remain in contact with the ground during the first step.

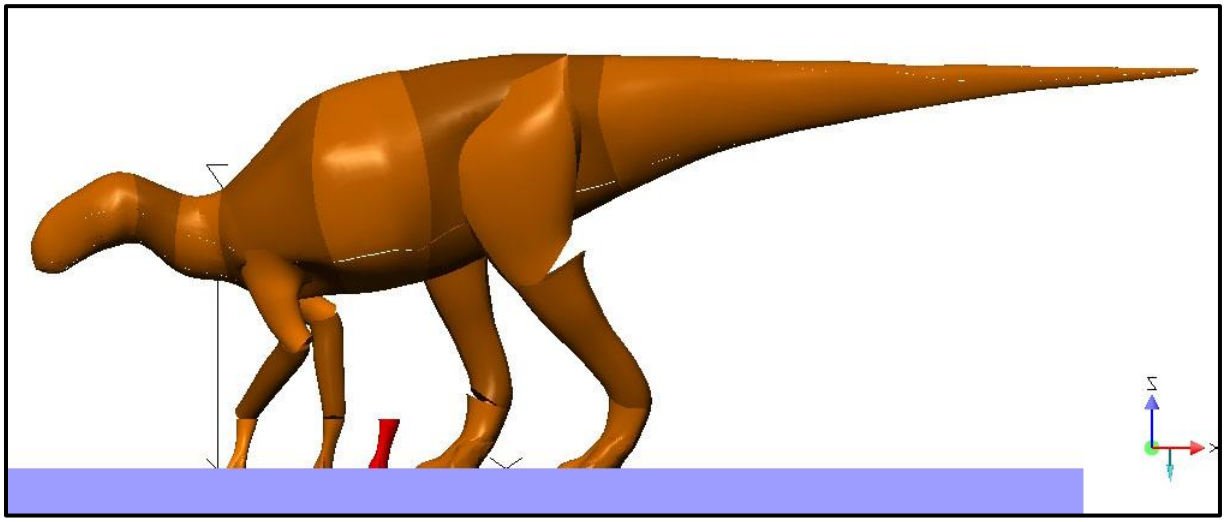

Figure 167: The *Brachylophosaurus* model in semibipedal gait F body posture from lateral view after the first step at 1.0s. In contrast to Figure 166 the body was slightly rotated downwards cranial and the right arm was set on the ground. However, the required position (red colored hand) is again out of reach. The bending of the left arm may be critical again.

In the fossil trackway foot length of the track-maker is nearly the same as the modeled one of *Brachylophosaurus*, possibly indicating a similar body size (Table 3). Trackway width is also nearly identical in both trackways, which would match considering body size. Step and stride length of the foot prints, step and stride length of the hand prints, and the distance between hand and foot print are a little higher in the fossil trackway, but

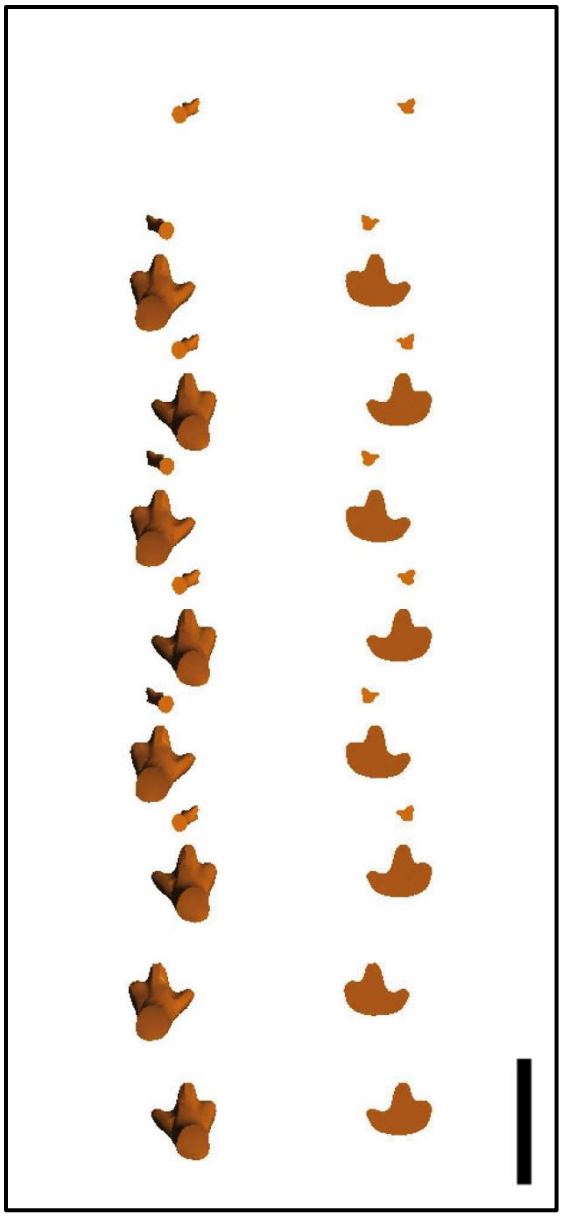

within the tolerance (Table 3). Further, both trackways show also inward rotation of the foot prints (Figure 168).

Figure 168: Model trackway of semibipedal gait F from dorsal view. The left trackway shows the position and orientation of hands and feet. The right trackway shows the corresponding hand and foot prints; scale bar = 1 m.

The curves which display the movement of the center of mass along the y-axis (Figure 169) and the z-axis (Figure 170) in semibipedal gait F show a great similarity with those of the other semibipedal simulations, except semibipedal gait B (Figure 155). The range of lateral movement along the y-axis in gait F is larger as in gait D (Figure 160), but smaller than in gait A (Figure 145). In gait E (Figure 164) and F it is nearly the same. This would coincide again with the overlapping of the feet, which is smaller as in gait A (Figure 128B), but larger than in gait D (Figure 132B), and widely accordant in gaits E (Figure 133B) and F (Figure 134B). Therefore, trackway width gets broader from gait A to gaits F / E to gait D (Table 3). The curve of the y-axis is less symmetrical in semibipedal gait F as in gait E, but resembles those of gaits A and D, with a slight shift of the center of mass to the left during progression.

However, as in semibipedal gaits D and E the range of lateral movement of the center of mass decreases during forward motion, but only to a little extent.

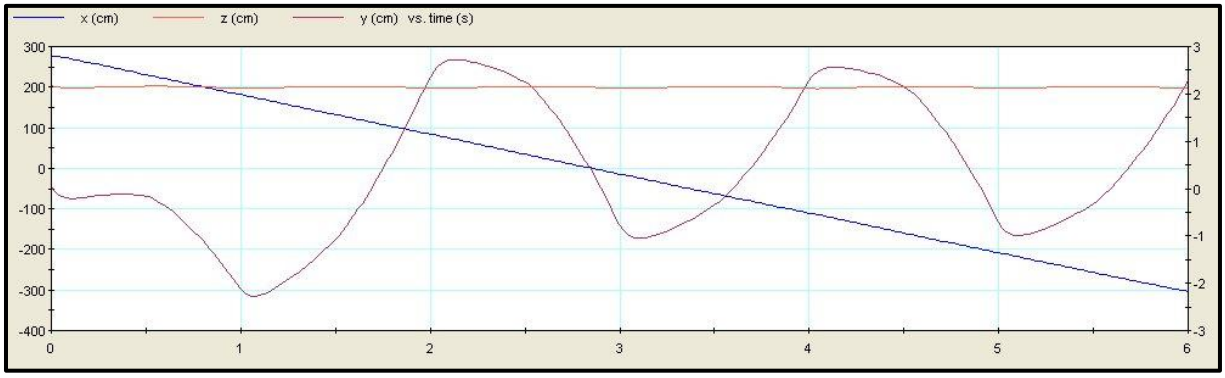

Figure 169: The diagram displays the position of the center of mass along the y-axis during the semibipedal gait F simulation.

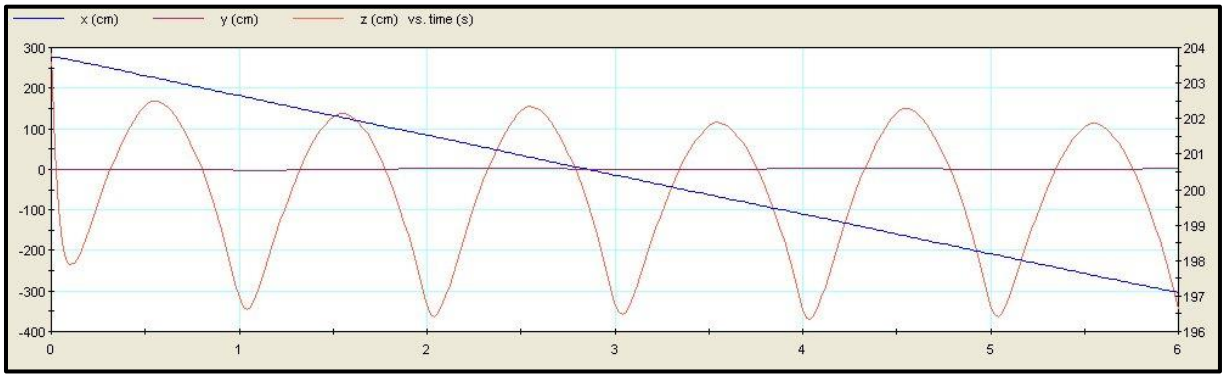

Figure 170: The diagram displays the position of the center of mass along the z-axis during the semibipedal gait F simulation.

The transition from **quadrupedal to bipedal locomotion** during progression was simulated based on two different quadrupedal gaits. However, this motion change is quite easier in semibipedal gait D (Figure 132) as in the cross gait (Figure 125), due to the different use of the arm in locomotion.

The model trackway of motion change from **cross gait to bipedal gait** (Videos 14A-E / Figure 171) shows an increase in pace angulation and a correlated decrease in trackway width of the foot prints, as described by THULBORN (1989, 1990). However, an increase in stride length of the foot prints, which was also described by THULBORN (1989, 1990), was not realized in the simulation. In semibipedal gait D trackway width (Figure 172) is already smaller as in the cross gait (Figure 171). Therefore, it was not reduced further during the transition to bipedal locomotion.

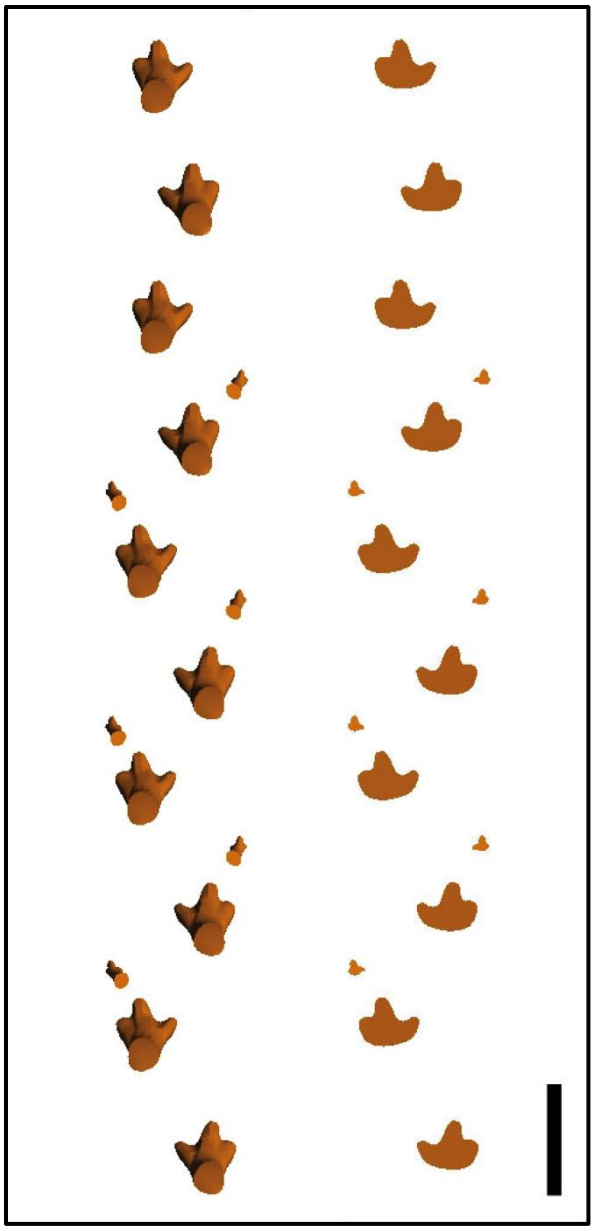

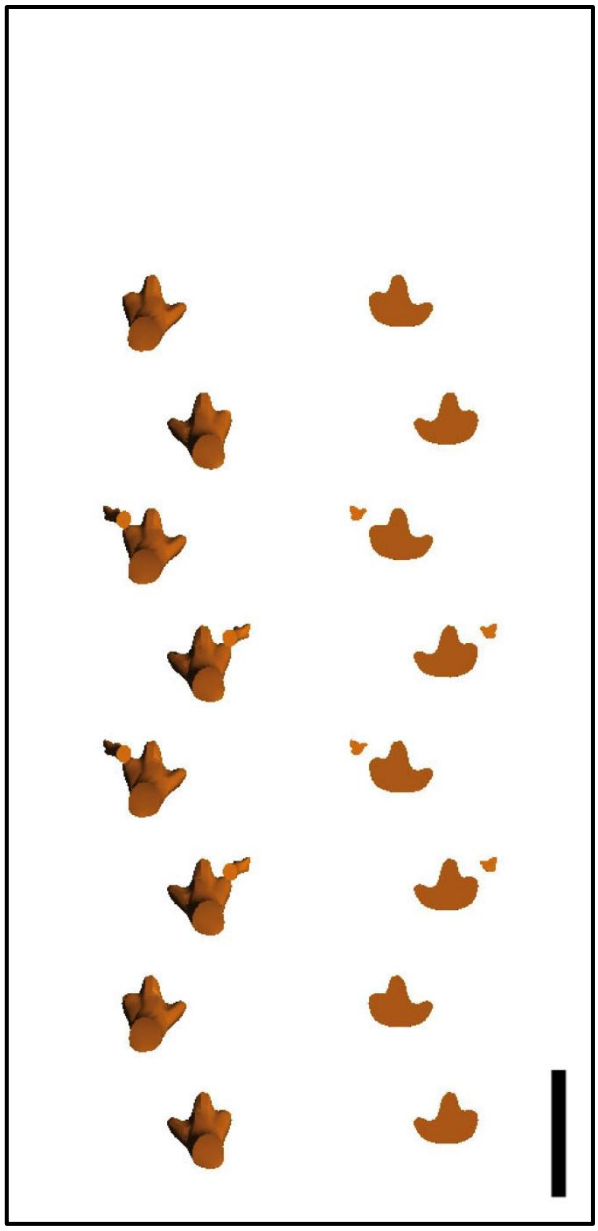

Figure 171 (left): Model trackway of motion change from cross gait to bipedal gait from dorsal view. The left trackway shows the position and orientation of hands and feet. The right trackway shows the corresponding hand and foot prints; scale bar = 1 m.

Figure 172 (right): Model trackway of motion change from semibipedal gait D to bipedal gait from dorsal view. The left trackway shows the position and orientation of hands and feet. The right trackway shows the corresponding hand and foot prints; scale bar = 1 m.

Hence, the only difference the model trackway of motion change from semibipedal gait D to bipedal gait (Figure 172) shows is the lack of the hand prints during progression. This transition is of course no real gait change compared to that one using the cross gait, but was included as both alternatives are possible.

The movement of the center of mass along the y-axis in the simulation on basis of the cross gait (Figure 173) shows clearly the transition from quadrupedal to bipedal locomotion.

Especially the range of lateral movement of the center of mass is considerably higher in the bipedal part of the motion sequence and its motion is more regular in this section. As in the cross gait, the movement of the center of mass is accordant with body motion during the quadrupedal part of the simulation, but this changes to an opposite movement during the bipedal part, showing also a direction change which is clearly more accordant to step transition.

In the diagram which displays the movement of the center of mass along the z-axis (Figure 174) the transition between quadrupedal and bipedal part is also clearly visible due to the more erect posture in bipedal locomotion, which causes a higher position of the center of mass. Further, the progression of the curve is more regular in the bipedal part of the simulation, presumably based on the less complex motion in the bipedal gait.

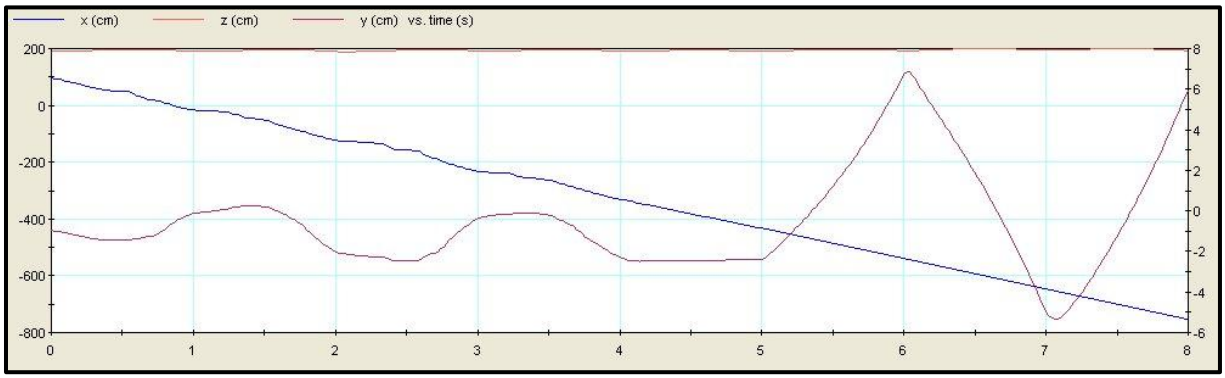

Figure 173: The diagram displays the position of the center of mass along the y-axis during motion change from cross gait to bipedal gait.

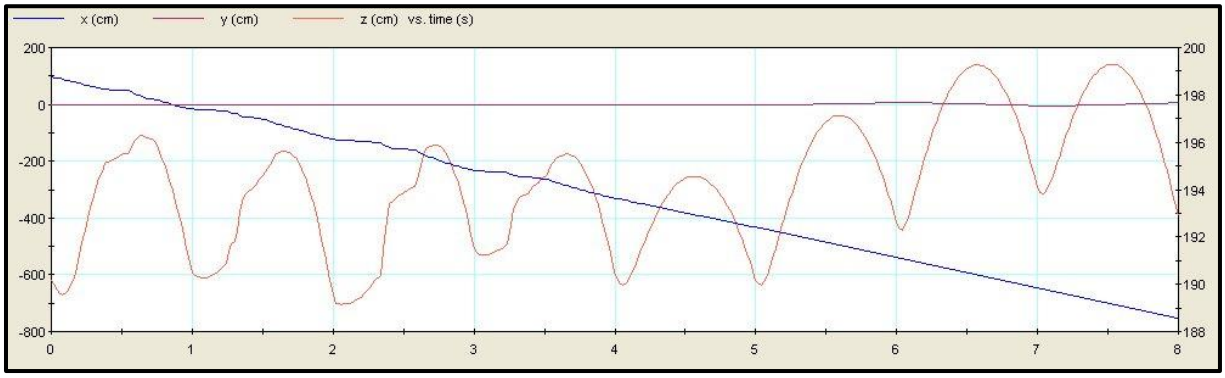

Figure 174: The diagram displays the position of the center of mass along the z-axis during motion change from cross gait to bipedal gait.

In the motion change from **semibipedal gait D to bipedal gait** (Videos 13A & B) the movement of the center of mass along the y-axis (Figure 175) and the z-axis (Figure 176) is widely accordant with its motion in the semibipedal gait D simulation (Figures 160 & 161).

However, the movement along the y-axis is a little more extended lateral between 4.0s and 6.0s, the bipedal part of the simulation, as in the same period in semibipedal gait D. In addition, along the z-axis the center of mass moves slightly higher between 4.0s and 6.0s. Although these differences are minimal compared to semibipedal gait D, and the motion of body and legs was not changed from quadrupedal to bipedal locomotion, the nonuse of the arms seems to have at least a minor effect on the movement of the center of mass.

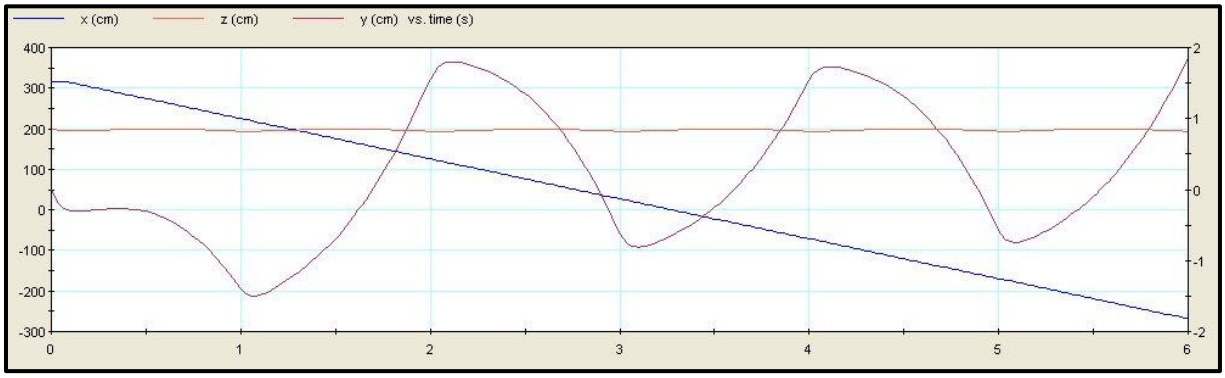

Figure 175: The diagram displays the position of the center of mass along the y-axis during motion change from semibipedal gait D to bipedal gait.

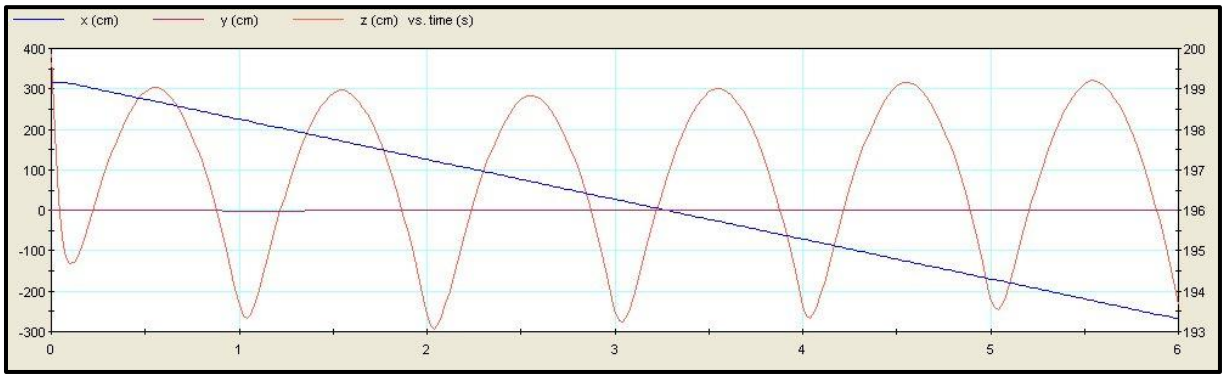

Figure 176: The diagram displays the position of the center of mass along the z-axis during motion change from semibipedal gait D to bipedal gait.

5.2 Bipedal locomotion

Regarding the bipedal gait, only the position and movement of the legs have to be considered. However, as in the quadrupedal gaits, the bipedal locomotion can also comprise different postures of body and legs, which were tested in the simulations.

In contrast, it was not possible to simulate a hopping gait, as presented by SELLERS et al. (2009), because of the simultaneous aerial phase of the legs.

5.2.1 Results

In the bipedal gait again the descriptions of THULBORN (1990) were used, to define an initial posture of the legs:

- The feet produced fairly narrow trackways with foot prints arranged in a slightly zig-zag pattern.
- The foot prints are turned inwards to the midline of the trackway, and there is rarely any trace of a tail-drag.

In **bipedal gait A** the body is hold horizontally and the feet are placed close to the midline (Figures 177A & B). This posture of body and legs correlates with that one shown in semibipedal gait A.

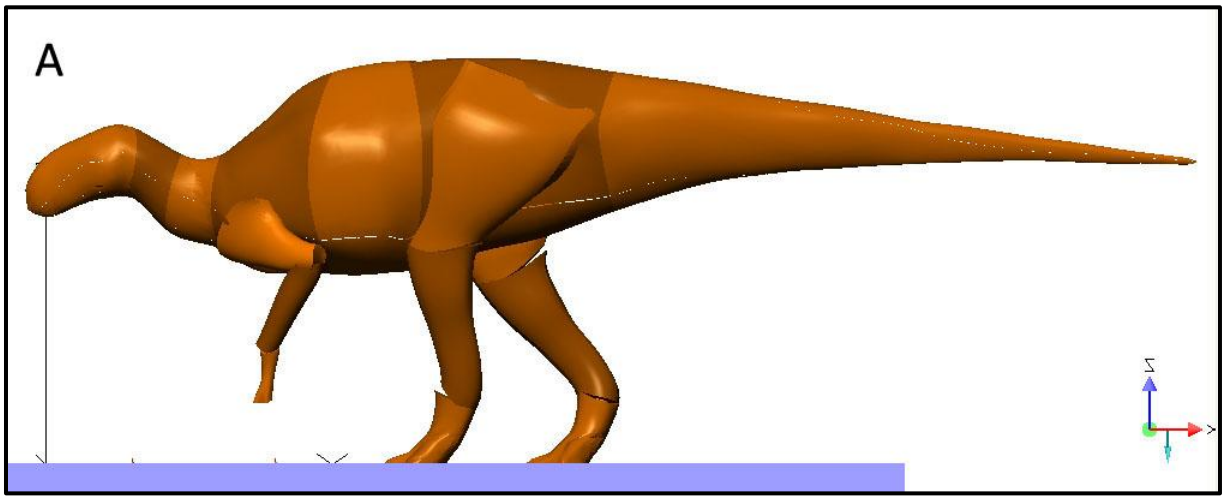

Figure 177A: The *Brachylophosaurus* model in bipedal gait A body posture from lateral view.

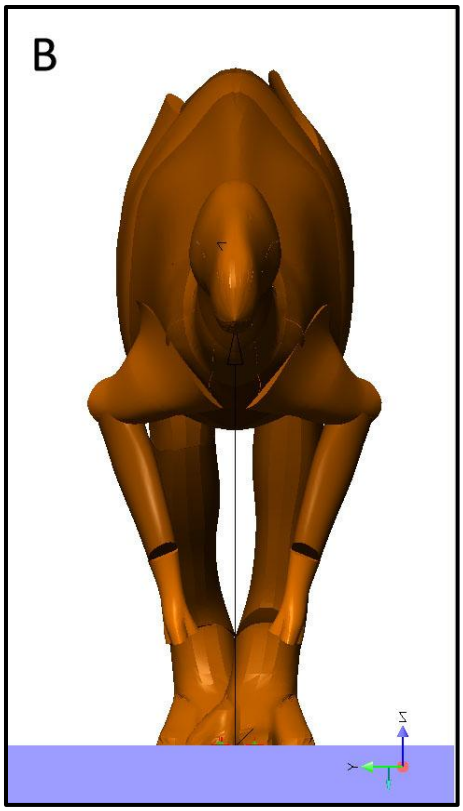

Figure 177B: The *Brachylophosaurus* model in bipedal gait A body posture from cranial view.

The following videos show the results of the **bipedal gait A** simulation:

- **Video 16A** shows bipedal gait A IS1 from cranial view.
- **Video 16B** shows bipedal gait A IS2 from cranial view.
- **Video 16C** shows bipedal gait A IS3 from lateral view.
- **Video 16D** shows bipedal gait A IS3 from dorsal view.
- **Video 16E** shows bipedal gait A IS3 from cranial view.
- **Video 16F** shows bipedal gait A IS3 from dorsocraniolateral view.
- **Video 16G** shows bipedal gait A IS3 from caudal view.

In **bipedal gait B** the body posture of the cross gait (also pace gait, semibipedal gaits B and C) was maintained with the head directed downwards. Compared to bipedal gait A the posture of the legs was not changed (Figure 178).

The following videos show the results of the **bipedal gait B** simulation:

- **Video 17A** shows bipedal gait B IS3 from lateral view.
- **Video 17B** shows bipedal gait B IS3 from cranial view.
- **Video 17C** shows bipedal gait B IS3 from dorsocraniolateral view.
- **Video 17D** shows bipedal gait B IS3 from caudal view.

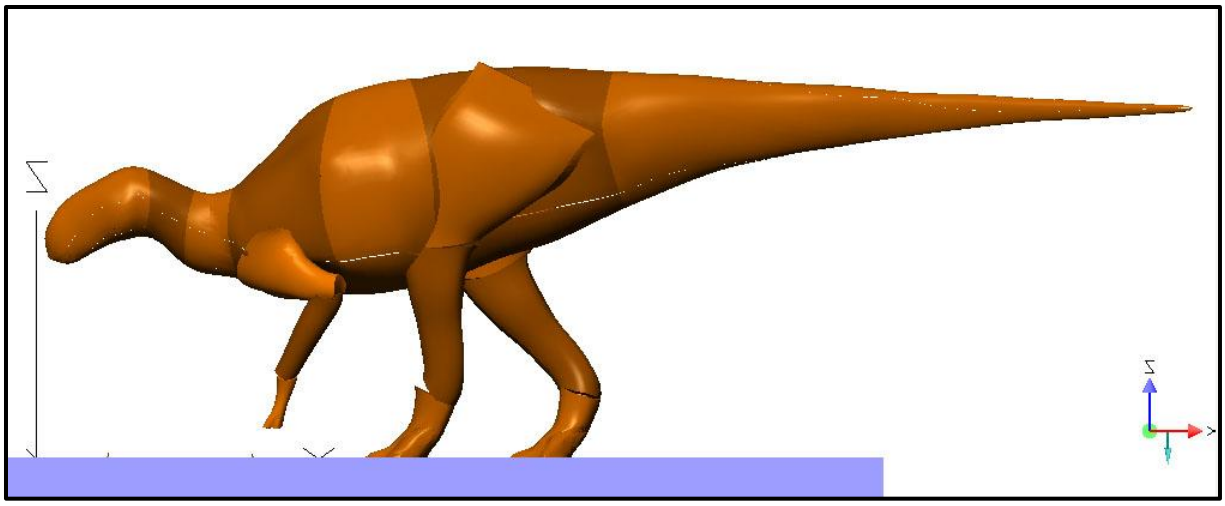

Figure 178: The *Brachylophosaurus* model in bipedal gait B body posture from lateral view.

In **bipedal gait C** the model shows a semi-erect posture inspired by old kangaroo-like hadrosaur reconstructions (e.g. from Charles R. Knight). However, the body posture is less erected as in the old reconstructions and the stiff tail touches not the ground and is not angled. The position of the legs is the same as in bipedal gaits A and B (Figure 179).

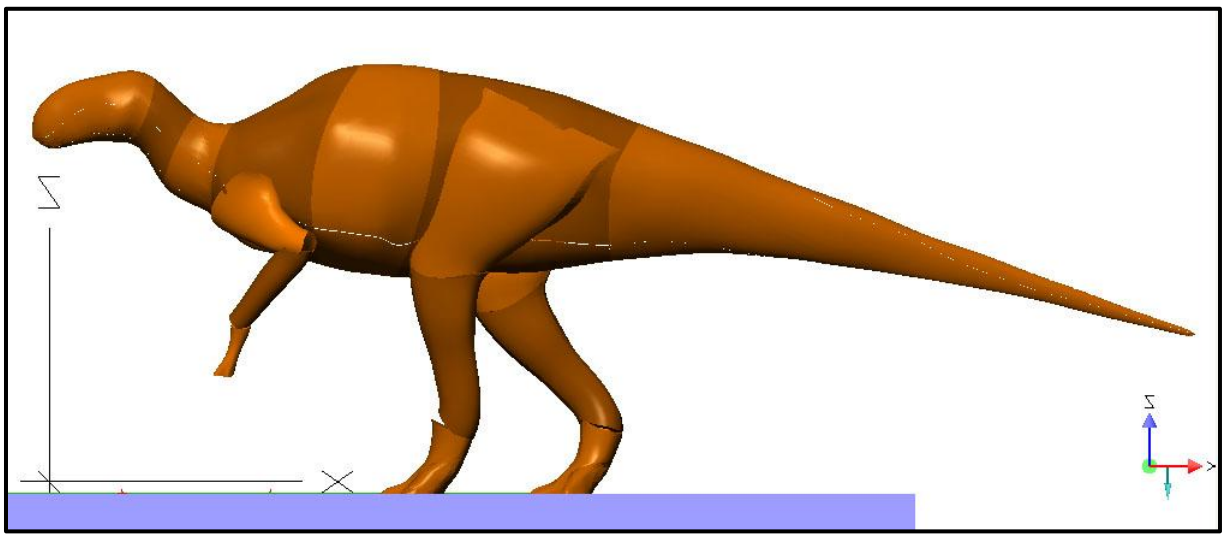

Figure 179: The *Brachylophosaurus* model in bipedal gait C body posture from lateral view.

The following videos show the results of the **bipedal gait C** simulation:

- **Video 18A** shows bipedal gait C IS3 from lateral view.
- **Video 18B** shows bipedal gait C IS3 from cranial view.
- **Video 18C** shows bipedal gait C IS3 from dorsocraniolateral view.
- **Video 18D** shows bipedal gait C IS3 from caudal view.

Bipedal gait D (Figure 180) shows the same horizontally body posture as bipedal gait A, but with a wider spacing of the legs along the y-axis and therefore a minor overlapping of the feet. In contrast, the positioning of the legs along the x-axis is the same as in the other bipedal gaits. The intention was to test walking stability with a slightly greater distance of the feet to the center of mass, and to produce a slightly broader trackway as in bipedal simulations A, B, and C, as trackway width of bipedally walking hadrosaurs can vary to a little extent (THULBORN 1990).

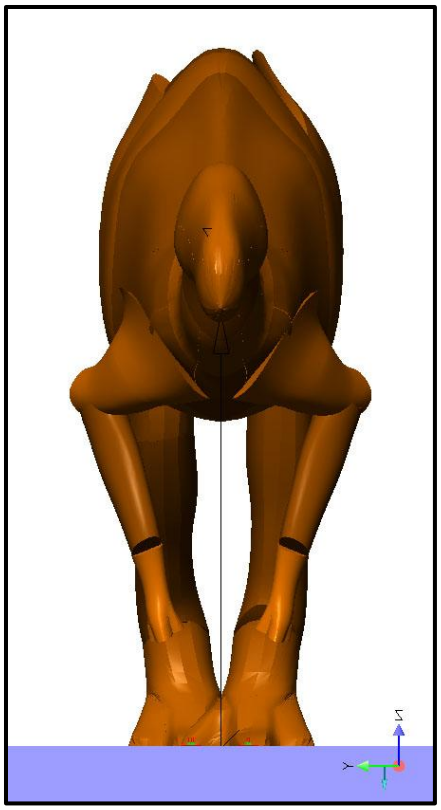

Figure 180: The *Brachylophosaurus* model in bipedal gait D body posture from cranial view.

The following videos show the results of the **bipedal gait D** simulation:

- **Video 19A** shows bipedal gait D IS3 from lateral view.
- **Video 19B** shows bipedal gait D IS3 from cranial view.
- **Video 19C** shows bipedal gait D IS3 from dorsocraniolateral view.
- **Video 19D** shows bipedal gait D IS3 from caudal view.

The horizontally body posture, which was shown in bipedal gaits A and D, was also used in **bipedal gait E** (Figure 181). Along the y-axis the feet were positioned with a wider spacing as in bipedal gaits A, B, and C, but not as wide as in gait D. Along the x-axis the feet

were placed with a considerably wider spacing as in the other bipedal simulations. Through this wider distance of the feet walking stability with increased step length could be tested. Further, bipedal gait E was also used to simulate higher velocities in bipedal locomotion, assuming that these are associated with an increased step length.

However, it is not possible to simulate these higher velocities using a 'real' running mode, as presented by SELLERS et al. (2009), since this would require a simultaneous aerial phase of the legs, which is not realizable using the generic constraints. Therefore, the 'running' shown in bipedal gait E is rather a fast walking.

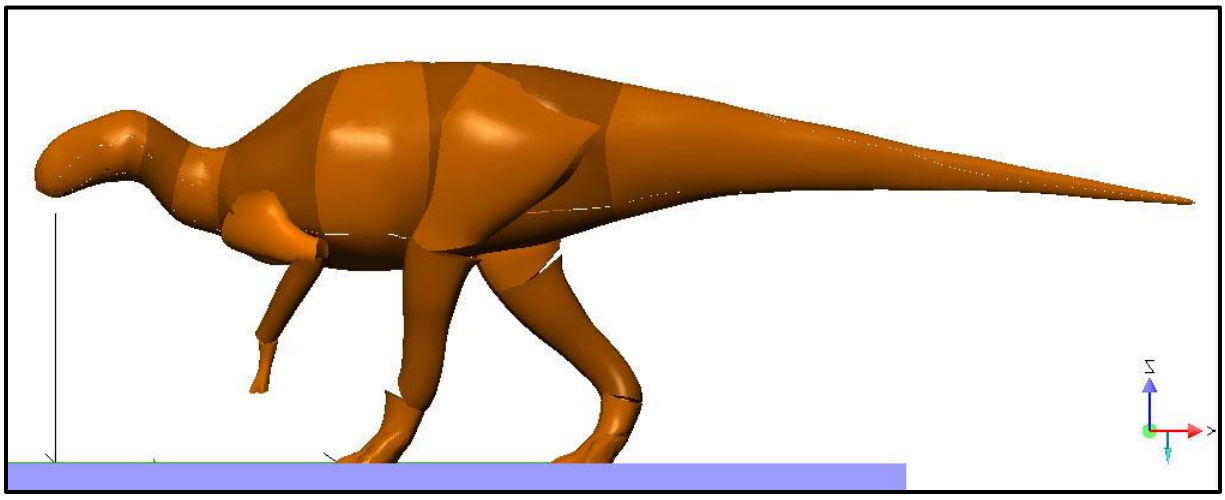

Figure 181: The *Brachylophosaurus* model in bipedal gait E body posture from lateral view.

The following videos show the results of the **bipedal gait E** simulation:

- **Video 20A** shows bipedal gait E IS3 from lateral view.
- **Video 20B** shows bipedal gait E IS3 from cranial view.
- **Video 20C** shows bipedal gait E IS3 from dorsocraniolateral view.
- **Video 20D** shows bipedal gait E IS3 from caudal view.

- **Video 20E** shows bipedal gait E IS3 with double velocity from lateral view.
- **Video 20F** shows bipedal gait E IS3 with double velocity from cranial view.
- **Video 20G** shows bipedal gait E IS3 with quadruple velocity from lateral view.
- **Video 20H** shows bipedal gait E IS3 with quadruple velocity from cranial view.
- **Video 20I** shows bipedal gait E IS3 with octuple velocity from lateral view.
- **Video 20J** shows bipedal gait E IS3 with octuple velocity from cranial view.
- **Video 20K** shows bipedal gait E IS3 with octuple velocity from lateral view with arms directed straight back (according to GALTON 1970).
- **Video 20L** shows bipedal gait E IS3 with octuple velocity from cranial view with arms directed straight back (according to GALTON 1970).

In his studies about the posture of hadrosaurian dinosaurs, GALTON (1970) presented a reconstruction of *Anatosaurus annectens* while running (Figure 182). The vertebral column is shown nearly horizontal and the forelimbs are directed backwards. This posture was also simulated using bipedal gait E (Figure 183), but with the known limitations concerning the running ability of the model.

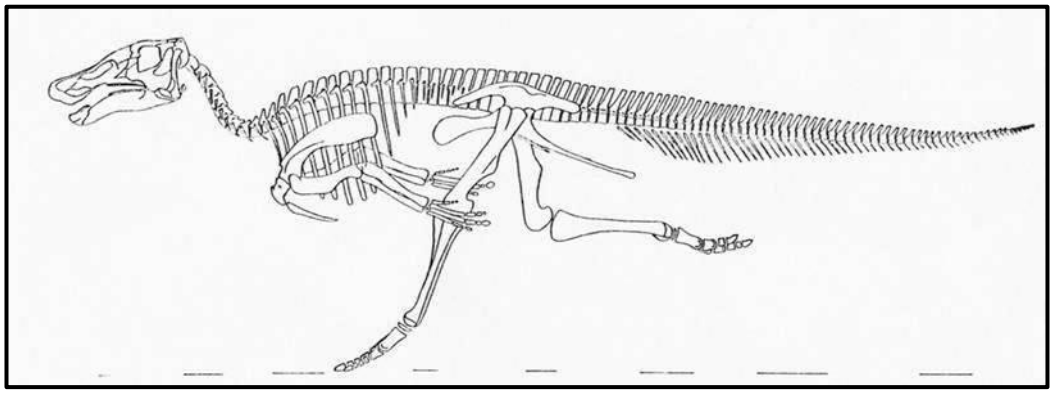

Figure 182: Reconstruction of *Anatosaurus annectens* while running (GALTON 1970).

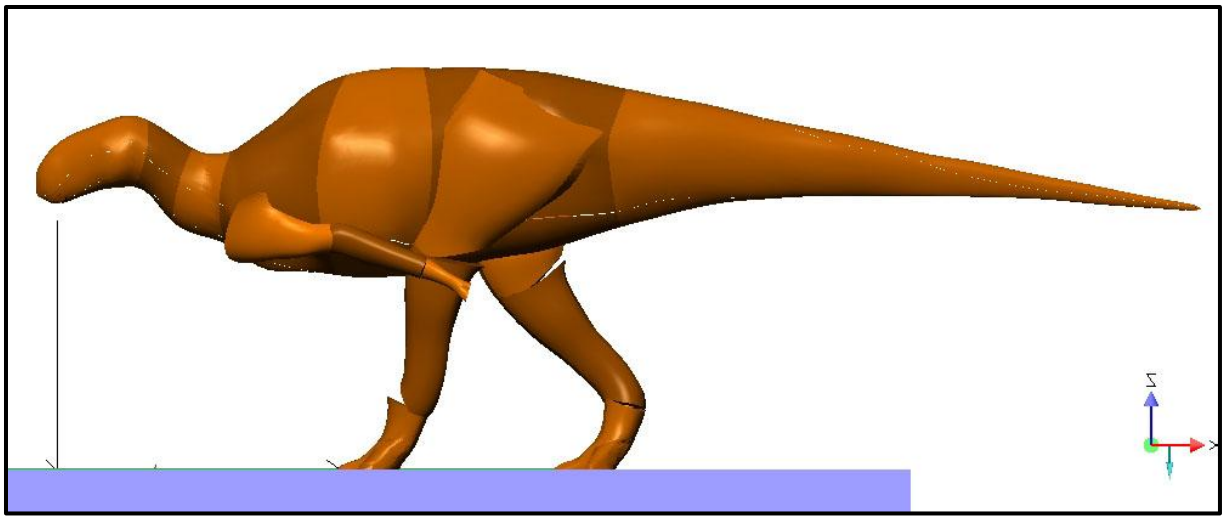

Figure 183: The *Brachylophosaurus* model in bipedal gait E body posture from lateral view with arms directed backwards after GALTON (1970).

5.2.2 Discussion

The simulations of quadrupedal locomotion in hadrosaurs show that trackways can help determine different body postures, as they require specific postures of arms and legs and therefore of the whole body. In contrast, in trackways of bipedally walking hadrosaurs and other advanced ornithopods only the foot prints are present, making it more complicated to find the correct body posture. The simulations of **bipedal gaits A, B, and C** (Videos 16A-G / 17A-D / 18A-D) show that as long the posture of the legs is identical, there are only little differences visible in the model trackways (Figures 184, 185 & 186), although the three simulations include three different body postures.

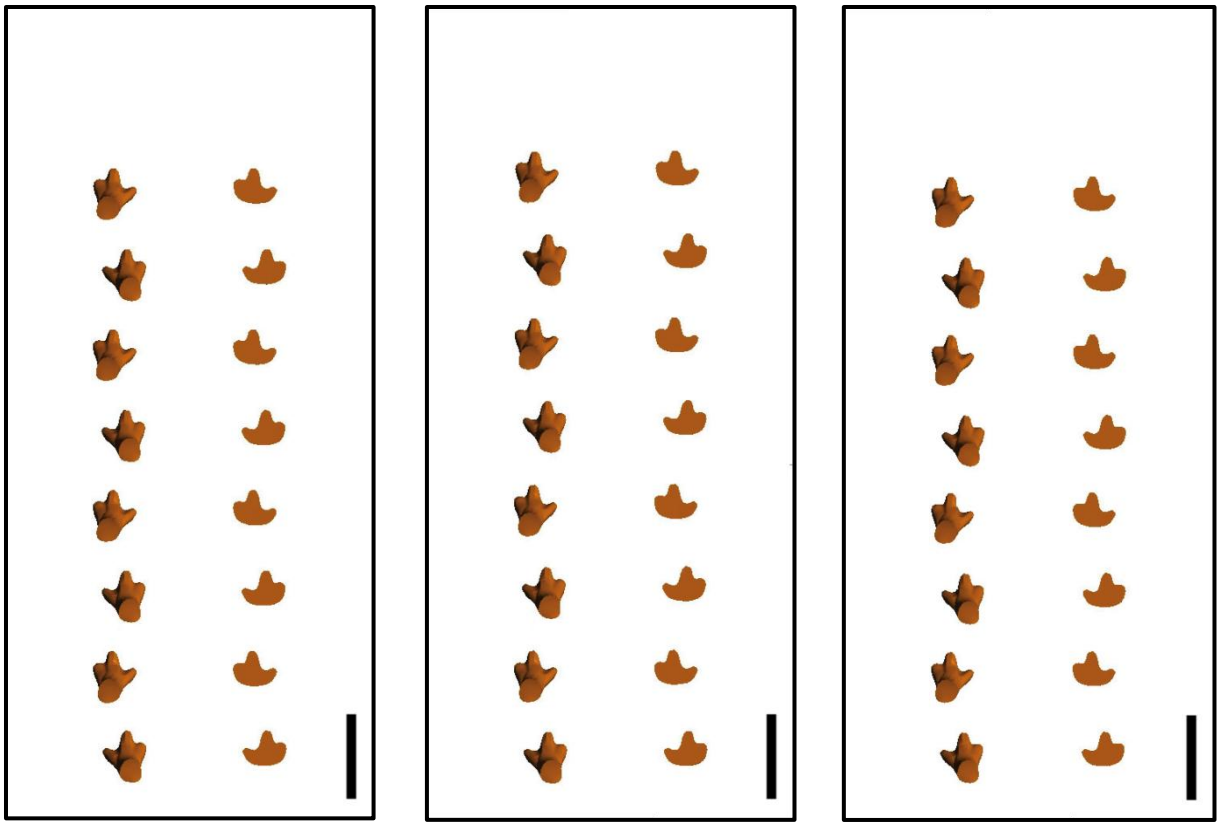

Figure 184 (left): Model trackway of bipedal gait A from dorsal view. The left trackway shows the position and orientation of the feet. The right trackway shows the corresponding foot prints; scale bar = 1 m.

Figure 185 (center): Model trackway of bipedal gait B from dorsal view. The left trackway shows the position and orientation of the feet. The right trackway shows the corresponding foot prints; scale bar = 1 m.

Figure 186 (right): Model trackway of bipedal gait C from dorsal view. The left trackway shows the position and orientation of the feet. The right trackway shows the corresponding foot prints; scale bar = 1 m.

The only difference between the model trackways is the increase of step length of the foot prints during progression in bipedal gait B (Figure 185). Despite this, the three trackways are almost identical considering other characteristics, as trackway width and inward rotation of the foot prints. This inward rotation is also shown by the right trackway in Figure 127 from the Purbeck Limestone Group, and was also described by THULBORN (1990). The model trackways are also fairly narrow and the foot prints are arranged in a slightly zig-zag pattern (THULBORN 1990).

However, as all three model trackways show the required characteristics, it is not possible to determine which body posture the animal used when walking bipedally. Therefore, bipedal trackways of hadrosaurs are presumably not as useful as quadrupedal trackways in defining corresponding body postures. In quadrupedal simulations especially the correct posture of the arms is a limiting factor concerning different alternatives.

Since bipedal gait A and semibipedal gait A base on the same body posture, the movement along the y-axis (Figure 187) is virtually identical. In contrast to motion change from semibipedal gait D to bipedal gait (Figure 175), seems the nonuse of the arms to have no influence on the center of mass, which moves also opposite to body motion in all bipedal simulations.

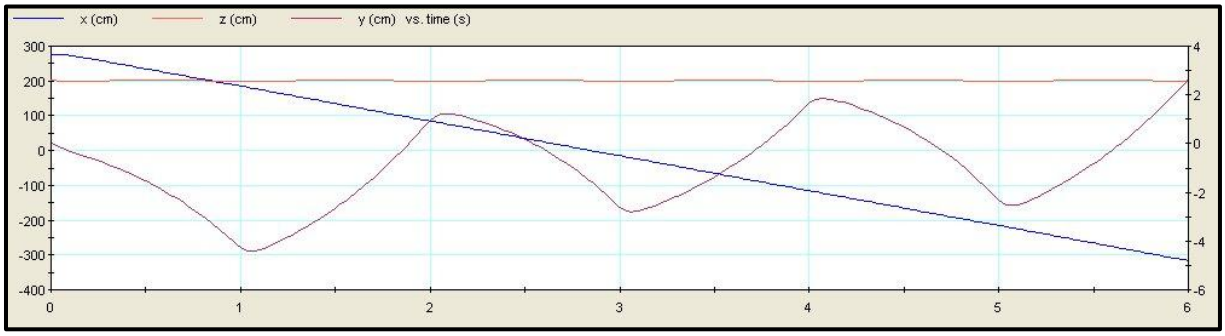

Figure 187: The diagram displays the position of the center of mass along the y-axis during the bipedal gait A simulation.

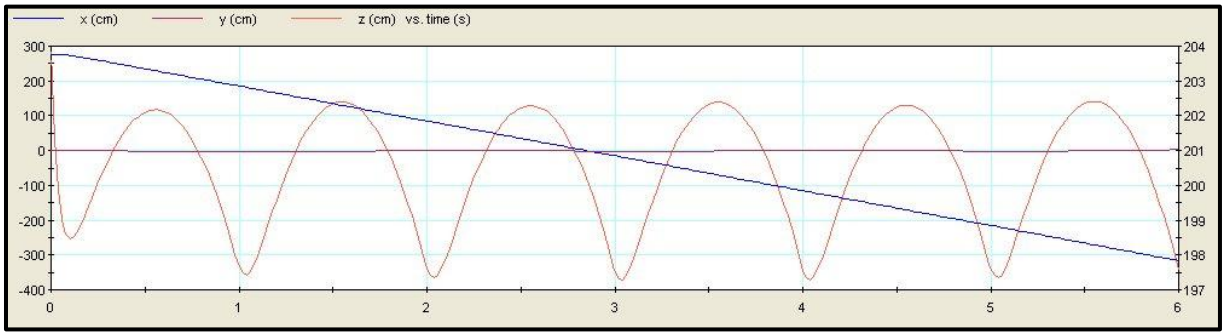

Figure 188: The diagram displays the position of the center of mass along the z-axis during the bipedal gait A simulation.

Compared to the curve of the y-axis, the curve of the z-axis in bipedal gait A (Figure 188) shows a little difference to the one of semibipedal gait A (Figure 146), as the movement of the center of mass is slightly shifted dorsally. This is accordant to its motion in the transition from semibipedal gait D to bipedal gait (Figure 176) after gait change has taken place.

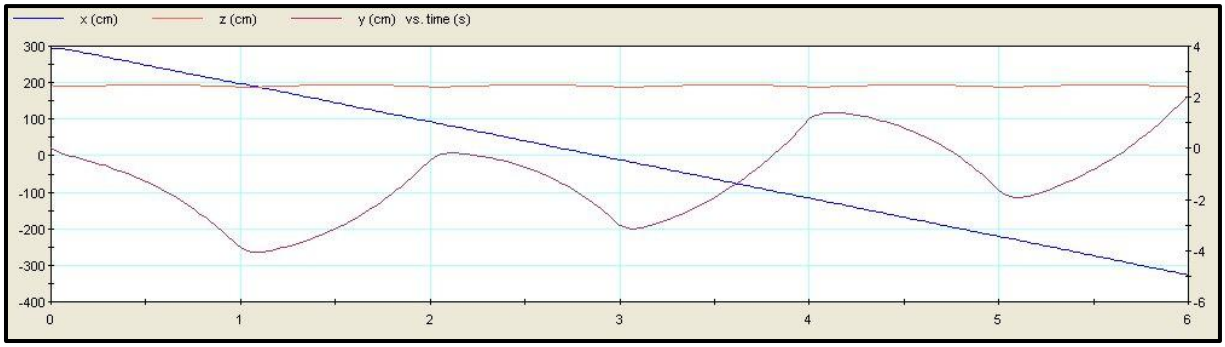

Figure 189: The diagram displays the position of the center of mass along the y-axis during the bipedal gait B simulation.

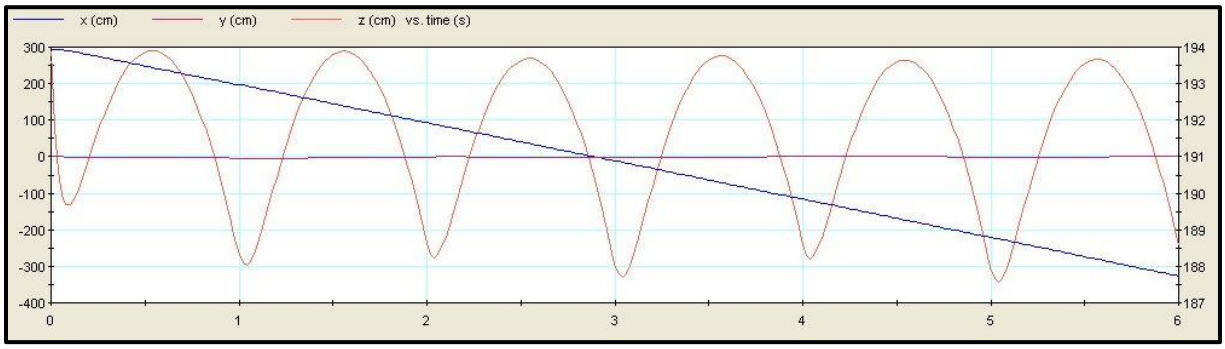

Figure 190: The diagram displays the position of the center of mass along the z-axis during the bipedal gait B simulation.

Whereas semibipedal gait A (Figure 128) and bipedal gait A (Figure 177) differ only in the nonuse of the arms in the latter simulation, bipedal gait B (Figure 178) shares only its body posture with cross and pace gait (Figures 125 & 126) and their corresponding semibipedal gaits (Figures 129 & 130). Compared to these simulations, the posture of the legs was changed in bipedal gait B, which provides a different movement of the center of mass along the y-axis (Figure 189) and the z-axis (Figure 190). The curve of the y-axis displays a minor range of lateral motion than in the diagrams of bipedal gaits A (Figure 187) and C (Figure 191), but as in bipedal gait A the center of mass shifts slightly to the left during progression. Along the z-axis the center of mass moves on a lower level than in bipedal gaits A (Figure 188) and C (Figure 192), according to the more ducked body posture in bipedal gait B.

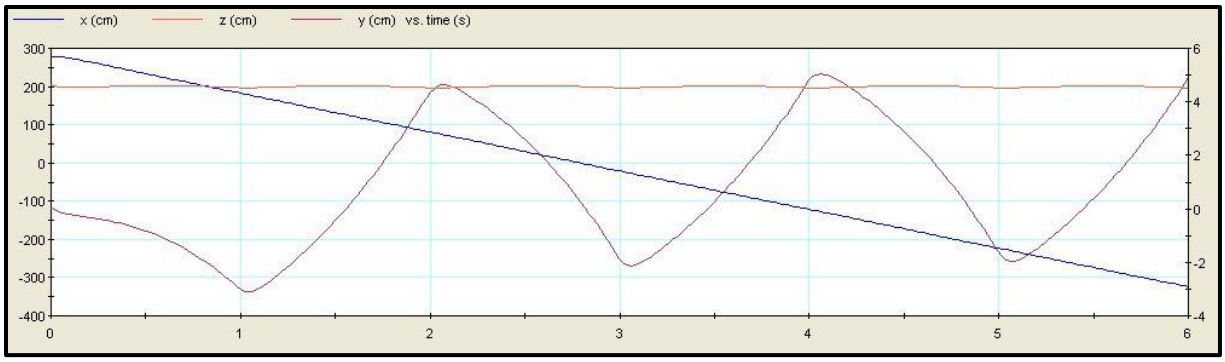

Figure 191: The diagram displays the position of the center of mass along the y-axis during the bipedal gait C simulation.

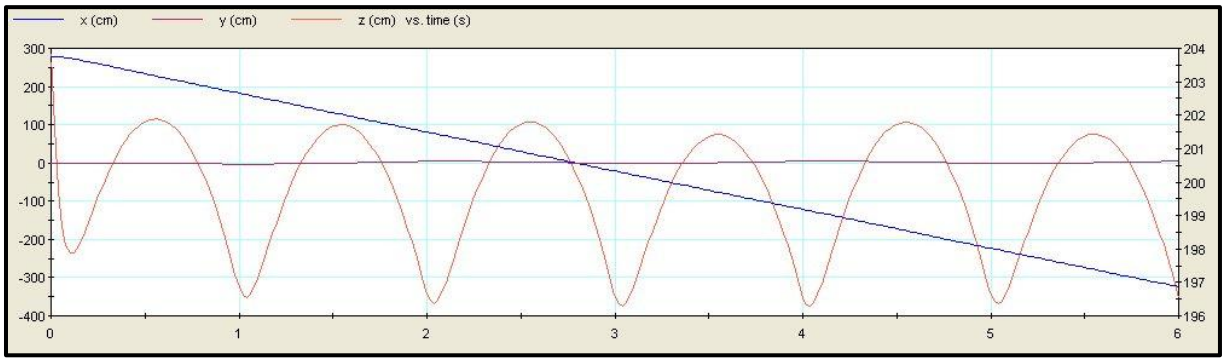

Figure 192: The diagram displays the position of the center of mass along the z-axis during the bipedal gait C simulation.

In bipedal gait C the center of mass shows the largest range of lateral motion along the y-axis (Figure 191), but only less shifting to the left or right during progression. Along the z-axis (Figure 192) the curve runs on a lower level as in bipedal gait A (Figure 188), but only with a minor difference.

In summary, the motion of the center of mass along the y-axis in bipedal gaits A, B, and C (Figures 187, 189 & 191) indicates that a more erected body posture causes a larger range of lateral movement of the center of mass, which increases from bipedal gait B to gait C. However, on basis of the simulations it is not possible to determine which body posture is preferable. The bipedal gait A body posture (Figure 177) seems to be most likely, as it correlates most with the neutral standing pose, but hadrosaurs may have used all three postures in bipedal locomotion.

According to the gallop in the quadrupedal gait simulations, it was also not possible to simulate a hopping hadrosaur (SELLERS et al. 2009) due to the generic constraints. However, as in case of the gallop, there are no tracks indicating this kind of motion, and there is no evidence that any extinct dinosaurs hopped (HUTCHINSON 2005).

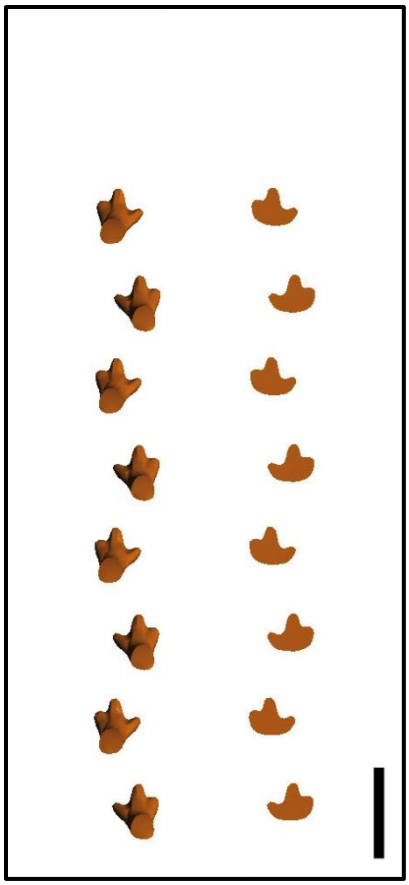

The model trackway of **bipedal gait D** (Videos 19A-D / Figure 193) shows the same characteristics as the trackways of the other bipedal motion sequences. Compared to these, the trackway is only a little broader, but a more increased trackway width would have been no longer in accordance with the fossil record. Nevertheless, the simulation shows that the wider spacing of the feet has no influence on walking stability.

Figure 193: Model trackway of bipedal gait D from dorsal view. The left trackway shows the position and orientation of the feet. The right trackway shows the corresponding foot prints; scale bar = 1 m.

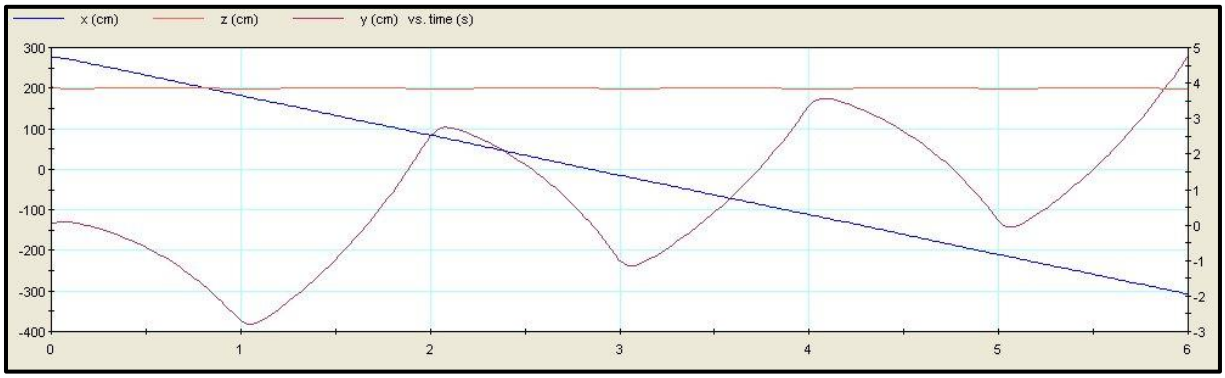

Figure 194: The diagram displays the position of the center of mass along the y-axis during the bipedal gait D simulation.

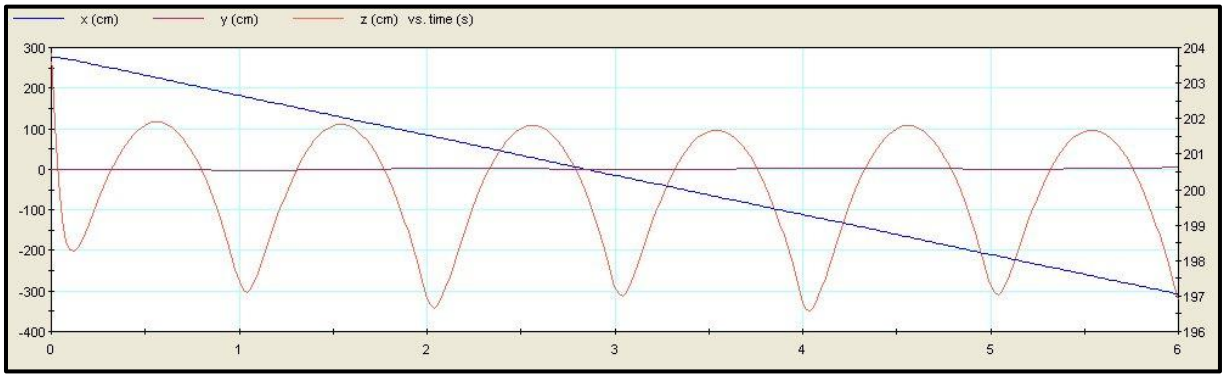

Figure 195: The diagram displays the position of the center of mass along the z-axis during the bipedal gait D simulation.

The range of lateral movement of the center of mass along the y-axis in bipedal gait D (Figure 194) is larger than in bipedal gaits A (Figure 187) and B (Figure 189), but smaller than in gait C (Figure 191). In contrast to semibipedal gaits A, D, E, and F, the wider spacing of the feet increases slightly lateral motion range of the center of mass when comparing bipedal gaits A and D. However, both bipedal simulations base on the same body posture, which is not the case in the semibipedal motion sequences. Further, bipedal gait C shows a minor spacing of the feet as gait D, but a larger range of lateral motion of the center of mass, which correlates with the quadrupedal gait results.

Along the z-axis (Figure 195) the center of mass moves on a slightly lower level in bipedal gait D than in gait A (Figure 188), despite the accordance in body posture in both simulations. The wider spacing of the feet in bipedal gait D presumably caused this discrepancy.

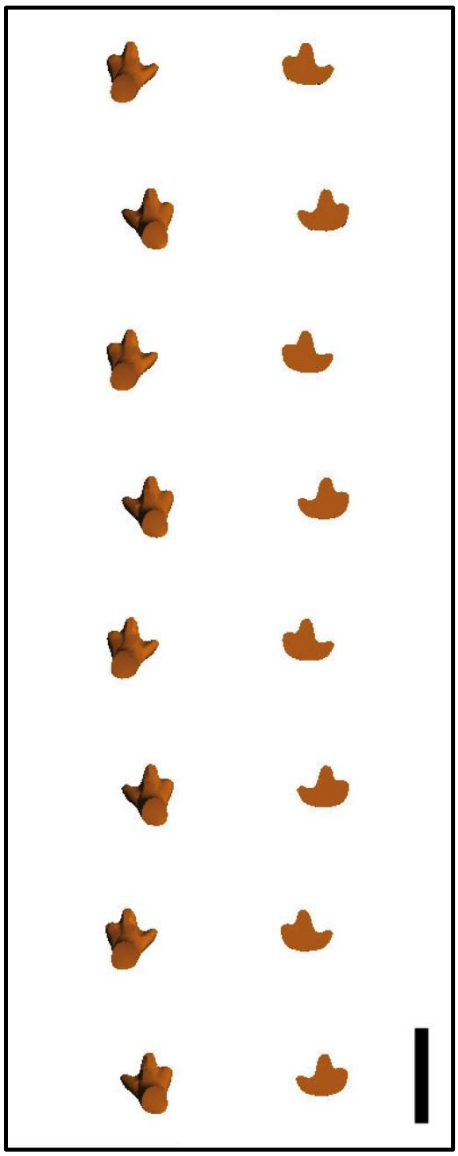

The wide spacing of the feet along the x-axis is clearly visible in the model trackway of **bipedal gait E** (Videos 20A-L / Figure 196), which displays also the characteristics of bipedal locomotion as the inward rotation of the foot prints. The bipedal gait E simulations show that walking stability is maintained with larger step length, even if velocity increases. Based on the technical limitations, mainly due to the generic constraints, a 'real' running could not be simulated, but it was decided to test higher velocities using instead a fast walking. In contrast to this work, the simulations of SELLERS et al. (2009) include a running hadrosaur. However, their simulation runs not stable as the model tilts over forward during progression.

Figure 196: Model trackway of bipedal gait E from dorsal view. The left trackway shows the position and orientation of the feet. The right trackway shows the corresponding foot prints; scale bar = 1 m.

The range of lateral movement of the center of mass along the y-axis in bipedal gait E (Figure 197) is nearly identical with the one in bipedal gait C (Figure 191), but the progression of the curve differs in both diagrams. In gait E direction change happens more fluently but less directly, maybe caused by the larger step length. The latter presumably caused also the larger range of lateral motion in gait E compared with bipedal gaits A (Figure 187) and B (Figure 189), and the accordance with gait C, despite the wider spacing of the feet in gait E. In contrast, as in bipedal gait D the distance between the feet is a little higher as in gait E, lateral motion is slightly smaller.

The vertical motion of the center of mass along the z-axis (Figure 198) differs from those of the other bipedal gaits (Figures 188, 190, 192, & 195), since the center of mass moves on a higher level and shows also a larger vertical motion range due to increased step length in bipedal gait E.

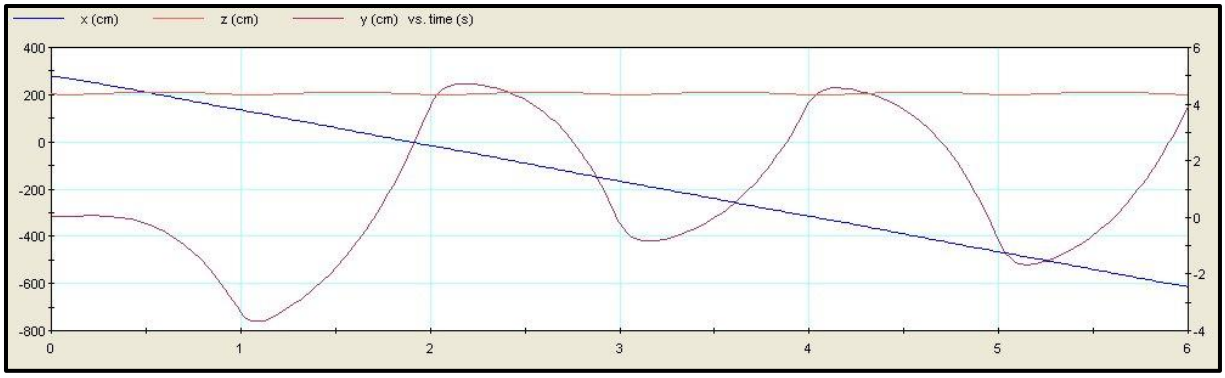

Figure 197: The diagram displays the position of the center of mass along the y-axis during the bipedal gait E simulation.

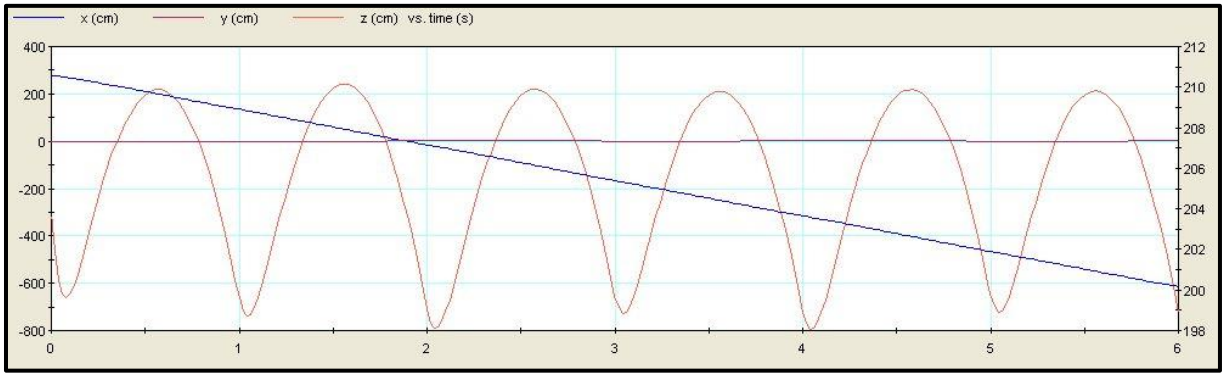

Figure 198: The diagram displays the position of the center of mass along the z-axis during the bipedal gait E simulation.

When the model moves with double speed, the delay in direction change along the y-axis (Figure 199) becomes larger as the inertia effect increases. Simultaneously curve progression is now strongly rounded and symmetrical in turning from right to left and vice versa, different to the other simulations.

Whereas the range of lateral motion is highly similar to normal speed (Figure 197), the vertical motion of the center of mass shows a smaller range in the double speed diagram (Figure 200). The decrease of range in vertical motion continues with increasing speed as the diagrams of the z-axis show (Figures 202, 204, 206). In addition, curve progression gets less rounded and more serrated from normal to octuple velocity. Therefore, increasing speed and correlated inertia effect seem to hinder the motion of the center of mass along the z-axis. According to that, also the range of lateral movement of the center of mass decreases with quadruple and octuple velocity (Figures 201, 203, 205).

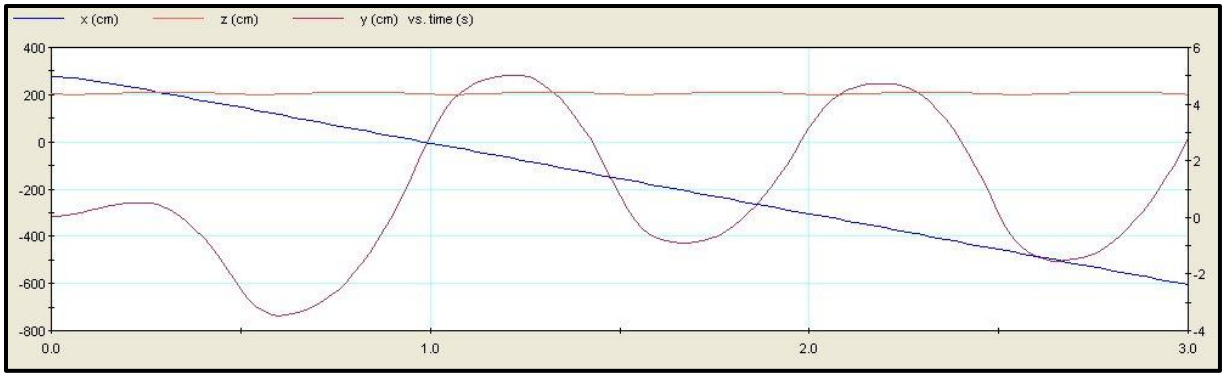

Figure 199: The diagram displays the position of the center of mass along the y-axis during the bipedal gait E simulation with double velocity.

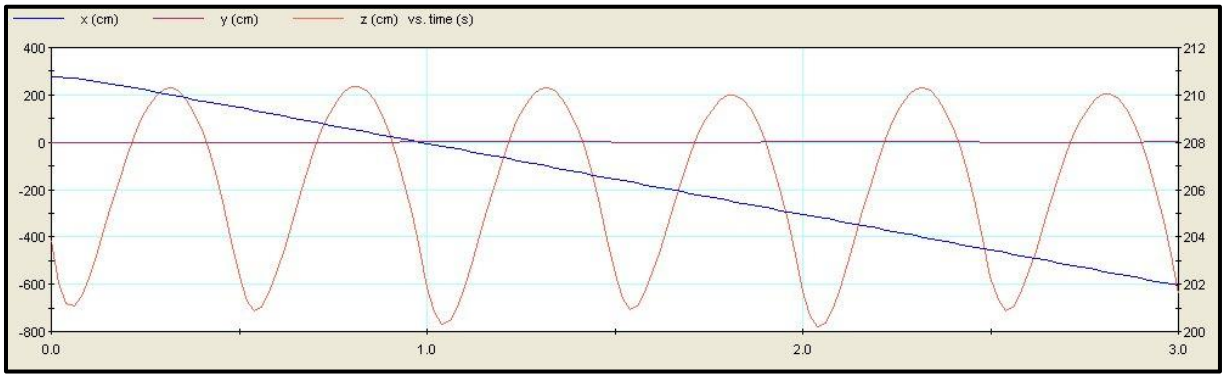

Figure 200: The diagram displays the position of the center of mass along the z-axis during the bipedal gait E simulation with double velocity.

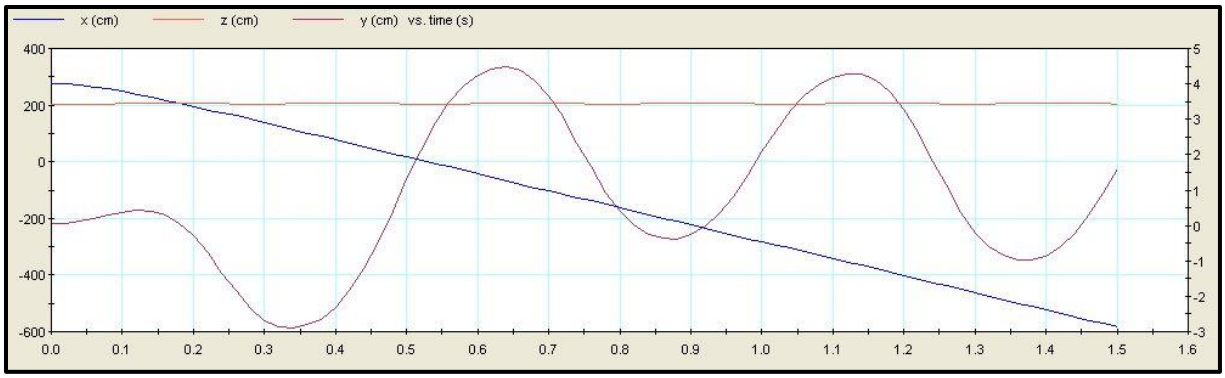

Figure 201: The diagram displays the position of the center of mass along the y-axis during the bipedal gait E simulation with quadruple velocity.

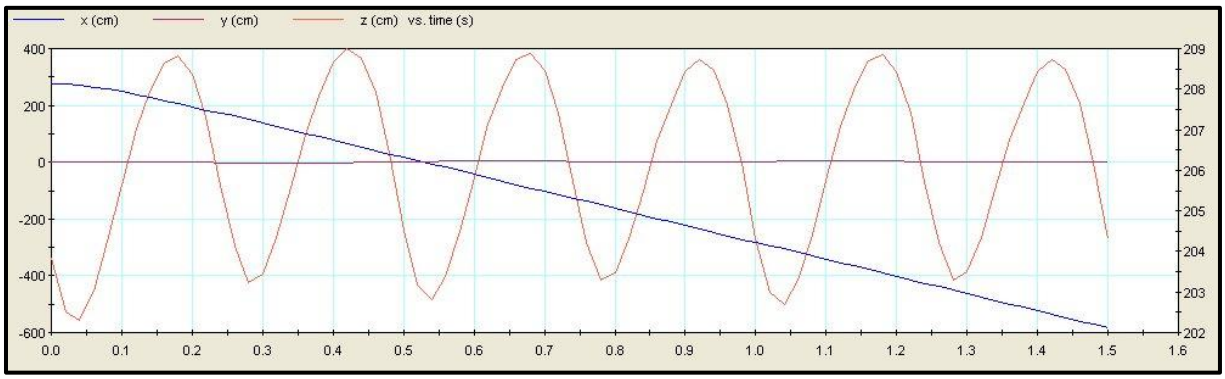

Figure 202: The diagram displays the position of the center of mass along the z-axis during the bipedal gait E simulation with quadruple velocity.

In the simulations with octuple velocity a second body posture was tested. According to GALTON (1970) the arms were directed straight back, following his supposed body posture of a running hadrosaur. The comparison of normal and modified posture shows no differences concerning the movement of the center of mass along the y-axis (Figures 203 & 205). However, along the z-axis the center of mass moves on a slightly higher level when the arms are directed straight back (Figures 204 & 206).

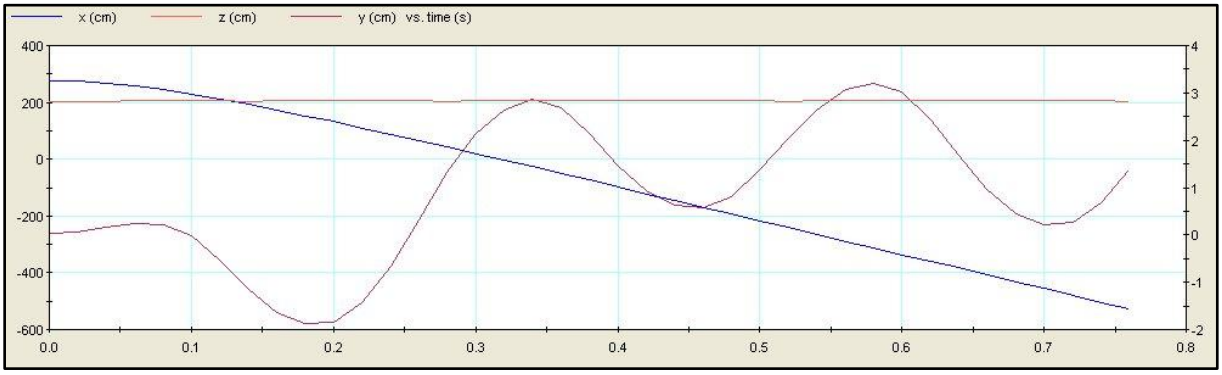

Figure 203: The diagram displays the position of the center of mass along the y-axis during the bipedal gait E simulation with octuple velocity.

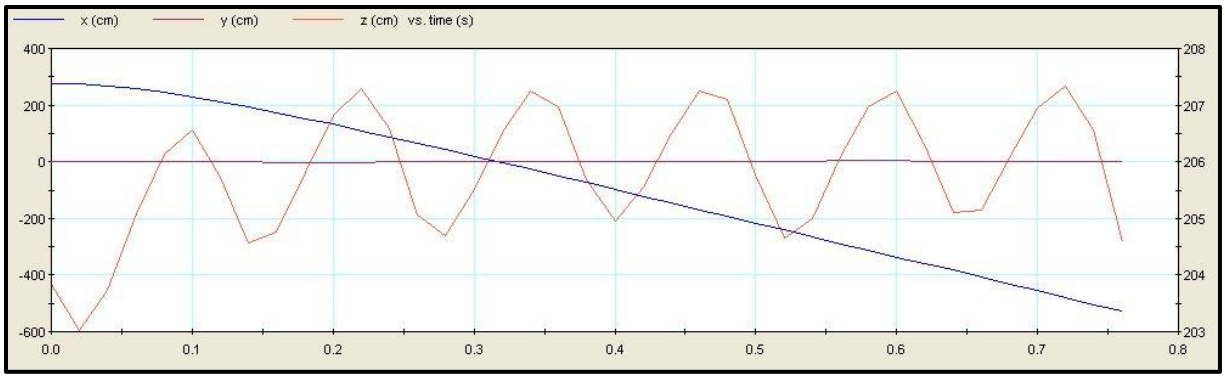

Figure 204: The diagram displays the position of the center of mass along the z-axis during the bipedal gait E simulation with octuple velocity.

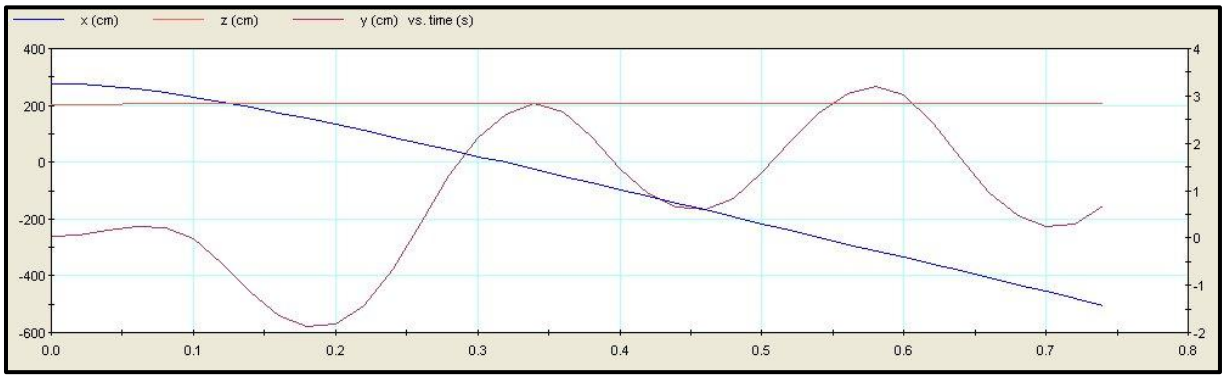

Figure 205: The diagram displays the position of the center of mass along the y-axis during the bipedal gait E simulation with octuple velocity and arms directed straight back.

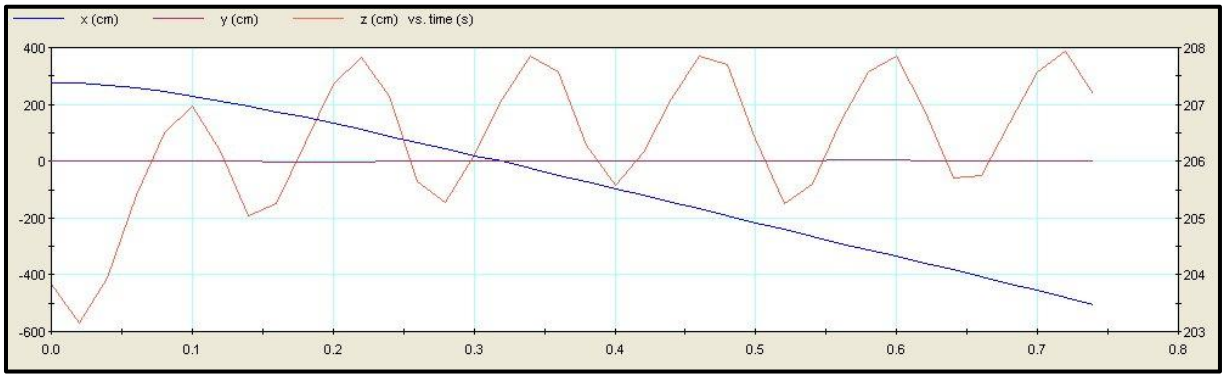

Figure 206: The diagram displays the position of the center of mass along the z-axis during the bipedal gait E simulation with octuple velocity and arms directed straight back.

5.3 Other body postures

In addition to the walking simulations, also other possible body movements were simulated. However, when simulating high- or low-browsing, it is not possible to control these movements using tracks or trackways. Therefore, gravity is the main control factor to determine the probability of a certain body movement respectively posture.

5.3.1 Results

In the **high-browsing** simulation the ability of the hadrosaurian body to achieve an erect stance was tested, as described for example by MARYANSKA and OSMOLSKA (1984). In contrast to their illustration (Figure 207), the tip of the tail of the model nearly touches the ground, but the tail was not bended because of its stiffness (Figure 208).

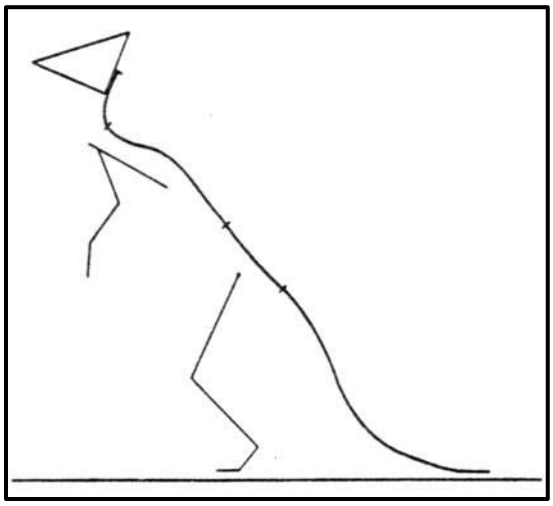

Figure 207: Diagrammatic reconstruction of *Saurolophus angustirostris* in high-browsing stance (MARYANSKA and OSMOLSKA 1984).

The following videos show the results of the **high-browsing** simulation:

- **Video 21A** shows high-browsing stance from lateral view, based on a bipedal body posture.
- **Video 21B** shows high-browsing stance from cranial view, based on a bipedal body posture.
- **Video 21C** shows high-browsing stance from lateral view, based on a quadrupedal body posture.
- **Video 21D** shows high-browsing stance from cranial view, based on a quadrupedal body posture.

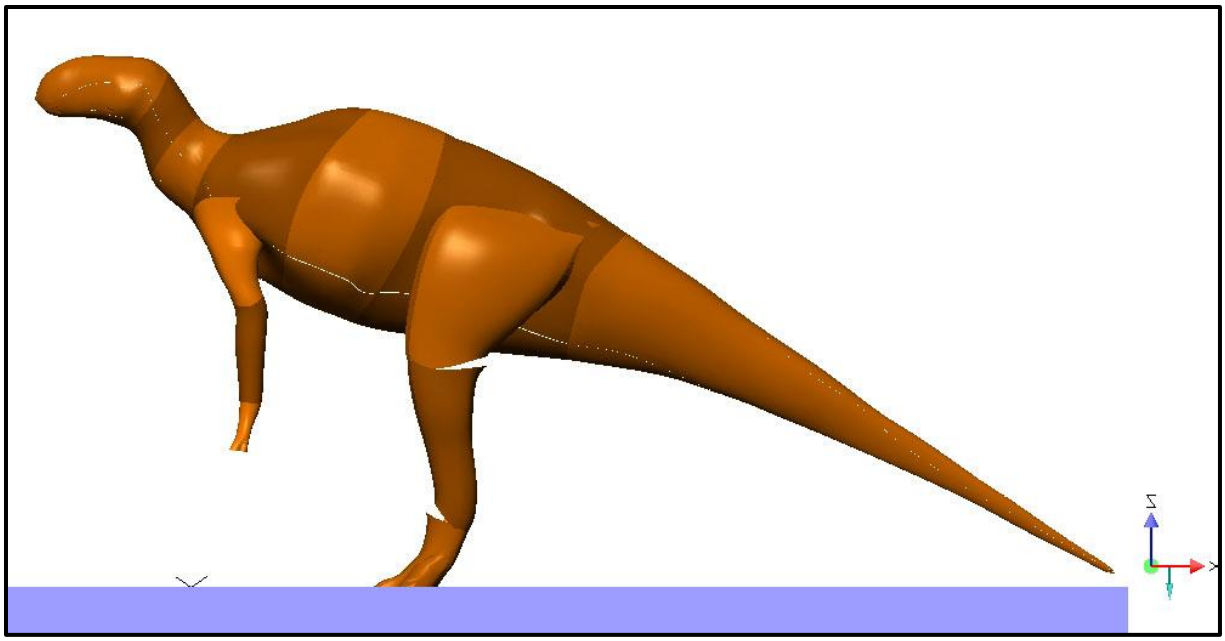

Figure 208: The *Brachylophosaurus* model in high-browsing stance from lateral view.

The second simulated body posture is the **low-browsing and drinking posture**, which bases also on an illustration of MARYANSKA and OSMOLSKA (1984) (Figure 209). In contrast to their illustration and the high-browsing stance, two low-browsing postures were simulated, as the arms could be used in body support or not (Figures 210 & 211). Further, the tail was again not bended.

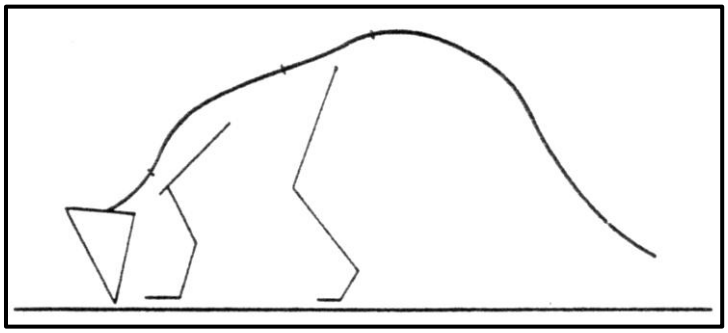

Figure 209: Diagrammatic reconstruction of *Saurolophus angustirostris* in low-browsing stance (MARYANSKA and OSMOLSKA 1984).

The following videos show the results of the **low-browsing** simulations:

- **Video 22A** shows low-browsing stance from lateral view, without using the arms in body support.
- **Video 22B** shows low-browsing stance from cranial view, without using the arms in body support.
- **Video 22C** shows low-browsing stance from lateral view, using the arms in body support.
- **Video 22D** shows low-browsing stance from cranial view, using the arms in body support.

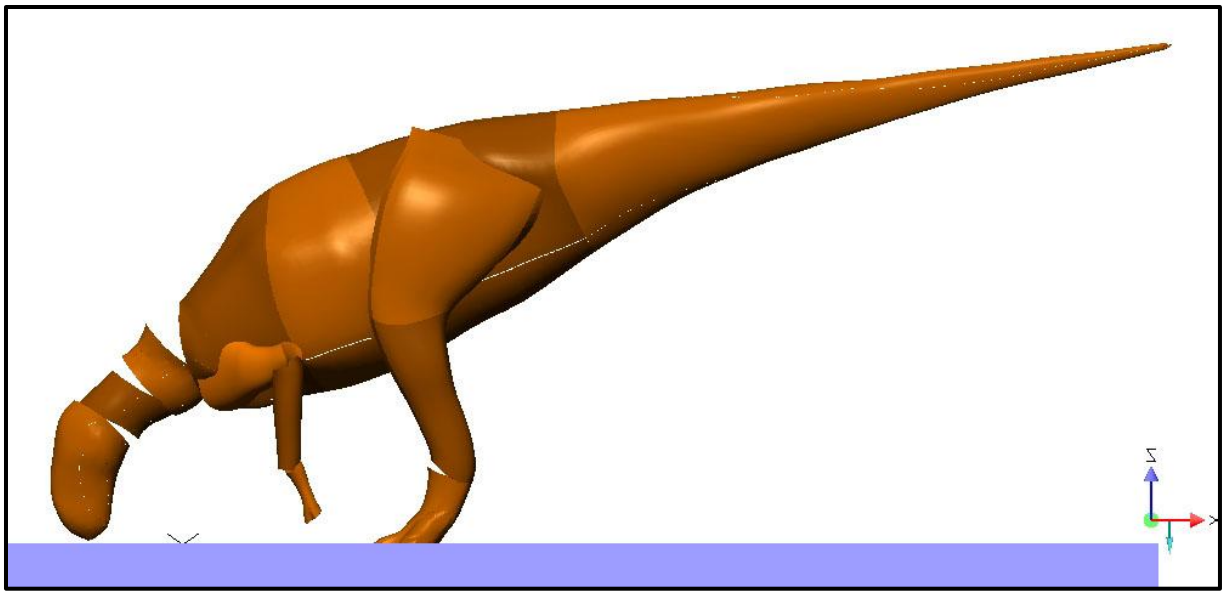

Figure 210: The *Brachylophosaurus* model in low-browsing stance from lateral view, without using the arms in body support.

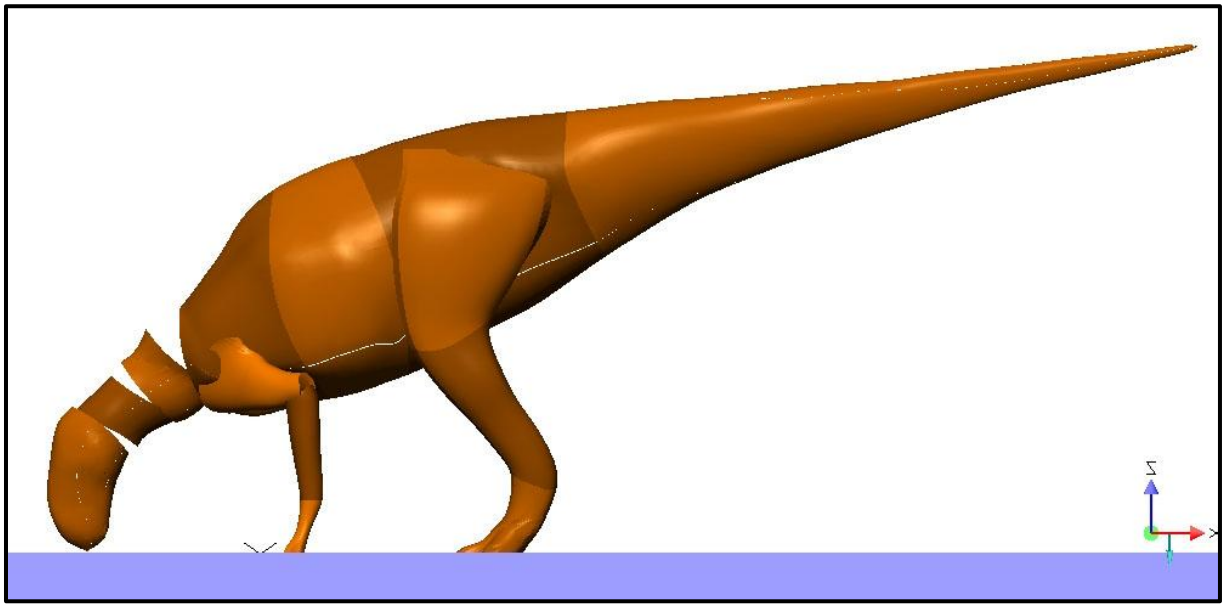

Figure 211: The *Brachylophosaurus* model in low-browsing stance from lateral view, using the arms in body support.

After simulating the transition from quadrupedal to bipedal gait (see chapter 5.1.1), also the transition from **quadrupedal to bipedal stance** was simulated.

The following video shows the change from quadrupedal to bipedal stance:

- **Video 23A** shows the change from quadrupedal to bipedal stance and back from lateral view.

5.3.2 Discussion

The **high-browsing** simulations (Videos 21A-D) show that it would have been possible for *Brachylophosaurus* to achieve an erect stance (Figure 208), based either on a bipedal or a quadrupedal body posture. Therefore, the assumption of MARYANSKA and OSMOLSKA (1984) (Figure 207) seems to be proved, but a bending of the tail is not possible due to the ossified tendons (Figure 4). According to the simulation, the *Brachylophosaurus* model would have a high-browsing reach of approximately 3.5 m. However, despite the possibility to achieve an erect stance, it is not provable if hadrosaurs actually used this body posture.

Concerning the **low-browsing and drinking posture** (Videos 22A-D), the simulations show that this posture can be achieved with or without using the forelimbs (Figures 210 & 211). In contrast, MARYANSKA and OSMOLSKA (1984) correlated this body posture solely with the quadrupedal stance (Figure 209). Further, their illustration shows again a bended tail.

The bipedal and quadrupedal low-browsing body postures differ in the position of the legs, which are placed more cranially in the bipedal stance. Otherwise the nonuse of the arms would not be possible as a gravity test with the quadrupedal stance illustrates (Video 24A).

- **Video 24A** shows the gravity test with the quadrupedal low-browsing body posture.

The gravity test shows that the more caudally position of the legs in the quadrupedal stance requires the use of the arms, as otherwise stability is not ensured.

In contrast to the high-browsing posture, the low-browsing stance was definitely part of hadrosaurian motion, at least for drinking. However, if bipedal and quadrupedal stance were used by these animals, or if one posture was preferred, cannot be resolved.

Finally, the simulation of the transition from **quadrupedal to bipedal stance** and back (Video 23A) indicates that this motion is possible without a backward motion of the head for example, to facilitate the shift of the center of mass.

6. Conclusions

The locomotion of hadrosaurs has been examined for a long time, with different approaches producing often controversial results. However, with the exception of SELLERS et al. (2009), computer based simulations of hadrosaurian locomotion were not part of this research. The use of CAD (computer aided design) and NASTRAN-based CAE (computer aided engineering) software provide the possibility to investigate hadrosaurian balance and postures, range of motion, body mass distribution, and motion sequences.

For these simulations the used model has to be as accurately as possible, based first on the virtual skeleton. Within this work it was not possible to digitize a complete skeleton, but the bones of shoulder and pelvic girdle and of arms and legs were most important and were also sufficient to build the locomotory parts of the model highly accurate. Although some bones of the *Brachylophosaurus* material from Malta were damaged or incomplete, the assembling of the virtual skeleton demonstrates that it is of great advantage if most of the bones belong to one specimen, as scaling of bones from different specimens can always cause inaccuracies. Essential in creating the virtual skeleton were photos (e.g. from museum mounts) and drawings (e.g. BAKKER (1986); BRETT-SURMAN and WAGNER (2007)). Fortunately, in case of hadrosaurian dinosaurs these tools are frequently available due to the huge amount of material from this common dinosaur group. Possible inaccuracies in assembling the virtual skeleton caused by the unknown amount of epiphyseal (articular) cartilage are not avoidable, but this problem occurs in every scientific work handling with fossilized bone material.

The newly introduced method of reworking digitized bones shows that if this work is done carefully, these bones are clearly more useful in assembling the virtual skeleton than using the non-reworked ones. Most complex was the transformation of the two *Dryosaurus* bones, but widely correct shapes of astragalus and calcaneus could be achieved. Although the reworking method should only be a compromise, it can be quite useful if no complete bone is available for digitizing.

The use of the *Parasaurolophus* desk model to create the model body was also problematical, due to its unsure scientific correctness, but in combination with the skeletal drawings, the virtual skeleton, and the carefully done freehand modeling of arms and legs a realistic model of a *Brachylophosaurus* could be created. Concerning body length, body

weight, and the position of the center of mass the *Brachylophosaurus* model coincides with other reconstructions and calculations (e.g. ALEXANDER (1989); BATES et al. (2009); Scott Hartman [www.skeletaldrawing.com]; HENDERSON (1999); PAUL (2010)).

Therefore, the procedure in creating the *Brachylophosaurus* model can be used also for the creation of other dinosaur models. However, the plenty of information about hadrosaurian dinosaurs is not available for each dinosaur group, and the more information the higher the accurateness of the model.

The simulations are influenced by some technical limitations, especially regarding the generic constraints. However, although it was not possible to simulate a 'real' running hadrosaur, this kind of motion was not needed in most of the simulations. Further, to work without the generic constraints would not have been possible using MSC.visualNastran 4D®.

Beside this limitation there is another problem concerning the constraints in general, as the range of motion of each constraint could only be estimated in the simulations. Based on the virtual skeleton alone, it was not possible to specify the range of motion of a certain constraint exactly. For that purpose reconstructions of hadrosaurian musculature would have been necessary, but this was beyond the scope of this work.

Therefore, it was important to achieve accordance between fossil and model trackway in a simulation, as motion sequence should be widely realistic then and also the used constraint settings. In addition, as no extreme motions were necessary, constraint settings should be also realistic in those simulations which could not be controlled by tracks. Concerning the latter, HUTCHINSON and GATESY (2006) are of the opinion that fossil footprints tell little about how the whole limb or body moved, because of redundancy within the limb skeleton. However, some postures of body and legs are more likely than others, and in most cases, especially in the simulations of quadrupedal locomotion, there exist only few alternatives to achieve the correct trackway, or even only one. Hence, tracks and trackways are nevertheless the best way to control the simulation results.

Regarding quadrupedal locomotion, it is obvious that in most simulations the semibipedal way of motion has to be used to be in accordance with the fossil tracks. The cross gait could have been used as well, but it is not sure if the rotation of the arm around the shoulder joint would have been possible as shown in the simulation. This would require a closer look on the range of motion of the shoulder joint, especially of the musculature of the shoulder girdle. Although the cross gait bases on problematic tracks, its model trackway

coincides with the description of THULBORN (1989), which is not the case regarding the pace gait. Therefore, the cross gait seems to be more likely, but if it was actually part of hadrosaurian locomotion remains unsolved, especially as its trackway characteristics could be also achieved using semibipedal gait B.

The results indicate that hadrosaurs used in general the semibipedal way of motion when walking quadrupedally. The arms were used as additional body support, but the legs played the major supportive role in bearing the body mass, which is also shown by the position of the center of mass. Further, the simulations show that there is no uniform semibipedal motion, but different postures of bodies, arms, and legs according to a huge variety of tracks and trackways in the fossil record. Although the use of the arms is undeniable, the simulations cannot answer why or to what extent they were used in locomotion.

In those simulations showing bipedal locomotion it was not possible to define which body posture is the correct one. However, as in quadrupedal motion, hadrosaurs may have used different body postures when walking bipedally, as indicated by the motion sequences. Despite the fact that a 'real' running hadrosaur could not be realized, the 'fast walking' simulations can give an idea how this may have looked like. In addition, they show that higher velocities and larger step length have no influence on walking stability.

In all simulations the center of mass moves within a small range, but differences between the individual gaits are visible, as for example the influence of a wider spacing of the feet. In those simulations showing transition from quadrupedal to bipedal gait, this change is also reflected by the motion curves in the diagrams. Altogether, regarding the motion of the center of mass, the differences between quadrupedal and bipedal locomotion are relatively small.

This would match with the conclusions of MORATALLA et al. (1992). Based on the inward rotation of the foot prints, which is part of bipedal and quadrupedal trackways, they concluded that ornithopods used a similar type of locomotion during both bipedal and quadrupedal progression. This indicates that the use of an optional quadrupedal gait does not significantly modify the slight rotation of the pelvic girdle or the role of the swinging tail during progression. Therefore, following their interpretation, the use of the arms would influence locomotion only to a minor extent, which can be deduced also from the movement of the center of mass in the bipedal and quadrupedal motion sequences.

Since the different hadrosaur species are so similar, the simulation results using the *Brachylophosaurus* model should be widely transferable to other hadrosaur genera. However, the simulations show that there are several ways of walking bipedally or quadrupedally. If these were all part of the range of motion of the individual hadrosaur species is unknown and also not provable for *Brachylophosaurus* itself. Further, concerning skeletal morphology, some differences exist between hadrosaurine and lambeosaurine hadrosaurs (e.g. EGI and WEISHAMPEL (2002)), which may have also caused differences in the range of motion. In addition, if there was actually habitat differentiation among hadrosaur species (RUSSELL 1967a, 1967b; DODSON 1971; HORNER 1983; HORNER et al. 2001), this could have influenced range of motion of the respective species as well.

Nevertheless, the results show that it is possible to simulate hadrosaurian locomotion using fossil tracks and trackways, but it is essential to achieve a high accordance between fossil and model trackway to make locomotion as realistic as possible.

In summary, the simulations of hadrosaurian locomotion and other motion sequences help to achieve a quite better understanding of which gaits hadrosaurs may have used or not, and how these different gaits may have appeared.

7. References

- ALEXANDER, R.McN. (1985): Mechanics of posture and gait of some large dinosaurs. – Zoological Journal of the Linnean Society, **83**: 1-25.
- ALEXANDER, R.McN. (1989): Dynamics of dinosaurs and other extinct giants. – Columbia University Press, New York.
- BAKKER, R.T. (1978): Dinosaur feeding behaviour and the origin of flowering plants. – Nature, **274**: 661-663.
- BAKKER, R.T. (1986): The Dinosaur Heresies. – Kensington, New York.
- BARRETT, P.M., BUTLER, R.J., TWITCHETT, R.J., & HUTT, S. (2011): New material of *Valdosaurus canaliculatus* (Ornithischia: Ornithopoda) from the Lower Cretaceous of southern England. - Special Papers in Palaeontology, **86**: 131–163.
- BATES, K.T., MANNING, P.L., HODGETTS, D. & SELLERS, W.I. (2009): Estimating mass properties of dinosaurs using laser imaging and 3D computer modelling. – PLoS ONE, **4**(2): 1-26.
- BRETT-SURMAN, M.K. & WAGNER, J.R. (2007): Discussion of character analysis of the appendicular anatomy in Campanian and Maastrichtian North American hadrosaurids – variation and ontogeny. In: CARPENTER, K. (Ed.): Horns and beaks - ceratopsian and ornithopod dinosaurs: 91-115. – Indiana University Press, Bloomington and Indianapolis.
- BROWN, B. (1912): The osteology of the manus in the family Trachodontidae. – Bull. Am. Museum Nat. History, **31**: 105-108.
- BROWN, B. (1913): A new trachodont dinosaur, *Hypacrosaurus*, from the Edmonton Cretaceous of Alberta. – Bull. Am. Museum Nat. History, **32**: 395-406.
- CHRISTIANSEN, P. (2000): Dinosaur biomechanics. In: PAUL, G.S. (Ed.): The Scientific American book of Dinosaurs: 64-75. – Byron Press, New York.
- COPE, E.D. (1869): Synopsis of the extinct Batrachia, Reptilia, and Aves of North America. – Transactions of the American Philosophical Society, **14**: 1-252.
- CURRIE, P.J. (1983): Hadrosaur trackways from the Lower Cretaceous of Canada. - Acta Palaeontologica Polonica, **28**(1/2): 63-73.

- CURRIE, P.J., NADON, G.C. & LOCKLEY, M.G. (1991): Dinosaur footprints with skin impressions from the Cretaceous of Alberta and Colorado. – Canadian Journal of Earth Sciences, **28**: 102-115.
- DAGG, A.I. (1977): Running, Walking and Jumping. – Wykeham Publications (London) Ltd. London and Basingstoke.
- DILKES, D.W. (1993): Growth and locomotion in the hadrosaurian dinosaur *Maiasaura peeblesorum* from the Upper Cretaceous of Montana. – Ph.D. thesis, The University of Toronto, Toronto.
- DILKES, D.W. (2000): Appendicular myology of the hadrosaurian dinosaur *Maiasaura peeblesorum* from the Late Cretaceous (Campanian) of Montana. – Transactions of the Royal Society of Edinburgh: Earth Sciences, **90**: 87-125.
- DILKES, D.W. (2001): An ontogenetic perspective on locomotion in the Late Cretaceous dinosaur *Maiasaura peeblesorum* (Ornithischia: Hadrosauridae). - Canadian Journal of Earth Sciences, **38**: 1205-1227.
- DODSON, P. (1971): Sedimentology and taphonomy of the Oldman Formation (Campanian), Dinosaur Provincial Park, Alberta (Canada). – Palaeogeography, Palaeoclimatology, Palaeoecology, **10**: 21–74.
- DODSON, P. (1975): Taxonomic implications of relative growth in lambeosaurine hadrosaurs. – Systematic Zoology, **24**: 37-54.
- DOLLO, L. (1888): Iguanodontidae et Camptonotidae. – C. R. Acad. Sci. Paris, **106**: 775-777.
- EGI, N. & WEISHAMPEL, D.B. (2002): Morphometric analyses of humeral shapes in Hadrosaurids (Ornithopoda, Dinosauria). – Senckenbergiana lethaea, **82**(1): 43-58.
- ELLENBERGER, P. (1974): Contribution à la classification des Pistes de Vertébrés du Trias: les types du Stormberg d'Afrique du Sud (II). - Palaeovertebrata, Mémoire Extraordinaire, Montpellier.
- FARLOW, J.O. (1987): Speculations about the diet and digestive physiology of herbivorous dinosaurs. - Paleobiology, **13**: 60-72.
- FIORILLO, A.R. & GANGLOFF, R.A. (2001): The caribou migration model for arctic hadrosaurs (dinosauria: ornithischia): a reassessment. – Historical Biology, **15**: 323-334.

- FORSTER, C.-A. & SERENO, P.C. (1994): Phylogeny of the Hadrosauridae. - Journal of Vertebrate Paleontology, **14**(Suppl.): 25A.
- FORSTER, C.-A. (1997): Hadrosauridae. In: CURRIE, P.J. & PADIAN, K. (Eds.): Encyclopedia of Dinosaurs: 293-299. - Academic Press, San Diego.
- GALTON, P.M. (1970): The posture of hadrosaurian dinosaurs. – Journal of Paleontology, **44**: 464-473.
- GALTON, P.M. (1977): The ornithopod dinosaur *Dryosaurus* and a Laurasia-Gondwanaland connection in the Upper Jurassic. - Nature, **268**: 230-232.
- GALTON, P.M. (1981): *Dryosaurus*, a hypsilophodontid dinosaur from the Upper Jurassic of North America and Africa. Postcranial skeleton. - Paläontologische Zeitschrift, **55**: 271-312.
- GODEFROIT, P., ZAN, S. & JIN, L. (2001): The Maastrichtian (Late Cretaceous) lambeosaurine Dinosaur *Charonosaurus jiayinensis* from north-eastern China. – Bulletin de l´Institut Royal des Sciences Naturelles de Belgique, Sciences de la Terre, **71**: 119-168.
- GODEFROIT, P., BOLOTSKY, Y.L., & VAN ITTERBEECK, J. (2004): The lambeosaurine dinosaur *Amurosaurus riabinini*, from the Maastrichtian of Far Eastern Russia. - Acta Palaeontologica Polonica, **49** (4): 585–618.
- GUNGA, H.-C., SUTHAU, T., BELLMANN, A., FRIEDRICH, A., SCHWANEBECK, T., STOINSKI, S., TRIPPEL, T., KIRSCH, K. & HELLWICH, O. (2007): Body mass estimations for *Plateosaurus engelhardti* using laser scanning and 3D reconstruction methods. – Naturwissenschaften, **94**: 623-630.
- HARTMAN, S. (2004): Stance and carriage in *Brachylophosaurus*: evidence from articulated specimens. – Journal of Vertebrate Paleontology, **24**(3): 68A.
- HENDERSON, D.M. (1999): Estimating the masses and centers of mass of extinct animals by 3-D mathematical slicing. – Paleobiology, **25**(1): 88-106.
- HENDERSON, D.M. (2006): Burly gaits: centers of mass, stability, and the trackways of sauropods dinosaurs. – Journal of Vertebrate Paleontology, **26**(4): 907-921.
- HOLLIDAY, C.M., SEDLMAYR, J.C., RIDGELY, R.C., & WITMER, L.M. (2001a): The articular cartilage of extant archosaur long bones: implications for dinosaur functional morphology and allometry. – Journal of Morphology, **248**(3): 241-242.

- HOLLIDAY, C.M., RIDGELY, R.C., & SEDLMAYR, J.C., (2001b): The articular cartilage of extant archosaur limb bones: implications for dinosaur functional morphology and allometry. – Journal of Vertebrate Paleontology, **21**(3): 62A.
- HOLLIDAY, C.M., SEDLMAYR, J.C., RIDGELY, R.C., & WITMER, L.M. (2002): The articular cartilage of extant archosaur limb bones: implications for dinosaur functional morphology and allometry. – American Zoologist, **41**(6): 1473-1474.
- HOLLIDAY, C.M., RIDGELY, R.C., SEDLMAYR, J.C., & WITMER, L.M. (2010): Cartilaginous epiphyses in extant archosaurs and their implications for reconstructing limb function in dinosaurs. – PLoS ONE, **5**(9): 1-16.
- HOPSON, J.A. (1975): The evolution of cranial display structures in hadrosaurian dinosaurs. – Paleobiology, **1**: 21-43.
- HORNER, J.R. & MAKELA, R. (1979): Nests of juveniles provides evidence of family structure among dinosaurs. – Nature, **282**: 296-298.
- HORNER, J.R. (1982): Evidence for colonial nesting and "site fidelity" in ornithischian dinosaurs. - Nature, **297**: 675-676.
- HORNER, J.R. (1983): Cranial osteology and morphology of the type specimen of *Maiasaura peeblesorum* (Ornithischia: Hadrosauridae), with discussion of its phylogenetic position. – Journal of Vertebrate Paleontology, **3**: 29-38.
- HORNER, J.R. (1984): The nesting behavior of dinosaurs. – Scientific American, **250**(4):130-137.
- HORNER, J.R. (1999): Egg clutches and embryos of two hadrosaurian dinosaurs. – Journal of Vertebrate Paleontology, **19**: 607-611.
- HORNER, J.R. (2000): Dinosaur reproduction and parenting. – Annu. Rev. Earth Planet. Sci., **28**: 19-45.
- HORNER, J.R., DE RICQLES, A. & PADIAN, K. (2000): Long bone histology of the hadrosaurid dinosaur *Maiasaura peeblesorum*: Growth dynamics and physiology based on an ontogenetic series of skeletal elements. – Journal of Vertebrate Paleontology, **20**(1): 115-129.
- HORNER, J.R., PADIAN, K. & DE RICQLES, A. (2001): Comparative osteohistology of some embryonic and perinatal archosaurs: Phylogenetic and behavioral implications for dinosaurs. – Paleobiology: **27**: 39-58.

- HORNER, J.R., WEISHAMPEL, D.B. & FORSTER, C.A. (2004): Hadrosauridae. In: WEISHAMPEL, D.B., DODSON, P. & OSMÓLSKA, H. (Eds.): The Dinosauria (2nd Edition): 438-463. - University of California Press, Los Angeles.
- HÜBNER, T.R. & RAUHUT,O.W.M. (2010): A juvenile skull of *Dysalotosaurus lettowvorbecki* (Ornithischia: Iguanodontia), and implications for cranial ontogeny, phylogeny, and taxonomy in ornithopod dinosaurs. - Zoological Journal of the Linnean Society, **160** (2): 366–396.
- HÜBNER, T.R. (2012): Bone Histology in *Dysalotosaurus lettowvorbecki* (Ornithischia: Iguanodontia) – Variation, Growth, and Implications. - PLoS ONE, **7**(1): e29958.
- HUTCHINSON, J.R. (2005): Dinosaur locomotion. – Encyclopedia of Life Sciences.
- HUTCHINSON, J.R. & GATESY, S.M. (2006): Beyond the bones. – Nature, **440**: 292-294.
- LAMBE, L.M. (1918): On the genus *Trachodon* of Leidy. – Ottawa Nat., **31**: 135-139.
- LANGSTON, W. (1960): A hadrosaurian ichnite. – National History Papers of the National Museum of Canada, **4**: 1-9.
- LEIDY, J. (1858): *Hadrosaurus foulkii*, a new saurian from the Cretaceous of New Jersey. - Proc. Acad. Nat. Sci. Philadelphia, 1858: 215-218.
- LOCKLEY, M.G. (1986): A guide to dinosaur tracksites of the Colorado Plateau and American Southwest. – Geology Department, University of Colorado, Denver.
- LOCKLEY, M.G. (1991): Tracking dinosaurs-a new look at an ancient world. – Cambridge University Press, Cambridge.
- LOCKLEY, M.G. & WRIGHT, J.L. (2001): Trackways of large quadrupedal ornithopods from the Cretaceous: a review. In: TANKE, D.H. & CARPENTER, K. (Eds.): Mesozoic Vertebrate Life: 428-442. – Indiana University Press, Bloomington and Indianapolis.
- LOCKLEY, M.G., JANKE, P. & THEISEN, L. (2001): First reports of bird and ornithopod tracks from the Lakota Formation (Early Cretaceous), Black Hills, South Dakota. In: TANKE, D.H. & CARPENTER, K. (Eds.): Mesozoic Vertebrate Life: 443-452. – Indiana University Press, Bloomington and Indianapolis.
- LULL, R.S. & WRIGHT, N.E. (1942): Hadrosaurian dinosaurs of North America. – Geological Society of America, Special Papers, Number 40, pp. 1-242.
- MAIDMENT, S.C.R., LINTON, D.H., UPCHURCH, P. & BARRETT, P.M. (2012): Limb-bone scaling indicates diverse stance and gait in quadrupedal ornithischian dinosaurs. – PLoS ONE, **7**(5): e36904.

- MAIDMENT, S.C.R. & BARRETT, P.M. (2012): Does morphological convergence imply functional similarity? A test using the evolution of quadrupedalism in ornithischian dinosaurs. – Proceedings of the Royal Society B.
- MALLISON, H. (2007): Virtual dinosaurs. – Ph.D. thesis, University of Tübingen, Tübingen.
- MALLISON, H., HOHLOCH, A. & PFRETZSCHNER, H.-U. (2009): Mechanical digitizing for paleontology-new and improved techniques. – Palaeontologia Electronica, **12**(2): 41p.
- MARSH, O.C. (1881): Principal characters of American Jurassic dinosaurs. Part V. – American Journal of Science (Series 3), **21**: 417-423.
- MARYANSKA, T. & OSMÓLSKA, H. (1983): Some implications of hadrosaurian postcranial anatomy. - Acta Palaeontologica Polonica, **28**(1/2): 205-207.
- MARYANSKA, T. & OSMÓLSKA, H. (1984): Postcranial anatomy of *Saurolophus angustirostris* with comments on other Hadrosaurs. - Palaeontologia Polonica, **46**: 119-141.
- MCDONALD, A.T., KIRKLAND, J.I., DE BLIEUX, D.D., MADSEN, S.K., CAVIN, J., MILNER, A.R.C. & PANZARIN, L. (2010): New basal iguanodonts from the Cedar Mountain Formation of Utah and the evolution of thumb-spiked dinosaurs. - PLoS ONE, **5**(11): e14075.
- MCDONALD, A.T. (2012): Phylogeny of basal iguanodonts (Dinosauria: Ornithischia): an update. - PLoS ONE, **7**(5): e36745.
- MEYER, C.A. & THÜRING, B. (2003): The first iguanodontid dinosaur track from the Swiss alps (Schrattenkalk Formation, Aptian). - Ichnos, **10**: 221-228.
- MILNER,A.R. & NORMAN, D.B. (1984): The biogeography of advanced ornithopod dinosaurs (Archosauria: Ornithischia)-A cladistic-vicariance model. In: REIF, W.E. & WESTPHAL, F. (Eds.): Third Symposium on Mesozoic Terrestrial Ecosystems: 145-159. – Attempto Verlag, Tübingen, Germany.
- MORATALLA, J.J., SANZ, J.L., JIMENEZ, S. & LOCKLEY, M.G. (1992): A quadrupedal ornithopod trackway from the Lower Cretaceous of La Rioja (Spain): inferences on gait and hand structure. – Journal of Vertebrate Paleontology, **12**(2): 150-157.
- MORENO,K., CARRANO, M. & SNYDER, R. (2004): Morphological changes in pedal phalanges and the evolution of quadrupedalism in ornithopods: a biomechanical approach. – Journal of Vertebrate Paleontology, **24**(3): 96A.

- MORENO,K., CARRANO, M.T. & SNYDER, R. (2007): Morphological changes in pedal phalanges through ornithopod dinosaur evolution: a biomechanical approach. – Journal of Morphology, **268**: 50-63.
- MOTANI, R. (2001): Estimating body mass from silhouettes: testing the assumption of elliptical body cross-sections. – Paleobiology, **27**(4): 735-750.
- NORMAN, D.B. (1980): On the ornithischian dinosaur *Iguanodon bernissartensis* from Belgium. - Mémoires de l´Institut Royal des Sciences Naturelles de Belgique, **178**: 1-103.
- ÖZKAYA, N. & NORDIN, M. (1999): Fundamentals of Biomechanics. – Springer-Verlag, New York.
- OLSEN, P.E. & GALTON, P.M. (1984): A review of the reptile and amphibian assemblages from the Stormberg of southern Africa, with special emphasis on the footprints and the age of the Stormberg. - Palaeontologia Africana, **25**: 87-110.
- ORGAN, C.L. (2006): Biomechanics of ossified tendons in ornithopod dinosaurs. – Paleobiology, **32**(4): 652-665.
- OSBORN, H.F. (1912): Integument of the iguanodont dinosaur *Trachodon*. – Mem. Am. Museum Nat. History, **1**:33-54.
- OSTROM, J.H. (1961): Cranial morphology of the hadrosaurian dinosaurs of North America. – Bulletin of the American Museum of Natural History, **122**(2): 35-186.
- OSTROM, J.H. (1964): A reconsideration of the paleoecology of hadrosaurian dinosaurs. – American Journal of Science, **262**: 975-997.
- PADIAN, K. & HORNER, J.R. (2004): Dinosaur physiology. In: WEISHAMPEL, D.B., DODSON, P. & OSMÓLSKA, H. (Eds.): The Dinosauria (2nd Edition): 660-671. - University of California Press, Los Angeles.
- PAUL, G.S. (1987): The science and art of restoring the life appearance of dinosaurs and their relatives: a rigorous how-to guide. In: CZERKAS, S.J. and OLSON, E.C. (Eds.): Dinosaurs Past and Present Volume II – an exhibition and symposium organized by the Natural History Museum of Los Angeles County: 4-49. – The University of Washington Press, Seattle.
- PAUL, G.S. (1997a): Migration. In: CURRIE, P.J. & PADIAN, K. (Eds.): Encyclopedia of Dinosaurs: 293-299. - Academic Press, San Diego.

- PAUL, G.S. (1997b): Dinosaur models: the good, the bad, and using them to estimate the mass of dinosaurs. In: WOLBERG, D.L., STUMP, E., & ROSENBERG, G. (Eds.): Dinofest International: Proceedings of a Symposium held at Arizona State University: 129-154.
- PAUL, G.S. (2007): Turning the old into the new: a separate genus for the gracile iguanodont from the Wealden of England. In: CARPENTER, K. (Ed.): Horns and beaks - ceratopsian and ornithopod dinosaurs: 91-115. – Indiana University Press, Bloomington and Indianapolis.
- PAUL, G.S. (2010): The Princeton field guide to dinosaurs. – Princeton University Press, Princeton and Oxford.
- PRIETO-MARQUEZ, A., WEISHAMPEL, D.B. & HORNER, J.R. (2006): The dinosaur *Hadrosaurus foulkii*, from the Campanian ofthe East Coast of North America, with a reevaluation of the genus. - Acta Palaeontologica Polonica, **51** (1): 77–98.
- PRIETO-MARQUEZ, A. (2007): Postcranial osteology of the hadrosaurid dinosaur *Brachylophosaurus canadensis* from the Late Cretaceous of Montana. In: CARPENTER, K. (Ed.): Horns and beaks - ceratopsian and ornithopod dinosaurs: 91-115. – Indiana University Press, Bloomington and Indianapolis.
- RUSSELL, D. (1967a): A census of dinosaur specimens collected in western Canada. - Natl. Mus. Can. Nat. Hist. Pap., **36**: 1–13.
- RUSSELL, D. (1967b): Cretaceous vertebrates from the Anderson River N.W.T. – Canadian Journal of Earth Sciences, **4**: 21–38.
- SANDER, M. (1994): Reptilien. – Ferdinand Enke Verlag, Stuttgart.
- SCHWARZ, D., WINGS, O., & MEYER, C.A. (2007a): Super sizing the giants: first cartilage preservation at a sauropod dinosaur limb joint. – Journal of the Geological Society, London, **164**: 61-65.
- SCHWARZ, D., FREY, E., & MEYER, C.A. (2007b): Pneumaticity and soft−tissue reconstructions in the neck of diplodocid and dicraeosaurid sauropods. – Acta Palaeontologica Polonica, **52**(1): 167-188.
- SEEBACHER, F. (2001): A new method to calculate allometric length-mass relationships of dinosaurs. – Journal of Vertebrate Paleontology, **21**(1): 51-60.
- SELLERS, W.I., MANNING, P.L., LYSON, T., STEVENS, K. & MARGETTS, L. (2009): Virtual palaeontology: gait reconstruction of extinct vertebrates using high performance computing. – Palaeontologia Electronica, **12**(3): 26p.

- SENTER, P. (2012): Forearm orientation in Hadrosauridae (Dinosauria: Ornithopoda) and implications for museum mounts. – Palaeontologia Electronica, **15**(3): 10p.
- SERENO, P.C. (1986): Phylogeny of the bird-hipped dinosaurs (Order Ornithischia). - Natl. Geogr. Soc. Res., **2**: 234-256.
- SERENO, P.C. (1997): The origin and evolution of dinosaurs. – Annu. Rev. Earth Planet. Sci., **25**: 435-489.
- SERENO, P.C. (1999): The evolution of dinosaurs. - Science, **284**: 2137-2147.
- STERNBERG, C.M. (1953): A new hadrosaur from the Oldman Formation of Alberta: Discussion of nomenclature. – Ca.Dept.Res.Devel.Bull., **128**: 1-12.
- THULBORN, R.A. (1989): The gaits of dinosaurs. In: GILLETTE, D.D. & LOCKLEY, M.G. (Eds.): Dinosaur Tracks and Traces: 39-50. – Cambridge University Press, Cambridge.
- THULBORN, R.A. (1990): Dinosaur Tracks. – Chapman and Hall, UK.
- VARRICCHIO, D.J. & HORNER, J.R. (1993): Hadrosaurid and lambeosaurid bone beds from the Upper Cretaceous Two Medicine Formation of Montana: Taphonomic and biologic implications. In: CURRIE, P.J. (Eds.): Results from the Sino-Canadian Dinosaur Project. – Canadian Journal of Earth Sciences, **30**: 997-1006.
- VIRCHOW, H. (1919): Atlas und Epistropheus bei den Schildkröten. - Sitzungsber. Ges. naturf. Freunde Berlin, **1919**: 303-332.
- WEDEL, M.J. (2003): Vertebral pneumaticity, air sacs, and the physiology of sauropod dinosaurs. – Paleobiology, **29**(2): 243-255.
- WEISHAMPEL, D.B. (1981a): Acoustic analysis of potential vocalization in lambeosaurine dinosaurs (Reptilia: Ornithischia). – Paleobiology, **7**: 252-261.
- WEISHAMPEL, D.B. (1981b): The nasal cavity of lambeosaurine hadrosaurids (Reptilia: Ornithischia): comparative anatomy and homologies. – Journal of Paleontology, **55**: 1046-1057.
- WEISHAMPEL, D.B. & WEISHAMPEL, J.B. (1983): Annotated localities of ornithopod dinosaurs: Implications to Mesozoic paleobiogeography. – Mosasaur, **1**: 43-87.
- WEISHAMPEL, D.B. (1984): Interactions between Mesozoic plants and vertebrates: Fructifications and seed predation. – Neues Jahrbuch für Geologie und Paläontologie-Abhandlungen, **167**: 224-250.
- WEISHAMPEL, D.B. (1990): Dinosaurian distribution. In: WEISHAMPEL, D.B., DODSON, P. & OSMÓLSKA, H. (Eds.): The Dinosauria: 63-139. - University of California Press, Berkeley.

- WEISHAMPEL, D.B., NORMAN, D.B. & GRIGORESCU, D. (1993): *Telmatosaurus transsylvanicus* from the Late Cretaceous of Romania: the most basal hadrosaurid Dinosaur. – Palaeontology, **36**(2): 361-385.
- WEISHAMPEL, D.B, BARRETT, P.M., CORIA, R.A., LE LOEUFF, J., XING, X., XIJIN, Z., SAHNI, A., GOMANI, E.M.P. & NOTO, C.R. (2004): Dinosaur distribution. In: WEISHAMPEL, D.B., DODSON, P. & OSMÓLSKA, H. (Eds.): The Dinosauria (2nd Edition): 517-606. - University of California Press, Los Angeles.
- WRIGHT, J.L. (1999): Ichnological evidence for the use of the forelimb in iguanodontid locomotion. – Special Papers in Palaeontology, **60**: 209-219.
- XING, L., BELL, P.R., HARRIS, J.D. & CURRIE, P.J. (2012): An unusual, three-dimensionally preserved, large hadrosauriform pes track from “Mid”-Cretaceous Jiaguan Formation of Chongqing, China. – Acta Geologica Sinica (English Edition), **86**(2): 304-312.
- YATES, A.M., WEDEL, M.J. & Bonnan, M.F. (2012): The early evolution of postcranial skeletal pneumaticity in sauropodomorph dinosaurs. – Acta Palaeontologica Polonica, **57**(1): 85-100.
- ZELENITSKY, D., THERRIEN, F., CURRIE, P., HENDERSON, D. & HORNER, J. (2006): Locomotory behavior in the lambeosaurine *Hypacrosaurus stebingeri*. – Journal of Vertebrate Paleontology, **26**(3): 143A.